Structural and molecular characterisation of the penetration process of *Fusarium graminearum* during fusarium head blight infection

Dissertation

to achieve the doctoral degree

Dr. rer. nat.*: *Doctor rerum naturalium

Presented To

Department Of Biology,

Faculty For Mathematics, Informatics And Natural Science

UNIVERSITY OF HAMBURG

Provided by

Marike Johanne Boenisch

Hamburg, Germany

2013

DEPARTMENT BIOLOGY

Genehmigt vom Fachbereich Biologie
der Fakultät für Mathematik, Informatik und Naturwissenschaften
an der Universität Hamburg
auf Antrag von Professor Dr. W. SCHÄFER
Weiterer Gutachter der Dissertation:
Priv.-Dz. Dr. S. SCHOLTEN
Tag der Disputation: 28. März 2013

Hamburg, den 14. März 2013

Professor Dr. J. Fromm
Vorsitzender des Promotionsausschusses
Biologie

Table of content

Abbreviations

AC	Adenylate cyclase
ADON	Acetyldeoxynivalenol
bp	Base pairs
CCD	Charge coupled device
cDNA	Coding deoxyribonucleic acid
CM	Complete medium
CP	Critical point
Cp	Crossing point
CWDE	Cell wall degrading enzymes
cv	Cultivar
cyc	Cycle
DAPI	4,6-diamidino-2-phenylindol
DEPC	Diethylpyrocarbonate
DHS	Deoxyhypusine synthase
DIG	Digoxygenin
DNA	Deoxyribonucleic acid
dNTP	Deoxynucleotide triphosphate
DOHH	Deoxyhypusine hydroxylase
DON	Deoxynivalenol
dpi	Days post inoculation
DsRed	Red fluorescent protein
DW	Dry weight
EC	European Comission
e.g.	Exempli gratia
EST	Expressed sequence tags
EVA	Ethylene vinyl acetate
FGDB	*Fusarium graminearum* genome database
FAC	*Fusarium graminearum* adenylate cyclas
FGL1	*Fusarium graminearum* lipase 1
FHB	Fusarium head blight
gDNA	Genomic deoxyribonucleic acid
GFP	Green fluorescent protein
eGFP	Enhanced Green fluorescent protein
gpdA	Glycerol-3-phosphate dehydrogenase promotor
Gpmk1	*Gibberella* pathogenicity MAP kinase 1
GS	Growth stage
hpi	Hours post inoculation
IC	Infection cushion
IR	Infrared
kb	Kilo bases
L.	Linnaeus
LD-PCR	Long distance polymerase chain reaction
LM	Light microscopy
LMD	Laser microdissection
LPC	Laser pressure catapulting
LSM	Laser scanning microscopy
M	Molar (mol/L)
MM	Minimal medium

MAPK	Mitogen activated protein kinase
min	Minute
MIP	Maximun intensity projection
MIPS	Munich Information Center for Protein Sequences
NGS	Next generation sequencing
NIV	Nivalenol
PALM	Name of a subdivision of the company Carl Zeiss
PCR	Polymerase chain reaction
Q-PCR	Quantitative polymerase chain reaction
RAW data	Unprocessed data
RH	Runner hyphae
RIN	RNA integrity number
RNA	Ribonucleic acid
rRNA	Ribosomal ribonucleic acid
ROS	Reactive oxygen species
RT	Room temperature
S	Svedberg
s	Second
SEM	Scanning electron microscopy
SMART	Switching mechanism of 5'end of RNA template
SNA	Synthetic nutrient poor agar
SNP	Single nucleotide polymorphism
ssRNA	Single stranded ribosomal ribonucleic acid
TEM	Transmission electron microscopy
Tri	Name of trichothecene cluster genes
TRI5	Trichodien synthase 5
USA	United Staates of America
UV	Ultra violet
v	Volume
v/v	Volume per volume
Wt	Wild type
w/v	Weight per volume
ZEA	Zeralenon

List of figures and tables

1 Introduction

1.1 The plant pathogen *Fusarium graminearum*

The ascomycete fungus *Fusarium graminearum* Schwabe (teleomorph *Gibberella zeae* (Schwein) Petch) causes the Fusarium head blight (FHB) disease of small grain cereals including wheat (*Tritticum aestivum* L.), barely (*Hordeum vulgare* L.), and rice (*Oryza sativa* L.) as well as cob rot of maize (*Zea mays* L.) [1-3]. Outbreaks of FHB on fields throughout the world are usually caused by a complex of different *Fusarium* species, which exhibit biological and pathological characteristics e.g. mytoxin production, virulence, and host range [4-8]. The species *Fusarium graminearum* is described to be the main causal agent in the USA, in Canada, and Europe [2, 3, 9]. However, outbreaks of *F. graminearum* infections are described in Asia, Australia, and South-America [10]. Relevance of *F. graminearum* for human kind is mainly caused by the economical importance of FHB due to losses of grain yield in many of the world's wheat-growing areas with humid to semi-humid climate [3, 5]. The disease cycle of FHB in fields is initiated by airborn ascospores germinating on spikelets (figure 1). The open florets during anthesis provide opportunities for the pathogen to contact the primary penetration sites of the host. The developing caryopses as well as the adaxial surfaces of lemma and palea are preferred sides for penetration [3, 11, 12]. Pollen grains of wheat, which are extruded during anthesis contain high concentrations of choline and betaine [13], which promote hyphal growth and vitality of the fungus [13-15]. After penetrating the floret tissues by unspecialised infection hyphae [12] or specialised infection structures [14, 16-18], the fungus colonises the floret tissue [12, 19, 20]. Finally, the fungus spreads systemically through the parenchyma and vascular tissue of the wheat spike [21-23] and reaches remaining florets of the spike. Symptoms appear as water soaking spots with partially necrotic and chlorotic tissue of the spike [3, 5, 23]. Premature bleaching of infected heads is a typical symptom of FHB and results from vacular occlusions following systemic spread of hyphae [3, 5]. During prolonged wet periods pink to salmon-orange masses of conidia of the fungus, so-called sporodochia, are often observed on infected spikelets of wheat and barley [5]. Through vegetative conidia a secondary inoculation can take place within the same vegetation period and, thus, can lead to severe FHB epidemics. Infection of wheat heads cause shriveled and underweight grains, which are contaminated with harmful mycotoxins. Fusarium toxins

such as trichothecenes (e.g. deoxynivalenol (DON) and nivalenol (NIV)) threaten humans and animals by contaminated food [24]. DON can cause vomiting and is harmful to central inner organs of mammals [3, 25, 26]. Additional mycotoxins, such as the polyketid zearalenone, cause reproductive defects, due to its analog effect as estrogenic hormones [24]. After harvest, *F. graminearum* overwinters in its sexual stage *G. zea* on crop residues on the field [27]. The dikaryotic mycelium of *G. zea* forms fruiting bodies, the perithecia, in which haploid ascospores are produced [27]. The matured meiotic ascospores then serve as inoculum for infection in the next vegetative period [3].

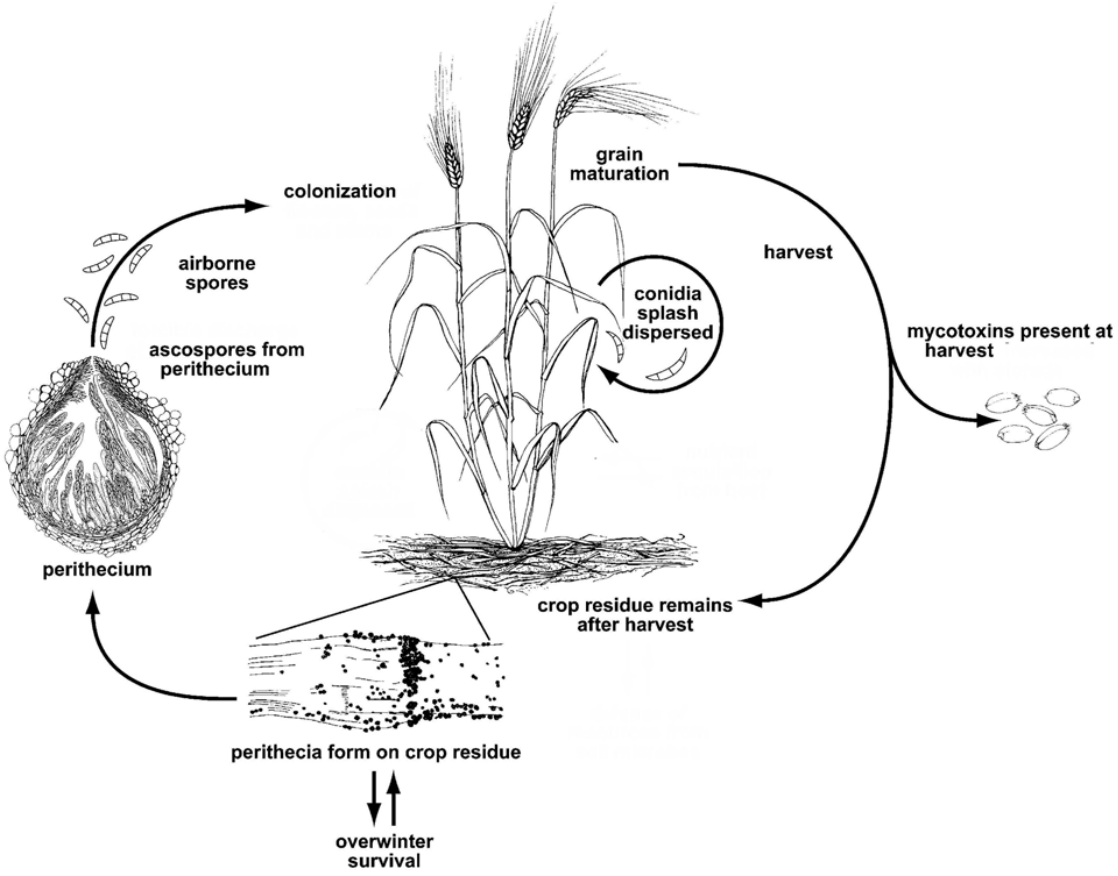

Figure 1: The life cycle of *F. graminearum.* Haploid ascospores are discharged from overwintering perithecia formed by the sexual stage of the fungus, called *Giberella zea.* The ascospores land on flowers of wheat heads were they germinate. The growing haploid mycelium of the fungus, then called *F. graminearum*, penetrates and colonises the spike systemically. By asexual spores (conidia) a secondary inoculation takes place. Following infection, kernels are contaminated with mycotoxins at harvest. The fungus develops perithecia on remaining crop residues and overwinters until ascospores are released in the next season. Source: Figure from Trail, 2009 [3] was modified.

1.2 Trichothecene mytoxins of *Fusarium graminearum*

Fusarium toxins including the trichothecenes nivalenol (NIV), deoxynivalenol (DON) and its derivatives 3- and 15-acetyldeoxynivalenol (3-ADON, 15-ADON) contaminate cereal products and have been shown to be harmful to humans, animals, and plants [24]. Hence, the European Union and the United States set limits for DON in final products for human consumption of 0.75 µg/g [Commission Regulation [EC] no. 1881/2006] and of 1 µg/g [Council for Agricultural Science and Technology, 2003]. The toxic effect of trichothecenes is mainly due to their ability to bind to the 60S ribosomal subunit of eukaryotes, resulting in inhibition of protein synthesis and induction of apoptosis [28]. Trichothecenes are potent phytotoxins for many plants. They can produce symptoms including wilting, chlorosis and necrosis at concentrations of 10^{-5} to 10^{-6} M [29]. DON is known as a virulence factor in wheat, causing tissue necrosis [30, 31]. Furthermore, DON production enables the fungus to spread from infected florets into the wheat rachis [21, 30-33]. Although detailed information of the *TRI* gene cluster (figure 2) is available [34], the factors inducing mycotoxin production during infection are nearly unknown. The first step of the trichothecene biosynthesis is catalysed by the enzyme trichodiene synthase encoded by the *TRI5* gene [35, 36]. Thus, the *TRI5* gene is used as a marker gene for the induction of trichothecene biosynthesis of the fungus [22, 37-39]. Induction assays using axenic cultures revealed several *TRI5* inducing conditions and substances under laboratory conditions [22, 37, 38, 40, 41]. Wheat infection of a fungal mutant with a *TRI5* promoter GFP (green fluorescent protein) fusion showed a tissue specific *TRI5* induction in rachis nodes during systemic colonisation and in caryopses during initial establishment of wheat infection [22]. A major role of trichothecenes for the initial establishment in the host tissue was suggested [39], after induction of *TRI5* expression was detected during early infection stages on barley spikes infected with *F. graminearum* [42] as well as on seedlings of wheat, infected with *F. culmorum* [39]. Contrary to that, infection studies with *TRI5* knockout mutants revealed that the trichothecene deficient mutant is still able to infect the primarily inoculated wheat spikelet like wild type [21, 30, 32, 33]. Thus, trichothecenes appeared to be of minor importance for initial infection on wheat. However, it was recently published that *TRI5* expression is highly induced in infection structures of *F. graminearum* during initial infection of different floret tissues of wheat [18]. It was further demonstrated that a high DON concentration is measured in caryopses and glumes, after *TRI5* expression was

visible in infection structures by GFP fluorescence using a fungal reporter strain with a *TRI5* promoter GFP fusion. Therefore, a role of trichothecenes during penetration of wheat was assumed.

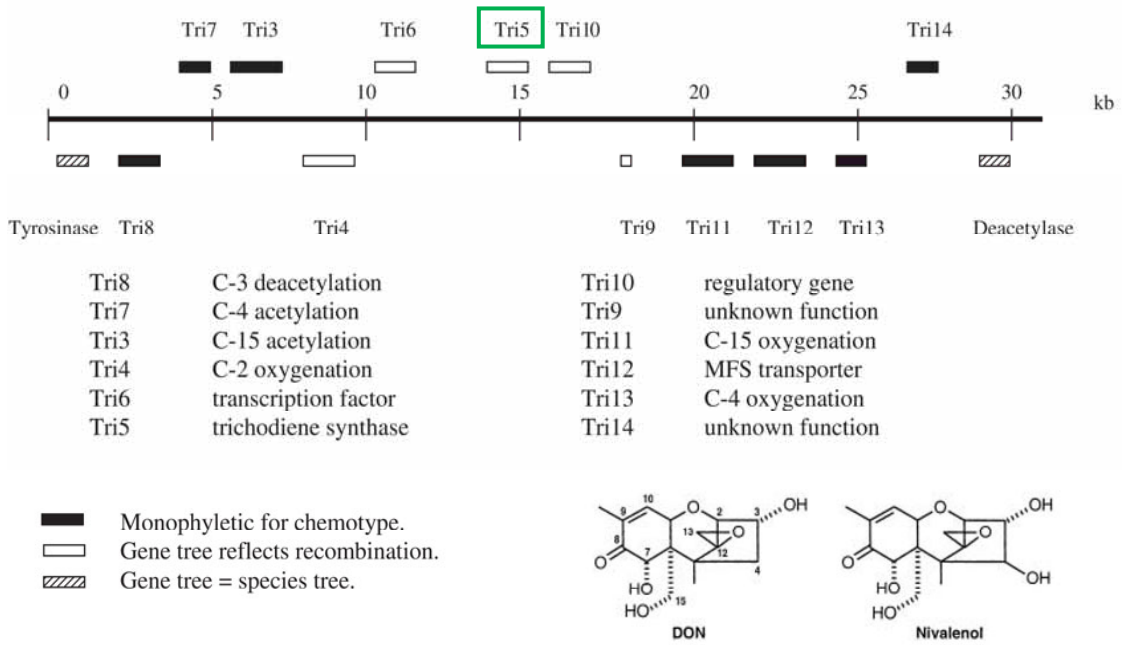

Figure 2: Diagram of the trichothecene (Tri) biosynthetic gene cluster of *F. graminearum*. The genes for secondary pathways of fungi are often arranged in clusters closely located to each other within the genome. The TRI genes encode for different enzymes involved in the trichothecene biosynthesis of the fungus. The boxes indicate the relative positions of genes on the genomic DNA strand. The tri5 gene coding for the trichodiene synthase is marked with a green square. The chemical structure of the major trichothecene molecules, deoxinivalenol (DON) and nivalenol produced by *F. graminearum* are illustrated at the bottom right. Source: [5].

1.3 Infection structures of phytopathogenic fungi

Phytopathogenic fungi invade living plant in order to obtain nutrients. For actively entering the host, the natural barrier of plant cells, namely the plant the cell wall, has to be overcome. In order to penetrate cell walls, different types of infection structures are produced by the various phytopathogenic fungi. In general, infection structures of phytopathogenic fungi are defined as modified hyphae specialised in the invasion of plant tissues. In general, infection structures with minor modifications e.g. infection hyphae (figure 3, A and B) are distinguished from specialised infection structures appressoria (figure 3, C and D) with specific morphological characteristics. The term "appressorium" was introduced 1883 by Frank [43] for *Colletotrichum lindemuthianum* and several other fungi in order to describe "spore-like organs" formed on germ tubes and serve as adhesive discs to attach a parasitic fungus to its host during the early stages of infection [44]. A classical appressorium is known as a domeshaped swollen cell at the tip of the conidial germ tube. A mature classical appressorium is separated from the germ tube by a septum and darkly pigmented by melanized cell walls in order to stand a high turgor pressure, which is built up to perforate the host cell wall by a so-called penetration peg or hyphae [45].

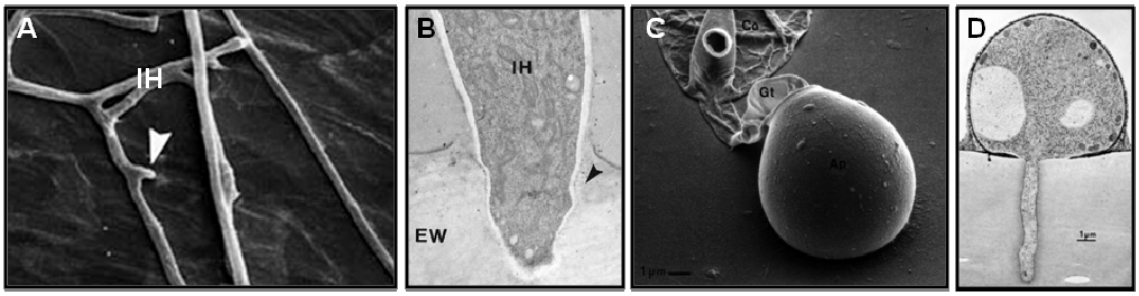

Figure 3: Unspecialised infection structures (A and B) and specialised appressoria (C and D) of phytopathogenic fungi. A and **B** Infection hypha of *Fusarium culmorum* on the surface of a lemma of wheat by SEM (A) and TEM (B). **C** and **D** Classical appressorium of *Magnaporthe oryzae* on artifitial surfaces by SEM (C) and TEM (D). Sources: A and B [20], C [46], D [47].

By accumulation of osmotic substances such as glycerol [48], a high turgor pressure up to 80 bars is determined in appressoria of *Magnaporthe oryzae* (former called *Magnaporthe grisea*) [49], while 54 bars are described for *Colletotrichum graminicola*. The thin (approx. 1 µm) penetration peg usually accumulates components of the

cytoskeleton in the tip, while the cell wall is less pronounced in order to secrete a variety of cell wall–degrading enzymes [45]. It is suggested that a combination of turgor pressure and enzymatic digestion enables direct penetration [45, 47, 50]. Various modifications of the classical approssorium e.g. smaller, unmalanised or unsepted types are described for different fungal plant pathogens [44, 50, 51]. Another group of appressoria types are the so-called compound appressoria. Compound appressoria include multicellular types of specialised infection structures, namely lobate appressoria and infection cushions. Both types are formed by epiphytic mycelium and usually not by germ tubes [44]. The hyphae from which compound appressoria originate are termed runner or running hyphae in publications about *Rhizoctonia solani* [52, 53] and several *Sclerotinia* species [54-56], but also mycorrhiza fungi [57, 58]. A development from lobate appressoria into infection cushions is described for *R. solani* [59], *Botrytis cinerea* [60], and *Sclerotinia sclerotiorum* [44]. For *R. solani* it is known that one-celled foot structures develop initially from runner hyphae (figure 4, A), develop further into lobate appressoria and finally into to infection cushions (figure 4, B) [52, 61, 62]. Lobate appressoria are smaller and formed by fewer cells than infection cushions. Lobate appressoria can consist a single lobate cell, but two-celled to multi-celled types are described as well [44]. In general, hyphae of lobate appressoria are short, swollen and highly septate cells [44]. Each lobe of a lobate appressorium is described to be able to form an infection peg [44]. Many penetration events resulting from penetration pegs of infection cushions were demonstrated by ultrastructural studies on *S. sclerotiorum* [54] and *R. solani* [53, 63].

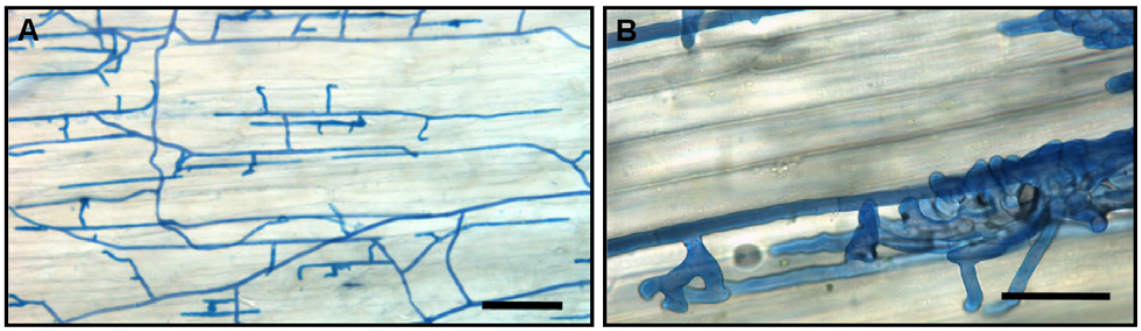

Figure 4: Compound appressoria of phytopathogenic fungi. A and **B** Light microscopy of compound appressoria development of *R. solani* on cauliflower hypocotyls after trypan blue staining of hyphae. **A** Bulbous foot structures branch from runner hypae on the plant. **B** Lobate appressoria and infection cushions consist of agglomerated and highly ramified hyphae. Scale bars=100 µm. Source: [62].

1.4 Infection structures of *Fusarium graminearum*

Most *Fusarium* species enter husks of wheat and barley by natural openings, such as stomata, or penetrate epidermal cell walls with short infection hyphae [9, 12, 20, 45, 64-66]. In contrast to the other species, previous publications for *F. graminearum* provided the first light microscopic evidences for specialised infection structures, which were named coral-like hyphal mats [14, 16, 17] and bulbous infection hyphae [14]. Coral-like hyphal structures were further specified by lobed, thickened, and branched hyphae [14, 16, 17]. In previous studies an i*n vitro* bioassay with detached floret organs was established and compound appressoria identified by different microscopic techniques, such as stereomicroscopy, laser scanning microscopy (LSM), and scanning electron microscopy (SEM) [18]. Due to constitutive expression of the *dsRed* gene in the mycelium of a *TRI5prom*::*GFP* reporter strain, three successive infection stages (stage I-III) were identified on wheat floret tissues including the glume, lemma, palea, and caryopses. The main characteristics of the respective infection stages are summarised in table 1. The stages of infection appear similar on caryopses and husks, yet at different time points after inoculation. It was demonstrated that *F. graminearum* develops compound appressoria including foot structures, lobate appressoria, and infection cushions during stage II of infection (figure 5,). Therby, striking morphological similarities to other fungal plant pathogens e.g. *R. solani* [61-63, 67, 68], *B. cinerea* [60, 69], and *S. sclerotiorum* [44, 54] were noted [18]. The expression of *GFP* gene driven by the endogenous *TRI5* promoter in the *TRI5prom*::*GFP* reporter strain enabled monitoring of the trichothecene induction during infection in real time. Thereby, DON induction was identified using fluorescence microscopy specifically in infection structures (figure 5, A-D). Morphological characteristics of compound appressoria, lobate appressoria, and foot structures were further visible by scanning electron microscopy (figure 5, E-F). Consequently, a relation between DON production and direct penetration was indicated. The observations regarding infection stages and infection structures for the *TRI5prom*::*GFP* reporter strain were shown to be similar for different wheat cultivars with varying degree of resistance towards FHB [18].

Table 1: Infection stages I-III on floret organs of wheat and their omnipresent characteristics in detached *in vitro* bioassays. Observations made on glumes, lemmas, paleas, and caryopses were similar for the susceptible wheat cultivar Nandu (n=80/organ) and the resistant cultivar Sumai 3 (n=24/organ), infected with *TRI5prom::GFP* mutant. Source: [18].

	Stage I	**Stage II**	**Stage III**
Main event	Surface colonisation	Penetration	Sporulation
Typical fungal morphology	Runner hyphae Infection hyphae	Runner hyphae, Foot structures Lobate appressoria Infection cushions	Aerial hyphae Sporodochia
Necroses	No	Some	Many
DON-Induction	No	Yes	No
Organ	**Apperance of stage at days post inoculation (dpi)**		
Caryopsis	0-2	2-3	3-4
Palea	0-4	4-8	8-10
Glume and lemma	0-7	7-14	14-21

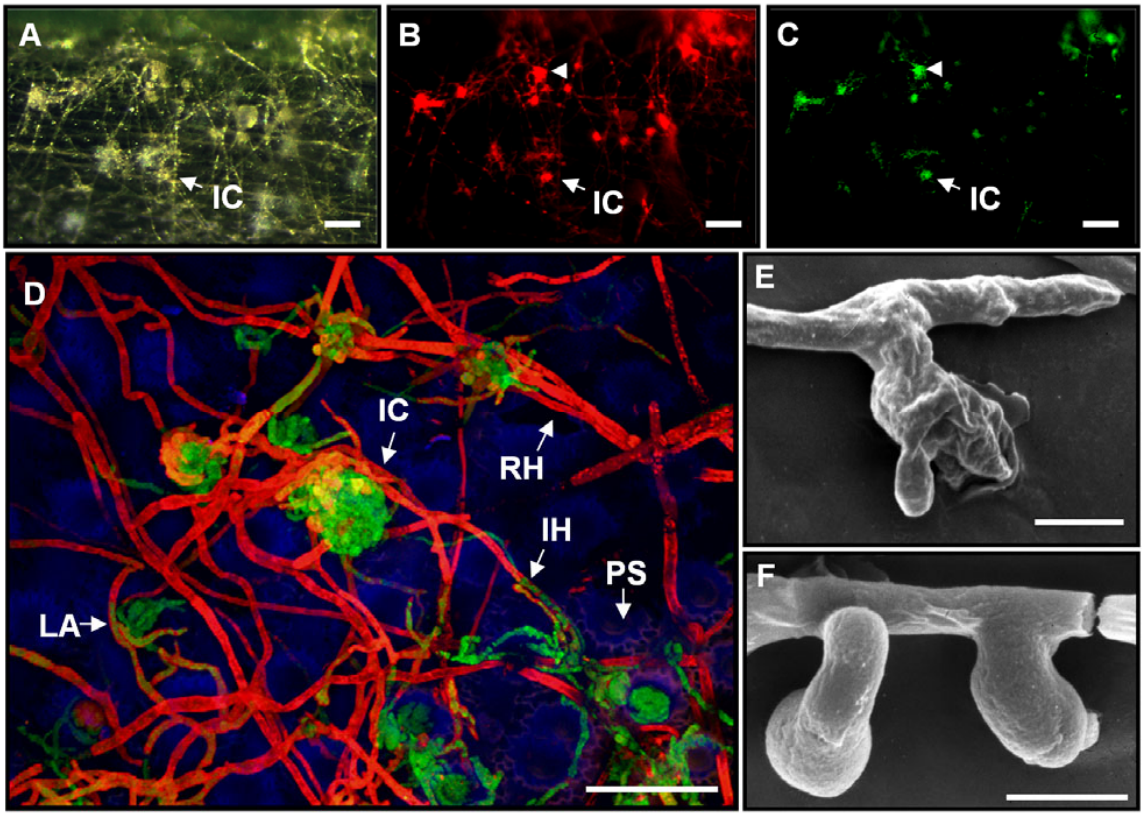

Figure 5: Compound appressoria and *TRI5* induction of *F. graminearum TRI5prom::GFP* on the wheat cultivar Nandu. A-C White light and fluorescence micrographs of infection cushions on palea at 8 dpi. Scale bars=100 µm. **A** Natural appearance of the inoculated surface of palea. **B** Infection cushions are visible by dsRed fluorescence. **C** GFP fluorescence demonstrates *TRI5* induction in infection structures. **D** Laser scanning microscopy of GFP inductive fungal structures (white arrowhead in B and C). Overlay image of individually detected dsRed and GFP fluorescence of the fungus as well as blue plant autofluorescence. The image represents a maximum intensity projection of a z-stack. Scale bar=50 µm. **E** and **F** Scanning electron micrographs of different infection structures on a palea 7 dpi. **E** Lobate appressorium, and **F** foot structures. Scale bars=5 µm. **Abbreviations**: **FS** Foot structures, **IC** infection cushion, **IH** infection hypha, **LA** lobate appressorium, **PS** papillae silica cell, **RH** runner hyphae. Source: A-D from [18].

1.5 Mutants of *F. graminearum* with altered infection phenotype

Due to the fact that, until very recently, it was unknown that *F. graminearum* forms compound appressoria on wheat [18], no data about genes or molecular characteristics of compound appressoria were available at the time experiments were performed. Therefore, accessible deletion or overexpression mutants of *F. graminearum*, which showed an altered (reduced or increased) infection phenotype, were selected for microscopic studies of infection structures and infection stages. Other mutants were selected for this experiment, since mutants of the respective homologous gene in other phytopathogenic fungi are known to be related to infection structure formation or function. Another criterion to pick the respective mutant was that it was co-transformed with a reporter gene for constitutive fluorescence detection of the mycelium during infection. The later named feature was beneficial for the clarity of microscopy results and, thus, improved the validity of observations made.

The secreted lipase encoded by the *FGL1* gene of *F. graminearum* was chosen, because it is known to be a virulence factor for infection of cereals and maize [70]. The gene disruption mutant of *F. graminearum* showed significantly reduced extracellular lipolytic activity in culture and reduced infection of wheat spikes and maize cobs [70]. In contrast to wild type strain infections, lipase deficient mutants were restricted to directly inoculated spikelets [70]. Transcription was detected one day after infection of wheat spikes. The importance of lipases in pathogenicity has been shown for other fungal plant pathogens, such as *Alternaria brassicicola* [71] and *B. cinerea* [72]. Inhibition of an extracellular lipase of *B cinerea* by polyclonal antibodies suppressed lesion formation on detached tomato leaves [72].

The disruption mutant of the MAP kinase *GPMK1* of *F. graminearum* was unable to cause disease symptoms of the inoculated spikelet [73] and, thus, was reported as the first apathogenic mutant of *F. graminearum* on wheat. MAP kinases regulate the pathogenic stages of many filamentous fungi [74-77]. The homologous sequence has been reported to be involved in appressorium formation [74-76].

The disruption mutant of the PLS1 gene of *F. graminearum* showed remarkably reduced spread of wheat spikes in previous infection experiments performed by Dr. Long Nam Nguyen [78]. *PLS1* deletion mutants of other plant pathogenic fungi (*M. oryzae*, *B. cinerea,* and *C. lindemuthianum*) were studied previously and displayed a

loss of pathogenicity on their respective host plants [79-81]. Mutants of the *PLS1* homologe of *M. oryzae* developed normally shaped appressoria, but were unable to form functional penetration pegs [79]. Furthermore, the *PLS1* gene of *C. lindemuthianum* is required for the correct positioning of a penetration peg at the base of the appressorium [82].

The gene disruption mutant *FAC* of *F. graminearum* is defective to produce an endogenous adenylate cyclase. Adenylyl cyclases are membrane bound enzymes that can be activated by the α-subunits of G-protein-coupled-receptors (GPCRs). GPCRs may perceive external signals leading to conformational changes and dissociation of a heteromeric G-protein that consists of one α, β, and γ subunit. The dissociated α-subunits then results in the conversion of ATP to cAMP and pyrophosphate. Increasing levels of intracellular cAMP bind to regulatory subunits of the protein kinase A (PKA). Following dissociation the activated catalytic subunits PKA activates downstream effectors such as transcription factors or further signal cascades. [83, 84]. The Δ*FAC-dsRed* disruption mutant exhibited a non pathogenic phenotype in wheat infection in previous experiments performed by Elena Brückner and Dr. Jörg Bormann (Molecular Phytopathology and Genetics, Biocenter Klein Flottbek, University of Hamburg). Deletion of the adenylate cyclase gene MAC1 in *M. oryzae* resulted in mutants that can not form appressoria [85, 86] developed a model of the cAMP/PKA signaling pathway of the ascomycete *M. oryzae* and showed that surface recognition and initiation of appressorium formation is regulated by the corresponding pathway.

The overexpression mutants of the two enzymes deoxyhypusine synthase (OE *DHS-GFP*) and deoxyhypusine hydrolase (OE *DOHH-GFP*) as well as the overexpression mutant of both enzymes (OE *DHS/DOHH-GFP*) were selected for microscopic studies on initial infection stages, because these mutants appear to be involved in aggressiveness of FHB infection [87, 88]. While the OE *DHS-GFP* exhibited a more severe infection of wheat spikes, the OE *DOHH-GFP* mutant caused a reduced infection compared to the wild type. Interestingly, the double mutant OE *DHS/DOHH-GFP* appeared to be between the *DHS* and *DOHH* infection phenotype and caused similar FHB symptoms like the wild type.

1.6 The genome of *Fusarium graminearum*

The genome sequence was publicly released 2003 and is provided by the Broad institute (www.broad.mit.edu/annotation/ genome/fusarium_group/MultiHome.html) [65]. Since 2004, the sequenced and annotated genomic data of *F. graminearum* are publicly available via the FGDB (*Fusarium graminearum* genome data base) by http://mips.helmholtz-muenchen.de/genre/proj/fusarium [89]. The genome sequence release has greatly increased research activity and possibilities on *F. graminearum* [3] by making large-scale omic studies more practicable. The size of the *F. graminearum* genome (36.1 mega bases) is relatively common for a filamentous fungus. Some genomic data from other, well studied phytopathogens are provided in table 2.

Table 2: The genome size, number of genes and chromosomes of *F. graminearum* as well as other fungal plant pathogens. (Data were queried at the 22.12.2012 by: www.broad.mit.edu/annotation/ genome/)

Species	Size	Genes	Chrs
***Fusarium graminearum* (PH-1)**	36.1 Mb	13.321	4
***Botrytis cinerea* (B05.10)**	42.66 Mb	16.448	16[§]
Ustilago maydis	19.68 Mb	6.522	N/A
***Magnapothe oryzae* 70-15 (MG6)**	41.7 Mb	11.074	N/A
***Neurospora crassa* OR74A (NC10)**	41.04 Mb	9.733	7

§ Shirane et al., (1989) [90]. N/A = not annotated.

The genome of the sequenced *F. graminearum* strain PH-1 contains genes encoding 13.321 genes distributed over four chromosomes [3, 65]. Of these genes, 2.001 are not similar to those of any other sequenced organism, the so-called orphans. This shows that only a small proportion of genes are unique for *F. graminearum*. An amount of 5.812 genes show homology to proteins of unknown function [3]. This demonstrates that the annotation of the genome of this fungus not entrely elucidated yet. The genome of *F. graminearum* contains fewer repeat sequences than the genomes of other filamentous ascomycetes [3, 65] and, thus, can be considdered as a compact genome. Genes of *F. graminearum,* associated with the basal metabolism and other highly conserved

regions, are usually represented in the low SNP (single nucleotide polymorphism) regions. In contrast, high SNP regions are enriched for genes unique to *F. graminearum* e.g. genes related to pathogenicity, secreted proteins, and gene clusters involved in secondary metabolism [65]. Interrestigly, genes necessary for niche specificity are often located in subtelomeric regions, as already described for other organisms.

1.7 Aim of the study

The subject of the presented thesis is the Fusarium head blight (FHB) disease of wheat, caused by the fungal plant pathogen *F. graminearum*. Previously, it was discovered that *F. graminearum* forms specialised infection structures, so-called compound appressoria, during infection of wheat floret tissues [18]. However, the penetration mechanism of compound appressoria of *F. graminearum* was not elucidated in detail. Therefore, one aim of this study was to clarify the penetration mechanism of compound appressoria on wheat by histological and microscopical methods. The biology and cytology of compound appressoria of phytopathogenic fungi had been intensively studied by means of microscopy for 40 years until in the 90s. Nevertheless, the underlying molecular regulations of compound appressoria are nearly unknown for fungal plant pathogens and, completely unique for a member of the *Fusarium species*. Thus, additional goals of the study were to provide first insights about molecular processes in compound appressoria and, even more important, to identify fungal genes activated during plant penetration leading to FHB. For this purpose infection cushions and runner hyphae were chosen as biological samples for comparative expression analysis by next generation sequencing techniques. Thus, the transcriptome of both tissues was aimed to provide by the presented thesis. While infection cushions penetrate wheat tissues, runner hyphae colonise the plant surface during initial infection of wheat floret tissues. Due to the different biological functions between infection cushions and runner hyphae during initial steps of FHB, they were supposed to be appropriate to gain expression profiles of both plant penetration and epiphytic growth. In order to identify genes of *F. graminearum* involved in initial infection of wheat and in particular in plant penetration through infection structures, an additional strategy was followed. Several mutants of *F. graminearum* were screened on defects in the infection stages on wheat husks by means of microscopic studies. Thereby, observations were focused on the development of infection structures, penetration, and invasion of the host to identify phenotypes in this concern. In the end, the relevance of the previously described induction of trichothecenes specifically in infection structures of *F. graminearum* [18] for initial infection stages of FHB was another question adressed within the scope of this thesis.

2 Material and Methods

2.1 Material

2.1.1 Plant material

The susceptible spring wheat (*Triticum aestivum* L.) cultivar Nandu (EWDB, accession no. RICP 01C0203421) was used in this study. Nandu was grown in the greenhouse in plastic pots at 18–20°C, 60% relative humidity, and a photoperiod of 16 h. At the early stages of anthesis (GS (growth stage) 61-65 [91]) wheat plants were transferred to a growth chamber (Weiss-Technik) and cultivated under 16 h illumination and a temperature of 18 °C at day, and 16 °C at night.

2.1.2 Fungal strains

To identify genes of *F.graminearum* that play a role during initial infection and penetration of wheat, reporter mutants with genetic modifications were investigated in bioassays with detached floret tissues of wheat (see section 2.2.1.) using different microscopy/imaging methods. The mutants used were chosen, because they showed a decreased infection of wheat spikes in preliminary experiments. The experiments were performed by different scientist in the group of Prof. Dr. Wilhelm Schäfer (Molecular Phytopathology and Genetics, University of Hamburg, Germany).

The constitutive expression of fluorophores of all fungal reporter strains used was achieved by a fusion construct of the respective reporter gene (either eGFP or dsRed) with the glycerol-3-phosphate dehydrogenase (*gpdA*) promoter of *Aspergillus nidulans* and transformation of the respective fungal strain according to Jansen et al., 2004 [21].

Fg. 8/1-Wt

The wild type strain Fg.8/1 of the fungus *F. graminearum* Schwabe (teleomorph: *G. zeae* [Schwein] Petch) is a commonly found strain in fields in Europe. The strain was

isolated and kindly provided by Thomas Miedaner (Landessaatzuchtanstalt, Hohenheim, Germany) [92]. The used wild type strain will be named in the followimg Fg.8/1-Wt.

Fg. 8/1-Wt-GFP

The wild type strain Fg.8/1-Wt was transformed by plasmid mediated homologous integration as described previously [33, 93] to provide a constitutively GFP expressing strain for histological studies. The used reporter strain will be named in the followimg Fg.8/1-Wt-GFP.

Fg. PH-1-Wt

The wild type strain PH-1 of the fungus *Fusarium graminearum* Schwabe (teleomorph: *Gibberella zeae* [Schwein] Petch) is a common strain in the United States and warmer climates. The strain was kindly provided by Prof. Dr. Henriette Giese (Department of Biotechnology, Chemistry and Environmental Engineering, University of Aalborg, Denmark). The used reporter strain will be named in the followimg Fg.PH-1-Wt.

Fg. PH-1-Wt-dsRed

The Fg.PH1-Wt-dsRed reporter strain used expresses dsRed constitutively and was created as described for the Fg.8/1-Wt-GFP strain (see above). The used reporter strain will be named in the following Fg.PH-1-Wt-dsRed.

TRI5prom::GFP

The *TRI5prom*::*GFP* mutant consists of a functional *TRI5* gene and exhibits GFP (green fluorescence protein) expression driven by an endogenous *TRI5* promoter of the *TRI5* gene that is coding for the trichodiene synthase of the fungus [22]. This feature enables monitoring of trichothecene induction during wild-type-like infection in real time. The entire mycelium was visible due to constitutive expression of the *dsRed* gene. The *TRI5prom*::*GFP* mutant was generated in the genetic background of the *F. graminearum* wild type isolate Fg.8/1-Wt (see above).

Δ*TRI5-GFP*

The Δ*TRI5-GFP* reporter strain is trichothecene deficient due to gene replacement of the *TRI5* gene encoding for the trichodiene synthase of the fungus and expresses *GFP* constitutively. The constitutive production of GFP in the mycelium allowed us to monitor the infection of wheat plants under trichothecene deficient conditions. The Δ*TRI5-GFP* reporter strain was generated in the genetic background of the wild type isolate Fg.8/1-Wt (see above).

Δ*FGL1-GFP*

The Δ*FGL1-GFP* reporter strain is unable to produce the secreted protein lipase1 and expresses GFP constitutively. The mutant was generated by homologous gene replacement of the lipase1 gene as described by Voigt et al., 2005 [70]. The constitutive production of GFP in the mycelium allowed us to monitor the infection of wheat plants under lipase deficient conditions. The Δ*FGL1-GFP* reporter strain was generated in the genetic background of the wild type isolate Fg.8/1-Wt (see above).

Δ*GPMK1-GFP*

The Δ*GPMK1-GFP* reporter strain is deficient in the production of the so-called pathoginicity MAP kinase1 of *Gibberella zeae* (anamorph: *Fusarium graminearum*) wild type Fg.8/1-Wt (see above). The mutant was generated by homologous gene replacement of the *GPMK1* gene as described by Jenczmionka et al., 2003 [73]. Additionally, the mutant expresses GFP under the control of the constitutive promoter *gpdA*. By the constitutive production of GFP it was possible to monitor the infection of wheat plants under the absence of the *GPMK1* MAP kinase pathway.

Δ*PLS1-GFP*

The Δ*PLS1-GFP* reporter strain is unable to produce the tetraspanin protein of *F. graminearum* strain Fg.8/1-Wt (see above) and expresses GFP constitutively under the control of the *gpdA* promoter. The mutant was generated by Dr. Long Nam Nguyen under the supervision of Prof. Dr. Wilhelm Schäfer (Molecular Phytopathology and Genetics, University of Hamburg, Germany). The constitutive production of GFP in the

mycelium allowed us to monitor the infection of wheat plants under the absence of the endogenous tetraspanin protein.

Δ*FAC-dsRed*

The Δ*FAC-dsRed* reporter strain is unable to produce the adenylate cyclase of *F. graminearum* strain Fg.PH-1-Wt (see above) and expresses dsRed (from *Discosoma spec.*) constitutively under the control of the *gpdA* promoter. Conidia of the mutant were provided by Dr. Jörg Bormann from the group of Prof. Dr. Wilhelm Schäfer (Molecular Phytopathology and Genetics, University of Hamburg, Germany). By the constitutive production of dsRed in the mycelium we monitored the infection of wheat plants under the absence of the adenylate cyclase and its downstream signal cascade.

OE *DHS-GFP*, OE *DOHH-GFP* and OE *DHS/DOHH-GFP*

The *DHS* enzyme catalyses the first step of hypusine biosynthesis of the eukaryotic transcription initiation factor 5A (eIF5A) and produces an inactive intermediate of the mRNA transporting protein eIF5A [94]. The second enzyme deoxyhypusin hydroxylase (*DOHH*) activates the eIF5A intermediate by hydroxylation of deoxyhypusine in an irreversible reaction. The activated eIF5A binds certain mRNAs and transports them to the ribosoms. Overexpression mutants of *DHS* and *DOHH*, as well as the double mutant of the two enzymes, were generated by Dr. Mayada Woriedh [87, 88] from the group of Prof. Dr. Wilhelm Schäfer (Molecular Phytopathology and Genetics, University of Hamburg, Germany). All mutants are in the genetic background of the *F. graminearum* wild type Fg.8/1-Wt (see above). The overexpression of the enzymes and constitutive expression of GFP in the mutants were achieved by a coupled *gpdA* promoter. The expression of GFP allowed monitoring of the mycelium during infection of wheat plants by OE *DHS-GFP*, OE *DOHH-GFP*, or OE *DHS/DOHH-GFP* mutants.

2.1.3 Inoculum

The production of conidia of the *F. graminearum* wild type strain Fg.8/1-Wt and mutants with the genetic background of *F. graminearum* Fg.8/1-Wt was performed on SNA agar plates. The plate was inoculated at its centre with a plaque of either mycelium or conidia and incubated at 18 °C for 1,5-2 weeks under illumination with 16 h normal halogen light and 8 h long wave UV light per day. Conidia were washed from the plate surface by rinsing the agar twice thoroughly with 2 mL H_2O_{demin} cooled on ice. The suspension was filtered through a 100 µm sieve that passes the conidia but removes mycelium. Afterwards the amount of conidia were counted in a Fuchs-Rosenthal counting chamber and the concentration was adjusted to stock solutions of 100 conidia per µL. Aliquots of 50, 500, and 1000 µL were stored by -70°C until further use. Conidia of the *F. graminearum* wild type strain Fg.PH-1-Wt and mutants with its genetic background were produced on wheat agar plates or in liquid medium. The cultivation and harvesting procedure from agar plates is similar to the description for SNA plates, except the illumination with UV light and a temperature of 28°C during incubation for 5 to 7 days.

2.1.4 Media and solutions

CM complete medium

The CM complete medium [95] was prepared by autoclaving 1% (v/v) solution A, 0,1% (w/v) yeast extract, 0,1% (w/v) casein, and 1,6% (w/v) granulated agar (for solid media) with 80% H_2O_{demin} of the total volume in Schott bottles. 1% (w/v) D-glucose, was first solved with H_2O_{demin} in a 50 mL falcon tube. Afterwards the appropiate volume of solution B was added to the falcon tube and the mixture sterile filtered through a 0,2 µm pore filter into the down cooled, autoclaved bottle containing the remaining components of the medium. Finaly, 0,1% (v/v) MNS solution was added and the final volume was filled up with serile H_2O_{demin} under the clean bench.

Components of CM medium per liter

10 mL solution A

10 mL solution B

10 g D-glucose

1 g yeast extract

1 g casein mix

1 mL MNS solution

16 g granulated agar for solid medium

ad 1 liter with H_2O_{demin}

Solution A (100x) per liter

100 g $Ca(NO_3)_2$ x $4H_2O$

ad 1 liter with H_2O_{demin}

Solution B (100x) per liter

20 g KH_2PO_4

25 g $MgSO_4$ x $7H_2O$

10 g NaCl

ad 1 liter with H_2O_{demin}

Yeast extract (dry powder of bakers yeast, Carl Roth, Germany)

Casein mix

For 1 g of the casein mix the powder of casein hydrolyzed by enzymatic cleavage and casein hydrolyzed by acid degradation were mixed 1:1 (w/w).

MNS solution (100x) per liter

60 g H_3BO_3

390 mg $CuSO_4$ x $5H_2O$

13 mg KI

60 mg $MnSO_4$ x H_2O

51 mg $(NH_4)_6Mo_7O_{24}$ x $4H_2O$

5,5 g $ZnSO_4$ x $7H_2O$

932 mg $FeCl_3$ x 6 H_2O

2 mL chloroform

ad 1 liter with H_2O_{demin}

MM Minimal medium

Minimal medium MM [95] was prepared with the components described for CM complete medium, however, the casein mix and yeast extract are missing in MM medium.

Components of MM medium per litre

10 mL solution A

10 mL solution B

10 g D-glucose

1 mL MNS solution

16 g granulated agar for solid medium

ad 1 liter with H_2O_{demin}

Modified MM minimal medium

The MM minimal medium as described above was modified to achieve defined amount of different nitrogen species for the plate assay. Therefore, instead of solution A either 5 mM sodium nitrate $NaNO_3$ or 5 mM ammonium chloride NH_4Cl was used. For the modified MM of the respective nitrogen species 1% (v/v) of a 500 mM stock solution NH_4Cl or $NaNO_3$ was sterile-filtered into autoclaved agar and filled up to the respective total volume as described above for MM. A volume 25 mL of the respective modified MM medium was filled in a Petri dish (92×16 mm) and used for the penetration assays.

500 mM $NaNO_3$ stock solution

42,60 g $NaNO_3$ (MW 84,99 g/mol) per liter H_2O_{demin}

500 mM NH_4Cl stock solution

26,75 g NH_4Cl (MW 53,49 g/mol) per liter H_2O_{demin}

SNA medium

Synthetic nutrient poor (SNA) medium was prepared according to Nierenberg, 1981 [96]. The weighted components were solved in H_2O_{demin} and autoclaved.

Components of SNA medium per litre

1 g KH_2PO_4
1 g KNO_3
0,5 g $MgSO_4$ x $7H_2O$
0,5 g KCl
0,2 g D-glucose
0,2 g sucrose
(16 g agar)
ad 1 litre with H_2O_{demin}

Wheat medium

For the production of 1 litre wheat medium 15 g green wheat leaves are homogenised in a blender, added to H_2O_{demin} (and 16 g granulated agar for solid medium) and autoclaved for 20 min. Then the medium was filtered through a sieve and autoclaved again.

Selection media

For the selection of different *F. graminearum* transformants CM and SNA media containing 100 µg/mL hygromycin, geneticin or noseotricin were prepared. Antibiotics were added to the autoclaved medium after cooling the medium down to 30-40 °C, because of the instability of antibiotics at higher tempereratures.

PCR primer

Table 3: Used primers: The names of gene specific primer pairs, their respective nucleotide sequences, the targeted gene of *F. graminearum* and the encoding product is provided.

Primer	Nucleotide sequence	Gene*	Gene product*
$P_{FG\text{-}Rib\text{-}fw}$	GTTGTATCTGTGACCCTTGTTGAG	FGSG_00845.3	60S ribosomal protein L15
$P_{FG\text{-}Rib\text{-}rew}$	GATGTCGTTGCCTTCCTCCT		
$P_{FG\text{-}Ubi\text{-}fw}$	CTTCACTACACGCATCTACC	FGSG_10805.3	Putative Ubiquitin conjugating enzyme E2
$P_{FG\text{-}Ubi\text{-}rew}$	GGACAGAAGAACTTTAGAGATGG		

* Source http://www.broadinstitute.org (date of query: 07.01.2013)

Table 4: List of technical devices and software

Device	Company	Location
AxioCam MRc	Zeiss	Germany
AxioCam MRm	Zeiss	Germany
Axio Imager Z1	Zeiss	Germany
ApoTome	Zeiss	Germany
AxioVision software vers.4.8.1	Zeiss	Germany
Camera DFC 500	Leica	Germany
Critical point dryier CPD 030	BAL-TEC	Germany
Growth chamber	Weiss-Technik	Germany
Kern ABJ-80-4M	Kern und Sohn GmbH	Germany
LCS480 vers.1.5.0.39	Roche	Germany
Light Cycler 480	Roche	Germany
LSM 780	Zeiss	Germany
PALM MicroBeam	Zeiss	Germany
PALM Robo software	Zeiss	Germany
Primus Cycler	Avisio	Germany
LSM 780	Zeiss	Germany
Sputter Coater SCD 050	BAL-TEC	Germany
Stereomicroscope MZFLIII	Leica	Germany
Thermomixer Comfort	Eppendorf	Germany
ULTRACUT E	Reichert und Jung	Austria
ZEN Software 2010	Zeiss	Germany

Table 5: List of laboratory equipment

Equipment	Company	Location
AdhesiveCaps tubes clear	Zeiss	Germany
Advantage 2 PCR Kit	Clontech	Belgium
BEEM-capsules (1 x 2 cm)	BALTIC Präparation	Germany
Carbon tabs (12 mm) G3347	BALTIC Präparation	Germany
DifcoTM granulated Agar	Becton Dickinson	USA
End-It DNA End-Repair Kit	Epicentre an illumina Company	USA
Glass slides (76 x 26 x 1 mm)	Carl Roth	Germany
Liquid Cover Glass	Zeiss	Germany
Metal stubs (12,5 mm) G301D	BALTIC Präparation	Germany
mRNA direct Kit	Invitrogen Dynal	Germany
Parafilm	Pechiney	USA
PCR clean-up Gel extraction Kit	Macherey-Nagel	Germany
Petri dishes (92×16 mm)	Saarstedt	Germany
Platinum SYBR Green qPCR SuperMix-UDG	Invitrogen	Germany
Ponal - Classic	Henkel	Germany
Qiuashredder	Qiagen	Germany
Rasor blades (Wilkinson- Sword)	Wilkinson-Sword GmbH	Germany
RNeasy Micro Kit	Qiagen	Germany
SuperScript II Reverse Transcriptase	Invitrogen	Germany
SMARTer™ Pico PCR cDNA Synthesis Kit	Clontech	Belgium
SYBR Green qPCR SuperMix-UDG	Invitrogen	Germany

2.2 Methods

2.2.1 Inoculation of detached tissues of wheat

For the bioassay with detached floret tissues, spikelets of wheat plants were taken at anthesis to isolate floret organs including caryopses, paleas, and glumes. Organs were detached from the floret with a razor blade and placed in Petri dishes (92×16 mm) on 1,6% (w/v) granulated agar. Two Petri dishes contained 8 biological replicates of one floret organ and represented one independent experiment. The ventral side of caryopses and the adaxial side of glumes and paleas were inoculated with 5 µL sterile water containing 20 conidia per µL. After inoculation, the Petri dishes were sealed with Parafilm and incubated in a growth chamber at conditions described in section 2.1.1..
Infected floret organs, which were used for laser microdissection as well as organs used for electron microscopy were washed with 0,01% (v/v) Tween 20 (Carl Roth, Germany) for 10 min and afterwards rinsed twice with sterile H_2O_{demin} prior to inoculation. The washing step was included to remove wheat pollen from the glume surface.

2.2.2 Penetration assay on cellophane

Penetration assays on cellophane were performed as described by López-Berges et al., 2010 [103]. Autoclaved cellophane sheets were placed on agar plates (92 x 16 mm) with modified MM containing either 5 mM $NaNO_3$ or 5 mM NH_4Cl. The centre of each agar plate was inoculated with 5 µL of a suspension containing 20 conidia per µL sterile water. The *F. graminearum* reporter strain *TRI5prom*::*GFP* was used to monitor the penetration of cellophane foil and the *TRI5* induction of *F. graminearum* with response to different nitrogen sources. After 4 days at 28°C, the cellophane sheets with fungal colonies was folded in half and placed each on a water agar plate (1,6 % (w/v) of granulated agar in H_2O_{demin}). The presence or absence of fungal mycelium and on the underlying medium was recorded by the Nicon stereomicroscope 24 h after additional incubation of the agar plates at 28°C. Furthermore, the growth of hyphae at the folding edge of the cellophane sheet after 4 days incubation at room temperature was recorded with a stereomicroscope MZFLIII.

2.2.3 Histological and staining methods

2.2.3.1 Trypan blue staining

Inoculated paleas and glumes of wheat (section 2.2.1) were incubated in 96% ethanol for fixation and removal of chlorophyll. The mycelium was stained with 0.1% (w/v) trypan blue solution (Fluka analytical, Germany) in 10% (v/v) acetic acid for 10 min at room temperature after [62]. Excessive stain was removed by rinsing samples twice with H_2O_{dest}. Samples were cut in smaller pieces (1-3 mm^2) and transferred on glass slides for dark field microscopy with Axio Imager Z1 and colour camera AxioCam MRmc. The cytoplasm of fungal cells is stained with blue colour, while the fungal cell wall and plant cells are not stained. Trypan blue is commonly used as vital stain, because it colours only dead cells.

2.2.3.2 LR-White embedding

Inoculated floret tissues of wheat from detached bioassays were fixed after Huang et al., 2008 [54] with 3% (v/v) glutaraldehyde in 50 mM phosphate buffer (pH 6.8) for 8-10 h at 4°C, then rinsed with the same buffer 3 times over 3 h. Afterwards, samples were post-fixed with 1% (w/v) osmium tetroxide in the same buffer for 2 h at 4°C. After 3 washing steps with 50 mM phosphate buffer dehydration was performed for 24 h by a graded ethanol series at 4°C. The series was performed in five steps from 30-100% ethanol for 30 min. However, the last step with 100% ethanol was performed twice for 30 min. The infiltration of inoculated glumes with LR-White (Plano GmbH, Germany) was performed in 3 steps each for 3 h at room temperature (RT) using ethanol and LR-White (v/v) in the ratio 2:1, 1:1, and 1:2. Afterwards, 100% LR-White was infiltrated into the samples over night at RT. Then LR-White was exchanged once and incubated for further 2-4 hours. The following polymerisation was done under anaerobic conditions first for 2 h at RT and then at 50°C for 20-24 h. Semithin (1 µM) and ultrathin serial sections (0,5-0,7 µM) of inoculated embedded glumes were cut with a glass knife of an ultramicrotome Ultracut E. Semithin sections were collected on glass slides, stained with toloidine blue and observed by bright field microscopy (section

2.2.3.3). The ultrathin sections were collected on copper grids and used for transmission electron microscopy (section 2.2.4.5).

2.2.3.3 Toluidine blue staining

Semithin (1 µM) cross and transversal sections of inoculated glumes embedded in LR-White were collected on glass slides and dried at room temperature (RT). Sections were stained with 0,1% toluidine blue in 50 mM potassium phosphate buffer, pH 9 for 10 min at RT and washed 3 times with water. After slides dried, 87% (v/v) glycerol was applied on the slide for bright field microscopy with Axio Imager Z1. Photos were taken with colour camera AxioCam MRc.

2.2.3.4 Histology of living plants

The epidermal and subepidermal invasion of wheat floret tissues infected with different reporter strains of *F. graminearum* was studied by fluorescence microscopy of hand cut tissue cross sections. Therefore, inoculated floret organs were placed each in a gap, which was cut in a small block of styropor to fix samples physically during cutting with a razor blade. The cross sections were transferred on glass slide in sterile water and covered by a glass cover slip for microscopy.

2.2.4 Macroscopic and microscopic methods

2.2.4.1 Macroscopical studies on infection

Macroscopic studies of inoculated floral organs of wheat were done with the MZFLIII fluorescence stereomicroscope. Thereby, the entire surface of wheat floret tissues after inoculation with different reporter strains of *F. graminearum* was studied. Fungal development and stages of infection as described by Boenisch and Schäfer, 2011 [18],

were monitored daily for a period of 3 weeks. Infected floret organs were investigated in air without preparation, lying in Petri dishes. The dsRed fluorescence of all used dsRed expressing reporter strains was detected with the Leica dsRed filter set containing an excitation filter at 546/12 nm and a long pass filter at 560 nm. The GFP fluorescence of all used GFP expressing reporter strains was observed with a Leica GFP3 filter set with an excitation filter at 470/40 nm and a band pass filter transmitting light at 525/50 nm, as well as with a GFP2 filter set with an excitation filter at 480/40 nm and a long pass filter at 510 nm. Inclined reflected light of an external halogen lamp KL 1500 Electronic was used to visualise plant necroses as well as the mycelium under normal light conditions

2.2.4.2 Epifluorescence microscopy

Infection structures of reporter strains were investigated by fluorescence microscopy using Axio Imager Z1 microscope equipped with a Zeiss ApoTome. A UV (ultra violet) lamp HAL 100 served as UV light source. DsRed was excited in the range of 538 to 562 nm and detected in the 570 to 640 nm range. GFP was excited with 450 to 490 nm and detected at 500 to 550 nm wavelength. The plant apoplast was excited in the range of 335 to 383 nm. The blue autofluorescence was detected in the 420 to 470 nm range. Images were taken with Zeiss AxioCam MRm CCD camera. Image processing, including overlay of different fluorescence channels and generation of maximum intensity projections (MIP) of z-stacks, were done with Zeiss AxioVision software.

2.2.4.3 Laser scanning microscopy (LSM)

For LSM, a Zeiss LSM 780 microscope was used. DsRed was excited at 561 nm and its fluorescence detected at 570-640 nm. GFP was excited at 488 nm and its emission detected at 500-568 nm. The plant tissue was illuminated at 405 nm and its blue autofluorescence detected at 410-490 nm. Image processing of z-stacks was performed with Zeiss ZEN software 2009.

2.2.4.4 Scanning electron microscopy (SEM)

Inoculated glumes and paleas of wheat were prepared as described in 2.2.1 and were fixed according to Huang et al., 2008 [54] with 4% (v/v) glutaraldehyde in 50 mM phosphate buffer and were post-fixed with 1% (w/v) osmium tetroxide as described in section 2.2.3.2, however, acetone was used instead of ethanol in the graded series. Afterwards critical-point drying was performed by liquid carbon dioxide CO_2 and the machine CPD 030 SCD 050. Dried samples were mounted on stubs with carbon tabs and Ponal Classic (Henkel, Germany). After 48 h in a desiccator samples were sputter-coated with gold using apparatus SCD 050. The scanning electron microscope SEM LEO 1525 was used operating at 6 kV.

To identify penetration pores in the epidermis of inoculated glumes, the mycelium, including infection structures, was removed from the plant surface. The removal was performed with critical point dried samples by using an adhesive tape (TESA, Germany). Afterwards, the samples were mounted on stubs and sputter-coated as described above.

2.2.4.5 Transmission electron microscopy (TEM)

Inoculated floret tissues of wheat from detached bioassays (section 2.2.1) were contrasted and fixed as described above for scanning electron microscopy. However, for TEM studies samples were embedded in LR-White (see section 2.2.3.2.) after a graded ethanol series. Ulrathin (0,5-0,7 µM) cross and transversal sections on copper grids were contrasted with 1% (w/v) uranyl acetate for 5 min. After washing twice with H_2O_{bidest} contrasting with lead citrate (according to Reynolds, 1963 [97]) was performed for 5 min. with subsequent incubation in 0,02 M NaOH solution. Grids were examined with a LEO 906 transmission electron microscope at 100 kV.

2.2.4.6 Laser microdissection (LMD)

For laser microdissection (LMD) glumes were inoculated with conidia of the *TRI5prom*::*GFP* mutant and incubated as described in section 2.2.1. Glumes at 8 dpi were taken for isolation of 1-2 mm^2 tissue samples containing infection cushions and runner hyphae. The constitutive expression of dsRed under the control of the *gpdA* promoter enabled to distinguish living hyphae from degenerated mycelium of the *TRI5prom*::*GFP* mutant using the fluorescence stereomicroscope MZFLIII. During preparation of specimens with a razor blade for approx. 1 h, samples were collected in 99% ethanol on ice. After collection of 20-30 specimens, the ethanol was removed and samples were lyophilized for 30-40 min. Samples were then stored at -80°C over night. Afterwards, the mycelium was transferred from the glume surface on RNase-free glass slides at room temperature. To provide an adhesive surface of the glass slides, they were covered on one side with Liquid Cover Glass. The slides were sprayed 1-2 times with Liquid Cover Glass, a resin containing solution of isopropanol, and were dried at room temperature for 5 min. After slides dried, the tissue was pressed with its inoculated side on a glass slide. Afterwards the glume tissue was carefully removed with forceps. 4-6 individual tissue samples were put on one glass slide and used for LMD. Identification and isolation of runner hyphae and infection cushion was done with the inverse microscope PALM MicroBeam. Identification was done by bright field microscopy in air with a 20x objective. Infection cushions and runner hyphae were selected using the auto-LPC-function (freehand circle for infection cushions and or line marking for runner hyphae) of the PALM Robo software. Catapulting points for the UV-A laser (λ 355 nm) was set automatically within the selected area or along the selected line by the software. The following settings were used: Cutting energy 32 at a focus of 63, catapulting at delta 25 of the cutting energy and a focus of -2. The selection of the respective tissues using PALM microscope was done for 1 h at room temperature (20°C). Selected elements were then catapulted upwards (against gravity) in an adhesive cap of a 500 µL eppendorf tube. The isolation of either infection cushions or runner hyphae in the cap was verified by a so-called „CapCheck“, using 5x and 20x objectives. After catapulting, the collection tubes were carefully removed from the tube holder and stored at -80°C until mRNA isolation was performed (see section 2.2.5.5). Runner hyphae and infection cushions were collected on separate days to avoid contamination

by the respective unwanted tissue. Figure 6 provides a scheme about the workflow performed to isolate runner hyphae and infection cushions by laser microdissection.

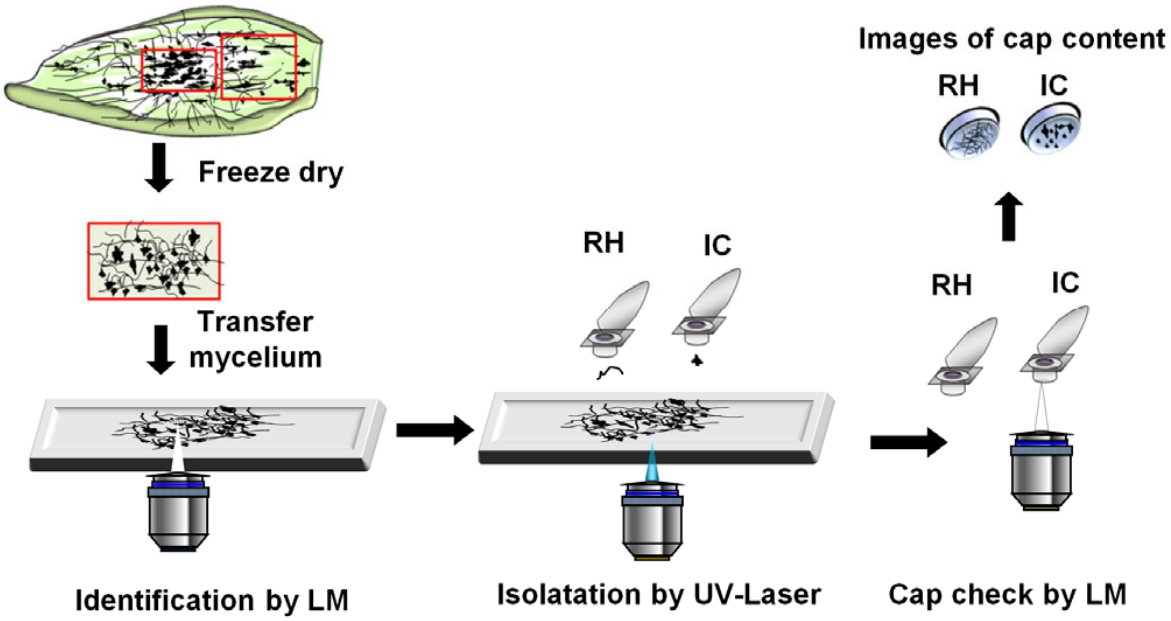

Figure 6: Scheme of the isolation of infection cushions and runner hyphae by laser microdissection (LMD). Small samples of glumes containing runner hyphae (RH) and infection cushions (IC) were dehydrated by ethanol, lyophilized and transferred on an adhesive microscopy slide. RH and ICs were identified and selected by light microscopy (LM). Afterwards ICs and RH were isolated in individual adhesive caps by UV-laser impulses. The content of the cap after isolation of RH and IC was controlled by LM of the tube caps, by a so-called “cap check”.

2.2.5 Molecular methods

2.2.5.1 Total RNA isolation

Mycelium was grown in Erlenmeyer flasks with 25 mL liquid SNA medium for 5 days at 28 °C, starting from $5*10^5$ conidia of *F. graminearum* reporter strain *TRI5prom::GFP*. The mycelium was harvested by Gaze sieves and washed with sterile water 3 times prior to incubation in 99 % ethanol for 1 h on ice. Afterwards, the mycelium was lyophilized for 40 min. Samples were then stored at -80°C over night. The lyophilized mycelium was homogenised by cutting with a razor blade at room temperature (22 °C) and the resulting powder weighted with a fine balance Kern ABJ-80-4M. Three repetitions of 5, 2,5, 1, 0,5 and 0,1 mg were weighted each in a 500 µL adhesive cap tube and used for total RNA isolation with the RNeasy Micro Kit. The procedure was performed according to the manufactures protocol for microdissected cryosections from "non-Leica LMD systems". The Zeiss system PALM was applied here. To remove cell debris e.g. fungal cell wall from the lysate after vortexing in 350 µL RLT buffer for 30 s, lysates were homogenised by a Qiuashredder spin columns as recommended for fibrous animal and human tissues. After removing cell debris from cell lysates by the Quiashredder, RNA isolation was continued according to steps 5-14 of the protocol for microdissected cryosections. Total RNA was eluted from RNeasy MiniElute spin columns with 14 µL of RNase-free water (Qiagen, Kit supplement).

2.2.5.2 Reverse transcription polymerase chain reaction (RT-PCR)

In order to test for mRNAs of *F.graminearum* in laser microdissected (LMD) hyphae, RT-PCR conditions were established first with low amounts (1-0,1 mg) of lyophilized hyphae, which were treated like LMD samples, despite laser micro dissection (PCR1 and PCR2). Afterwards, the most sensitive PCR conditions were used for LMD infection cushions (PCR3). DNAse treatment of RNA extracts was performed with Revert Aid H-Minus–RT-Kit according to manufactures protocol. For first-strand reaction the manufactures protocol for RT-PCR was applied. To prime polyadenylated mRNAs $Oligo(dT)_{18}$ primers were used. Total RNA extracts isolated with the RNeasy Micro Kit were used as template in the PCR.

Table 6: PCR conditions (PCR 1-3) tested for low amounts of mycelium.

Test PCR	PCR1	PCR2	PCR3
Fungal material	mycelium*	mycelium*	infection cushions+
Dry weight mycelium	1, 0,5 and 0,1 mg	0,5 and 0,1 mg	260455 µm^2
total RNA in RT-PCR	49, 33 and 12 ng	165 and 60 ng	22 ng
Volume in PCR	1 µL each	5 µL each	5 µL each
PCR cycles	35	25 and 35	35
Result figure 44	A	B	C

***** Mycelium was grown in liquid SNA medium for 4 days at 28°C, dehydrated by incubation in concentrated ethanol, lyophilized, and stored at -80 °C. + 128 infection cushions isolated by LMD.

PCR was performed as follows:

5 µL of single stranded cDNA was used as a template in each PCR with a total volume of 25 µL. Denaturation was done at 95°C for 5 min, followed by 25 and/ or 35 amplification cycles (see table 6, line 6) with 95°C for 30 s, annealing at 55°C for 30 s, and extension at 72°C for 60 s. The final extension was done at 72°C for 5 min. From the resulting PCR reactions 5 µL were loaded on a 0,8% agarose gel and size separated by gel electrophoreses. 1 µg of a DNA ladder SM 0321 (Fermentas) was loaded in one lane of the gel for size estimation of the resulting DNA fragment. The primers $P_{FG\text{-}Rib\text{-}fw}$ and $P_{FG\text{-}Rib\text{-}rev}$ were used to amplify a *F. graminaerum* strain Fg.PH-1-Wt specific mRNA coding for a protein associated to the 60S ribosomal subunit (FGSG_00845.3) of the translation machinery.

The used Mastermix for one reaction contained the following components:

5 µL 5x GoTaq Reaction Buffer

0,5 µL dNTP mix (10 mM)

1 µL of fw and rw primer (10 µM each)

0,25 µL of 5 U/ µL of the GoTaq polymerase (Promega)

12 µL H_2O

Total volume 20 µL

2.2.5.3 Quantitative real time PCR (Q-PCR)

Q-PCR was conducted in a Roche Light Cycler 480, using Roche SYBR Green Master Mix. For first-strand synthesis, SuperScript II Reverse Transcriptase was used according to manufacturer's instructions (Invitrogen, MAN001342, 2010). The resulting single stranded cDNA served as template in quantitative real-time PCR (Q-PCR) reactions. Q-PCR was performed using the Platinum SYBR Green qPCR SuperMix-UDG in a volume of 20 µL. Specific primers for *F. graminearum* Fg.PH-1-Wt m RNA of the Q-PCR reactions were carried out in a light Cycler 480. The PCR program was as follows: Incubation for 2 min at 50°C, then 2 min at 95°C, followed by 40 cycles of denaturation at 95°C for 30 s, annealing at 55°C for 30 s and extension at 72°C for 30 s, followed by melting curve analysis at 95° C for 10 s to check specificity of fragment amplification. Three replicates for each sample were measured. Cp values and absolute quantification of transcript concentration in ng per µL was determined by means of statistical analyses applying the "2nd Derivative Maximum" and the "Fit-Point" methods (software LCS480 version 1.5.0.39) of the light Cycler 480. For the fit point method a specific calibration curve with similar primer (efficiency >1,98) was used.

2.2.5.4 Transcriptome analysis of infection cushions and runner hyphae

Figure 7 provides an overview about the workflow to achieve expression patterns from runner hyphae and infection cushions following laser microdissection. Isolation of mRNA from infection cushions and runner hyphae with magnetic beads was performed. The entire mRNAs bound on beads were used for first-strand synthesis by SMART (switching mechanism at 5' end of the RNA transcript)-PCR. Thereby, ss cDNAs were provided, which served as templates for ds cDNA synthesis by LD-PCR. The amplified cDNA libraries were purified and send to the company LGC Genomics (Berlin, Germany), where Illumina sequencing was performed. The resulting sequencing data were mapped to the reference genome of *F. graminearum* and used for differential expression analysis by means of bioinformatic and statistics by Sebastian Piehler and Dr. Ulrich Güldener (Institute of Bioinformatics and Systems Biology, Munich, Germany).

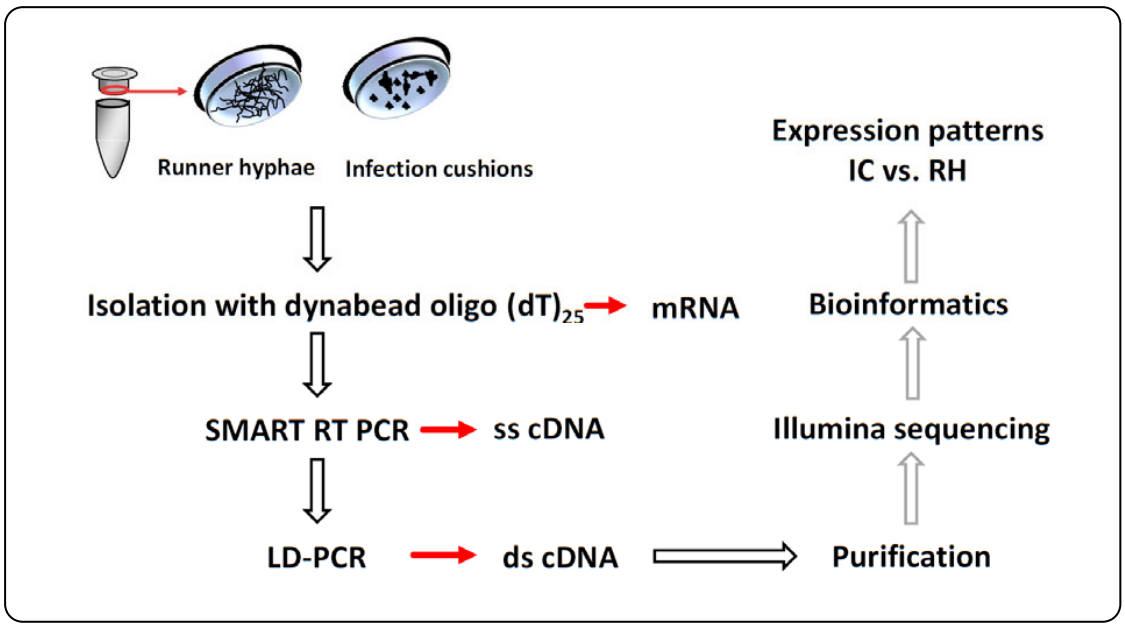

Figure 7: Scheme of the methodical workflow performed to provide expression data from runner hyphae and infection cushions isolated by laser microdissection. Isolation of mRNA from infection cushions and runner hyphae with magnetic beads was performed. The mRNAs were used for first-strand synthesis by SMART-PCR. Thereby, ss cDNAs were provided, which served as templates for ds cDNA synthesis by LD-PCR. The resulting cDNA libraries were purified and sequenced by Illumina Sequencing. The resulting sequencing data were mapped to the reference genome of *F. graminearum* and used for differential expression analysis.

2.2.5.5 mRNA isolation

Isolation of mRNA from infection cushions and runner hyphae was performed each with 15 µL oligo(dT)$_{25}$ magnetic beads from mRNA direct Kit. Prior to the use of Dynabeads the storage buffer was removed and the beads were washed with 50 µL lysis/binding buffer, using a magnet and pipette. Cell lyses was performed with 50 µL lysis/binding buffer in collection tubes from LMD containing infection cushions or runner hyphae. The tube was vortexed with the cap downwards for 1 min at room temperature. Afterwards the washed beads were added to the cell lysate and were resuspended thoroughly by pipetting. mRNAs were hybridised to the beads by incubation on a roller for 10 min at room temperature. Then the supernatant was removed and the beads/mRNA complex was washed twice with 50 µL washing buffer and twice with 50 µL first-strand buffer. After removing the supernatant the beads/mRNA complex was suspended in 3 µL H_2O and transferred into a 200 µL PCR tube for first-strand cDNA synthesis by SMART-PCR (section 2.2.5.6).

Dynabeads Oligo(dT)$_{25}$

Approx. 5 mg beads per mL were supplied in PBS pH 7.4, containing 0,02% NaN_3 as a preservative. The used beads had a size of 2,8 µm in diameter and a density of approx. 1,6 g/cm^3. 1 mg of the beads has the capacity to bind up to 2 µg of mRNA.

Lysis/binding buffer

100 mM Tris-HCl, pH 7,5
500 mM LiCl
10 mM EDTA, pH 8
1% LiDS
5 mM dithiothreitol (DTT)

Washing buffer

10 mM Tris-HCl, pH 7,5
0.15 M LiCl
1 mM EDTA
0.1% LiDS

2.2.5.6 First-strand synthesis by SMART-PCR

The first-strand ss cDNA synthesis was performed with mRNAs of infection cushions and runner hyphae using the SMARTer™ Pico PCR cDNA Synthesis Kit. For the SMART (**s**witching **m**echanism **a**t 5' end of the **R**NA **t**ranscript) PCR 1 µL 3' SMART CDS-PrimerIIA (12 µM) was added to 3 µL beads bound to mRNA runner hyphae or infection cushions, and incubated at 72°C for 2 min in a PCR cycler Primus. Then 6 µL Mastermix were added to a total volume of 10 µL per reaction. The PCR was performed at 42°C for 90 min with a following termination step at 72°C for 10 min. PCR tubes were placed on ice for 10 min and subsequently LD (long distance)-PCR was performed (section 2.2.5.7).

1x Mastermix for 10 µL SMART-PCR reaktions

2 µL 5x First-Strand buffer
0,25 µL DTT (100 mM)
1 µL dNTP Mix (10 mM)
1 µL SMARTer II A Oligonucleotide (12 µM)

0,25 µL RNase Inhibitor
1 µL SMARTScribe™ Reverse Transcriptase (100 U)
0,5 µL H_2O
Total volume 6 µL

5x first-strand buffer:

250 mM Tris-HCl (pH 8.3)
375 mM KCl
30 mM $MgCl_2$

3’ SMART CDS Primer II A sequence

5’-AAGCAGTGGTATCAACGCAGAGTACT$_{(30)}$N$_{-1}$N-3’

SMARTer II A Oligonucleotide sequence

5'–AAGCAGTGGTATCAACGCAGAGTACXXXXX–3'

2.2.5.7 Amplification of cDNA by LD-PCR

The amplification of single stranded cDNA (ss cDNA) produced by SMART PCR (previous section) was performed with Advantage 2 PCR Kit according to the recommendation of the SMARTer™ Pico PCR cDNA Synthesis Kit. The optimal number of LD-PCR cycles was determined to ensure the cDNA remained in the exponential phase of amplification. The optimal number of cycle for runner hyphae and infection cushions was checked by two test LD-PCR reactions. A 50 µL LD-PCR reaction using 1 µL template was performed and the optimal cycle within 15, 18, 21, 24, 27, 30 and 32 cycles was determined by electrophoresis in 1,2 % agarose gels in 1x TAE. By an additional 25 µL LD-PCR reaction with 0,5 µL template the optimal cycle was determined for each cycle between the two cycles that showed the strongest increase of PCR product in the 50 µL reactions. After determination of the optimal cycle number for both tissues, the remaining volume of the first-strand reaction of each tissue was cycled to the respective optimal PCR cycle. The resulting LD-PCR products of each tissue were pooled and a 2 µL aliquot was loaded on a 1,2 % agarose gel in 1x TAE to determine the amount of cDNA. The pooled cDNAs were used further for purification (section 2.2.5.8) and 5’ phosphorylation of cDNAs (section 2.2.5.9).

LD-PCR Protocol for 50 µL reactions

After 1 µL template was added to 49 µL of a 1x Mastermix the PCR was performed in a thermal cycler (Primus) as follows:

1. 95°C 1 min
2. 95°C 15 sec
3. 65°C 30 sec
4. 68°C 6 min

(steps 2–4: 15 cycles)

5. Pause at 68°C and transfer 5 µL from the 15-cycle PCR for agarose gel analysis.
6. Three additional cycles were run with the remaining PCR mixture and 5 µL transferred from the 18-cycle PCR for agarose gelelectrophoresis. This step was repeated for 32 cycles.

1x Mastermix (for 50 µL PCR reactions)

5 µL 10x Advantage 2 PCR buffer
1 µL dNTP Mix (10 mM)
1 µL 5' PCR Primer II A (12 µM)
1 µL 10x Advantage 2 Polymerase Mix
41 µL H_2O
Total volume 49 µL

10x Advantage 2 PCR Buffer

400 mM Tricine-KOH pH 8,7
150 mM KOAc
35 mM $Mg(OAc)_2$
37,5 µg/ mL BSA
0,05% Tween
0,05% Nonidet-P40

10x Advantage 2 Polymerase Mix

The mixture contains a TITANIUM Taq DNA Polymerase, a proofreading polymerase, and TaqStart Antibody (1,1 µg/µl) in the following storage buffer:

10% Glycerol
3 mM Tris-HCl pH 8,0
15 mM KCl
0,01 mM EDTA

2.2.5.8 Purification of cDNA libraries

To remove primers, enzymes, and other substances of the LD-PCR from the cDNA libraries of infection cushions and runner hyphae, a purification step through silica membranes was performed. Following the recommendation of the SMARTer™ Pico PCR cDNA Synthesis Kit, NucleoSpin Exctract II columns of a PCR clean-up Gel extraction Kit were used according to the manufactures instructions. Two columns were used to purify 5-10 µg cDNA of each tissue type, and the elution step was performed twice with 35 µL NE Buffer (5 mM Tris/HCl pH 8,5) per column. A volume of 68 µL was eluted per column (1 µL dead volume per column) and, thus, 136 µL of purified cDNA from infection cushions and runner hyphae was reached in total. The purified cDNAs were further repaired by 5´-phosphorylation (section 2.2.5.9).

2.2.5.9 End-it-Reaction

To provide 5´-phosphorylated, blunt-ended cDNAs from infection cushions and runner hyphae, the End-It DNA End-Repair Kit was used according to the manufactures protocol. Two End-it-Reactions of 100 µL total volume were preformed each with 68 µL purified cDNA (5-10 µg) of runner hyphae or infection cushions.

<u>End-it-Reaction protocol</u>
68 µL cDNA in NE Buffer (5mM Tris/HCl pH 8,5)
5 µL 10x End-Repair buffer
5 µL dNTP Mix
5 µL ATP
1 µL End-Repair Enzyme Mix
Total volume 100 µL

The blunt-ended cDNAs from infection cushions and runner hyphae were purified again with the PCR clean-up Gel extraction Kit as described above, however, substances of the End-it-Reaction were removed here. The elution of cDNA was performed twice with 25 µL per column. Afterwards, the cDNA of each sample was pooled and the

amount of blunt-ended and purified cDNA for each tissues was determined by electrophoresis of 1,2% agarose gels. Finally, 3 µg of the blunt-ended and purified cDNAs were used for next generation sequencing (section 2.2.5.10).

2.2.5.10 Illumina sequencing of infection cushion and runner hyphae

The blunt-ended and purified cDNA from infection cushions and runner hyphae (3 µg each) was sent to the company LGC Genomics (Berlin, Germany). The cDNAs of each library were concatemerized prior to fragmentation and adapter ligation, to avoid underrepresentation of short cDNA fragments during bridge amplification. A TruSeq cDNA library for each tissue was created by and next generation sequencing was performed by LGC Genomics using the Illumina HiSeq 2000 technology. Both bar coded TruSeq cDNA libraries were loaded on one channel of a low cell. Single reads with a length of 50 bp were performed for each cDNA library. Thereby, an output of 150 million reads per channel was achieved theoretically. The sequencing results were provided as FASTQ-files for each tissue type. The FASTQ files were send to Dr. Ulrich Güldener (Institute of Bioinformatics and Systems Biology, Munich, Germany) for bioinformatic analysis (section 2.2.5.11).

The Illumina sequencing method

Illumina sequencing protocols require the preparation of a specific sequencing library from the cDNAs to be determined. The procedure includes a randomized fragmentation of 1 µg of DNA. Then so-called Y-shaped adapters are ligated to 5' and 3' ends of all DNA molecules. The adapters are required for solid phase binding to the flow cell and for bridge amplification. The DNA with ligated adaptors is size separated by gel electrophoresis and a band of 300-500 bp is excised and purified. The purified adapter-ligated fragments are denaturised and then loaded on the flow cell. The flow cell is coated with single stranded oligonucleotides complementary to the adapter sequences. Single-stranded molecules bind complementary to oligonucleotides on the surface of the flow cell. Priming from the double stranded adapter sequence, the reverse strand of each molecule is synthesised by polymerase chain reaction. The resulting covalently bound reverse strand is then amplified by the so-called bridge amplification. Due to the bridge amplifications, randomly scattered clusters on the flow cell are created. Each cluster

represents up to 1000 copies of one original bound molecule from the library. Illumina sequencing techniques use the reversible terminator chemistry. Therefore, single stranded, identically oriented copies are needed. The 3' ends of single stranded fragments are fixed and the sequencing primers hybridize to the adapter sequences. Afterwards, the polymerase chain reaction is performed by using four different fluorescent labelled and terminated nucleotides. After one base is incorporated the amplification reaction is stopped by the nucleotide terminator and fluorophores are excited by a laser. The emitted fluorescence of the incorporated nucleotide is detected and identified by image analysis. Then the terminator and fluorophore are removed from the nucleotide and the next cycle of nucleotide incorporation starts. Several images are recorded, overlaid and the light intensities estimated for each cluster and cycle. The provided intensity data serve as raw data for the software mediated identification of nucleotides and quality scores for base calling. For detailed information about Illumina sequencing the dissertation of Dr. Martin Kircher 2011 [98] is recommended.

2.2.5.11 Bioinformatics of sequencing data

The FASTQ files, provided by LGC Genomics were send to Dr. Ulrich Güldener (Institute of Bioinformatics and Systems Biology Munich, Germany) for detailed bioinformatic analyses, including genome mapping, gene annotation, and differential expression analyses. The bioinformatic tools TopHat [99]and Cufflinks [100] were used in this purpose [101]. The *F. graminearum* reference genome used for read mapping is available at the MIPS FGBD [89]. The genomic sequence derived from sequencing of the *F. graminearum* wild type isolate Fg.PH-1. *F. graminearum* consists of four chromosomes. The total known genomic sequences are assembled in 31 supercontigs, and consist of 36.446.046 base pairs in total. A total number of 13.826 coding genes (exons) of the genome are annotated (version at date of use: 3.2, August, 2012 [101]).

3 Results

3.1 Biological characterisation of infection structures

3.1.1 Infection structures of different wild type strains

In order to investigate, wether the compound appressoria are formed by different wild type isolates of *F. graminearum*, two different wild type strains called Fg.8/1-Wt and Fg.PH-1-Wt were tested for the formation of infection structures on wheat husks. Eight individual glumes and paleas were inoculated with conidia of the respective strain as described in section 2.2.1 and investigated by bright field microscopy at 4, 8, 10, and 12 dpi for glumes, and at 4, 7, 9, and 10 dpi for paleas. For each strain and time point, two glumes and paleas were sampled and stained with trypan blue as described in section 2.2.3.1. By microscopy of glumes and paleas at 4 dpi, spread of germinated blue stained hyphae as typical for the stage I was visible for both strains. Thereby, the vitality of the conidia used for inoculation and the functionality of the staining procedure to visualise the fungus were controlled. After this control was positive, infected glumes and paleas at the three other respective time points were investigated. From 8 to 12 dpi of glumes and at 7 to 10 dpi of paleas infection structures were observed similar for both wild type strains used (Fg.8/1-Wt and Fg.PH-1-Wt). Remarkably, less and smaller infection cushions were observed at earlier time points (7 and 9 dpi and 8 and 10 dpi respectively) compared to the latest time points for both strains investigated (12 dpi for glumes and 10 dpi for paleas). Thus, a developmental process is indicated. At these time points smaller infection structures, including foot structures and lobate appressoria as well as complex infection cushions are observed. Furthermore, brownish lesions surrounding big infection cushions were visible at this time point, characteristic for the stage II of infection. The characteristics of stage II on paleas and glumes of the wild type strain Fg.8/1-Wt are demonstrated in figure 1.

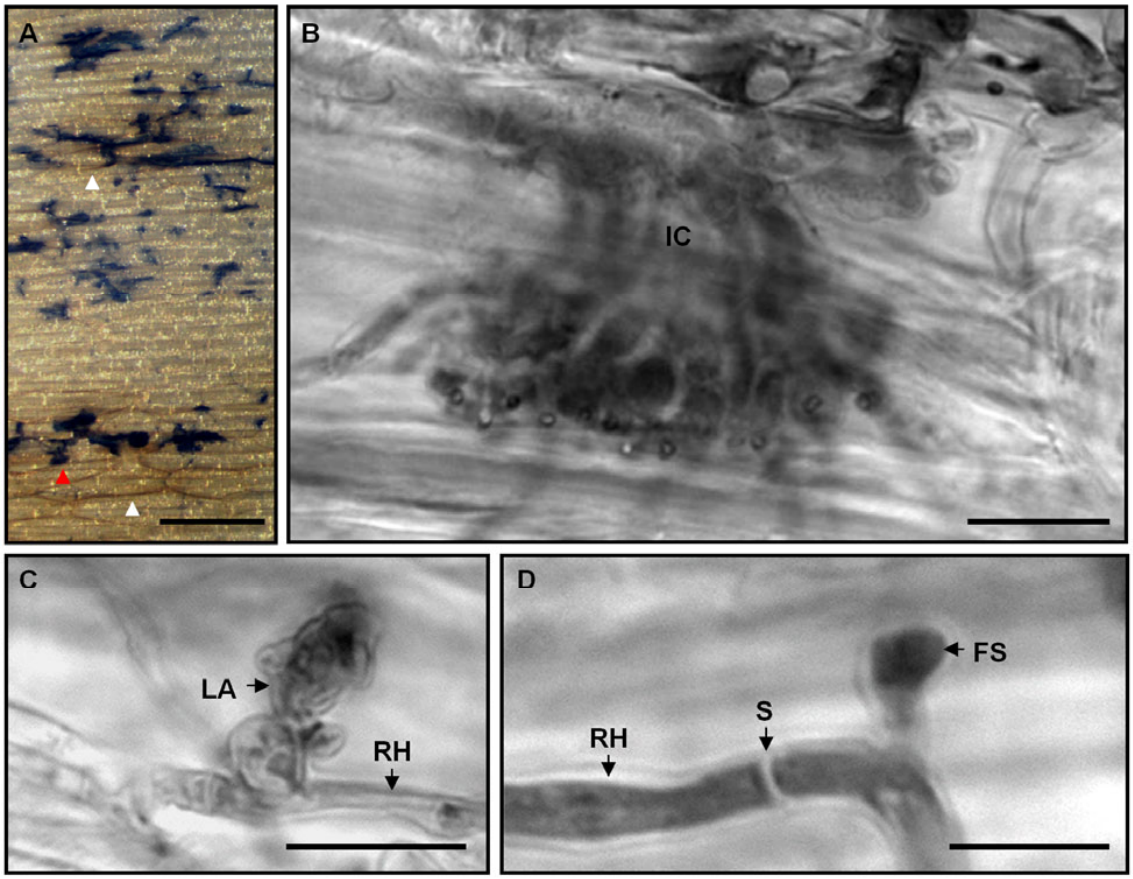

Figure 8: Compound appressoria of *F. graminearum* wild type isolate Fg.8/1-Wt on wheat. **A-D** Bright field microscopy of infected palea after trypan blue staining of mycelium at 10 dpi. **A** Abundance of infection cushions (blue) on the surface of palea under halogen light documented with the MZFLIII stereomicroscope. Different sizes of infection cushions and necroses of plant cells (white arrowhead) surrounding big infection cushions is remarkable. Scale bar=200 µm. **B-D** Higher magnification using Axio Imager Z1 reveals different infection structures. **B** Magnification of blue stained fungal structure (red arrowhead in A) showing a typical infection cushion. Scale bar=15 µm. **C** Typical cellular morphology of a lobate appressorium and **D** foot structure arising from runner hyphae. Scale bars=10 µm. **Abbreviations:** **FS** Foot structure, **IC** Infection cushion, **LA** Lobate appressorium, **RH** Runner hypha, **S** Septum.

The microscopic results of a palea at 10 dpi are shown representatively, because the thin, transparent tissue of paleas is more appropriate for imaging by light microscopy, than the thicker tissue of glumes. However, it must be pointed out that similar infection structures were observed for glumes, respectively. By removal of chlorophyll from palea tissues and trypan blue staining of hyphae necrotic plant cells surrounding big infection cushions became visible (figure 8, A). Higher magnifications of the fungal structures (figure 8, B-D) revealed cytological similarities to described infection

cushions of other fungal phytopathogens [44, 52-54, 56, 60-62, 68, 69, 102]. Large infection cushions were formed by highly branched and agglomerated hyphae (figure 8, B). Smaller fungal structures, namely lobate appressoria (figure 8, C) and foot structures (figure 8, D), were present in addition to infection cushions. All types of infection structures developed from epiphytic runner hyphae on the host surface.

Compound appressoria were observed to be formed by the wild type Fg.PH-1-Wt as described for the wild type Fg.8/1-Wt. By figure 9 typical compound appressoria of the Fg.PH-1-Wt on a palea at 10 dpi are demonstrated. Images were gained by light microscopy after trypan blue staining as performed with the wild type Fg.8/1-Wt. However, a colour camera was available for the microscope Axio Imager Z1 when experiments with Fg.PH-1-Wt were performed. Therefore, hyphae are coloured blue in images of figure 9 but black/white in figure 8. Typical for infection stage II of *F. graminearum* on wheat, a superficial network of runner hyphae and different types of infection structures are formed on the plant surface (figure 9). By higher magnification infection cushions can be identified by their agglomerated, multicellular appearance in contrast to runner hyphae (figure 9, B). Smaller fungal structures were formed on the plant surface and identified as lobate appressoria by higher magnifications (figure 9, C). Lobate appressoria emanated from runner hyphae and consisted of more than one up to a few lobed, swollen cells. Furthermore, foot structures of the wild type Fg.PH-1-Wt were observed (figure 9, D). The results indicate that the development of compound appressoria is not a strain specific feature of *F. graminearum*, hence similar results were obtained with the strain Fg.8/1-Wt and Fg.PH-1-Wt.

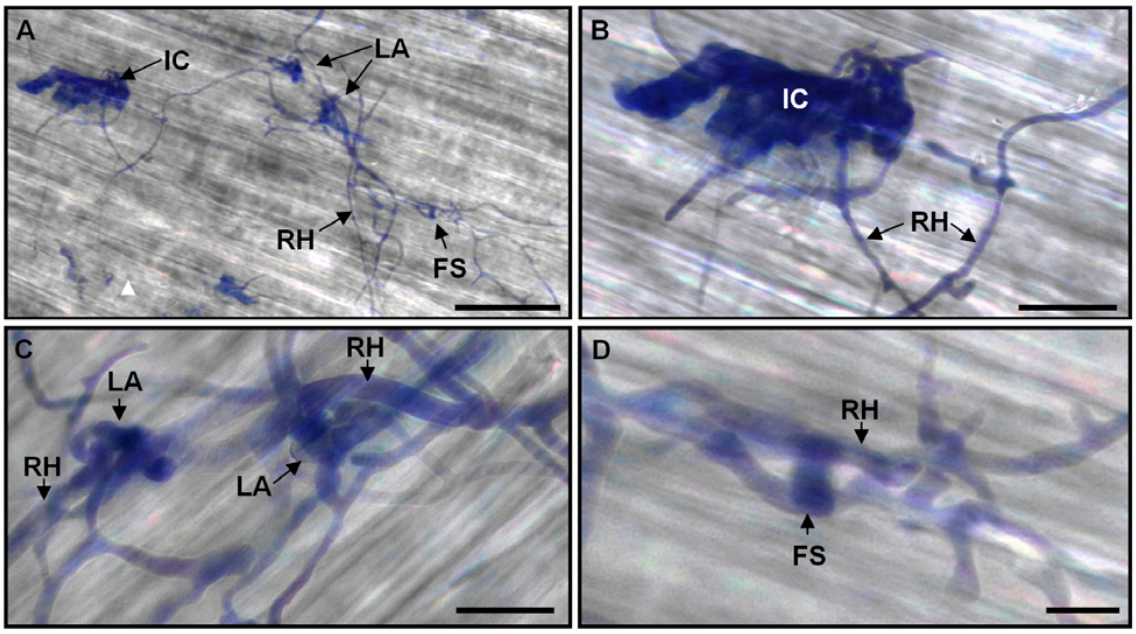

Figure 9: Compound appressoria are formed by *F. graminearum* wild type isolate Fg.PH-1-Wt on wheat. A-D Light microscopy of infected palea at 10 dpi after trypan blue staining of the mycelium. **A** Different types of infection structures, including foot structures, lobate appressoria, and infection cushions are formed on the inoculated plant surface. Scale bar=10 µm **B-D** Higher magnification of infection structures. **B** Typical morphology of an infection cushion. Scale bar=25 µm. **C** lobate appressoria, and **D** foot structures, which arise from runner hyphae. Scale bars: C=10µm, D=5µm. **Abbreviations: FS** Foot structure, **IC** Infection cushions, **LA** Lobate appressorium, **RH** Runner hypha.

3.1.2 Infection structures of wild type-like reporter strains

3.1.2.1 Fg.8/1-Wt-GFP and Fg.PH-1-Wt-dsRed

In the following we tested reporter mutants of the *F. graminearum* wild type strains Fg.PH-1-Wt and Fg.8/1-Wt for the formation of compound appressoria, which express dsRed or GFP constitutively. The used wild type Fg.8/1-Wt-GFP and the wild type Fg.PH-1-Wt-dsRed express their respective reporter gene under the control of the same constitutive promoter of *A. nidulans* (section 2.1.2). Thereby, the cytoplasm of living hyphae is visible by either red or green fluorescence under adequate excitation of the respective fluorescence protein. Paleas and glumes were inoculated with conidia of the Fg.8/1-Wt-GFP or the wild type Fg.PH-1-Wt-dsRed as described in section 2.2.1. Due to the constitutive expression of fluorescent proteins in the mycelium, it was possible to

observe the developing hyphae daily with a fluorescence stereomicroscope. Thereby, it was controlled when the three infection stages of *F. graminearum* on wheat florets appear during infection as described previously [18]. For both strains germination and spread of hyphae, as characteristic for stage I of infection, were observed prior to the formation of infection structures in stage II. First, smaller structures appear and later big infection cushions developed on both plant surfaces. The cellular structure of compound appressoria formed by the wild type Fg.8/1-Wt-GFP was visualised in more detail by z stack LSM images (figure 10).

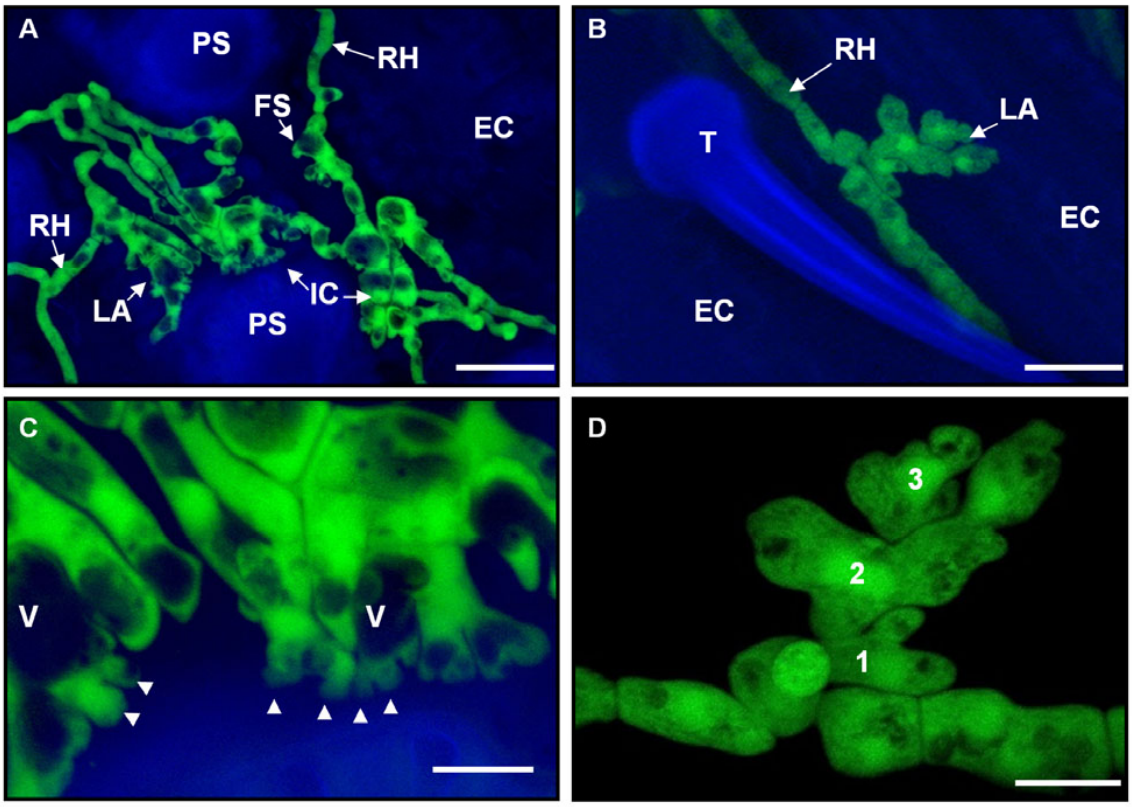

Figure 10: Laser scanning microscopy of compound appressoria formed by the wild type Fg.8/1-Wt-GFP on wheat. A-D Maximum intensity projection (MIP) images of z-stacks of infected glume at 12 dpi. **A** Cellular morphology of infection cushions originating from runner hyphae on the surface of a glume. The enlarged, swollen, and lobed appearance of cushion forming hyphae is noted. Furthermore, big vacuoles are visible as non fluorescent areas in the GFP-labled cytoplasm. **B** Typical morphology of a lobate appressorium originating from runner hyphae on the surface of a glume. **C** Higher magnification of cushion forming hyphae shows many small peg-like structures (white arrowhead) of 0,9-1,8 µm in diameter at the bottom of cushions. **D**. Higher magnification of the lobate appressorium shows that the apressorium is formed by more than one irregular shaped and lobed hyphal cell. Three cells (marked by numbers 1-3) can be identified. The blue channel was left out for better clarity of the fungal signal. Scale bars: A=25µm, B=10µm, C, and D= 5 µm. **Abbreviations: EC** Epidermal cell, **FS** Foot structure, **IC** Infection cushions, **LA** lobate appressorium, **PS** Papillae silica cell, **RH** Runner hypha, **T** Trichome, **V** Vacuole.

The cells of infection cushions and lobate appressoria are irregular in shape compared to the regular long and thin cells of runner hyphae (figure 10, A and B). The enlarged, swollen, and lobed appearance of cushion-forming hyphae is obviously in maximum intensity projections (MIPs) of z-stacks (figure 10, A). Several vacuoles are visible in cells forming infection cushions. By higher magnification of infection cushions small peg-like structures of 0,9-1,8 µm in diameter at the bottom of cushions became visible (figure 10, B). This indicates several penetration events at the junction of a papillae silica cell. MIPs of lobate appressoria show that lobate apressoria are usually formed by more than one irregular shaped and lobed hypha. Three cells separated by septa can be identified by studying the z-series of the appressorium shown in figure 3. It should be mentioned, that lobate appressoria were observed with one up to three cells. If more than 4 cells were involved in the formation of a compound appressorium, the morphology was similar to a small infection cushion. Therefore, discrimination of infection cushions and lobate appressoria was uncertain in these cases. Similar observations as described for the Fg.8/1-Wt-GFP were made by performing equal experiments and microscopic studies with glumes and paleas inoculated with the Fg.-PH-1-Wt-dsRed strain. In figure 11 the abundance of developing compound appressoria of the Fg.PH-1-Wt-dsRed on the plant surface during stage II of infection is demonstrated. Several compound appressoria with varying size, morphology, and complexity are visible, whereas all of them originate from runner hyphae (figure 11, A). Big infection cushions with a high cellular complexity were observed (figure 11, B), in addition to smaller structures, such as lobate appressoria (figure 11, C) and foot structures (figure 11, D)

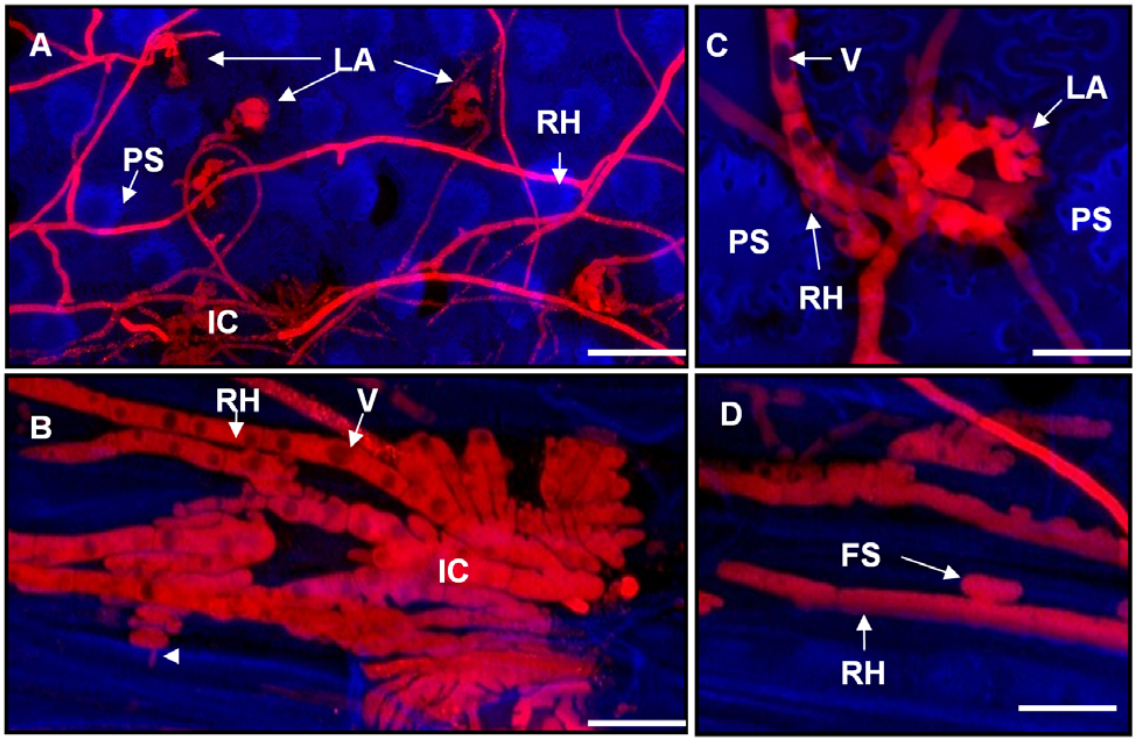

Figure 11: Laser scanning microscopy of compound appressoria formed by the wild type Fg.PH-1-Wt-dsRed on wheat. A-D Maximum intensity projection (MIP) images of z-stacks of an infected palea at 7 dpi. **A** Overview of developing infection structures on the plant surface demonstrates the abundance of compound appressoria that originate from runner hyphae. The varrying size and complexity of single compound appressoria is noted further. **B** Cellular morphology of infection cushions. Enlarged, swollen, and lobed appearance of cushion forming hyphae is shown. Furthermore, vacuoles are visible as non fluorescent areas in the dsRed-labled cytoplasm. **C** Typical morphology of a lobate appressorium and **D** foot structure originating from runner hyphae on the plant surface. Scale bars:A= 40 µm, B=20 µm, C, and D=15 µm. **Abbreviations: IC** Infection cushions, **LA** Lobate appressorium, **PS** Papillae silica cells, **RH** Runner hypha, **V** Vacuole.

In order to visualise penetration of the epidermal layer by compound appressoria of the Fg.8/1-Wt-GFP and Fg.PH-1-Wt-dsRed strain LSM z-series of glumes and paleas at 8 dpi were recorded. By observing the focal planes of the z-series, infection structures were followed from the surface into the plant tissue (figure 12). Thereby, hyphae from lobate appressoria were observed, which proceed in focal planes deeper than the outer epidermal layer. The invasion of epidermal cells through lobate appressoria of the Fg.8/1-Wt-GFP and Fg.PH-1-Wt-dsRed strain was evidential.

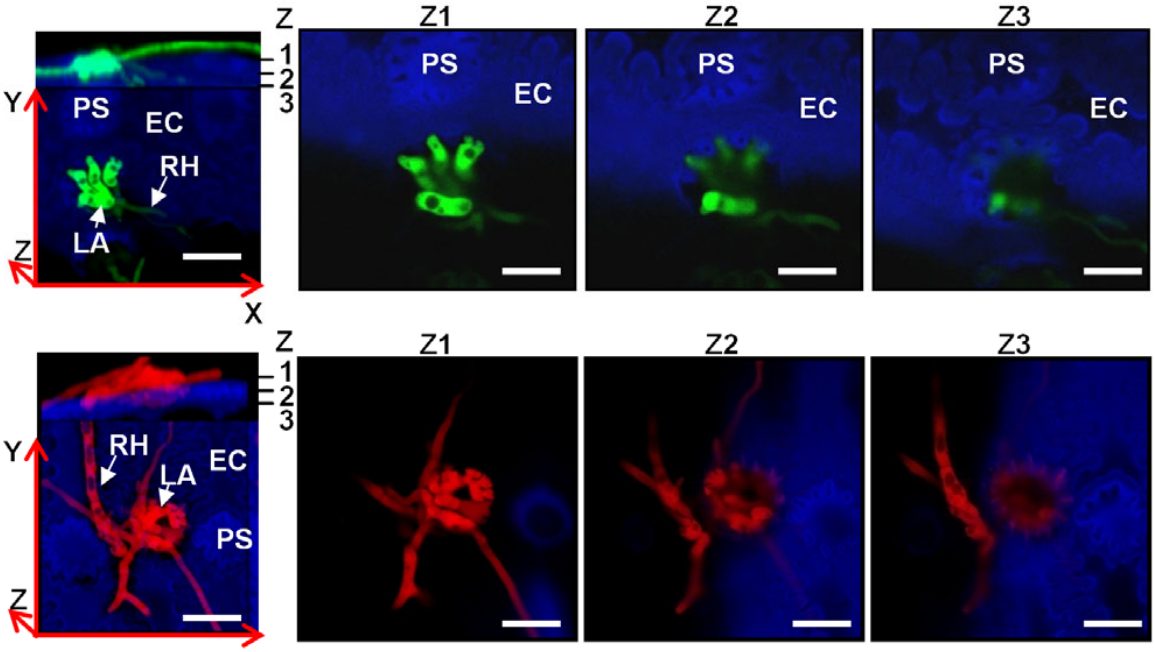

Figure 12: **Epidermal penetration of paleas of wheat by lobate appressoria of the wild type Fg.8/1-Wt-GFP (upper panels) and Fg.PH-1-Wt-dsRed (lower panels) at 7 dpi.** The very left LSM images are Maximum intensity projections (MIPs) from z-stacks of a lobate appressorium of each wild type strain on the epidermis of paleas (blue). The x-, y-, and z-directions of the recorded z-stacks are given by red axes. At the top of each MIP a cut view in x-z direction is provided to illustrate the approximate z-position of three slices (1-3) in the respective z-stack. The slices Z1-Z3 show a lobate appressorium proceeding from the outside (Z1) into focal planes inside (Z2 and Z3) of the epidermal cell. Thereby, epidermal penetration via lobate appressoria is demonstrated for the Fg.8/1-Wt-GFP and Fg.PH-1-Wt-dsRed strains. Scale bars = 30µm. **Abbreviations: EC** Epidermal cell, **LA** Lobate appressorium, **PS** Papillae silica cells, **RH** Runner hypha,

Hand cross sections of paleas infected with the Fg.8/1-Wt-GFP and Fg.PH-1-Wt-dsRed strain were prepared to study the mode of epidermal penetration by compound appressoria. LSM of tissue cross sections demonstrate several penetration pegs arising from infection cushions as well as subepidermal invasion of palea cells by intracellulary hyphae (figure 13).

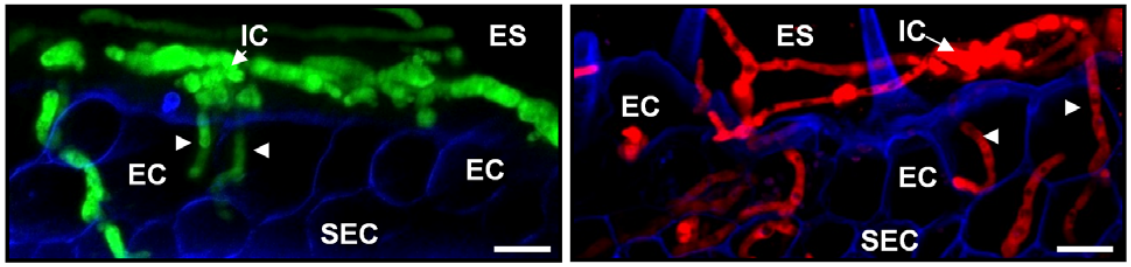

Figure 13: **Epidermal invasion by infection cushions formed by the wild type strain Fg.8/1-Wt-GFP (left pannel) and Fg.PH-1-Wt-dsRed (right panel) on paleas at 8 dpi .** Maximum intensity projections (MIPs) from z-stacks of tissue cross sections recorded by LSM.

Both images show an infection cushion of the Fg.8/1-Wt-GFP and Fg.PH-1-Wt-dsRed reporter strain on the outer epidermal cell wall of a palea (blue). Intracellular hyphae are visible in epidermal and subepidermal cells underneath infection cushions of both wild type strains. Scale bars =10 µm. **Abbreviations: EC** Epidermal cell, **ES** Extracellular space, **IC** Infection cushion, **RH** Runner hypha, **SEC** Subepidermal cell.

To sum up the results, it is demonstrated that compound appressoria types are formed by the reporter strains Fg.8/1-Wt-GFP (figure 10) and the Fg.PH-1-Wt-dsRed (figure 11) during stage II, as described for the respective strains without reporter genes (figure 8 and 9). Thereby, the wild type character with regard to the formation of compound appressoria is demonstrated for both reporter strains. Firstly, it was then possible to use the reporter strains for live cell microscopy of the penetration process (figure 12 and 13). Secondly, the two reporter strains were necessary as adequate wild type controls for experiments using deletion and overexpression reporter mutants in the background of Fg.PH-1-Wt and Fg.8/1-Wt.

3.1.2.2 *TRI5prom::GFP*

After it was observed that necrotic lesions appear around big infection cushions, it was tested, whether mycotoxins are involved during plant penetration by compound appressoria. An involvement of mycotoxins was suggested, since it was described that trichothecenes produced by *F. graminearum* can evoke necrosis of plant cells [29]. In order to evaluate the role of mycotoxins during infection in real time, the reporter strain *TRI5prom::GFP* was used for inoculation of wheat glumes and paleas by fungal conidia as described in section 2.2.1. Due to the constitutive expression of the dsRed protein in the mycelium of *TRI5prom::GFP* it was possible to observe the developing hyphae on the plant under a fluorescence stereomicroscope on a daily basis. In addition, the induction of *TRI5* gene expression in the mycelium was monitored during infection, due to GFP expression under the control of the *TRI5* promoter. It was investigated by a fluorescence stereomicroscopy, whether the three infection stages of *F. graminearum* on wheat florets appear during infection as described previously [18]. The studies of more than 20 independent experiments showed a wild-type-like progress of the infection stages I-III. During stage II compound appressoria were formed by the *TRI5prom::GFP* strain (figure 14) as observed during wild type infections (section 3.1.1 and 3.1.2).

Remarkably, compound appressoria of the *TRI5prom::GFP* strain showed a strong GFP fluorescence compared to the GFP fluorescence of runner hyphae (figure 14, A). By higher magnifications it was visible, that the GFP fluorescence occurs exclusively in infection structures and not or significantly less in runner hyphae (figure 14, B). However, in some runner hyphae directly involved in the formation of infection structures, a GFP induction was visible. Furthermore, it is obvious that the *TRI5* induction of infection structures occurs independently of the cellular complexity, hence lobate appressoria (figure 14, B), big infection cushions (figure 14, C), as well as small foot structures (figure 14, D) show GFP fluorescence.

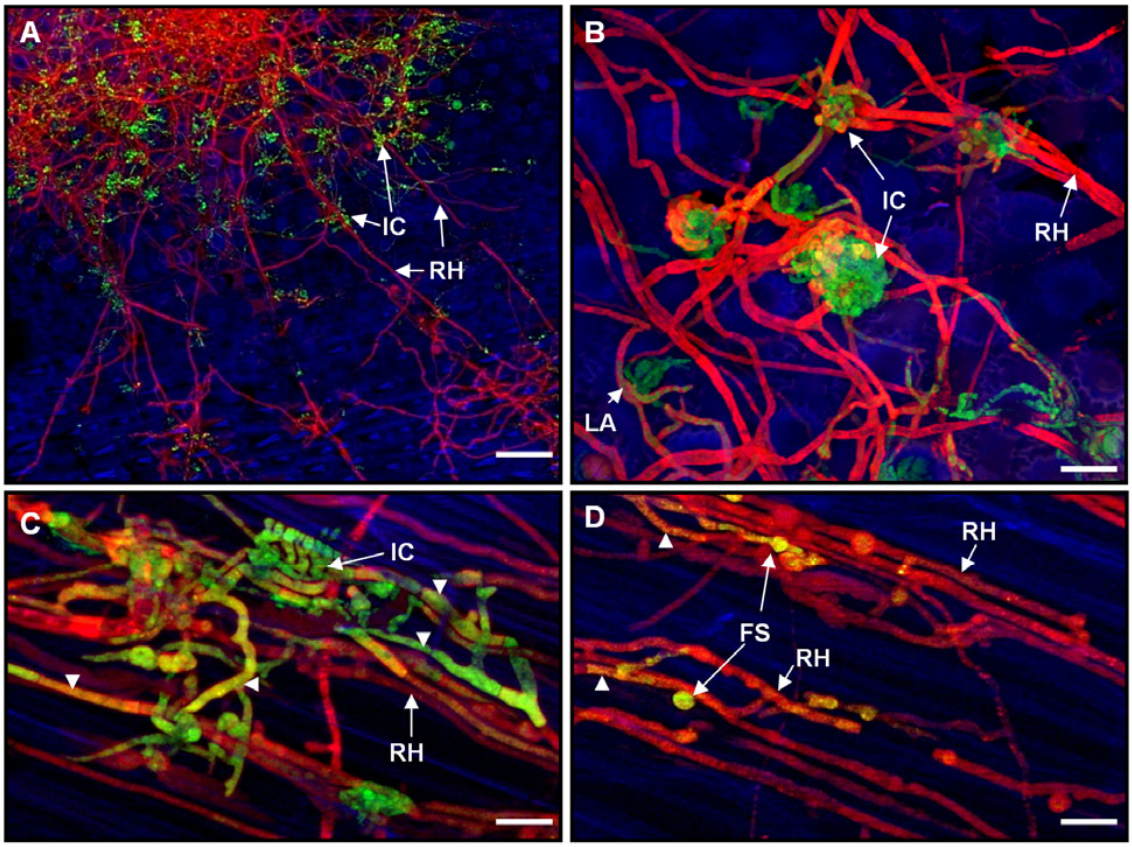

Figure 14: Mycotoxin induction takes place in compound appressoria of *F. graminearum*. **A-D** Fluorescence microscopy of compound appressoria formed by the *TRI5prom::GFP* reporter strain on inoculaed paleas (blue) at 8 dpi. **A** Abundance of infection cushions exhibiting GFP fluorescence in contrast to dsRed fluorescent runner hyphae showing no, or remarkably less GFP fluorescence. **B** Infection cushions with different size and lobate appressoria can be observed that show a strong GFP fluorescence. **C** Structurally complex infection cushions showed a high GFP fluorescence compared to runner hyphae. **D** A high GFP fluorescence compared to runner hyphae was also detected in foot structures. Runner hyphae which were involved in the formation of compound appressoria showed GFP fluorescence in some, but minor cases (white arrowheads in C and D). Scale bars: A= 100 µm, B=30 µm, C and D=20 µm. **Abbreviations: FS** Foot structures, **IC** Infection cushions, **LA** Lobate appressorium, **RH** Runner hyphae.

Although the GFP fluorescence in foot structures was less intense than in more complex structures like lobate appressoria and infection cushions, it was observed to be induced also in foot structures. 3D reconstruction of GFP inductive compound appressoria of the *TRI5prom::GFP* reporter strain on glumes and paleas revealed that the natural autofluorescence of the plant cell wall is strongly reduced underneath compound appressoria (figure 15). The loss of autofluorescence is an indication for alterations of the plant cell wall due to compound appressoria. The adhesion of infection cushion to the plant surface was not detectable by fluorescence microscopy or LSM in many cases, due to the loss of plant autofluorescence.

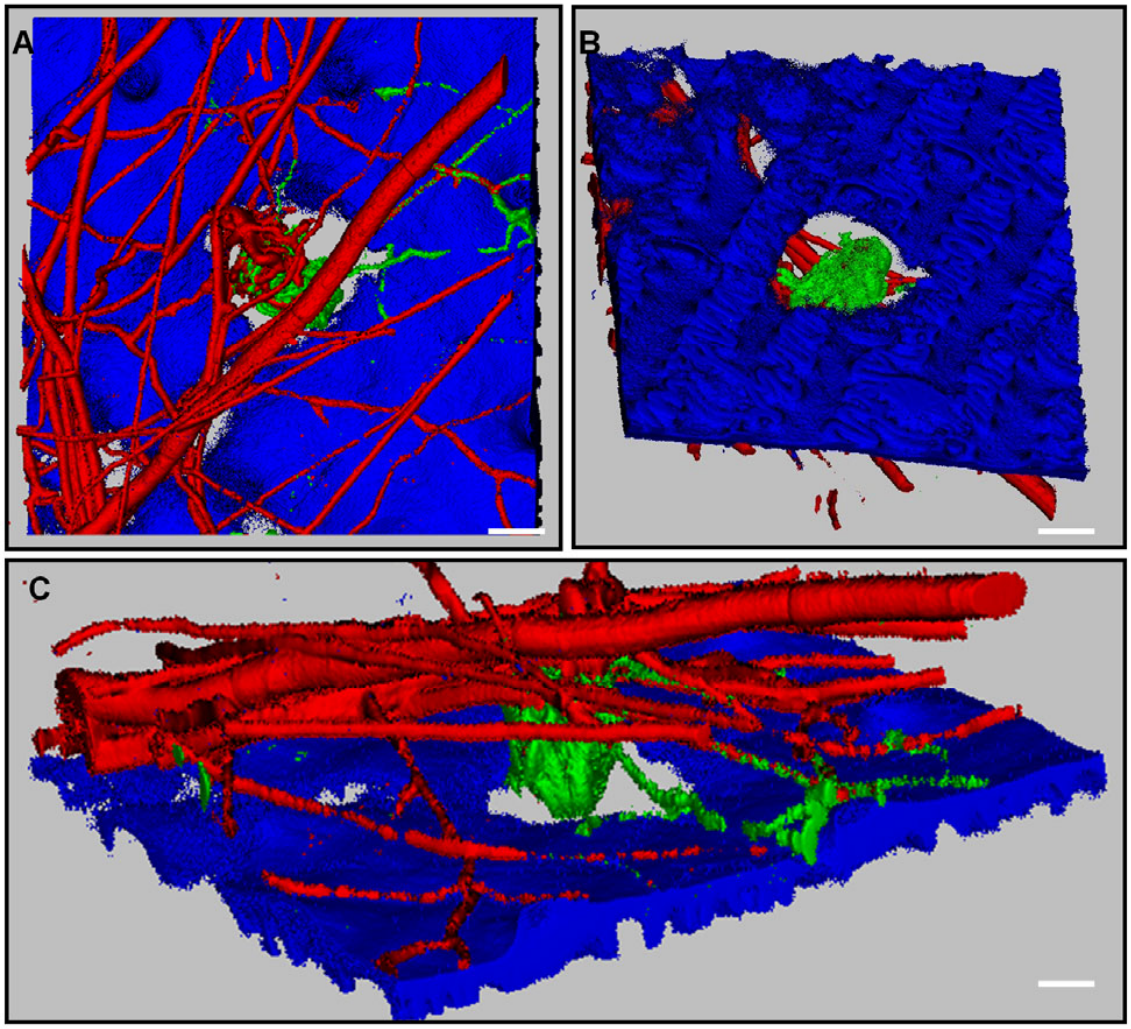

Figure 15: 3D imaging visualises plant alterations underneath toxin producing compound appressoria of *F. graminearum.* A-D 3D reconstruction of LSM z-stack of a typical GFP fluorescent compound appressorium (green) and dsRed fluorescent runner hyphae (red) formed by the *TRI5prom::GFP* strain on inoculated glumes (blue) at 8 dpi. **A** The top view shows a lack of blue plant autofluorescence underneath the appressorium. **B** The view from the bottom of the sample clearly demonstrates the loss of fluorescence of the plant cell wall especially underneath the appressorium. **C** In the cut view of the sample, it appears as if no adhesion of the appressorium to the plant surface takes place. Scale bars:A and B = 10 µm, C= 5µm.

In order to investigate, whether adhesion of compound appressoria to the plant surface takes place scanning electron microscopy (SEM) was performed. By SEM the surface of the inoculated plant is visualised independently of fluorescence characteristics of the cell wall components. Thereby, direct contact of different types of compound appressoria to the plant surface can be identified more reliably by SEM than by fluorescence microscopy. By SEM studies of infected glumes at 8 dpi the adhesion of compound appressoria was observed for lobate appressoria (figure 16, A) and infection cushions (figure 16, B).

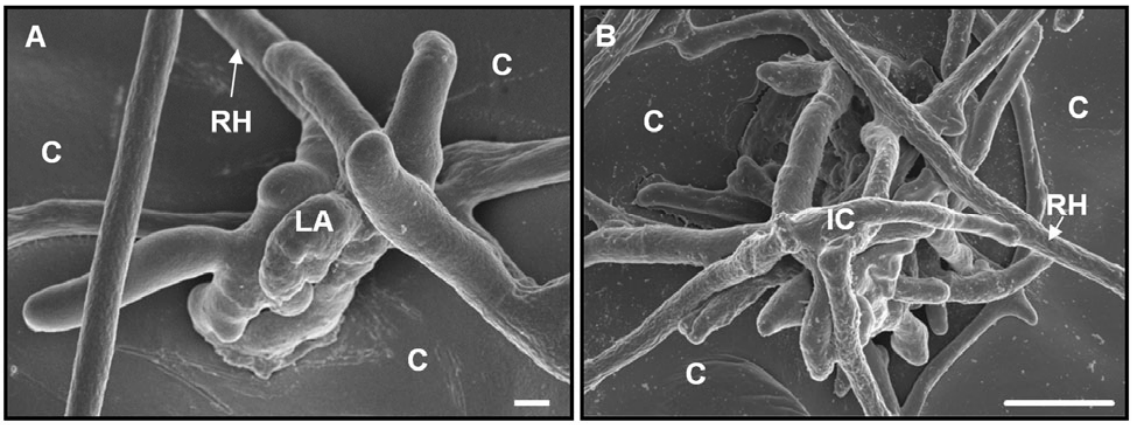

Figure 16: Adhesion of compound appressoria to the plant surface. A and **B** Scanning electron micrographs of compound appressoria formed by the *TRI5prom::GFP* strain on a glume of wheat at 8 dpi. **A** For lobate appressoria direct contact to the surface of wheat glumes was evident as well as for **B** infection cushions. Scale bars: A=2µm, B=50 µm. **Abbreviations**: **C** Plant cuticle, **IC** Infection cushion, **LA** Lobate appressorium, **RH** Runner hypha.

In other words, no compound appressoria were observed in SEM studies without direct contact to the inoculated plant surface. Consequently, the loss of cell wall autofluorescence observed by fluorescence microscopy as shown in figure 15 probably does not reflect a loss of cell wall material in total. It is unclear, whether the change in the autofluorescence results from degradation, synthesis or modification of one or more cell wall compounds, because the components of the cell wall responsible for the autofluorescence are not known. Nevertheless, plant alterations due to compound appressoria are indicated by the change in plan cell wall autofluorescence as demonstrated in figure 15.

3.1.3 Penetration mechanisms on wheat husks

3.1.3.1 Penetration by compound appressoria

In order to study mode of penetration by toxin infection cushions under real time conditions, free hand sections of glumes and paleas with GFP fluorescent infection cushions of the *TRI5prom::GFP* strain were made. Applying fluorescence microscopy tissue sections were studied by z-stacks. Thereby, penetration pegs arising from cushion forming hyphae were observed (figure 17). In cut views of z-stacks penetration penetration pegs were indicated (figure 17, A) and identified clearly by 3D reconstructions of the z-stack (figure 17, B)

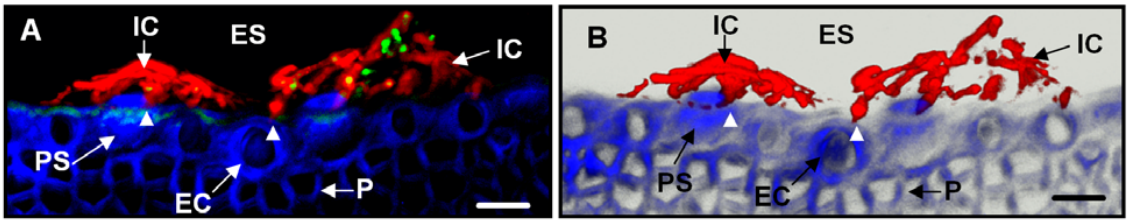

Figure 17: Epidermal penetration by toxin producing infection cushions of *F. graminearum.* **A** and **B:** Fluorescence microscopy of a cross section of a glume inoculated with the *TRI5prom::GFP* reporter strain at 7 dpi. **A** Maximum intensity projection of a recorded z-stack shows two infection cushions by constitutive dsRed fluorescence on the glume tissue (blue). Only a slight induction of GFP in infection cushions (green to yellow due to dsRed and GFP overlay) was detectable after cutting and imaging. The penetration of the epidermal layer by penetration pegs (marked by white arrowheads) arising from an infection cushion is indicated. **B** Penetration pegs of cushion forming hyphae are clearly visible by 3D reconstruction of the z-stack. The GFP channel was omitted, because of disturbing plant autofluorescence. Scale bar = 20 µm. **Abbreviations**: **EC** Epidermal cell **ES** Extracellular space, **IC** Infection cushion, **PC** Parenchyma cell, **PS** Papillae silica cell.

By toluidine blue staining of LR White sections, it was observed that several penetration pegs are formed by an infection cushion (figure 18, A). Penetration pegs inside the epidermal cell wall were identified more easily by toluidine blue staining than by fluorescence microscopy, because the cell wall is stained more reliable by toluidine than by autofluorescence, and since thinner LR White sections improve the clarity of images, compared to free hand cross sections used for fluorescence microscopy.

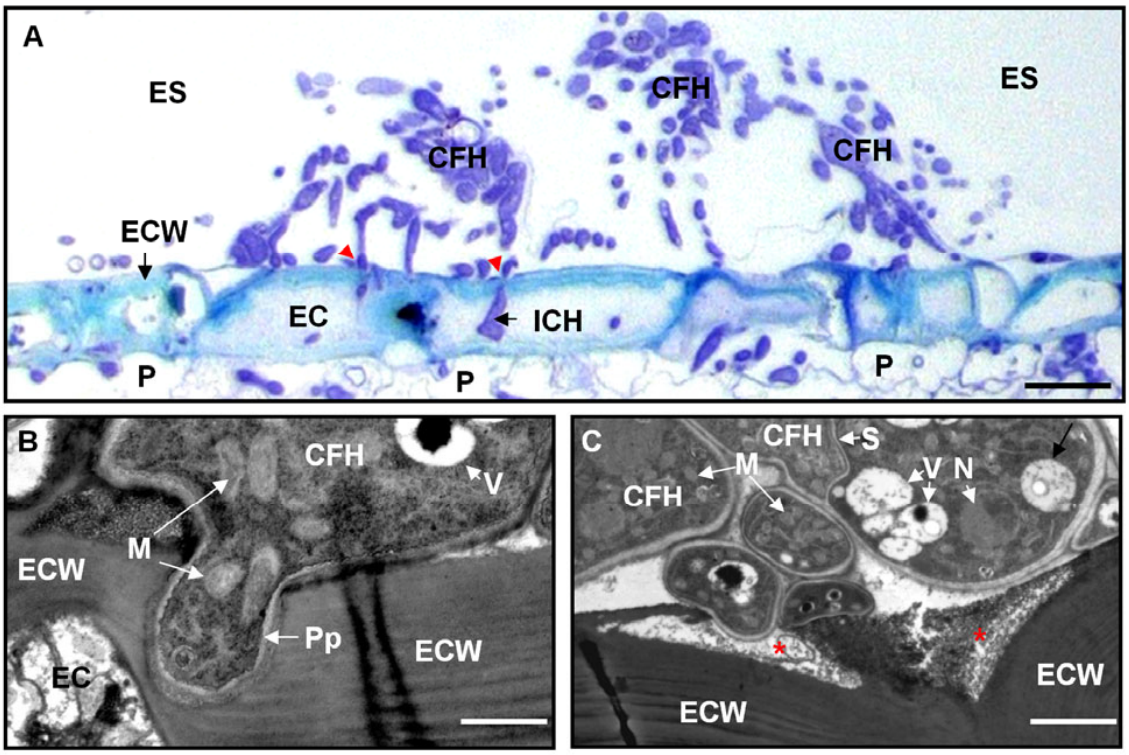

Figure 18: Epidermal penetration of wheat glumes through infection cushions formed by *F. graminearum* 11 dpi. A-D Histology of LR White cross sections of wheat glumes infected with the *TRI5prom::GFP* strain by light microscopy (A) and transmission electron microscopy (B-C). **A** Longitudinal cut infection cushion on the outer epidermis of a glume. After toluidine blue staining intracellular colonisation of epidermal and subepidermal glume tissues (blue) by hyphae (violet) were observed. Direct penetration of the outer epidermal cell wall (blue) by penetration pegs (marked by red arrowheads) is visible. **B** TEM provides ultrastructural resolution images of a penetration peg arising from a cushion forming hypha. **C** A loose and degraded appearance of the plant cell wall (marked by red star) next to contacting hyphae of an infection cushion is further visible by TEM. Scale bars: A=25 µm, B=1 µm, and C=2µm **Abbreviations**: **CFH** Cushion-forming hyphae, **EC** Epidermal cell, **ECW** Epidermal cell wall, **ES** Extracellular space, **ICH** Intracellular hypha, **M** Mitochondria, **N** Nucleus, **P** Parenchyma cell, **Pp** Penetration peg, **S** Septum, **V** Vacuole.

By TEM studies of infection cushions higher resolution of penetration pegs were provided (figure 18, B). The predominant cellular compartments observed in the cytoplasm of hyphae by TEM were mitochondria, the nucleus and vacuoles. No remarkable difference in cellular pattern of penetration pegs was observed compared to hyphae without a penetration peg. By TEM a loose and disorganised appearance of the fibrillary structure of the plant cell wall was visible next to hyphae of an infection cushion (figure 18, C). Considering the formerly described results from fluorescence microscopy as demonstrated in figure 15, alterations of the plant cell wall underneath infection cushions are supported by TEM observations.

3.1.3.2 Penetration through lobate appressoria and foot structures

The penetration of outer epidermal cell walls of glumes by foot structures and lobate appressoria (figure 19) was investigated by light microscopy and TEM of LR White sections, as described before for infection cushions. By light microscopy of toluidine blue stained tissue sections, 1-2 penetration pegs arising from lobate appressoria were observed (figure 19, A). Furthermore, the invasion of the glume tissue was evident by intra- and intercellular hyphae in epidermal and subepidermal plant cells. Foot structures adhering to the surface of glume were observed by light microscopy (figure 19, A) and TEM (figure 19, B).

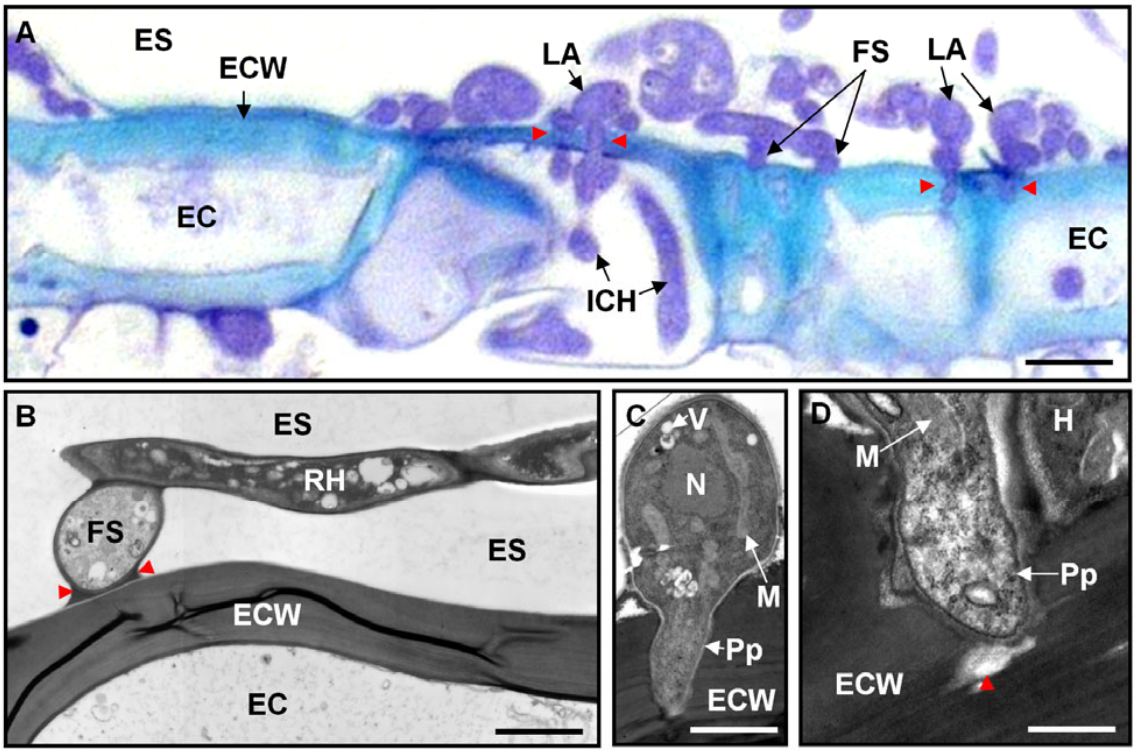

Figure 19: Epidermal penetration by foot structures and lobate appressoria of *F. graminearum* at 11 dpi. A-D: LR White cross sections of wheat glumes infected with the *TRI5prom::GFP* strain were studied histologically by means of light microscopy (A) and transmission electron microscopy (B-D). **A** Toluidine blue staining visualises fungal cells (violet) including lobate appressoria and foot structures on the outer epidermal cell wall of a glume (blue). Penetration of the epidermal cell wall by penetration pegs (red arrowheads) arising from lobate appressoria. Furthermore, intracellular hyphae were visible in epidermal and subepidermal cells. **B** TEM shows a foot structure arising from a runner hyphae. The bulbous foot structure adheres to the outer epidermal cell wall and exhibts an extracellular material (red arrowhead) at its bottom. **C** TEM further demonstrates direct penetration by a penetration peg arising from a bulbous hyphae similar to foot structures. **D** In many cases the cell wall surrounding penetation pegs appeared loose and disintegrated. Scale bars: A= 10µm, B= 5 µm, C=2 µm, D=0,5µm. **Abbreviations**: **EC** Epidermal cell, **ECW** Epidermal cell wall, **ES** Extracellular space, **FS** Foot structure, **ICH** Intracellular hyphae, **M** Mitochondrium, **N** Nucleus, **Pp** Penetration peg, **RH** Runner hypha, **V** Vacuole.

By TEM, an extracellular material was observed covering the fungal cell wall at the bottom of a foot structure (figure 12, B). TEM further demonstrated direct penetration by a penetration peg arising from bulbous hyphae similar to foot structures (figure 19, C). Additionally, a loose and disintegrated appearance of the cell wall surrounding penetation pegs was noted by TEM that indicates enzymatic degradation of the plant cell wall (figure 19, C). After penetration of the epidermal layer by compound appressoria types was elucidated, the further vertical colonisation of glumes tissues was evaluated. Light microscopy of LR White sections showing big (matured) infection cushions demonstrated a dense intracellular colonisation of the epidermal layer following penetration by penetration pegs (figure 20, A). Subepidermal colonisation by intracellular hyphae (violet dots) is also visible in tissue sections of glume, but less severe than in the epidermal layer. Thus, a progress of vertical colonisation following penetration by infection cushions is demonstrated. Under higher magnifications several penetration pegs can be observed arising from infection cushions (figure 20, B).

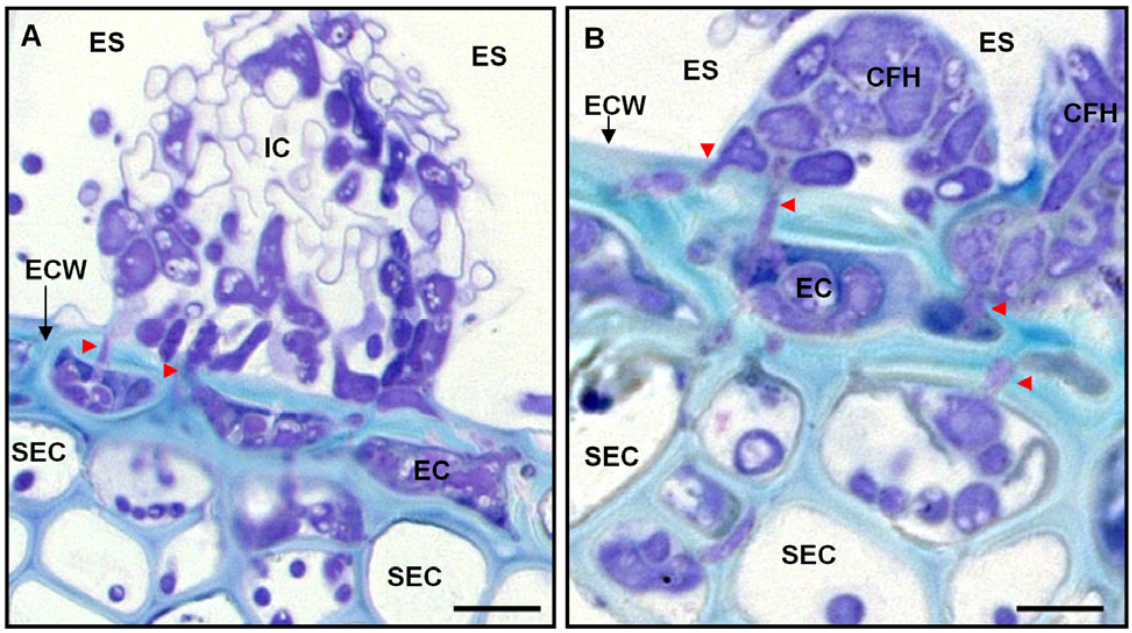

Figure 20: Invasion of wheat glumes through infection cushions formed by *F. graminearum* at 11 dpi. A and **B** LR White sections of a glume infected with the *TRI5prom::GFP* strain were stained with toluidine blue to visualise fungal cells (violet stained) as well as the plant tissue (blue stained) for light microscopy. **A** In addition to the penetration of the epidermal cells by penetration pegs (marked by red arrowheads), a massive intracellular colonisation of the epidermal layer by fungal cells is observed. Subepidermal colonisation by intracellular hyphae is visible, however, less severe than in the epidermal layer. **B** Higher magnification of another section of the same infection cushion demonstrates that several penetration pegs (marked by red arrowheads) are formed. Scale bars: A= 15µm, B= 5 µm. **Abbreviations**: **CFH** Cushion forming hyphae, **EC** Epidermal cell, **ECW** Epidermal cell wall, **ES** Extracellular space, **IC** Infection cushion.

In figure 14 the vertical colonisation inside the tissue is documented. Neighbouring cells are usually invaded by penetration on the cell wall (figure 21, A). This was investigated further by serial cuts observed with a TEM (figure 21, B and C). It was observed that the plant cell wall appears loose and digested surrounding the penetration peg (figure 21, B). In a second proximal section it is visible how the penetration peg of the same intracellular hyphae perforated the entire cell wall to enter the neighbouring cell (figure 21, C).

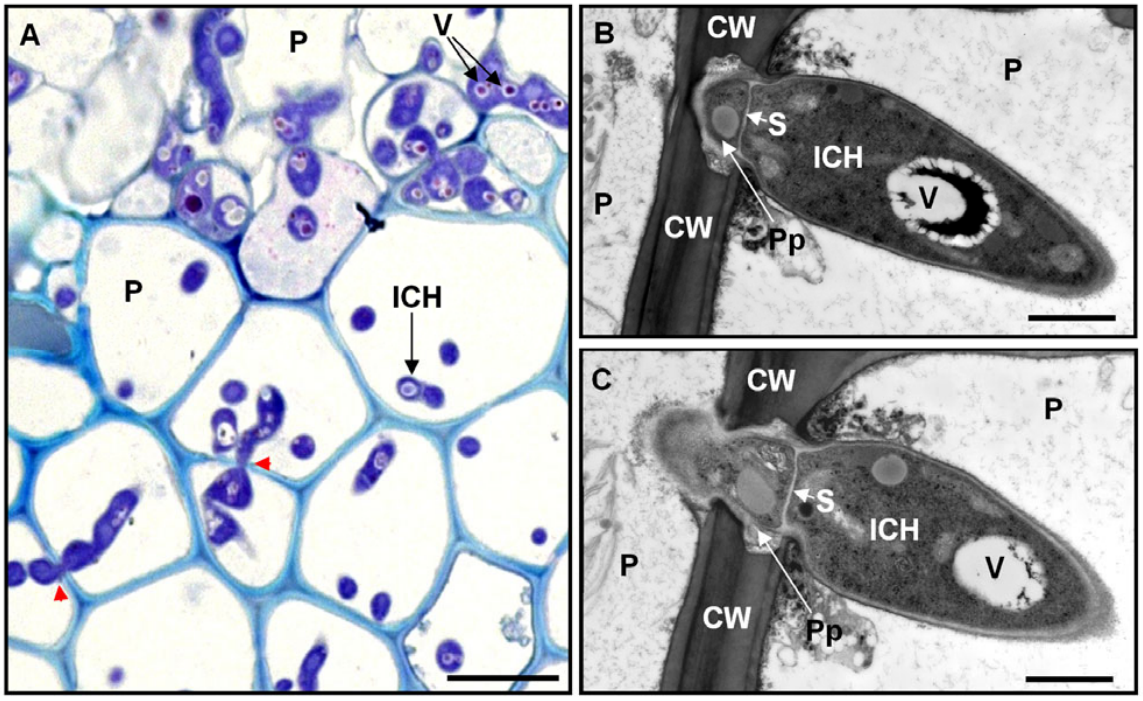

Figure 21: Subepidermal colonisation of wheat glumes by *F. graminearum* at 11 dpi. A-C. LR White embedded cross sections of wheat glumes infected with the *TRI5prom::GFP* strain studied histologically by light microscopy (A) and transmission electron microscopy (B and C). **A** Toluidine blue stained cross section of a glume shows many intracellular hyphae, and vertical colonisation of the tissue by penetrating neighbouring cells (marked by red arrow head). **B** and **C** TEM images of a serial cut show an intracellular hypha entering a neighbouring host cell by penetration. **B** The plant cell wall is not completely perforated by the penetration peg in an ultrathin section distal of the intracellular hyphae. A loose appearance of the plant cell wall surrounding the penetration peg is noted here. **C** In a more proximal section of the same hyphae the penetration peg perforated the entire cell wall and entered the neighbouring host cell. Scale bars:A=20 µm, B and C=1 µm **Abbreviations**: **CW** Plant cell wall, **ICH** Intracellular hypha, **P** Parenchyma cell, **Pp** Penetration peg, **S** Septum, **V** Vacuole.

3.1.3.3 Direct penetration identified by pores in host cells walls

In order to study penetration via penetration pegs, compound appressoria were removed from the plant surface with an adhesive plastic tape (see figure 22). Infection cushions and runner hyphae of the *TRI5Prom::GFP* strain formed on the surface of glumes were imaged before and after removing fungal structures. By bright field illumination and dsRed detection the removal of former existing infection structures was documented (figure 22, A-D). With the exception of a few remaining hyphae, the entire mycelium was removed successfully from the plant (compare figure 22 A and B (before removal) with figure 22 C and D (after removal). Plant necroses at former infection cushions became clearly visible by bright field images (figure 22 A, C). The absence of infection cushions and runner hyphae after removal through an adhesive tape has been proven by dsRed images (figure 22 B, D). DsRed image of the adhesive tape demonstrated that infection cushions und runner hyphae were present on the tape after removal (figure 22, E). The areas where infection cushions have been removed were clearly identifiable on the plant surface by SEM (figure 22, F). Similar samples as shown in figure 22, F were used to look for penetration pores in the epidermal cell wall caused by penetration pegs (see next section). The epidermal cell wall underneath removed infection cushions was investigated for the presence of round pores (holes) with a defined edge by SEM (figure 23). Areas next to removed infection structures, treated equally, were used as the methodical control (figure 23 C, E). By SEM areas of removed infection cushions were clearly distinguishable from areas without infection cushions (compare figure 23 B with C and D with E). Remaining parts of extracellular and subcuticular hyphae were usually visible at margins of removed cushions (figure 23, B). The predominant part of the removed area underneath infection cushions provided a view of the outer epidermal cell wall. Under higher magnifications, numerous circular pores of about 1 µm in diameter are observed in the epidermal cell walls (figure 23, D, F and G). Usually, more than one pore was observed under removed infection cushions.

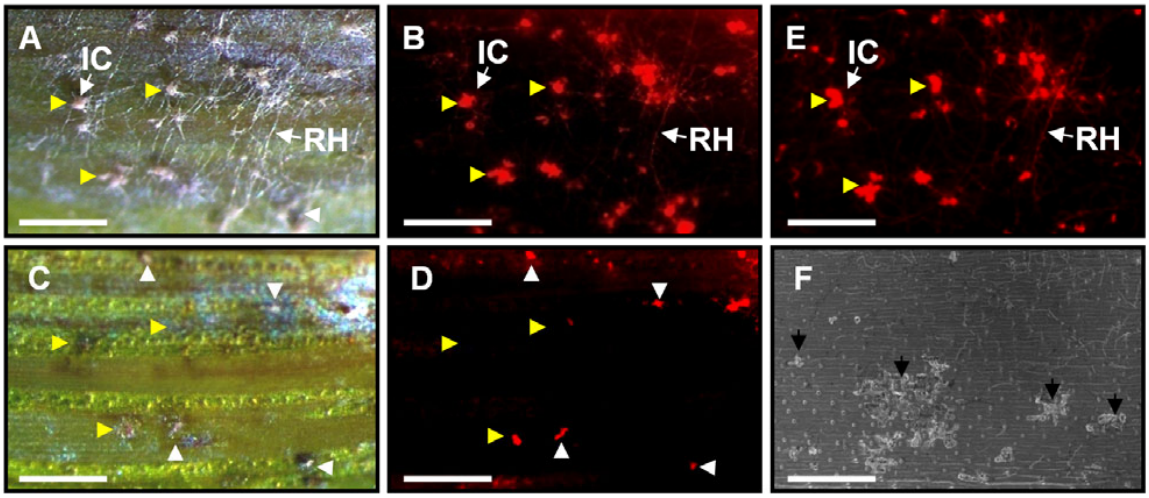

Figure 22: Removal of infection cushions and runner hyphae of *F. graminearum* from wheat glumes with adhesive tape. A-D The surface of a glume inoculated with the constitutively dsRed expressing *TRI5Prom::GFP* strain before removal of mycelium by an adhesive tape (A-B) and afterward (C-D). To illustrate the removal of infection cushions, some cushios are marked by yellow arrowheads in panels C and D. **A** and **B** Images of infection cushions and runner hyphae on a glume under **A** bright field illumination and **B** dsRed detection. **C** and **D** Images of the glume shown in panels A and B after removing the mycelium under bright field illumination (C) and dsRed detection (D). **C** Plant necroses surrounding former infection cushions are visible by bright field images. **D** DsRed detection of the mycelium confirms the absence of mycelium on the glume, with a few exceptions of remaining hyphae (white arrowheads in C and D). **E** DsRed image of the adhesive tape after removal demonstrates that infection cushions (yellow arrowheads) and runner hyphae were transferred on the tape. **F** Scanning electron micrograph of a similar treated glume, as shown in panels A-D. The areas of the plant surface, where infection cushions were removed (black arrows) are clearly visible by SEM. Similar samples were further investigated by SEM for the presence of penetration pores in the epidermal cell wall (see next figure). Scale bars: A-E=400µm, F=100 µm. **Abbreviations**: **IC** Infection cushion**, RH** Runner hypha.

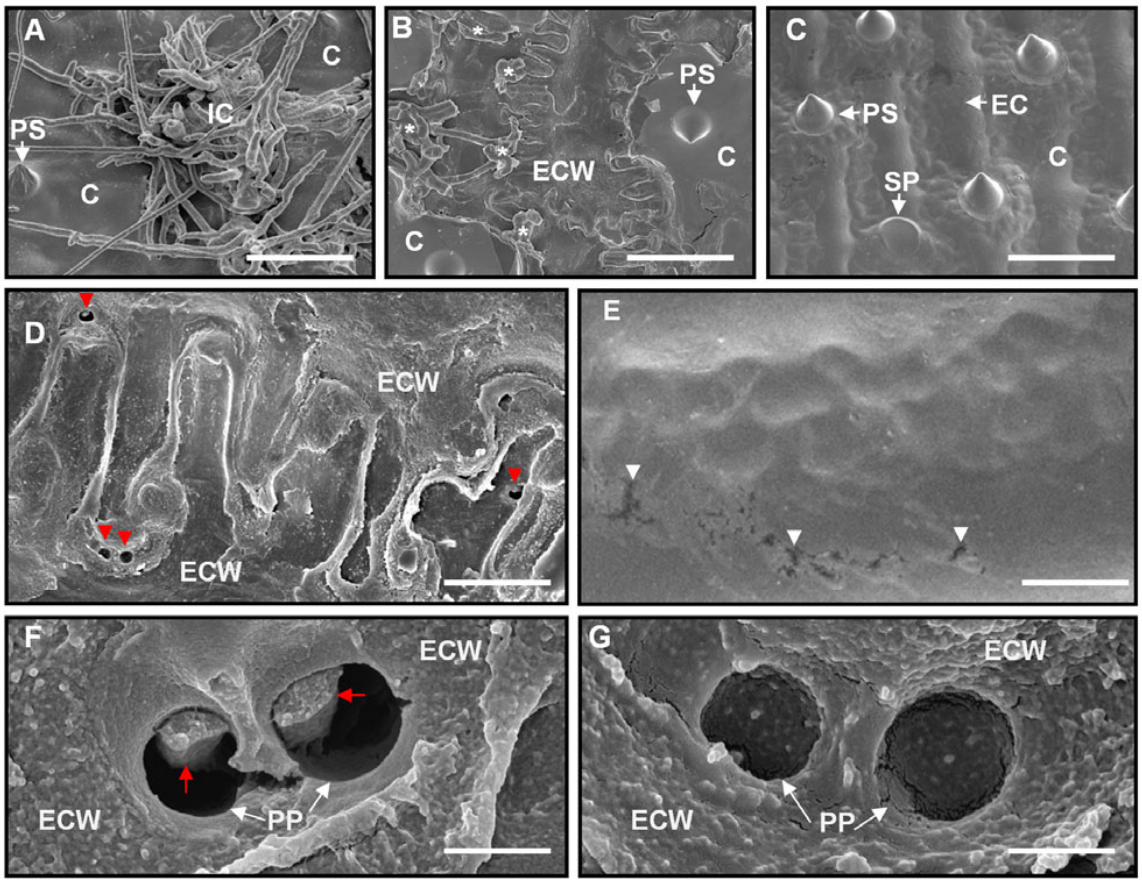

Figure 23: Infection cushions of *F. graminearum* perforate plant cells by penetration pegs. **A-G** Scanning electron microscopy infection cushions formed by *TRI5prom::GFP* on a glume at 8 dpi (A) and the plant surface after removal of infection cushions with an adhesive tape (B-G). **A** Typical infection cushion grown on a glume before removal. **B** The surface of a glume after removal of infection cushions. The plant cell wall is visible at regions where infection cushions are removed. Parts of remained hyphae (white stars) are observed at the margin of the removed infection cushions. **C** The surface of a glume similarly treated as in B without infection cushions served as a control for the removing procedure. **D** Higher magnification of the epidermal plant cell wall below infection cushions show several penetration pores (red arrowheads) of about 1 µm in diameter. **E** The plant cuticle of a control as in C shows irregular alterations (white arrowheads) due to the removing procedure. **F** The penetration pegs (red arrows) inside the penetration pores were visible. **G** Attempts of penetration were observed were the cell wall was not completely perforated. Scale bars: A-C= 30µm, D and E= 15 µm, F and G=1 µm **Abbreviations**: **C** Plant cuticle, **EC** Epidermal cell, **ECW** Epidermal cell wall, **IC** Infection cushion,, **PP** Penetration pore, **PS** Papillae silica cell.

3.1.3.4 Subcuticular growth is related to compound appressoria

An additional way of plant invasion through compound appressoria was subcuticular growth of hyphae. Irregular deformations of the plant surface were detected by SEM, which originated from lobate appressoria and infection cushions (figure 24, A). Due to the deformations around infection cushions an extensive subcuticular colonisation of hyphae was indicated. Furthermore, severe damages of the plant cuticula, such as cuts and cracks, were observed predominately at those areas, where subcuticulary growth of hyphae was assumed (figure 24, B).

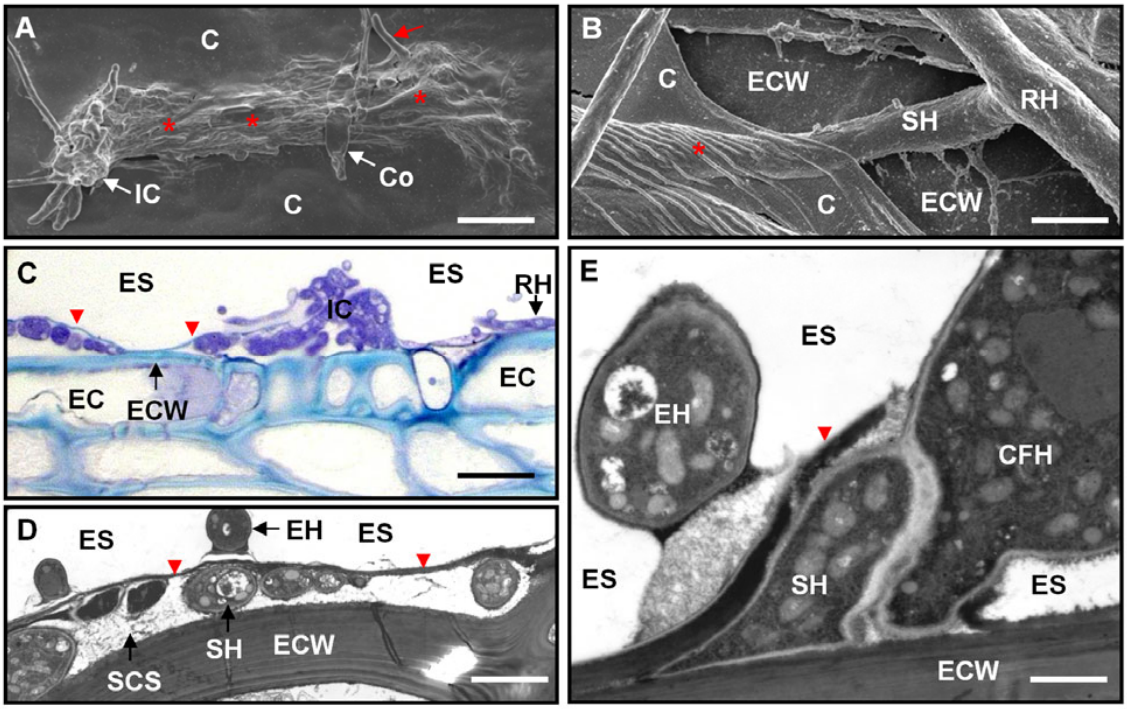

Figure 24: Infection cushions formed by *F. graminearum* are associated with subcuticular spread of hyphae. A-E The *TRI5prom::GFP* strain on wheat glumes were sampled at 8 dpi for Scanning electron microscopy (SEM) studies (A and B) but at 11 dpi for histological studies of LR White sections by light microscopy (C) and transmission electron microscopy (D-E). **A** By SEM of infected glumes irregular alterations of the plant surface (marked by red stars) were observed that extended from infection cushions. Furthermore, hyphae growing out of the cuticle (see red arrow) were visible. **B** Under higher magnification the plant cuticle is visible as a thin layer that covers parts of a subcuticular growing hyphae with extracellular origin. **C** LM of LR White section stained with toluidine blue shows an infection cushion (violet) on the outer epidermal cell wall of glume (blue). A distict blue layer (marked by red arrowhead) covering hyphae near to infection cushions further indicates subcuticulary spread by hyphae. **D** TEM image of the margin of an infection cushion also showed hyphae covered by a distinct, plant derived layer (marked by red arrow heads), namely the plant cuticle**. E** Pentration of the cuticula by tightly adhering hyphae was further observed by TEM at the margin of infection cushions. Scale bars: A = 20µm, B= 5 µm, C=15 µm, D=2 µm, E = 0,5 µm. **Abbreviations**: **C** Plant cuticle, **CFH** Cushion forming hyphae, **Co** Conidium,**EC** Epidermal cell, **ECW** Epidermal cell wall, **EH** Extracellular hypha, **ES** Extracellular space, **IC** Infection cushion, **RH** Runner hypha, **SCS** Subcuticular space, **SH** Subcuticular hypha.

Histological studies on infection cushions on glumes confirmed subcuticular growth at margins of cushions (figure 24, C-E). Toluidine blue staining of semi-thin (1 µm) LR-White sections resulted in a blue coloured plant cell wall and violet stained hyphae visible in bright field microscopy (figure 24, C). Longitudinal sections of infection cushions show dome-shaped accumulations of hyphae located on the outer epidermal plant cell wall. Especially at the margin of infection cushions hyphae were covered with a thin, blue layer representing the plant cuticle (figure 24, C). TEM of ultra-thin LR-White sections confirms the presence of subcuticular growing hyphae at the margin of infection cushions (figure 24, D) and further shows an amorphous substance in the subcuticular space that might be digested plant material (figure 24, E).

3.1.3.5 Compound appressoria can penetrate via papillae silica cells

Papillae silica cells are types of phytoliths (plant cells with SiO_2 deposits) in the epidermis of vegetative tissues of wheat and other grasses. They are circular cells that consist of a papillae-shaped, silicified cell wall. Papillae silica cells of wheat husks showed a characteric anatomy by microscopy (figure 25 E and F). The cell wall consists of pore-like intercellular spaces. The penetration by compound appressoria via papillae silica cells was studied, hence papillae silica are omnipresent cells of the inoculated plant tissues. The adhesion of compound appressoria to papillae silica cells was visible by scanning electron microscopy of glumes inoculated with the *TRI5prom::GFP* reporter strain (figure 25 A-B). The invasion of papillae silica cells by compound appressoria is supported by histological studies on cross sections of compound appressoria on wheat glumes (figure 25 C-D). Due to the morphological characteristics it was possible to distinguish papillae silica cells from other epidermal cell types e.g. stomata, trichomes, and unspecific epidermal cells. The penetration of papillae silica cells by infection cushions and lobate appressoria was also visible in z-series from LSM (figure 25, E and F). The infection structures were followed from the surface into the plant by the focal planes of the z-stack. Thereby, it was visible that papillae silica cells are colonised by hyphae originating from compound appressoria. In many cases the entire lumen of the papillae cells was filled with hyphae. The penetration via papillae silica cells of glumes and paleas was observed for all wild type like reporter strains Fg.8/1-Wt-GFP (figure 12, upper panels) and Fg.PH-1-Wt-dsRed (figure 12, lower

panels and figure 25, E and F) and the *TRI5prom::GFP* (figure 25 A-D). Although the general ability to penetrate the plant via papillae silica cells is demonstrated, it should be pointed out that inoculated areas consisting of epidermal cells without specific modifications are penetrated equally.

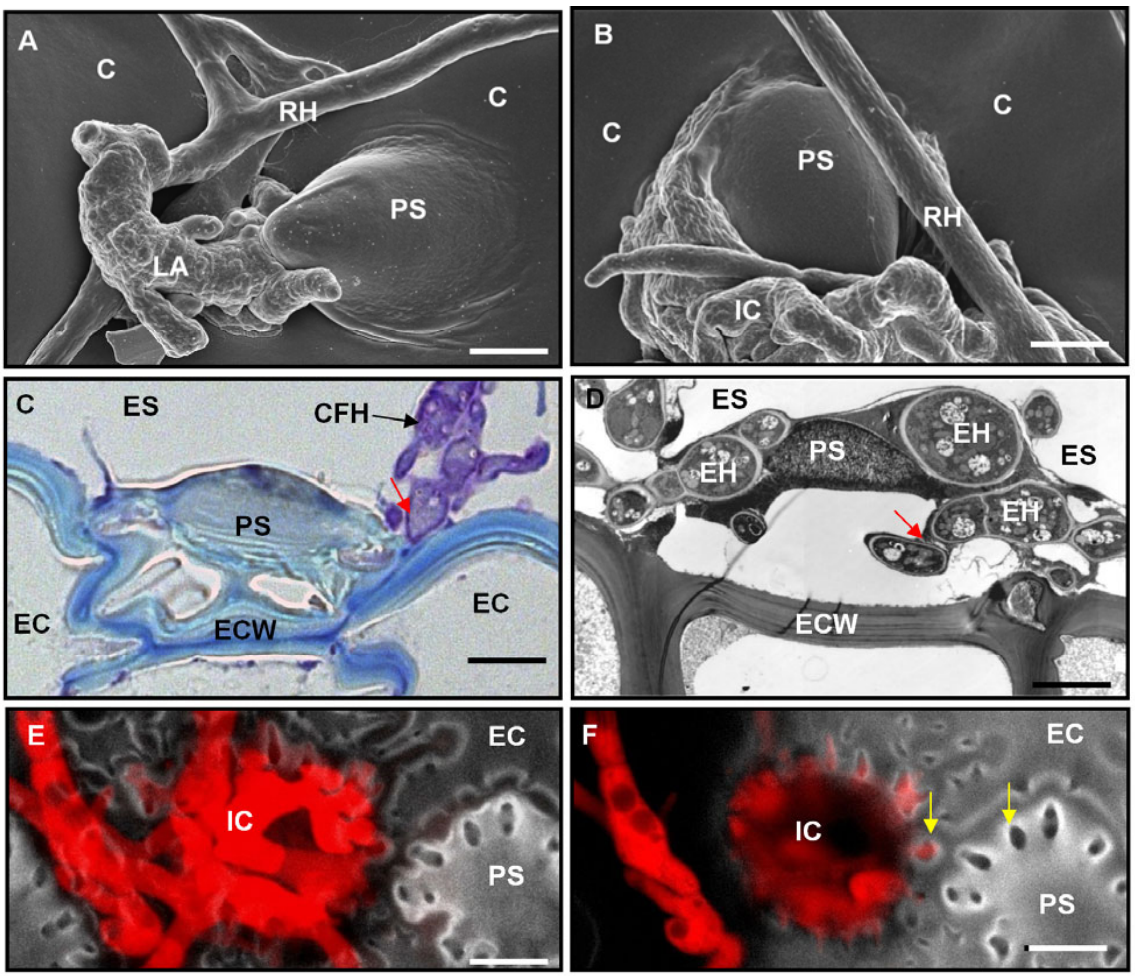

Figure 25: Penetration of silica cells by compound appressoria of *F. graminearum*. **A** and **B** Scanning electron microscopy (SEM) of compound appressoria of the *TRI5prom::GFP* strain on a glume at 8 dpi. A lobate appressorium (**A**) and an infection cushion (**B**) entering the glume by papillae silica cells are documented. **C** Light microscopy of LR White sections of glumes at 11 dpi stained with toluidine blue shows hyphae (violet stained) of an infection cushion that attempt to penetrate (red arrow) the junction of a papillae silica cell (plant cell wall is stained blue). **D** Transmission electron microscopy of infected glume at 11 dpi demonstrates successful penetration (red arrow) through the junctions of papillae silica cells by hyphae. **E** and **F** Laser scanning microscopy of an infection cushion of the wild type Fg.PH-1-Wt-dsRed strain penetrating a papillae silica cell of infected palea at 7 dpi (grey scale). **E** Maximum projection of a z stack provides a top view of the entire fungal structure on the plant. **F** In focal planes deeper than the surface intracellular hyphae in papillae silica cells are visible. Papillae silica cells consist of characteristic circularly distributed intercellular spaces (yellow arrow). Scale bars: A-D = 5µm, E and F= 15 µm. **Abbreviations**: **C** Plant cuticle, **CFH** Cushion forming hyphae, **EC** Epidermal cell, **ECW** Epidermal cell wall, **ES** Extracellular space, **EH** Extracellular hyphae, **IC** Infection cushion, **LA** Lobate appressorium, **PS** Papillae silica cell, **RH** Runner hypha.

3.1.3.6 Stomata penetration

In addition to the direct penetration of the plant cell wall by infection structures, stomatal pores provide an alternative path to enter wheat floret tissues. In case of wheat husks (glume, lemma, and palea) stomata are distributed in homogeneous in the adaxial (inoculated) epidermal layer. Stomata of the adaxial epidermis of glumes are arranged in discontinuous rows [16] and represent approx. 15-20 % of the inoculated surface. Even less stomata can be observed for the adaxial epidermis of paleas. Stomatal rows are completely absent on the adaxial epidermis, with the exception of the two lateral wings. Compared to the total area of the adaxial surface, the stomatal pores are less than 5% of the plant surface. In order to investigate penetration of stomata by *F. graminearum,* glumes were inoculated with conidia of the *TRI5prom::GFP* strain and investigated by different microscopic methods. Fluorescence microscopy (FM) and scanning electron microscopy (SEM) of the inoculated plant surface was performed to observe, whether hyphal growth is directed towards stomata. In both FM and SEM studies germinated hyphae were distributed on the glume surface, without preference to a certain direction, epidermal cell type or topography. The growth direction and branching of runner hyphae on the surface seemed to be random. In cases where hyphae were observed to grow close to stomata, they usually grew along without penetration. Nevertheless, growth of hyphae into the stomatal pore, as shown in figure 26 A by SEM, was observed twice. To investigate, whether the glume is colonised by hyphae underneath stomata, LR-White sections of infected glumes were studied by TEM (figure 26, B) and light microscopy (figure 26, C). In both microscopic studies, hyphae were observed inside stomata several times. Furthermore, colonisation of the substomatal space by hyphae was visible (figure 26, C). From the different microscopic studies it is indicated that stomatal penetration by *F. graminearum* occurs more coincidentally than directed. *F. graminearum* seems to be unable to detect stomata as convenient entry into the host tissue, because hyphae usually pass stomats without entering the pore. Considering the low amount of stomata on adaxial surfaces of glumes and paleas penetration via stomata seem to be of minor relevance for infection. However, the histological studies show that the substomatal space is easily colonised, when the fungus entered the tissue via stomatal pores. Thus, an alternative way to enter the plant tissue, independent of infection structure formation is demonstrated.

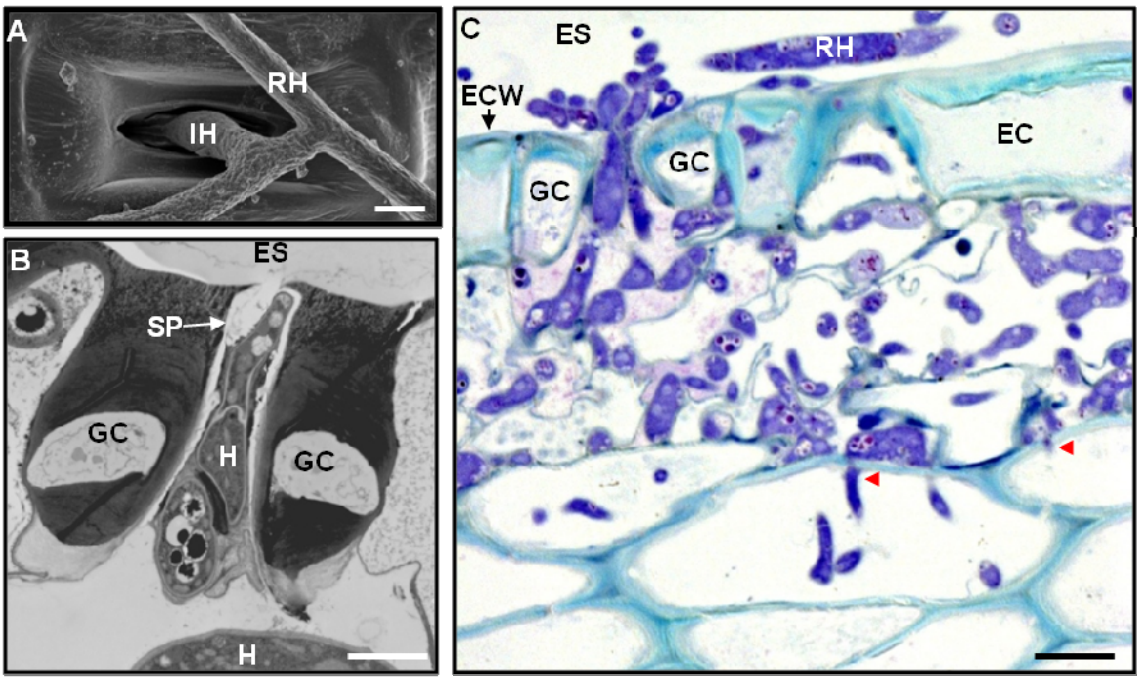

Figure 26: Stomatal penetration of wheat glumes by *F. graminearum*. A Scanning electron micrograph of a hypha of the *TRI5prom::GFP* strain entering the glume through the stomatal pore at 8 dpi. **B** Transmission electron microscopy of a similar infected glume at 11 dpi demonstrates hyphae in the stomatal pore and in the breathing chamber. **C** Light microscopy of LR White sections of glumes at 11 dpi stained with toluidine blue shows hyphae (violet stained) growing through the stomatal pore. Furthermore, intracellular hyphae (violett cells) were observed colonising substomatal parenchyma cells of the glume by penetration (red arrowheads) of neighbouring cells. Scale bars: A and B =5µm, C= 15 µm. **Abbreviations**: **EC** Epidermal cell, **ECW** Epidermal cell wall, **ES** Extracellular space, **GC** Guard cell, **H** Hypha, **IH** Infection hypha, **RH** Runner hypha, **SP** Stomata pore.

3.2 Penetration of cellophane foil

In the previous section it is demonstrated that *TRI5* gene expression is highly induced in different types of infection structures of *F. graminearum*. Therefore, it was suggested that toxin production might be induced due to penetration. In order to test, whether the induction of the *TRI5* gene is dependent on a plant derived factor, an *in vitro* penetration assay was performed with *F. graminearum* wild type Fg.8/1-Wt and the *TRI5prom::GFP* strain. The assay was performed after López-Berges et al., 2010 [103]. The authors performed an agar plate assay with cellophane foil inoculated with *Fusarium oxysporum* and demonstrated that cellophane is penetrated, when the fungus is cultured under nitrate as available nitrogen source, but not, when ammonium is present in the medium. In our experiments, conidia of *F. graminearum* wild type Fg.8/1-Wt and the *TRI5prom::GFP* strain were used for inoculation of cellophane foil placed either on 5mM nitrate or 5mM ammonium as available nitrogen source in solid MM medium. After four days of incubation at 28°C fungal colonies showed a different pigmentation and hyphal morphology depending on the nitrogen source available in the medium (figure 27). No difference in colony morphology and pigmentation was observed between the wild type Fg.8/1-Wt and the *TRI5prom::GFP* strain (figure 27, A). The centre of the colony of both strains used appeared red under the presence of nitrate, whereas it was pigmented yellow, when ammonium was present in the medium. Under higher magnification of the colony edge it was visible that hyphae grown on ammonium are highly branched, in contrast to hyphae grown on nitrate (figure 27 B). The toxin induction in the mycelium under presence of nitrate and ammonium was monitored by fluorescence microscopy of hyphal colonies from *TRI5prom::GFP* (figure 27, C). The dsRed fluorescence of the mycelium was visible under both conditions due to the constitutive dsRed expression of the *TRI5prom::GFP* strain. However, GFP fluorescence that visualises the induction of the *TRI5* gene, was observed in the mycelium under presence of ammonium (figure 27 C, lower panels), but not with nitrate in the medium (figure 27 C, upper panel). Thus, it is indicated that *TRI5* related toxin production is induced by ammonium, but not by nitrate.

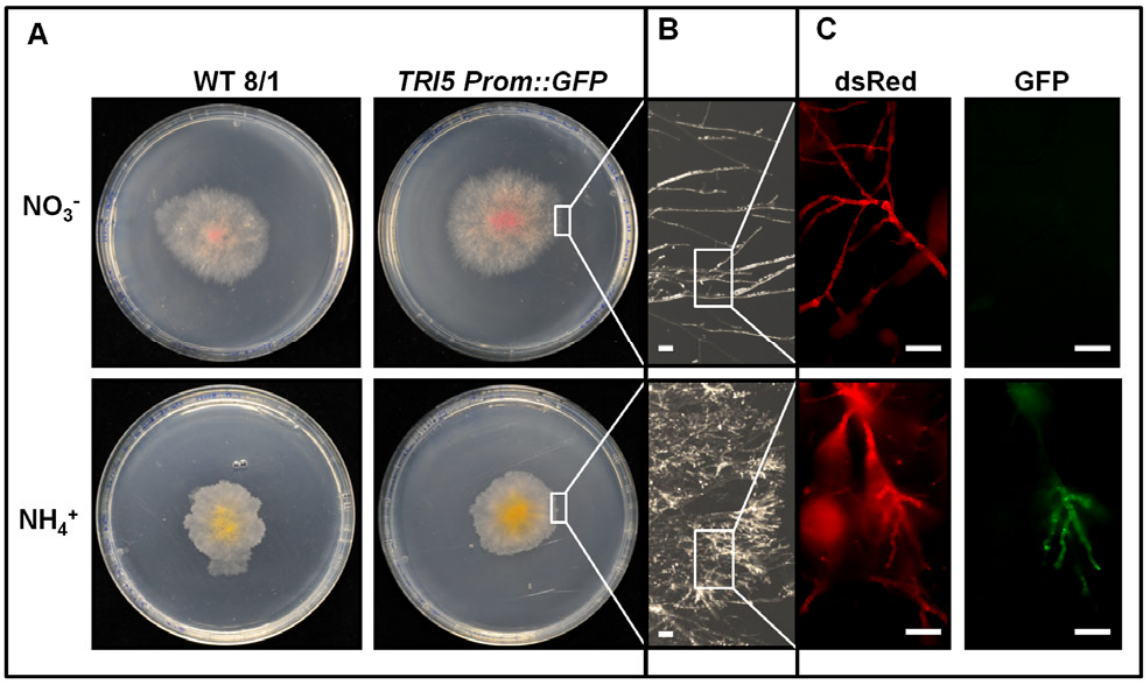

Figure 27: Colony morphology and toxin induction of *F. graminearum* under different nitrogen sources. A Fungal colonies of the wild type (WT) Fg.8/1-Wt (left panels) and the *TRI5Prom::GFP* strain (right panels) after 4 days on agar plates with either 5mM nitrate (upper panels) or 5mM ammonium (lower panels). The centre of the colony appears violet under the presence of nitrate, whereas it is pigmented yellow, when ammonium is present in the medium. **B** Higher magnification of the colony edge (marked by white squares in A) of the *TRI5prom::GFP* strain shows that hyphae grown on ammonium are highly branched, in contrast to hyphae grown on nitrate. **C** Fluorescence microscopy of hyphae shown in panel B (marked by white squares in B) under nitrate (upper panels) or ammonium (lower panels). The constitutive dsRed fluorescence of the mycelium is visible under both conditions (left panels). However, GFP fluorescence that indicates toxin induction, was visible in several parts of the mycelium under the presence of ammonium (lower right panel), but not with nitrate (upper right panel) in the medium. Scale bars = 20 µm**.**

Penetration through cellophane was tested by peeling off the cellophane foil after 4 days of growth at 28°C and further incubation of the agar plates for 4 more days (figure 28). Growth of hyphae on the agar containing nitrate or ammonium was checked for the *TRI5prom::GFP* strain with a fluorescence stereomicroscope (figure 28, A) and the wild type Fg.8/1-Wt (data not shown). However, similar results were observed for the wild type Fg.8/1-Wt and the *TRI5prom::GFP* strain. By dsRed fluorescence growth of mycelium was observed on agar containing nitrate, but not with ammonium as nitrogen source (figure 28, A, left panels). Thereby, it is indicated that the fungus penetrated the cellophane foil on nitrate containing medium, while cellophane placed on ammonium is not penetrated. No induction of toxins was observed by GFP fluorescence in the mycelium growing on agar with nitrate (figure 28, A, upper right panel). The agar

containing ammonium without growing hyphae is shown as the negative control for GFP detection. In order to observe hyphal growth through the cellophane foil under presence of nitrate or ammonium, removed foils were folded once in the middle and incubated for 4 days. By brightfield and dsRed images hyphae were documented growing out of the folded edge of cellophane foil derived from on nitrate containing agar plates, but not when ammonium was present (figure 28, B). No induction of toxins was detected in the mycelium by GFP fluorescence under both nitrogen sources (figure 28, B, right panels).

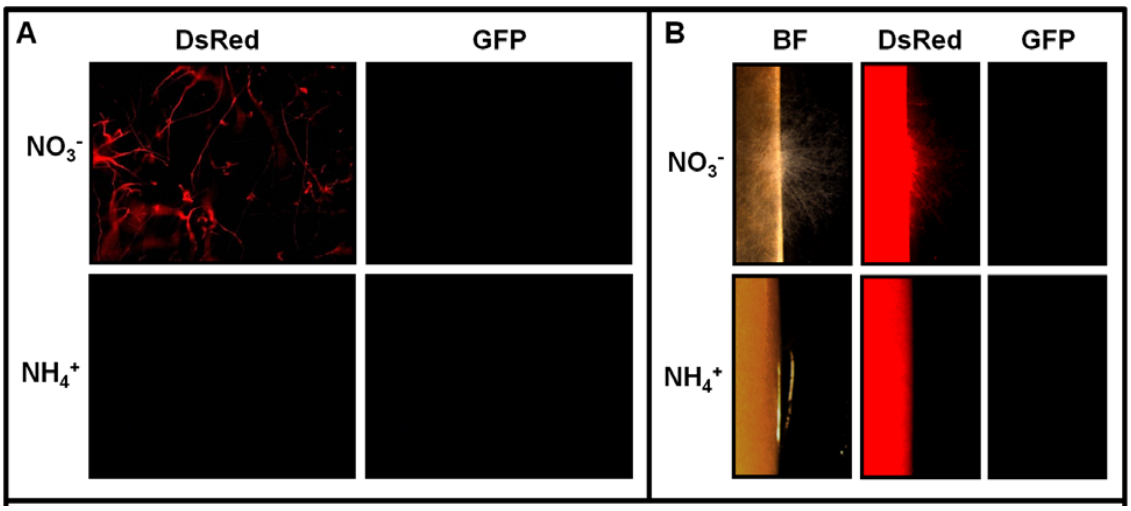

Figure 28: Penetration of cellophane foil the *TRI5prom::GFP* strain under different nitrogen sources and test for toxin induction. A Fluorescence microscopy of the agar surface four days after removal of inoculated cellophane foil from plates with either 5 mM nitrate (upper panels) or ammonium (lower panels). The growing mycelium on agar containing nitrate (upper left panel) is visible by dsRed fluorescence, but not when ammonium is supplied (lower left panel). No induction of toxins in the mycelium is indicated by the absence of GFP fluorescence under both conditions. **B** Images of the edge of half folded cellophane sheets four days after removal from agar plats with either 5 mM nitrate (upper panels) or ammonium (lower panels). Hyphal growth at the folding edge is visible by bright field (BF) images (left panels) and dsRed images (middle pannels) (upper panels), when cultured on nitrate, but on ammonium (lower panels). No induction of toxins in the mycelium was detected by GFP fluorescence under both nitrogen sources (right panels).

3.3 Screening of *F. graminearum* mutants for penetration defects

3.3.1 Infection structures of Δ*TRI5-GFP* deletion mutant

The *TRI5* mutant was investigated for the formation of infection structures, hence a reduced infection of wheat spikes was shown for this mutant in previous experiments [33]. To evaluate the role of trichothecenes for initial penetration the trichothecene deficient Δ*TRI5-GFP* mutant was used for inoculation of wheat glumes and paleas. The mycelium was visible on the plant due to constitutively expressed GFP in the hyphal cytoplasm. Microscopic investigations revealed no differences regarding formation of infection structures between the Δ*TRI5-GFP* mutant (figure 29) and the trichothecene-producing Fg.8/1-Wt strains studied (figure 8, 10, 14 and 16). Furthermore, similar to wild type infections, necrotic lesions around infection cushions were observed by stereomicroscopy (figure 29, A-C). Necrotic plant cells were visible after removal of chlorophyll by critical point drying (figure 29, C). They refer to plant destruction at fungal penetration sites.

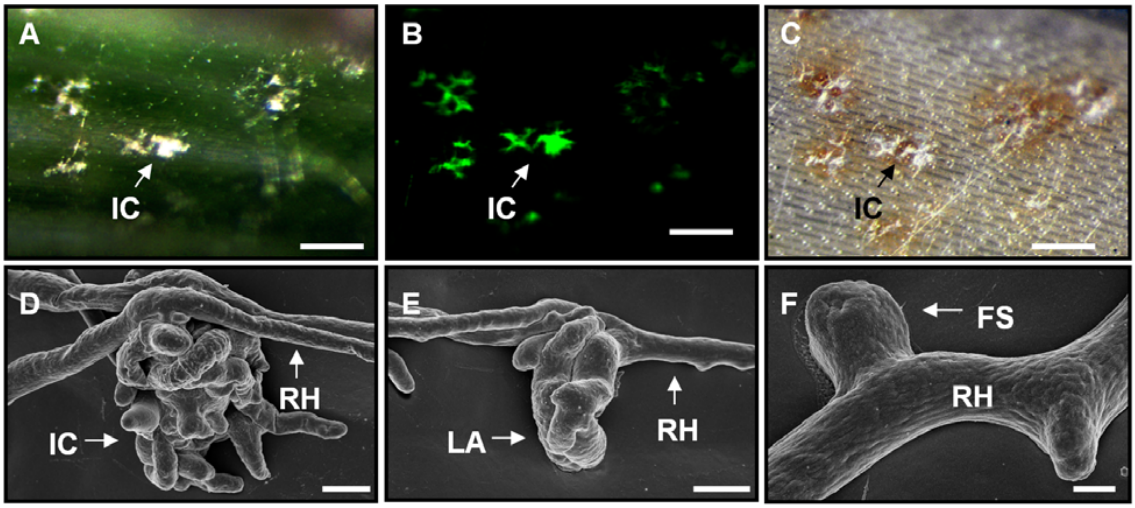

Figure 29: Infection structures of a trichothecene deficient Δ*TRI5-GFP* mutant of *F. graminearum* on wheat glumes. A-C White light and fluorescence micrographs of an infected glume at 13 dpi done with MZFLIII microscope. Scale bars = 200 µm. **A** White light image of infection cushions formed by the Δ*TRI5-GFP* mutant. **B** GFP fluorescence of the mycelium due to constitutive GFP expression. **C** Brownish necroses around infection cushions visible by white light microscopy after critical point drying. **D-F** Scanning electron micrographs show different infection structures of a Δ*TRI5-GFP* mutant on glume at 8 dpi. **D** Infection cushions, **E** lobate appressoria, **F** foot structures and infection hyphae, scale bars: D and E = 4 µm, F = 1 µm. **Abbreviations: FS** Foot structure, **IC** Infection cushion, **LA** Lobate appressorium, **RH** Runner hypha.

SEM of glumes infected by Δ*TRI5-GFP* mutant revealed that all types of infection structures including infection cushions (figure 29, D), lobate appressoria (figure 29, E), foot structures and infection hyphae (figure 29, F) were formed by the Δ*TRI5-GFP* mutant. In summary, DON production in infection structures is neither required for their development nor for formation of necrotic lesions.

3.3.2 Infection structures of Δ*FGL1-GFP* deletion mutant

The lipase 1 deficient *FGL1* knock-out mutant of *F. graminearum* was investigated for the formation of infection structures, hence a reduced ability to infect wheat spikes was shown for this mutant in previous experiments [70]. To evaluate the role of the secreted lipase 1 during initial steps of plant infection, we used the Δ*FGL1-GFP* strain for inoculation of glumes and paleas (section 2.2.1) and investigated the infection stages and infection structures (section 2.2.4.1 and 2.2.4.2). The mycelium was detected on the plant by constitutive expression of *GFP* in the fungal cytoplasm. Daily investigation of inoculated glumes and paleas by a stereomicroscope showed similar stages of infection as described for the wild type infection. However, compound appressoria were observed earlier as described for the wild type. As early as two days post inoculation (dpi), smaller structures like foot structures and lobate appressoria were observed on paleas, and even complex infection cushions were visible by fluorescence microscopy. Similar observations as described for infections of paleas were made with glumes of wheat inoculated with Δ*FGL1-GFP* strain. Although the infection stages I-III were exhibited on glumes equally, stage II occurred three to four days later than on paleas. This tissue specific delay at inoculated glumes compared to paleas has been described previously for wild type infections of *F. graminearum* [18]. Hence, infection structures formed on paleas and glumes are similar, fluorescence images of inoculated paleas are shown representatively. Maximum intensity projections from z stacks, recorded by fluorescence microscopy, show the typical appearance of compound appressoria during infection stage II of the Δ*FGL1-GFP* strain (figure 30). Different types of compound appressoria, arising from runner hyphae by side branches, were visible on the plant (figure 30, A). Higher magnifications demonstrate the characteristic lobed and agglomerated morphology of hyphae forming lobate appressoria (figure 30, B) and

infection cushions (figure 30, C). Several vacuoles in the cytoplasm of hyphae are visible due to a loss of GFP fluorescence in this cellular compartment.

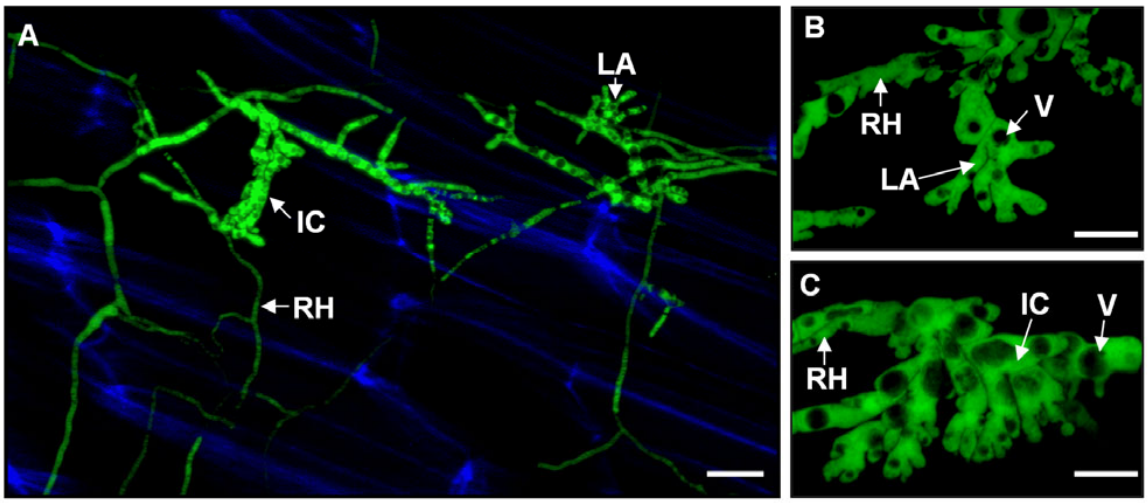

Figure 30: Infection structures of a lipase deficient Δ*FGL1-GFP* mutant of *F. graminearum* on husks of wheat. A-C Maximum intensity projection from fluorescence microscopy of compound appressoria on paleas at 2-3 dpi. GFP fluorescence of the mycelium is detected by constitutive GFP expression, while plant tissues is visualised by its blue autofluorescence under UV light excitation. **A** Different types of compound appressoria developed from runner hyphae, which spread on the surface of palea following germination of conidia. **B** and **C** Higher magnification of compound appressoria types at 2 dpi on inoculated palea. The blue plant autofluorescence is ommited here for a better visibility of the morphology of infection structures. **B** Typical morphology of a lobate appressorium and **C** infection cushion of the Δ*FGL1-GFP* mutant. The characteristic lobed and agglomerated appearence of hyphae forming lobate appressoria and infection cushions is demonstrated by panel B and C. Vacuols in the cytoplasm of hyphae are visible due to a loss of GFP fluorescence. Scale bars: A=10µm, B and C= 4µm, **Abbreviations**: **IC** Infection cushion, **LA** Lobate appressorium, **RH** Runner hypha, **V** Vacuole.

In summary, it is shown that the initial infection on wheat paleas and glumes is not affected negatively by the absence of the secreted lipase 1 in the Δ*FGL1-GFP* strain. All infection stages and infection structures were observed as described for the wild type, however, stage II occurred even earlier than usual for wild type infections. It should be mentioned here that all experiments and with the Δ*FGL1-GFP* strain were performed by the master student Jakob Weber.

3.3.3 Infection structures of Δ*GPMK1-GFP* deletion mutant

The Δ*GPMK1-GFP* mutant of *F. graminearum* showed a reduced ability to infect wheat spikes in previous studies [73], therefore, the initial infection stages of this mutant were studied microscopically in detail in the presented work. Furthermore, defects in the function of infection structures were described for deletion mutants of the homologous gene in the phytopathogenic fungi *M oryzae*. Consequently, infection structure development and function of Δ*GPMK1-GFP* mutant of *F. graminearum* was investigated here. The developing mycelium on the plant was monitored by fluorescence microscopy due to constitutively expressed GFP in the cytoplasm. By daily observations of inoculated glumes and pales by fluorescence stereomicroscopy, the stages I-III of infection as described for wild type infections were observed on paleas, but not on glumes.

Germination of conidia and colonisation of the palea surface by runner hyphae took place as characteristic for stage I of the wild type. However, the GFP fluorescence of the Δ*GPMK1-GFP* mutant was significantly lower compared to the responding Fg.8/1-Wt-GFP strain. Due to the low GFP signal of the hyphae of the Δ*GPMK1-GFP* mutant higher exposure times were necessary for the acquisition of fluorescence images. Thus, the autofluorescence signal of the plant detected in the GFP emission range increased and strongly lowered the clarity of fluorescence images of fungal structures. As a consequence, calcofluor-white staining was additionally performed with the Δ*GPMK1-GFP* mutant. By calcofluor-white staining the fungal cell wall, including the septa of hyphae, became visible on the plant. Foot structures and lobate appressoria as characteristic for the start of stage II appeared at 2 dpi on paleas (figure 31, A). Infection cushions developed in the following 1-2 days and their maturation proceeded until necroses become visible on paleas after 7 dpi. The single developmental stages of compound appressoria, including foot structures (figure 31, B), lobate appressoria (figure 31, C) and infection cushions (figure 31, D) were also observed by SEM studies of the Δ*GPMK1-GFP* on paleas at 3 dpi. Infection structures including foot structures seemed to adhere to the surface by a mucilage-like material (figure 31, B). Interestingly, on several inoculated glumes the infection structures were visible still at 27 dpi (figure 31, E), but no progress to stage III was observed, as typical for the wild type at 8-10 dpi.

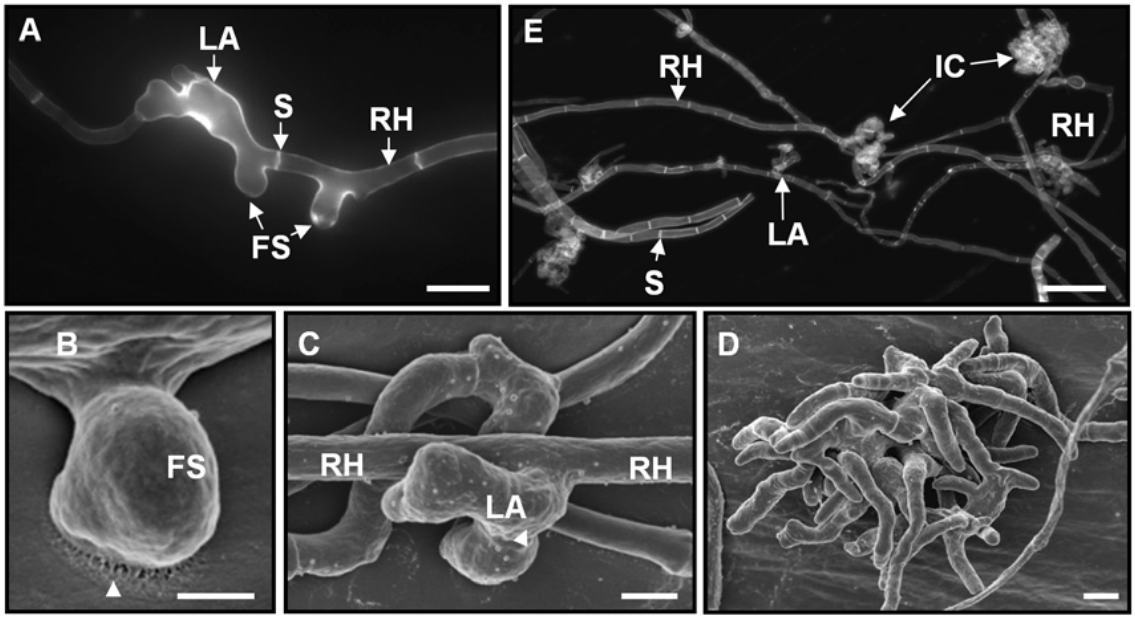

Figure 31: Infection structures of the *GPMK1-GFP* mutant of *F. graminearum* on wheat paleas. A and **E** Fluorescence microscopy after calcofluor-white staining to visualise compound appressoria at 2 dpi (A) and 27 dpi (E). **A** Infection structures, such as foot structures and lobate appressoria developed by runner hyphae at 2 dpi. The regular morphology and septation of runner hyphae in contrast to compound appressoria is visible due to stained septa. **B-D** Scanning electron microscopy of compound appressoria at 3 dpi. **B** Foot structure is arising from runner hyphae and adheres to the surface by mucilage-like material (white arrowhead) at the bottom of a foot structures. **C** Lobate appressorium is arising from runner hyphae. **D** Characteristic appearance of an infection cushion. **E** Complex infection cushions and lobate appressoria within the network of runner hyphae were still present at 27 dpi. Scale bars: A = 10 µm, B = 2 µm, C and D =5 µm **Abbreviations**: **FS** Foot structure, **IC** Infection cushion, **LA** Lobate appressorium, **RH** Runner hypha, **S** Septum.

Consequently, a stagnation of fungal development is indicated. Necroses of paleas were less severe compared to the wild type infection at the same time point. However, entire necroses of paleas occurred, when prolonging the time of infection. The degeneration of hyphae from 4-5 dpi onward is indicated by a continuous decrease of GFP fluorescence in the mycelium with increased time of infection. Subcuticulary colonisation of wheat palea by the *GPMK1-GFP* mutant was observed by scanning electron microscopy (figure 32).

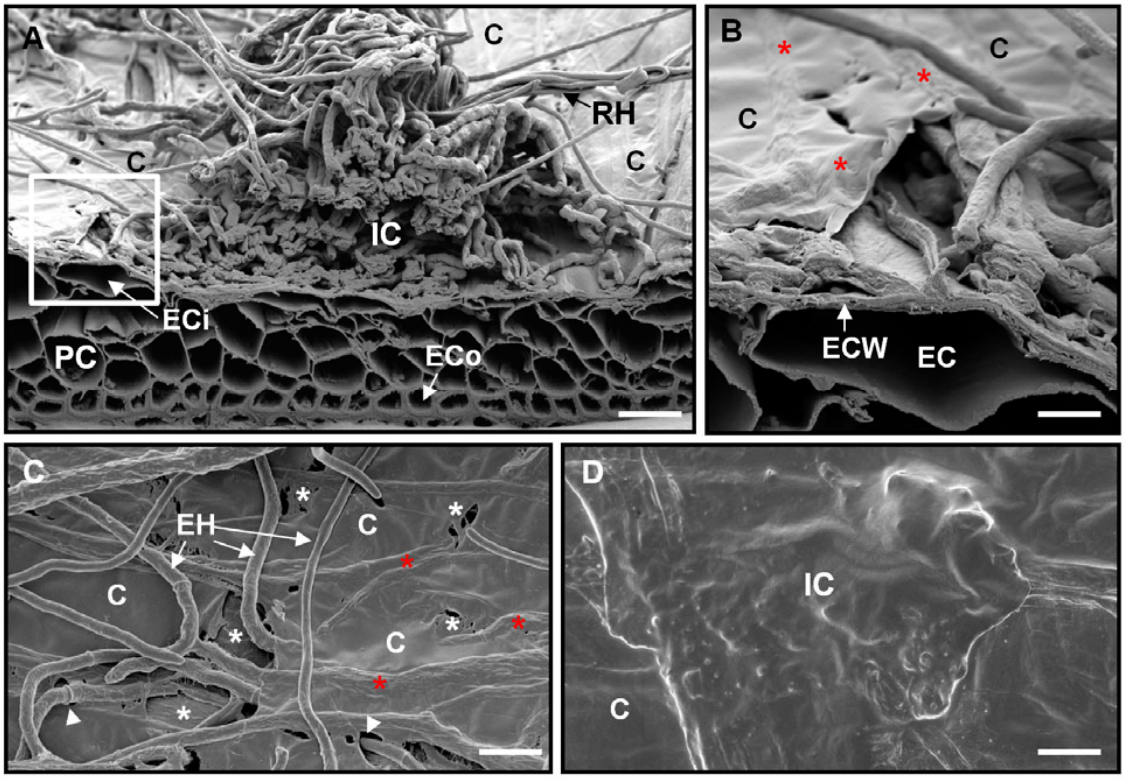

Figure 32: Subcuticulary colonisation of wheat palea by the *GPMK1-GFP* mutant of *F. graminearum*. A-D Scanning electron microscopy of compound appressoria development on palea at 2-3 dpi. **A** Scanning electron microscopy of a complex infection cushion on a palea cut in a cross section. No colonisation of the palea tissue by hyphae was visible. At the margin of infection cushions subcuticulary colonisation was observed (marked by white square). **B** Magnification of subcuticular hyphae (red stars) at the infection cushion as in A. **C** Subcuticulary hyphae (red stars) without co-localisation to compound appressoria. Penetration of the cuticle (white arrowheads) by extracellulary runner hyphae as well as disruption of the cuticle by subcuticular growing hyphae (white stars) was visible. **D** Surface of palea after removing a compound appressorium by an adhesive tape. Deformation and alterations of the cuticle are visible where infection cushions adhered to the plant surface, but no penetration pores are observed. Scale bars: A = 20µm, B =5µm, C= 10µm, D=2 µm **Abbreviations**: **C** Plant cuticle **ECi** Inner epidermal cell (adaxial side) **ECo** Outer epidermal cell (abaxial side), **EC** Epidermal cell, **ECW** Epidermal cell wall, **EH** Extracellular hyphae, **IC** Infection cushion, **PC** Parenchyma cell, **RH** Runner hyphae.

In a cross section of a complex infection cushion on palea at 2-3 dpi no horizontal colonisation of the palea tissue was visible (figure 32, A). Epidermal cells and subepidermal parenchyma cells appeared empty, without intracellular hyphae. However, at the margin of infection cushions subcuticular colonisation was remarkable (figure 32, A and B). Although subcuticular growth of hyphae was observed especially at infection cushions, this mode was also observed independently of compound appressoria (figure 32, C). No penetration pores were observed on the surface of inoculated palea after removal of compound appressorium by an adhesive tape (figure 32, D). Therefore, the results indicate that the mutant is able to penetrate the

cuticle and to colonise subcuticularly, but unable to break the plant cell wall and consequently abolished in tissue colonisation. On inoculated glumes the fungal development was strongly restricted compared to the wild type infection. After germination of conidia and colonisation of the glume surface by runner hyphae, the mycelium did not show further development.

3.3.4 Infection structures of Δ*PLS1-GFP* deletion mutant

Observation of infection structures formed by Δ*PLS1-GFP* mutant on the plant surface revealed that their hyphae had a reduced growth compared to the wild type. Germinated conidia were visible on glumes and paleas 24 h after inoculation in both wild type and Δ*PLS1-GFP*, but the spread of runner hyphae on the surface was strongly reduced in Δ*PLS1-GFP* (figure 33). However, hyphal morphology (shape and organisation) was similar in Δ*PLS1-GFP* and the wild type. The wild type forms compound appressoria such as lobate appressoria and infection cushions at 7-8 dpi (figure 33, A), while at this time of infection, Δ*PLS1-GFP* runner hyphae were much less abundant and did not differentiate appressoria (Fig. 33, B). The Δ*PLS1-GFP* mutant did form infection structures at 16-18 dpi.

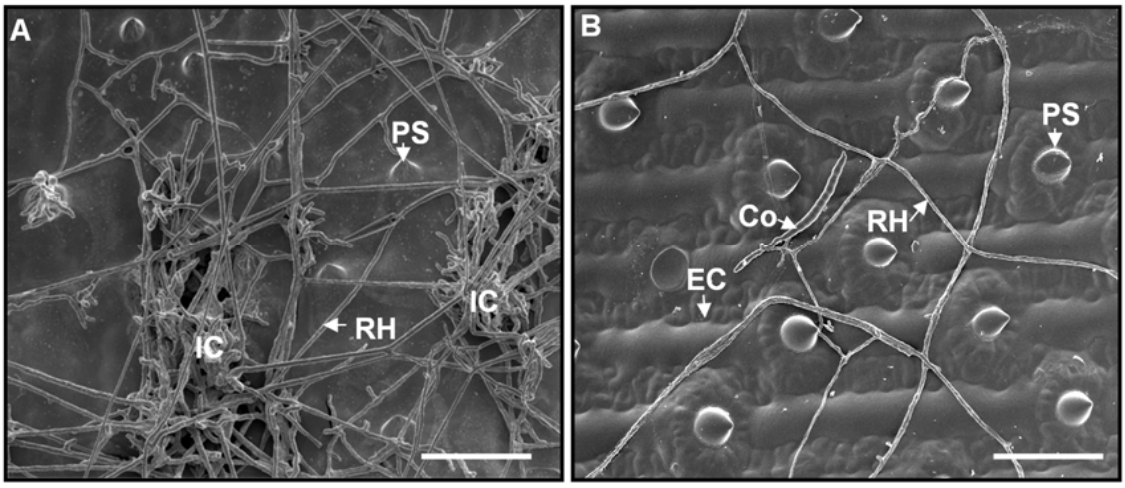

Figure 33: *F. graminearum* mutant Δ*PLS1-GFP* shows a delayed colonisation. **A** and **B** Scanning electron microscopy of the adaxial surface of glumes 8 days post inoculation (dpi) using the wild type (A) and Δ*PLS1-GFP* (B). **A** Network of runner hyphae and infection cushions formed by the wild type. **B** After germination of conidia, the Δ*PLS1-GFP* mutant colonises the surface of glume by long celled runner hyphae. Scale bars=50 µm **Abbreviations**: **Co** Conidium, **EC** Epidermal cell, **IC** Infection cushion, **PS** Papillae silica cell, **RH** Runner hypha.

After this delay, all types of infection structures observed for the wild type were also visible for Δ*PLS1-GFP*, yet at a much lower frequency. The amount of appressoria formed by Δ*PLS1-GFP* on infected glume samples is approx. 5-10% of wild type, although, infection structures of the mutant exhibit similar morphologies. Different stages of appressoria formation were observed for the Δ*PLS1-GFP* (figure 34). Infection structures, including foot structures (figure 34, A), lobate appressoria (figure 34, B), and infection cushions (figure 34, C) were observed. Penetration of the host surface by hyphae arising from infection cushions was observed indicating successful entering of the host tissue (figure 34, C).

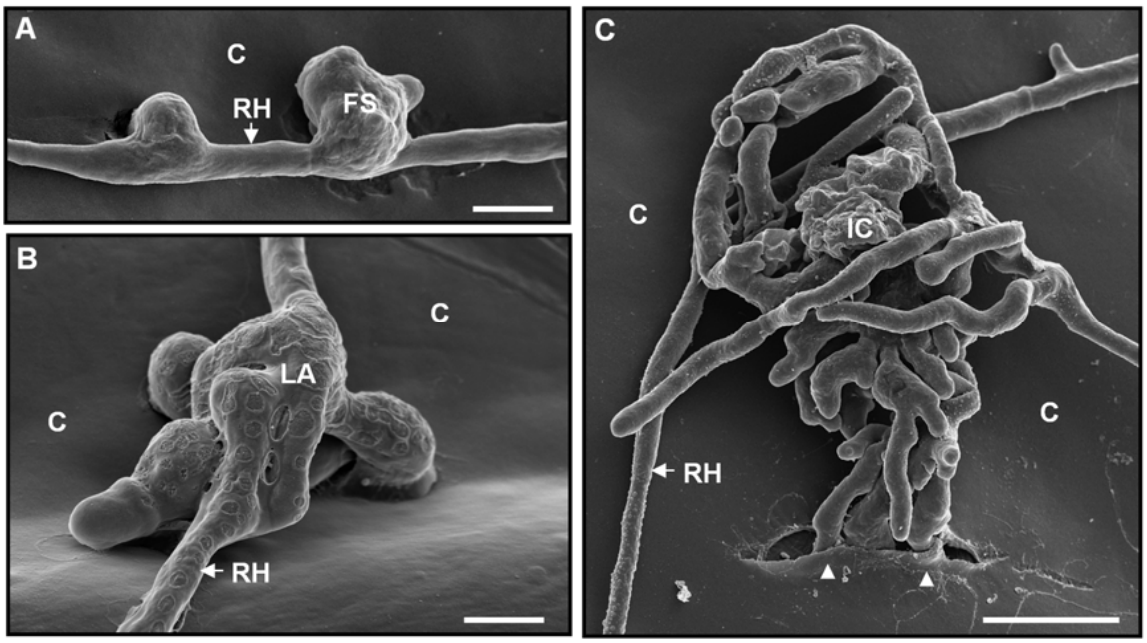

Figure 34: Infection structures of the Δ*PLS1-GFP* mutant of *F. graminearum* on glumes of wheat. A-C Scanning electron microscopy of compound appressoria of *F. graminearum* Δ*PLS1* mutant at 17 dpi. **A** Small foot structures originating from runner hyphae **B** Typical lobate appressorium. **C** Direct penetration (white arrowheads) of the glume surface by an infection cushion. Scale bars:A and B = 5 µm., C=20 µm. **Abbreviations**: **C** Plant cuticle, **IC** Infection cushion, **LA** Lobate appressorium, **RH** Runner hypha.

To investigate the penetration process of Δ*PLS1-GFP*, we removed infection cushions (IC) from wheat glumes and looked for penetration pores in the plant cell wall. SEM revealed penetration pores with 1-2 µm in diameter under infection cushions of wild type (figure 35, A) and Δ*PLS1-GFP* (figure 35, B). Penetration pores were visible under all Δ*PLS1-GFP* removed IC analyzed (n=7). The number of penetration pores differed

among individual ICs ranging from 5 to 28 penetration pores per IC (mean = 12). This variation may reflect the different stages of IC maturation, since the ICs range from 30 to 250 µm in diameter. The removal of a large IC of Δ*PLS1-GFP* (240 x 210 µm) (see figure 36, B) revealed 28 penetration pores underneath the cushion by SEM. This was the highest number of penetration pores observed in this study. Therefore, infection structures of the Δ*PLS1-GFP* mutant are functional with regard to cell wall penetration of the plant.

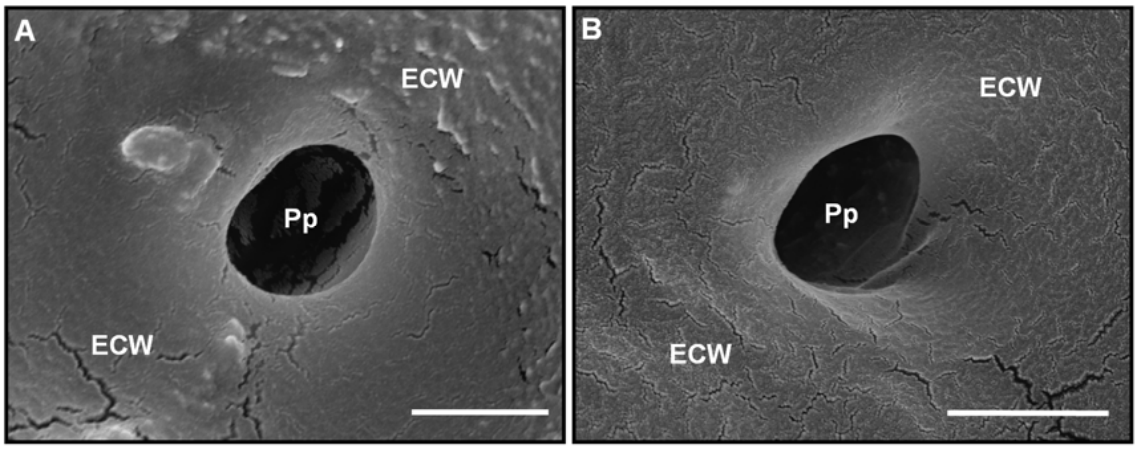

Figure 35: Penetration by compound appressoria of the Δ*PLS1-GFP* mutant is similar to the wild type. A and **B** Scanning electron microscopy of glume surface after removal of infection cushions of the wild type at 8 dpi with an adhesive tape (A) and similar samples of the Δ*PLS1-GFP* mutant at 17 dpi (B). **A** Circular penetration pores of about 1 µm in diameter in the outer epidermal cell wall of glumes underneath infection cushions of wild type strain and **B** Penetration pores of the Δ*PLS1-GFP* mutant. Scale bars = 1µm. **Abbreviations**: **ECW** Epidermal cell wall, **PP** Penetration pore.

Epidermal penetration and colonisation of glumes by compound appressoria the Δ*PLS1-GFP* mutant was observed by LSM of hand cut cross sections (figure 29, C and D). Epidermal penetration and following intracellular invasion took place (figure 29, C) prior to subepidermal colonisation of the glumes (figure 29, D). Intracellular colonisation of host cells as well as direct penetration of neighboring cells was observed. The results demonstrate that the Δ*PLS1-GFP* mutant is able to penetrate cell walls and spread inside tissue of wheat glumes horizontally. The collapse of host cells due to the spread of hyphae is indicated by a lack of blue autofluorescence from the plant tissue. Furthermore, blue fluorescent irregular structures indicate the degradation of the plant (figure 29, D).

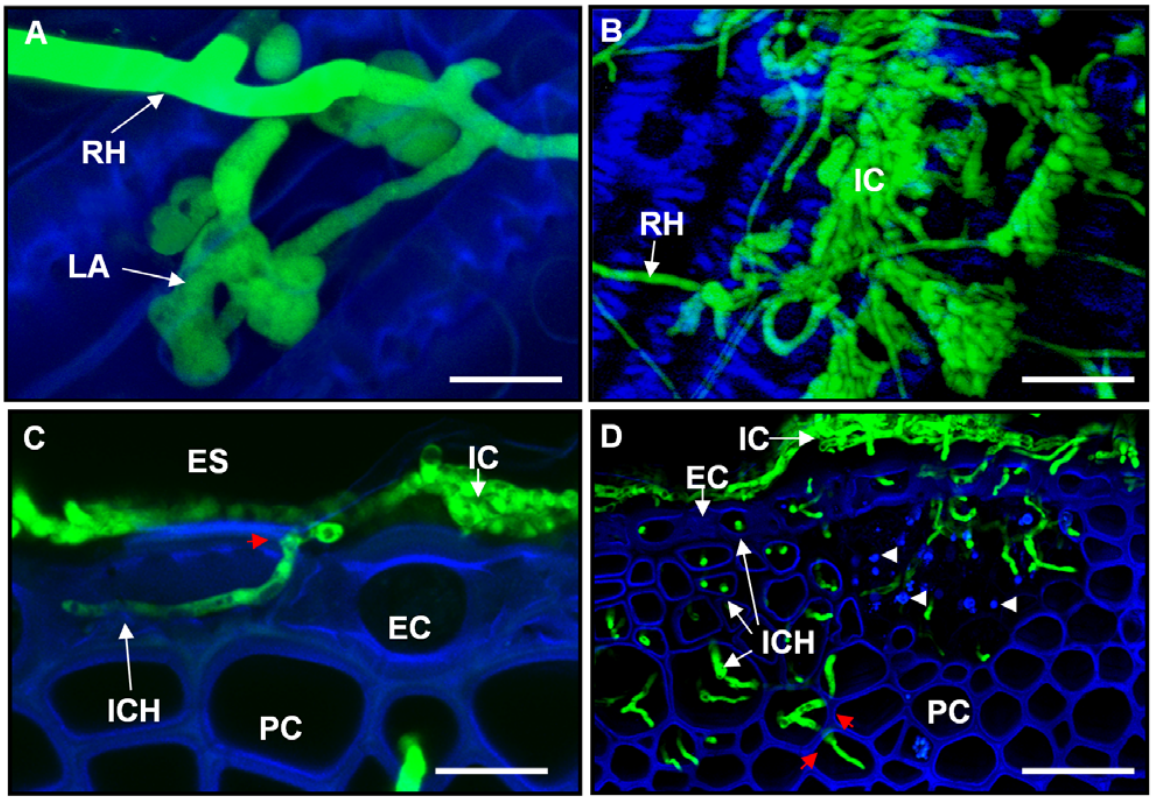

Figure 36: Colonisation of glume tissues by compound appressoria of Δ*PLS1-GFP* mutant. **A-D** LSM maximum intensity projection (MIP) images of constitutively GFP expressing Δ*PLS1-GFP* mutant on wheat glumes (blue) at 17 dpi. **A** and **B** Compound appressoria of the Δ*PLS1-GFP* mutant on the epidermis of glumes. **A** Lobate appressorium as well as **B** complex infection cushions originate from runner hyphae. **C** and **D** Cross sections of inoculated glumes with infection cushions of the Δ*PLS1-GFP* on the epidermal layer. **C** Following penetration (red arrow) of the outer epidermal cell wall intracellular growth of hyphae takes place. **D** Horizontal colonisation of glume tissue by intracellular hyphae is observed underneath infection cushions. Direct penetration (red arrow) of parenchyma cells by hyphae to invade neighbouring cells was visible. The collapse of host cells due to the spread of hyphae is indicated by a lack of blue autofluorescence from the plant cell walls and blue fluorescent remnants (white arrowheads). Scale bars: A and B= 10 µm, C =20 µm, D=50 µm. **Abbreviations**: **EC** Epidermal cell, **ES** Extracellular space, **IC** Infection cushion, **ICH** Intracellular hyphae, **LA** Lobate appressorium, **PC** Parenchyma cell, **RH** Runner hypha.

3.3.5 Infection structures of Δ*FAC-dsRed* deletion mutant

Germination of conidia and colonisation of surfaces of glumes and paleas by runner hyphae took place from 24 h after inoculation as characteristic for stage I of the wild type. However, in contrast to wild type infections, infection stage II is not exhibited by the Δ*FAC-dsRed* deletion mutant. Compound appressoria, such as lobate appressoria and infection cushions are not observed. Instead of compound appressoria, conidia are formed at 4 dpi by runner hyphae and by conidia of the primary inoculum. During ongoing time of infection more sporophores are formed and, even later, many sporodochia developed. In contrast to the wild type infection stage III, sprorodochia production of the mutant is not related to plant necrosis and not attended by the production of aerial hyphae. Compared to the wild type, necroses of palea and glumes were dramatically reduced in infections with the Δ*FAC-DsRed* mutant. Paleas showed slightly brownish necrosis after 3-4 weeks after inoculation with the Δ*FAC-dsRed* mutant, while paleas infected with wild type show first necrosis at 4-5 days after inoculation. Necroses of glumes inoculated with the Δ*FAC-dsRed* mutant were not observed within 4-5 weeks of infection for the majority of samples (approx. 80-90% of inoculated glumes (n=72)). The observed sporulation phenotype of the Δ*FAC-dsRed* mutant is demonstrated by LSM of a palea at 7 dpi (figure 37, A and B) and SEM studies of a glume at 8 dpi (figure 37, C and D). Blue autofuorescence of primary inoculated conidia was detected by LSM that indicates degenerated segments of conidia (figure 37, A and B).

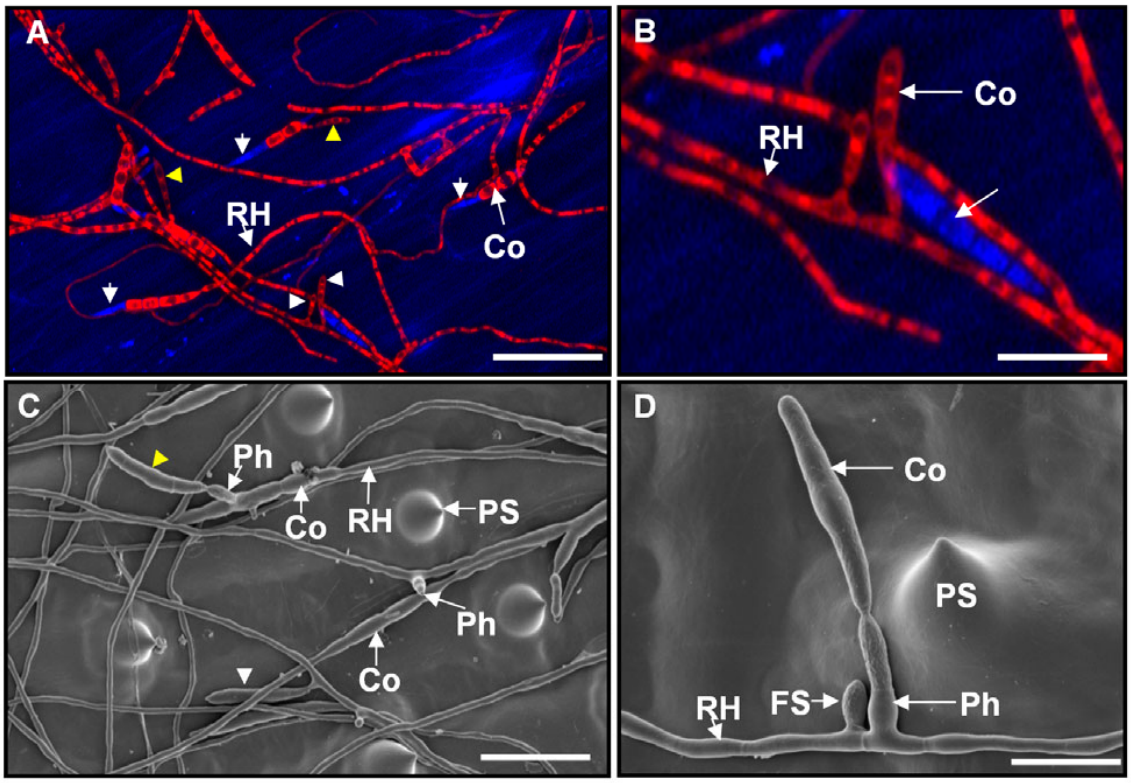

Figure 37: Sporulation phenotype of the Δ*FAC-dsRed* mutant *of F. graminearum* during surface colonisation of wheat husks. A and **B** LSM maximum intensity projections of the constitutively dsRed expressing Δ*FAC-dsRed* mutant (red) on a palea (blue) at 7 dpi. **A** Network of runner hyphae from inoculated conidia spread on the surface of palea. Development of new conidia was visible at runner hyphae (white arrowheads) and at primary inoculated conidia (yellow arrowheads). Blue autofluorescence of primary inoculated conidia (white arrow) is further noted, indicating for degenerated cells of conidia. **B** Higher magnification of developing conidia, which arise from runner hyphae and an autofluorescent conidium (white arrow) is shown. **C** and **D** SEM of the Δ*FAC-dsRed* mutant on the surface of a glume at 8 dpi. **C** New built conidia (white arrowheads) developed on phialides at runner hyphae and at primary inoculated conidia (yellow arrowheads). **D** Higher magnification of a conidium formed on a phialide of a runner hyphae. Foot shaped structure beneath a phialide is further visible, indicating small infection structures. Scale bars: A = 100µm, B= 20 µm, C= 50µm, D=15µm **Abbreviations**: **Co** Conidium, **FS** Foot structure, **Ph** Phialide, **PS** Papillae silica cell, **RH** Runner hypha.

By SEM new build conidia are visible developing apically on phialides (figure 38, C and D). Small infection structures, such as foot structures and infection hyphae, were observed by LSM and SEM studies (figure 38, A and B). For that reason, it was investigated further, whether the Δ*FAC-dsRed* mutant is able to penetrate the plant cell wall via these two types of infection structures. 3D reconstructions of foot structures and infection hyphae were studied for evidences for direct penetration events (figure 38, A). By studying 3D reconstructions direct penetration was not identified undoubtedly, due to varying intensities of the plant autofluorescence (figure 38, A). Applying SEM

the direct contact of infection structures to the surface was visualised reliably. Here, the adhesion of small infection hyphae to host surfaces was visible (figure 38, B). In order to check for successful penetration by infection structures of the Δ*FAC-dsRed* mutant, hyphae including infection structures were removed from the paleas at 7 and glumes at 8 dpi by using an adhesive tape. By SEM observation of the surface of paleas (n=3) and glumes (n=3) after mechanical removal, one single penetration pore was identified on a palea (figure 38, C). However, no penetration pore was observed at glumes (Figure 38, D).

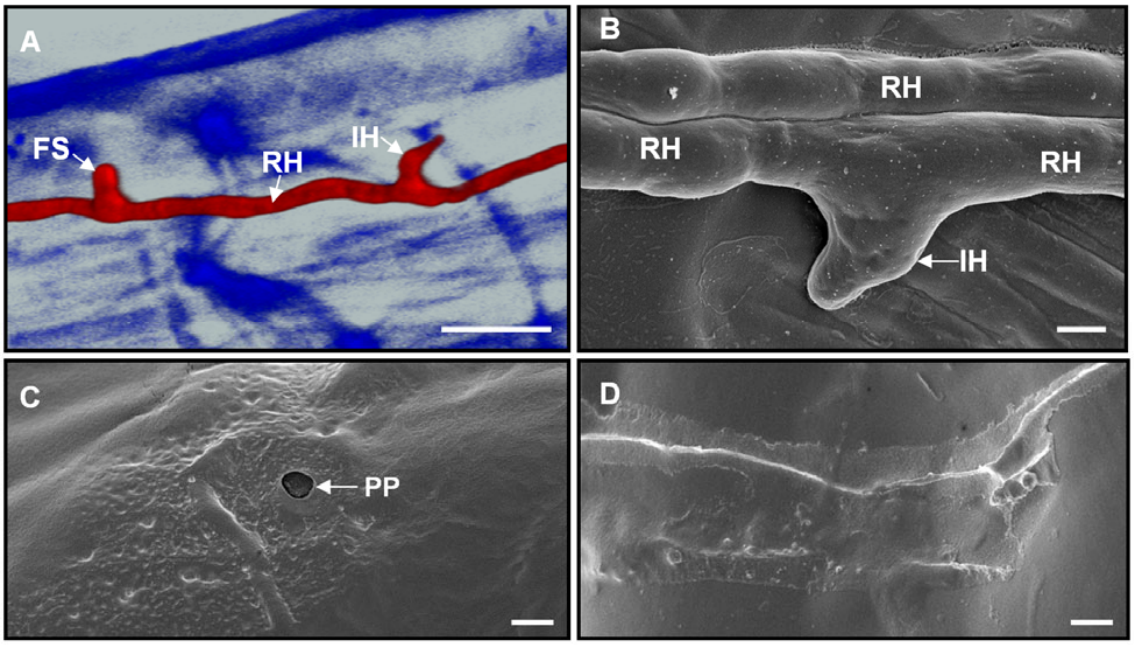

Figure 38: Reduced penetration of the Δ*FAC-dsRed* mutant of *F. graminearum* on wheat husks. A 3D reconstruction from LSM z-stack of an infection hyphae and a foot structure, which originate from a runner hyphae on the outer epidermal cell wall of a palea (blue) at 7 dpi. Although a peg-saped hyphae is visible, direct penetration of the plant is not clearly detected. **B-D** SEM of the Δ*FAC-dsRed* mutant on wheat palea (B and C) and glume at 8 dpi (D). **B** Infection hyphae at runner hyphae attach to the surface of palea. **C** Penetration pore of about 1 µm in diameter in the outer epidermal cell wall of palea after removal of hyphae with an adhesive tape. **D** The surface of a glume similarly treated as in C but without penetration pore at removed hyphae. Scale bars: A= 15µm, B= 2µm C and D= 1,5 µm **Abbreviations**: **FS** Foot structure, **IH** Infection hypha, **PP** Penetration pore, **RH** Runner hypha.

Considering that several hundred infection hyphae were removed from paleas, penetration is most likely an exceptional event. The results lead to the suggestions that the Δ*FAC-dsRed* mutant forms simple infection structures, namely infection hyphae and

foot structures without functional penetration pegs, and that compound appressoria development is completely defective in the Δ*FAC-dsRed* mutant. A defect in penetration of inoculated paleas by Δ*FAC-dsRed* mutant is indicated by the absence of colonisation observed in tissue cross sections of paleas by LSM (figure 39, B) compared to the wild type (figure 39, B). Furthermore, irregular autofluorescence signals are visible in parenchyma cells of the uninvaded palea tissue (figure 39, B). These fluorescence signals of the plant cells appear in the far red spectral range (approx. 640-750 nm) and in the blue range (420-470 nm).

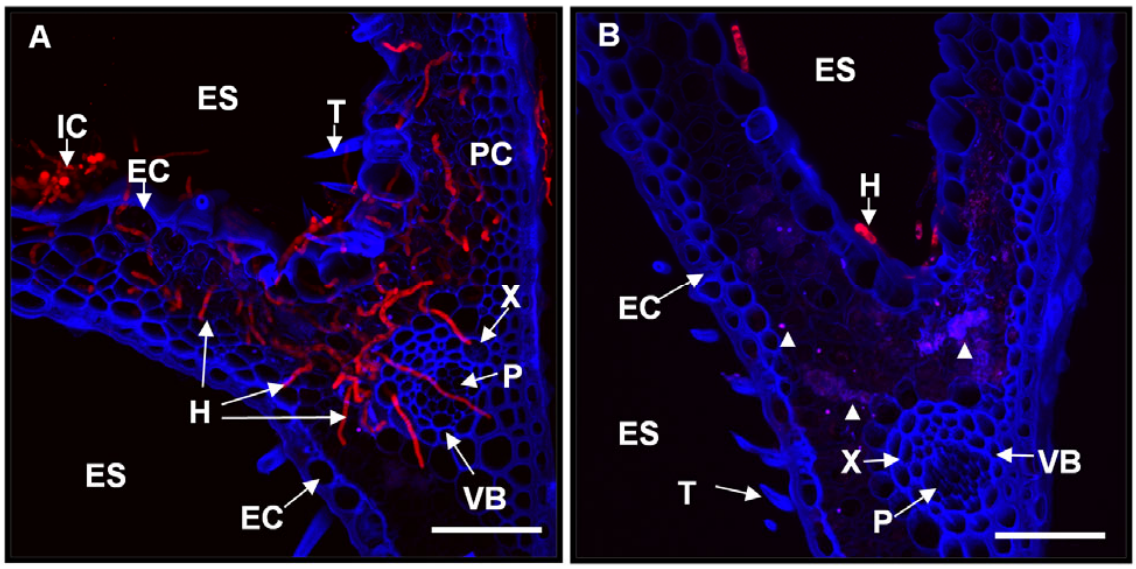

Figure 39: Reduced colonisation of paleas by *F. graminearum* Δ*FAC-dsRed* mutant compared to wild type infections at 8 dpi. A and **B** LSM of palea cross sections inoculated with the wild type Fg.PH-1-Wt-dsRed (A) or Δ*FAC-dsRed* deletion mutant (B)**.** Both fungal strains are visible by constitutive expression of dsRed, while the apolast of palea cells is detected by their blue autofluorescence. **A** Hyphae of the wild type are visible in epidermal cells, subepidermal parenchymya cells and in the xylem of the vascular tissue. **B** Hyphae of the Δ*FAC-dsRed* deletion mutant are detected on the surface of palea, but not inside the tissue. Irregular autofluorescence signals (white arrowheads) in parenchyma cells indicate cell wall alterations. A and B are Maximum intensity projections (MIPs) of z-sereies. Scale bars =80 µm. **Abbreviations: EC** Epidermal cell, **ES** Extracellular space, **H** Hyphae **IC** Infection cushion, **P** Phloem, **PC** Parenchyma cells, **T** Trichome, **VB** Vascular bundle, **X** Xylem.

Hence, no hyphae are co-localised to the fluorescence signals, a plant defense reaction is assumed. In contrast to the mutant, hyphae of the wild type are visible in epidermal cells, subepidermal parenchymya cells, and vascular cells at the same time point after infection (8 dpi). Even after 13-14 dpi hyphae were not visible in cross sections inoculated with Δ*FAC-dsRed* (data not shown) as observed for the wild type infections

(figure 39, A). Nevertheless, during histological studies in one palea cross section hyphae were observed inside an epidermal cell at 8 dpi (data not shown). Following this, it can be suggested that the mutant can penetrate the plant rarely by direct penetration, as shown by one pore by SEM (figure 38, C), but is further unable to precede colonisation inside the tissue. Alternative possibilities to enter epidermal host cells without direct penetration are provided by stomata and woundings of the plant surface. Thereby, the rare events of epidermal colonisation, observed for infections with Δ*FAC-dsRed* might be explained. The fluorescence signal visible in Δ*FAC-dsRed* inoculated tissue sections might reflect cell wall depositions or modifications of the plant as a response to the prolonged colonisation of the host surface by the fungus.

3.3.6 Infection structures of OE *DHS-GFP* overexpression mutant

Glumes and paleas inoculated with conidia of the OE *DHS-GFP* mutant exhibited stage I similar to the wild type. However, compound appressoria, which characterise infection stage II, occurred earlier during infection (2-3 dpi) than the wild type (4-5 dpi). Furthermore, the amount of compound appressoria formed during stage II of infection by the OE *DHS-GFP* mutant (figure 40) seemed slightly higher compared to the wild type at the same point of infection. A high density of compound appressoria was visible on the plant (figure 40, A). Many penetrating foot structures and lobate appressoria were observed (figure 40, B). Complex infection cushions were built up by the OE *DHS-GFP* mutant as well (figure 40, C). Necrosis of glumes and paleas and the following infection stage III were observed as usual for the wild type infection (10-12 dpi), though respectively earlier (6-7 dpi). In summary, all infection stages and infection structures described for the wild type are exhibited by OE *DHS-GFP* mutant more rapid then the wild type.

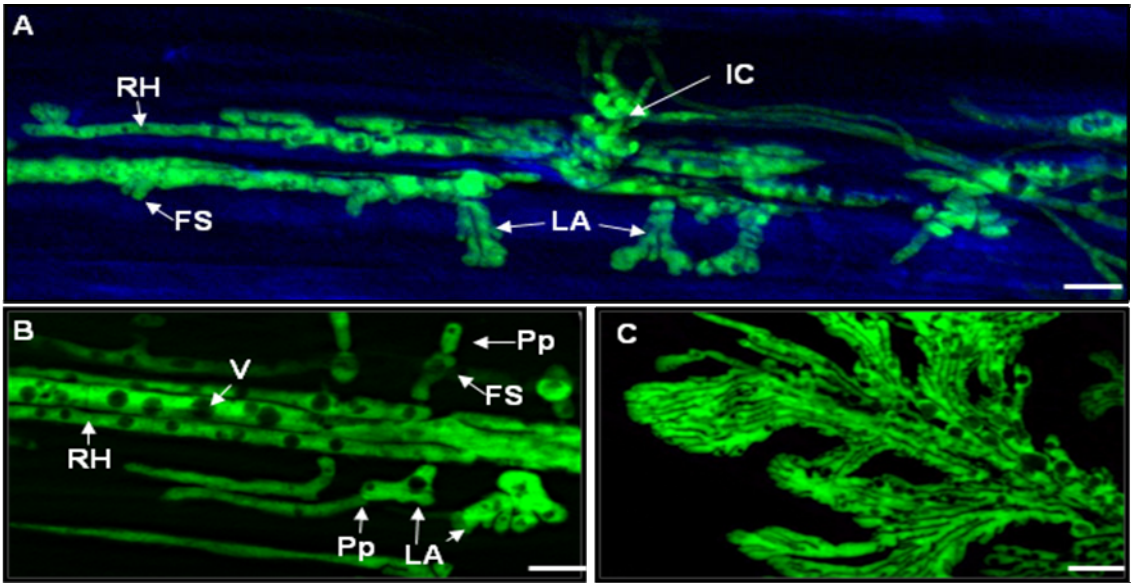

Figure 40: Infection structures of a *DHS* overexpression mutant OE *DHS-GFP* of *F. graminearum* on husks of wheat. A-C Fluorescence microscopy of compound appressoria of OE *DHS-GFP* mutant on paleas at 3 dpi (A) and 4 dpi (B and C). GFP fluorescence of the mycelium is detected by constitutive GFP expression, while the plant tissue is visualised by its blue autofluorescence under UV light excitation. **A** Different types of compound appressoria developed from runner hyphae on the surface of palea. **B** and **C** Higher magnification of compound appressoria. The blue plant autofluorescence is omitted here for a better visibility of infection structures. **B** Morphology of plant penetrating foot structures and lobate appressoria. **C**. Complex infection cushion with the characteristic lobed and agglomerated appearance of cushion forming hyphae. Vacuols in hyphae are visible due to a loss of GFP fluorescence. A and B show Maximum intensity projections (MIPs) of z-series. Scale bars=10µm. **Abbreviations**: **FS** Foot structure, **IC** Infection cushion, **LA** Lobate appressoria,**Pp** Penetration peg, **RH** Runner hypha.

3.3.7 Infection structures of OE *DOHH-GFP* overexpression mutant

In contrast to the OE *DHS-GFP* mutant, infections of glumes and paleas inoculated with the overexpression mutant OE *DOHH-GFP* were remarkably reduced. While germination of conidia and colonisation of the plant surface was exhibited by the OE *DOHH-GFP* mutant similar as described for stage I of the wild type, compound appressoria were not observed until 14 dpi. In figure 41 runner hyphae of the OE *DOHH-GFP* mutant are shown, growing on the surface of a palea at 7 dpi. A dense colonisation of the inoculated surface took place (figure 41, A), but no foot structures and no compound appressoria, such as lobate appressoria and infection cushions, were formed (figure 41, B). In other words, stage II was absent. Furthermore, infection stage III was not exhibited as described for the wild type. Necroses were absent on paleas and glumes until 14 dpi, however, conidia were formed by the OE *DOHH-GFP* mutant. The mycelium of OE *DOHH-GFP* seemed to degenerate from 7 to 14 dpi, which was indicated by a continuous reduction of GFP fluorescence in the mycelium.

3.3.8 Infection structures of *DHS/ DOHH-GFP* overexpression mutant

Infections of palea and glumes with the overexpression mutant of both enzymes *DHS* and *DOHH* were similar to the wild type infections. Infection stages I-III were observed at time points after inoculation similar to the wild type. Infection structures including foot structures, lobate appressoria, and infection cushions developing from runner hyphae were observed during stage II (figure 41, C), but also enlarged infection cushions were visible (figure 41, D). Disease symptoms, such as necroses of glumes and paleas, were undistinguishable from wild type infections.

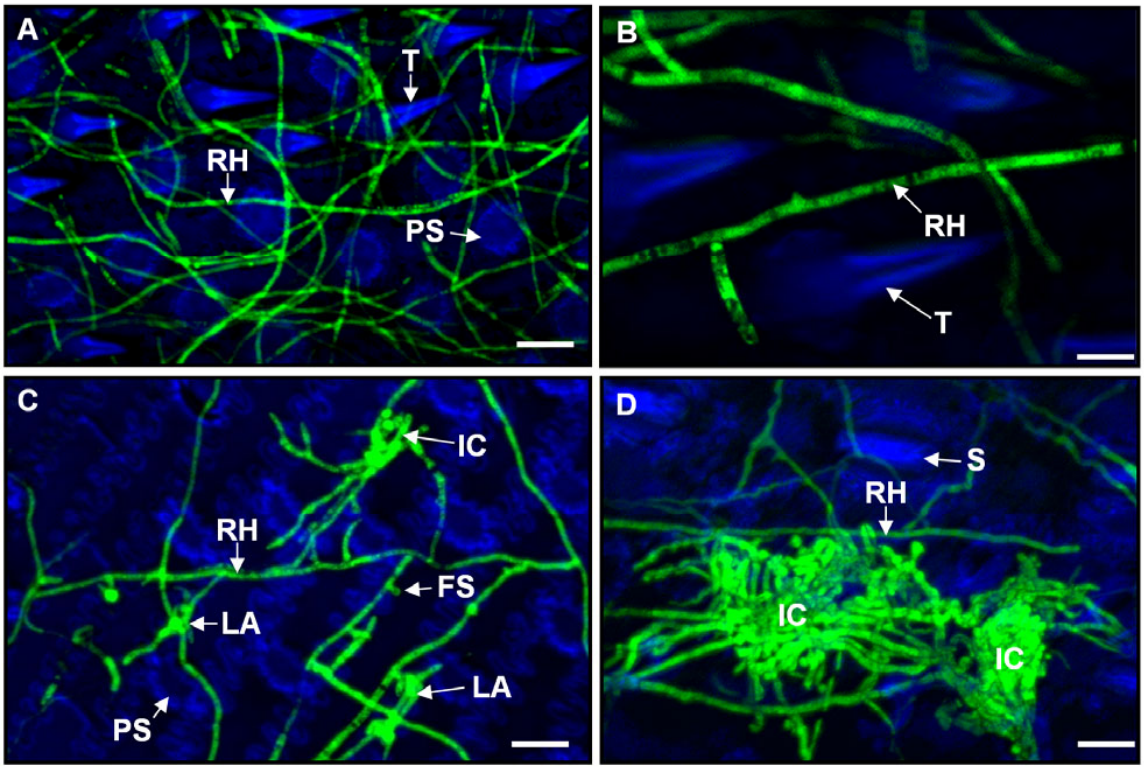

Figure 41: Infection structures of the OE *DOHH-GFP* (A and B) and the double overexpression mutant OE *DOHH*/*DHS-GFP* (C and D) of *F. graminearum* on paleas of wheat. A and **B** LSM of the constitutively GFP expressing OE *DOHH-GFP* mutant (green) on a palea (blue) at 7 dpi. **A** Network of runner hyphae from germinated conidia on the surface of palea. **B** Higher magnification of runner hyphae showed no compound appressoria formation. **C** and **D** LSM of the constitutively GFP expressing OE *DOHH-DHS-GFP* double mutant (green) on a palea (blue) at 7 dpi. **C** Typical development of compound appressoria by foot structures, lobate appressoria, and infection cushions originating from runner hyphae. **D** The characteristic dome shaped and agglomerated appearance of a complex infection cushion of the OE *DOHH/DHS-GFP* double mutant. All images show maximum intensity projections (MIPs) of z-series. Scale bars:A and C =30µm, B=15 µm, D 25µm. **Abbreviations**: **FS** Foot structure, **IC** Infection cushion, **LA** Lobate appressorium, **PS** Papillae silica cell, **RH** Runner hypha, **S** Stomata, **T** Trichome.

3.4 Molecular characterisation of infection structures

3.4.1 RNA isolation from low amounts of fungal material

3.4.1.1 Total RNA isolation

In order to establish work with microscopic amounts of fungal cells, like it is the case for LMD samples, RNA isolation was first established with hyphae of *F. graminearum* treated like LMD samples, except the laser dissection procedure. The RNeasy Micro Kit was applied on mycelium as described in section 2.2.5.1. Mycelium grown in SNA liquid culture was used, which was dehydrated with ethanol, lyophilized, and stored at -80 °C until further use, similar to LMD samples. Decreasing amounts of mycelium from 5 mg (max. amount recommended for by the Kit) down to 0,1 mg dry weight were used for total RNA isolation. To check for RNA degradation the total eluate of the isolated RNA was loaded on an agarose gel and size separated by electrophoresis (figure 42). Thereby, it was tested, whether the preparation procedure using ethanol, lyophilization, and storage at -80 °C had an effect on the intactness of RNA.

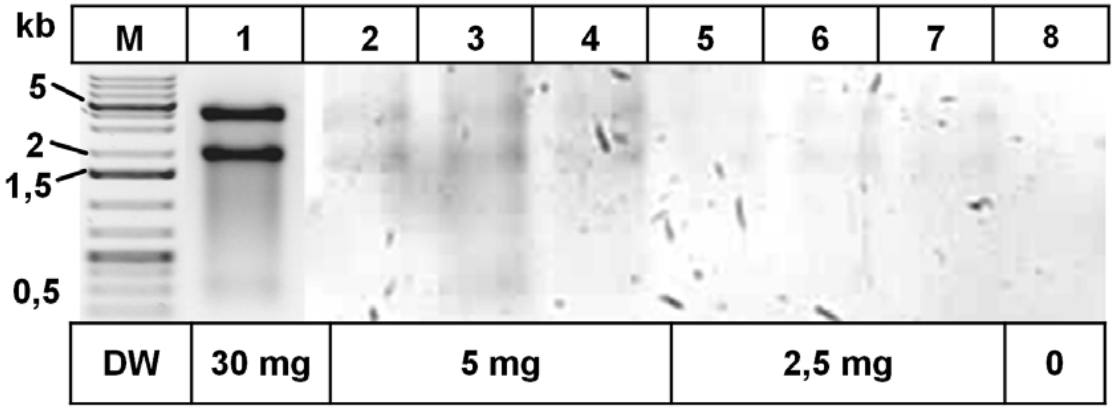

Figure 42: Gel electrophoresis of total RNA extracts from decreasing amounts of lyophilized mycelium of *F. graminearum*. Lane 1: Total RNA isolated from high amounts (30 mg) of lyophilized mycelium with a conventional extraction Kit (Macherey Nagel). Lane 2-7: Total amount of extracted RNA (three replicates) using 5 mg (lane 2-4) or 2,5 mg (lane 5-7) dry weight (DW) of lyophilized mycelium. Lane 8: Empty lane of the gel for background control. M: 1 kb Plus DNA marker.

Figure 42 shows that RNA from 5 mg (lanes 2-4), and 2,5 mg (lanes 5-7) mycelium exhibits two characteristic bands of the 18S and 28S ribosomal RNA (rRNA), similar to the positive control (lane 1). The intensity of bands is strongly reduced, demonstrating lower amounts of RNA according to the dry weight (5 mg and 2,5 mg) of mycelium used. RNA extracts from less than 2,5 mg mycelium (1 mg and 0,5 mg) were undistinguishable from background noise, when seperated in ethidium bromide gels (data not shown). The RNA concentration, the total amount of RNA in samples, and the RNA purity (A260nm/A280nm) in 14 µL total volume of eluted RNA were determined by means of photometry using the NanoVue. The results of three replicate isolations with different amounts of starting material are provided in table 7. The determination of RNA concentration in ng/µL extract (14 µL eluted volume) demonstrates that max. 80 ng RNA/ µL (61,8 ng RNA/ µL ±17,6 ng/µL) were gained from 5 mg of lyophilized mycelium and max. 16 ng/µL (11,6 ng RNA/ µL ±4,1 ng/µL), when 0,1 mg mycelium was used for the RNA isolation. The resulting RNA extracts contained total amounts of. 741,6 ng RNA ±246,8 ng isolated from 5 mg mycelium and 162 ng RNA ±56,7 ng from 0,1 mg mycelium. The results in table 7 show, that a maximum of 980 ng total RNA (mean of 741 ng) was isolated from 5 mg of lyophilized mycelium.

Table 7: Determination of total RNA amounts and RNA purity. The RNA concentration in ng/µL, the total amount of isolated RNA in ng per sample (elution volume), and the RNA purity (260nm/A280nm ratio) at decreasing dry weight of mycelium. Three independent isolations per dry weight were measured 3 times by the NanoVue. Mean values and respective standard deviations (σ_{n-1}) were calculated.

Dry weight (mg)	**5**	**2,5**	**1**	**0,5**	**0,1**
Mean RNA conc. (ng/µL)	61,8	49,5	49,2	32,6	11,6
$\pm\sigma_{n-1}$ RNA conc. (ng/µL)	17,6	11,9	13,2	12,2	4,1
Mean total RNA (ng) per sample	741,6	593,6	688,8	457,3	162,4
$\pm\sigma_{n-1}$ total RNA (ng)	246,8	166,7	184,3	171,4	56,7
Mean A260/A280	2,9	2,1	2,3	2,1	2,1
$\pm\sigma_{n-1}$A260/280	0,4	0,5	0,3	0,1	0,5

***** mycelium was grown in liquid SNA medium for 4 days at 28°C, dehydrated by incubation in concentrated ethanol, lyophilized and stored at -80 °C.

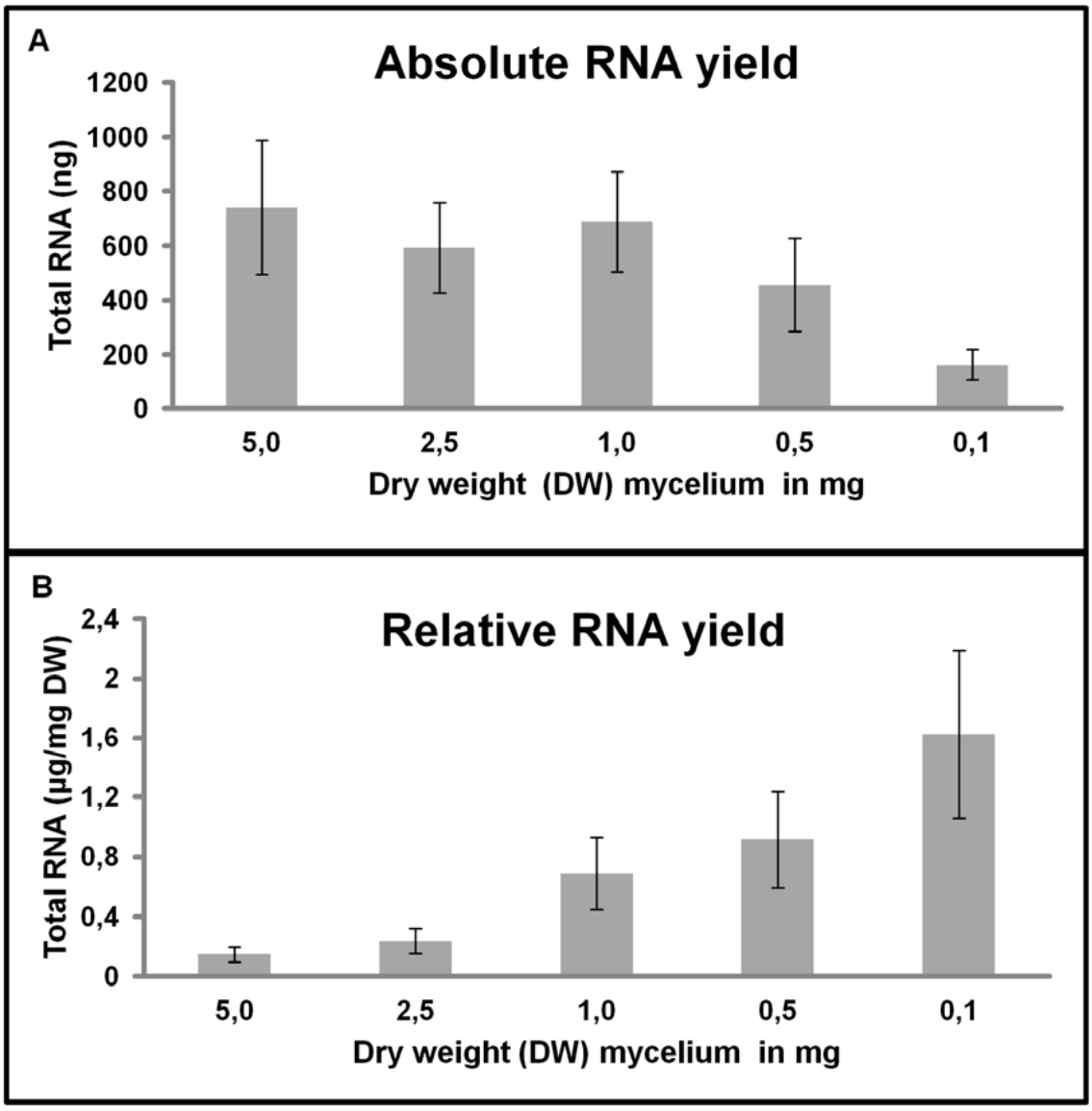

Figure 43: Yield of total RNA using decreasing amounts of hyphae. **A** Absolute yield of RNA in ng per sample using 5,0, 2,5, 1,0, 0,5, and 0,1 mg dry weight (DW) of mycelium. Mean values of ng RNA and respective standard deviations from three independent isolations per dry weight are shown (values in table 7). Each isolate was measured three times by the NanoVue and the resulting mean values were used for further calculations and statistics. **B** Mean values and standard deviations of the relative yield of RNA in ng per mg DW of mycelium are presented. It is demonstrated that the relative yield of isolated RNA increases with decreasing amounts of starting material.

For comparison, 4-20 µg RNA are described to be isolated from 5 mg of fresh mouse tissue (RNeasy Micro Handbook, 2007, p.11). However, RNA yields are described to vary strongly among different tissue/ cell types. Four to five µg RNA can be isolated from 5 mg mouse brain, heart, and lung tissue, while threefold more RNA (15 µg) can be extracted from equal amounts of kidney, liver or spleen tissue (RNeasy Micro Handbook, 2007, p.11). Surprisingly, only 20% less RNA (mean 593 ng) was extracted,

when half of the starting material (2,5 mg) was used for RNA extraction. Equal or even higher amounts of RNA (mean 688,8 ng) were isolated, when 1 mg material was used. Consistent to the decreasing amount of dry weight, less RNA (mean 457 ng) was isolated from 0,5 mg mycelium and 0,1 mg (162 ng) compared to 1 mg samples. An increase of starting material >1 mg dry weight for isolation did not result in a proportionally higher yield of RNA (figure 43, A and B). The higher affectivity of RNA isolation at low amounts (1 mg -0,1 mg) of material (figure 43, B) is consistent with the recommendation of the Kit manual to use less than 5 mg material. This is recommended to avoid overloading of the columns, which are specified for limiting amounts of starting material down to single cells. The standard deviations of RNA concentrations determined by replicate isolations ranged from 27-38%. The variations in RNA content along replicates might reflect the fact that weighing dry material in the <mg range with a fine balance might causes technical errors due to insufficient sensitivity below 1 mg.

The purity of RNA extracts was estimated by the relation of the absorbance at 260 nm (A260) and 280 nm (A280) (table 7). In general, RNA solutions are considered as pure RNA, when the ratio is higher or equal to 2,0. The relative absorbance of A260/A280 in extracts of 2,5-0,1 mg dry weight of mycelium ranged from 2,1 to 2,3 (table 7). This shows that the RNA content in extracts were 2,1-2,3 fold higher than those of proteins or aromatic substances, which can also absorb light of 280 nm wave length. The highest RNA purity with a A260/A280 ratio of 2,9±0,4 was measured in samples using 5 mg starting material. This indicates that a lower starting material results in a higher contamination of RNA extracts with unwanted material, such as proteins and aromatic substances. However, purity values of all isolates were higher than 2,0 and, thus, considered as high purity extracts of RNA.

In summary, it is shown that total RNA with a good purity was detected in all extracts of mycelium treated by ethanol dehydration prior to lyophylization. Although, standard deviations of replicate isolations are high, an estimation of isolated RNA content for the respective fungal material used is provided.

3.4.1.2 RT-PCR conditions for low amounts of fungal material

In order to test for *F. graminearum* specific mRNAs in laser microdissected (LMD) infection cushions, RT-PCR conditions were established with low amounts (1 mg to 0,1 mg dry weight) of lyophilized mycelium, treated like LMD samples, despite the laser dissection procedure (figure 44, A and B). After RT-PCR conditions for 0,1 mg samples were established, the same PCR conditions were performed with infection cushions isolated by LMD (figure 44, C). Detail of the RT-PCR conditions are provided by table 6 in section 2.2.5.2. In three RT-PCRs performed, the mRNA of the 60S ribosomal protein L15 of *F. graminearum* strain Fg.PH-1-Wt was targeted by gene specific primers P_{RSU}fw; P_{RSU}rev (primer details in table 3). Amplification of genomic DNA was excluded by exon-spanning designed primers. 5 µL of each RT-PCR reaction was electrophoresed on an 0,8 % agarose gel to visualise gene specific PCR products with the expected size of 495 bp. The results from gel electrophoresis show, that DNA bands were detected after 35 PCR cycles (figure 44, A) using 1 µL total RNA from 1 mg (49 ng RNA) and 0,5 mg (33 ng RNA) dry weight (DW) of mycelium. However, only a faint specific DNA band is detected using 1 µL RNA from 0,1 mg mycelium (12 ng RNA). Thus, the sensitivity of the PCR was sufficient for 49 to 33 ng total RNA but not for 12 ng total RNA in the RT reaction.

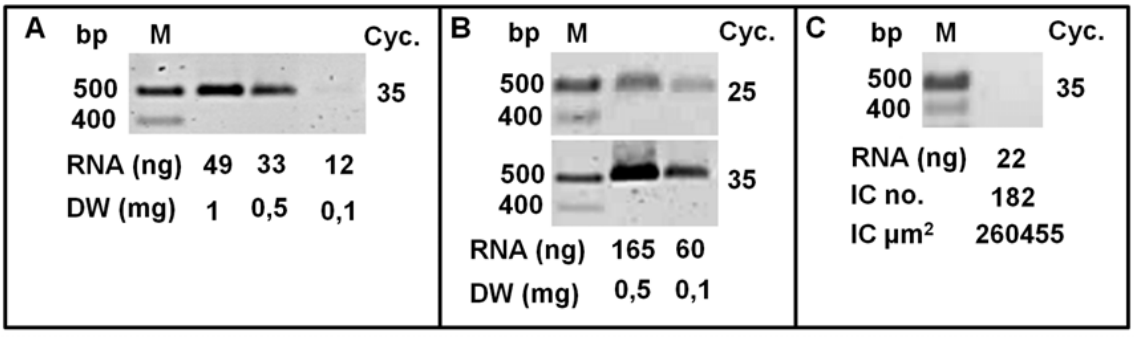

Figure 44: RT-PCR with low amounts of dry weight (DW) of mycelium (A and B) and infection cushions (C). A-C RT-PCR targeting the mRNA of the 60S ribosomal protein L15 of *F. graminearum* strain Fg.PH-1-Wt primers P_{RSU}fw; P_{RSU}rev. 5 µL of each PCR reaction was electrophoresed on an 0,8% agarose gel. For size determination a marker (M) is shown at the left side of each gel picture. **A** Specific PCR bands after 35 cycles for 1 mg and 0,5 mg samples, but a faint band for 0,1 mg samples (total RNA in ng below image). **B** Specific cDNA bands are detected in 0,5 mg samples and 0,1 mg samples already after 25 cycles using the double mount of total RNA (total RNA in ng below image). More intense bands are visible after 35 cycles. **C** No PCR product is detected with similar PCR conditions as shown in B with total RNA isolated from laser dissected infection cushions (IC). The total RNA in ng used for RT- PCR, as well as the total number and $\mu m^2$of isolated ICs are given below the image.

Figure 44 B shows PCR products from RT-PCRs using 5 µL RNA from 0,5 mg (165 ng RNA) and 0,1 mg (60 ng RNA) samples. Specific DNA bands are detected for 0,5 mg and 0,1 mg samples after 35 cycles, but already after 25 amplification cycles (figure 44, B). Accordingly, 5 µL of the total RNA (22 ng RNA) isolated from 128 infection cushions (260.455µm^2) were used for RT-PCR. However, no PCR product was detected on the gel, even after 35 amplification cycles (figure 44, C).

In summary, the results show that sensitive RT-PCR conditions for limiting amounts of RNA form 60 ng down to 33 ng were achieved. However, detection of transcripts in gel electrophoresis failed for infection cushions (n=128, 22 ng toal RNA in RT-PCR) tested. In the next step quantitative real time PCR was performed to improve sensitivity of the PCR method for specific transcripts of *F. graminearum* in LMD isolated infection cushions (section 3.4.1.3.).

3.4.1.3 Quantitative real time PCR of infection cushions

Quantitative real time PCR (Q-PCR) with SYBR Green, was performed to improve the sensitivity for the detection of gene specific transcripts in total RNA extracts of laser microdissected (LMD) material. Gene specific primers $P_{FG\text{-}Ubi\text{-}rew}$ $P_{FG\text{-}Ubi\text{-}rfw}$ (primer details in table 3) were used to amplify a sequence of 112 bp length of the transcript of the ubiquitin conjugating enzyme of *F. graminearum* Fg.PH-1-Wt. For this approach 128 isolated infection cushions (260.455µm^2) were tested. Furthermore, the amount of mRNA template in infection cushions was aimed to be estimated by Q-PCR. The resulting crossing points (Cp) values and quantification of transcripts (in ng/µL) are shown in table 8. The cDNA of *F. graminearum* Fg.PH-1-Wt extracted from hyphae from axenic SNA culture was used (Pos diluted 1:10 and 1:50) as a positive control for PCR detection of the constitutively expressed mRNA of the ubiquitin conjugating enzyme of *F. graminearum*. RNA isolates from laser dissected lyophilized mycelium from axenic SNA culture was used undiluted (Lyo.) and diluted (Lyo.1:5), and served as control for the dissection procedure. By a positive detection of transcript in the later named samples, we could exclude that LMD might degrade mRNA. The Q-PCR results of infection cushions demonstrate that statistically determined Cp values and template concentration differ using the Second-Derivative-Maximum method and the Fit-Point

method. The Cp value is 2 cycles lower using the Second-Derivative-Maximum method (Cp 35; 1,43 ng/µL). Consequently, also the template concentration of infection cushions calculated with the Second-Derivative-Maximum method is 5 fold higher than the respective values determined by the Fit-Point method (Cp 37; 0,29 ng/µL). In contrast to the Second-Derivative-Maximum method, which is an automatic calculation tool using internal standards and algorithms, the Fit-Point method includes a calibration curve, which was performed with similar primers and known template concentration. Furthermore, the specific primer efficiency was included in the Fit-Point method. Therefore, the the Fit-Point method is suggested to provide the more authentic results compared to the second Derivative Maximum method. The Cp values, determined by Fit-Point calculation method, are illustrated in figure 45, A.

Table 8: Determination of Cp (crossing point) and absolute template quantification by Q-PCR. Positive controls (Pos) with cDNA of *F. graminearum* Fg.PH-1-Wt (Pos 1:10 and Pos 1:50 diluted), for lyophilized mycelium* undiluted (Lyo.) and diluted (Lyo1:5) treated by laser microdissection (LMD), and for 128 infection cushions isolated by LMD were tested. Mean values and respective standard deviations ($\pm\sigma_{n-1}$) were calculated by the "Second-Derivative-Maximum" method and by the "Fit-Point" method of the Light Cycler 480 Software.

Calculationion method	Sample	Pos 1:10	Pos 1:50	Lyo	Lyo.1:5	IC
Second-Derivative-Maximum	**Mean Cp**	23,60	26,55	31,25	34,08$^{\$}$	35,00
	$\pm\sigma_{n-1}$	0,03	0,06	0,11	0,12	0,00
	Mean template conc. (ng/µL)	3870	499	19,2	2,70$^{\$}$	1,43
	$\pm\sigma_{n-1}$	71,5	22,2	1,45	0,22	0,00
Fit-Point	**Mean Cp**	21,34	26,05	30,92	33,38$^{\$}$	37,07
	±σn-1	0,72	0,1	0,06	0,21	0,22
	Mean template conc. (ng/µL)	17000	599	20,4	3,70$^{\$}$	0,29
	$\pm\sigma_{n-1}$	9000	0,85	0,54	0,11	0,05

*mycelium used as starting material was grown in liquid SNA medium for 4 days at 28°C, dehydrated by incubation in concentrated ethanol, lyophilized, and stored at -80°C. $^{\$}$One of three measurements was ommited for calculation due to lacking fluorescence detection in the PCR well.

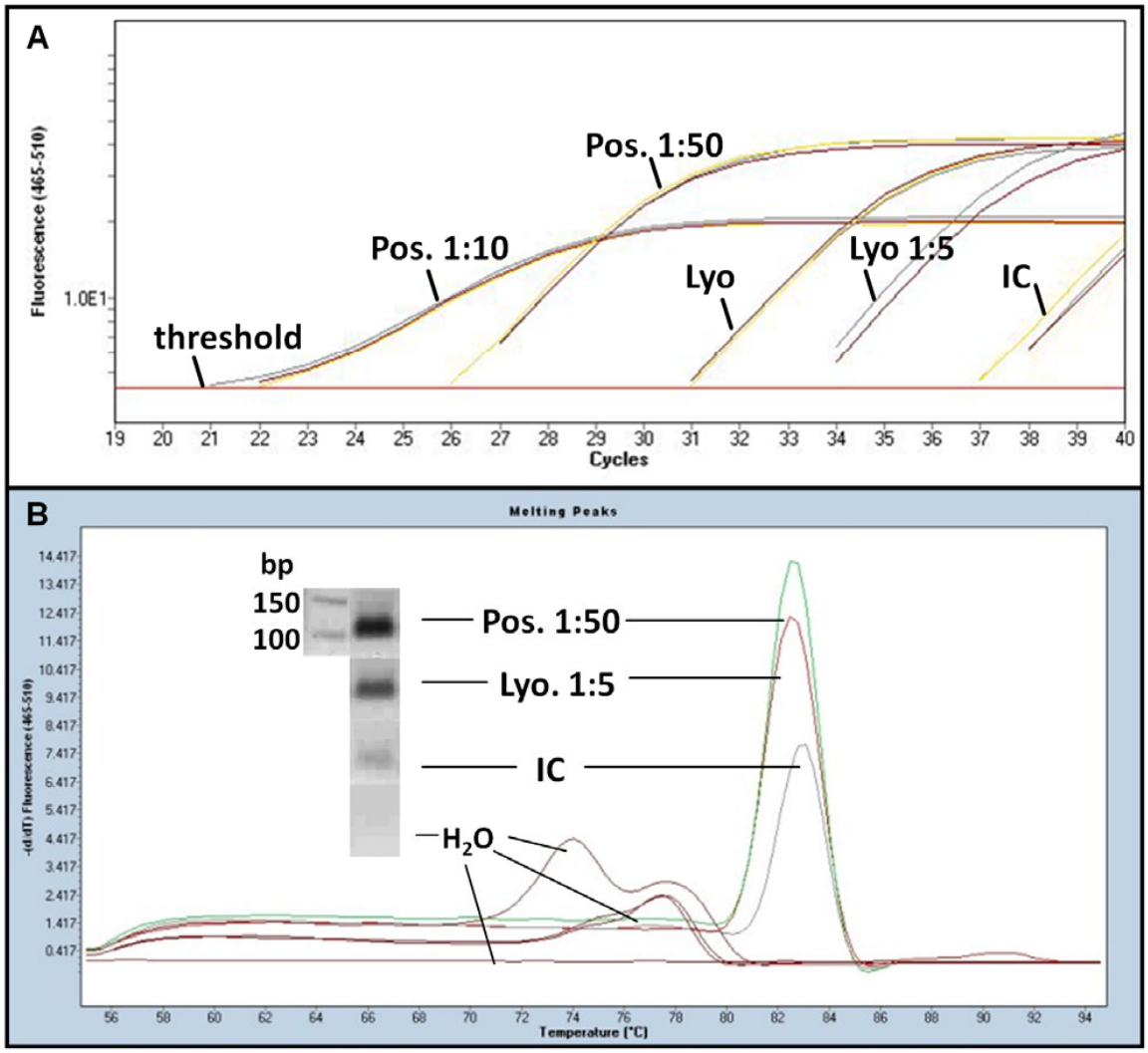

Figure 45: Transcript quantification in infection cushions of *F. graminearum* by quantitative real time PCR. A The logarithm of fluorescence is plotted versus the cycle number, calculated by the Fit-Point method. Three replicates from positive controls (Pos), using cDNA of *F. graminearum* Fg.PH-1-Wt (1:10 and 1:50 diluted), lyophilized mycelium undiluted (Lyo.) and diluted (Lyo 1:5), as well as 128 infection cushions are shown. Analysis (threshold) was set to a fluorescence level where measurements of crossing points (Cp) were done. Mean values and standard deviations ($\pm\sigma_{n-1}$) are given in table 8. **B** Melting curve of samples: Pos. 1:50, Lyo 1:5, infection cushions (IC), and water contols (n=6). A specific PCR product with the expected melting temperature (Tm 83°C) is detected in all samples, despite the water control. However, one or two different PCR products are detected between 70 and 80°C in 3 of 6 replicates using water instead of template. Gel electrophoresis of the Q-PCR products show one bands of about 112 bp (expected size) using $P_{FG\text{-}Ubi\text{-}rew}$.

Here the logarithm of fluorescence is plotted against the cycle number. The detected fluorescence was set to a level where measurements of crossing points were done (threshold line in figure 45, A). The Cp values reflect the decreasing amount of cDNA template in the different samples, with the lowest amount in infection cushions. The flat

fluorescence curve of the 1:10 diluted positive control might result from a too high template concentration, which can disturb fluorescence detection of SYBR green. Melting curves of the PCR products were done to identify possible unspecifically amplified products. In figure 45 B it is illustrated that one specific PCR product with a melting temperature of 83°C was amplified from infection cushions, dissected lyophilized mycelium (Lyo), and cDNA positive control (Pos). The detection of a DNA band with the expected size of 112 bp by gel electrophoresis of PCR products supports a specific amplification of the targeted cDNA (figure 45, B). In the melting point analysis three of 6 replicates of water controls showed one to two different products with melting temperatures (70-80°C). This result indicates unspecific amplifications in water controls. However, by gel electrophoresis of the PCR products no bands were detected in water controls, indicating artifacts during melting point measurements. Concatemerisation of primers by alignment or other secondary structures, which might interfere with SYBR green, can be suggested in this regard. In summary, it is shown that specific transcripts of *F. graminearum* are detectable in laser microdissected infection cushions by Q-PCR

3.4.2 Laser microdissection of infection structures

Laser microdissection (LMD) was used to isolate runner hyphae and infection cushions (see illustration in figure 6). Due to the fact that infection cushions are formed only on planta, the fungus had to be grown on glumes until infection cushions were formed. Then the mycelium had to be transferred on a microscopy slide for LMD, while the plant had to be removed to avoid plant contaminations. The viability of the mycelium as well as the toxin production of the fungus were checked by the fluorescence stereomicroscope MZFLIII, Leica (figure 46, A-C). The constitutive expression of dsRed under the control of the gpdA promoter enabled discrimination of living hyphae from degenerated mycelium of the *TRI5prom*::*GFP* reporter strain. Under the fluorescence stereomicroscope 1-2 mm^2 glume samples containing infection cushions and runner hyphae were selected (figure 46, A-C) and cut with a razor blade.

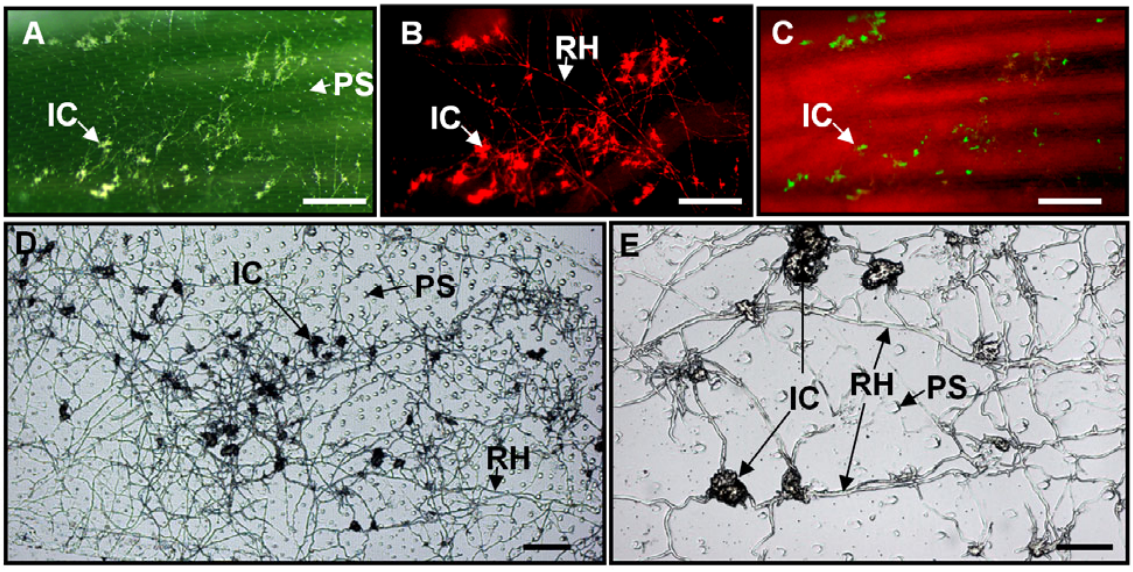

Figure 46: Microscopy of infection cushions (IC) and runner hyphae (RH) of the *TRI5prom*::*GFP* reporter strain on glume (A-C) and on glass slides for laser microdissection (LMD). A-C Typical glume sample selected for LMD by fluorescence microscopy using MZFLIII stereomicroscope (Leica). **A**. Bright field image of the fungus (whitish) on the plant (green). **B** DsRed image shows red fluorescent RH and IC. **C** GFP image shows *TRI5* induction in many IC, but usually not in RH. The plant is visible by red autofluorescence of chlorophyllic tissue. **D** and **E** Bright field microscopy of lyophilized IC and RH after transferring them from a glume on an adhesive glass slide. The PALM microscope was used. **D** Natural architecture of IC and RH is visible with a 5x objective. Regular distributed dots result from papillae silica cells of the epidermis of glumes. **E** IC and RH at magnifications applied for identification and isolation of RH and IC by laser microdissection using a 20x objective. Scale bars: A-C= 300 µm, D= 100 µm, E=20µm.

Cutting was necessary to remain the hyphal architecture after the transfer on microscopy slides by pressing the plant on it. After cutting 1-2 mm^2 samples, they were immediately dehydrated in ethanol and lyophilized to eliminate RNAse activity, which occurs in water solutions. In addition, dry samples instead of fresh samples were necessary for the successful transfer on a sticky microscope slide, sprayed with Liquid Cover Glass. fresh samples of infection cushions and runner hyphae were not transferred on slides sprayed with Liquid Cover Glass successfully. Dilutions of 1:2 and 1:4 v/v Liquid Cover Glass with isopropanol were tested in addition to undiluted Liquid Cover Glass (according to manufactures descriptions). However, the best structural maintenance was achieved without dilution of Liquid Cover Glass. While microscopy was approved using diluted Liquid Cover Glass on glass slides, hyphae adhered less on the slide surface and, thus, total yield of transferred hyphae was reduced. Moreover, the loose adherence of hyphae on diluted Liquid Cover Glass resulted in a higher contamination by the respective unwanted fungal material during isolation of either runner hyphae or infection cushions by the UV-laser. For the profit of less contamination, a lower clarity in light microscopy with undiluted Liquid Cover Glass was preferred. Despite this, identification of transferred infection cushions and runner hyphae by light microscopy was sufficient using undiluted Liquid Cover Glass on glass slides (figure 46, D and E, figure 47, A and E). Approximately 100-200 infection cushions or runner hyphae are possible to isolate within 1 hour. The yield of isolation by LMD was mostly dependent on the degree of maintenance after transferring the mycelium on the slide. The most time consuming part during LMD was the selection of infection cushions (figure 47, B) and runner hyphae (figure 47, F) per free hand draw lines. After selection of either infection cusions or runner hyphae, catapulting was performed by laser impulses. Infection cushions (figure 47, C) and runner hyphae (figure 47, G) were catapulted within seconds against gravity in separate adhesive caps (figure 47, D and H). A total number of 345 infection cushions (square of all elements 1.113.101 μm^2) and a total number of 767 runner hyphae (square of all elements 1.133.163 μm^2) were isolated and used further for mRNA isolation and cDNA library construction.

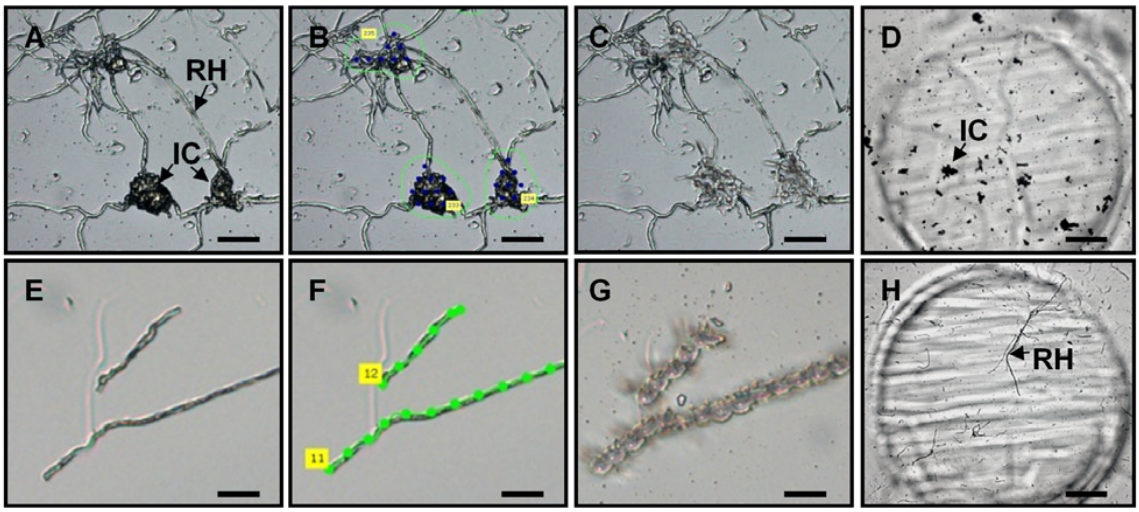

Figure 47: Laser microdissection (LMD) of infection cushions (A-D) and runner hyphae (E-H) with PALM system. **A** Bright field microscopy of infection cushions and runner hyphae on a glass slide. **B** Selection of infection cushions per free hand draw line (green). Blue dots localise where laser impulses for catapulting will take place, using the Auto-LPC function. **C** Infection cushions, shown in A and B, were removed by catapulting them upwards in adhesive caps. **D** Isolated infection cushions are visible in an adhesive cap. **E-G** Isolation of runner hyphae by LMD, as described for infection cushions in A-C, however, using the Line-Auto-LPC function. **H** Isolated runner hyphae in an adhesive cap. The dark rings, visible in D and H, are manufacture embossings at the outside of the adhesive caps. Scale bars: A-C= 20 µm, E-G 10µm, D and H= 150 µm.

3.4.3 cDNA libraries of infection cushions and runner hyphae

Amplification of isolated mRNA by SMART-PCR prior to (long distance) LD-PCR was established with low amounts (<0,1 mg dry weight) of lyophyllized mycelium treated like infection cushions, but grown in SNA liquid culture. Thereby, it was controlled that the mRNA isolation and amplification procedure, in principle, is functional for similarly treated, but more easily accessible material than laser microdissected samples. Determination of the optimal LD-PCR cycle with mycelium by gel electrophoresis revealed that no further increase of PCR product is detected after 18 amplification cycles (figure 48, A). Thus, exponential phase of the PCR reaction can be estimated to take place between 15 and 18 cycles. The optimal number of cyles for exponential phase of amplification in this case is 16, because two cycles below the maximum are recommended by the manufactures protocol. In case of doubt, fewer cycles instead of

many were chosen to avoid over-cycling of cDNA, which may affect representativeness of the transcripts insamples.

For mRNA amplification from laser microdissected infection cushions (total 345 cushions, 1.113.101 μm^2) and runner hyphae (total 767 hyphae, total 1.133.163 μm^2) every PCR cycle was checked by gel electrophoresis for the saturation of amplification (figure 48, B and C). Thereby, the optimal number for amplification was identified after 22 cycles for infection cushions, but after 24 cycles for runner hyphae samples. The lower cycles for amplification of transcripts derived from infection cushions indicate a higher amount of template compared to runner hyphae. A higher yield of mRNA from infection cushions might be explained by the multicellular anatomy of infection cushions, in contrast to runner hyphae. Due to the higher number of cells per isolated infection cushion, mRNA yield might be higher compared to runner hyphae, although comparable square µm were used for mRNA isolation. To provide the necessary amount (3 µg cDNA claimed by LGC genomics (Berlin, Germany)) of amplified cDNA for Illumina sequencing LD-PCR reactions were cycled to the respective optimal cycle number and were pooled.

In addition to the determination of the optimal number of amplification cycles, gel electrophoresis of the cDNA libraries from runner hyphae and infection cushions enables quality assessment of the produced libraries. As it was shown by gel electrophoresis of total RNA, quality assessment was not possible, when less than 2,5 mg dry weight of mycelium was used (figure 42). Considering that mRNA instead of total RNA was isolated from infection cushions and runner hyphae, it is obvious that only the amplified product of mRNAs (cDNA) can be used for optical assessment of template integrity by means of electrophoresis. Gel electrophoresis of cDNA from axenic mycelium (figure 48, A) and the infection cushions (figure 48, B) revealed certain bright bands, which appear within a smear from 0,5-5 kb fragment size. The distinct bands are suggested to reflect certain abundant transcripts of the sample. For comparison, manufactures descriptions are referred to the following. It is described that cDNA amplified from mammalian RNA appears as a smear between 0,5 to 4 kb. The number and position (size) of distinct bands in the smear are described to be different for individual types of tissue. For example, cDNA of mouse liver total RNA or human placenta tissue exhibits bright distinct bands, while human brain, spleen and thymus samples do not display only a homogenous smear. An absence of distinct bands was

explained by a high complexity of the respective RNA pool. Following this explanation a high complexity of the transcriptome of runner hyphae is indicated, because amplified cDNA of this tissue exhibits a homogenous smear after gel electrophoresis without distinct bands (figure 48, C). In general, a low integrity of the RNA used for amplification (e.g. by degradation through RNase activity) will be identified by electrophoresis of the amplified cDNA due to a strong signal at 0,2-0,5 bp size range. Hence, no distinct signal appeared in the samples investigated (figure 48, A-C), mRNA degradation by RNases was excluded and the integrity of RNA was controlled.

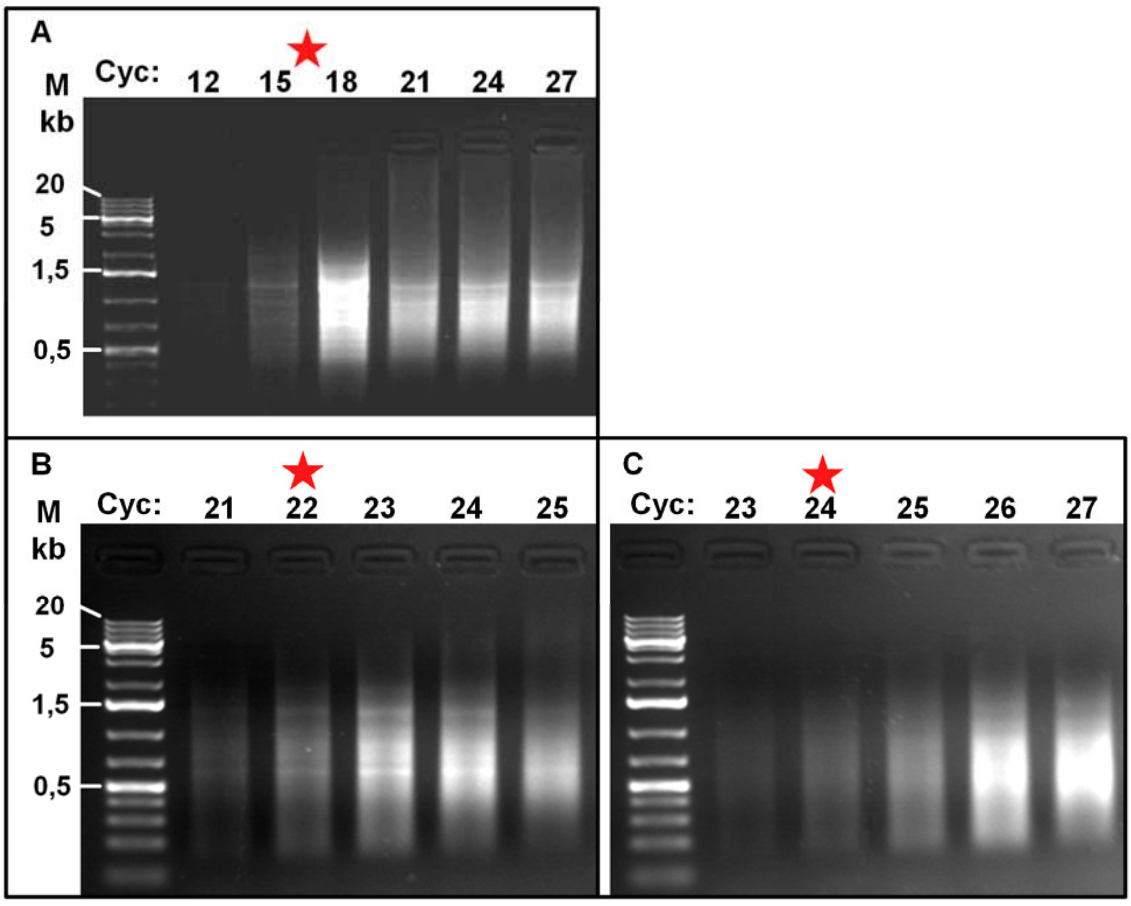

Figure 48: Determination of the optimal PCR cycle (red star) for the production of cDNA libraries by mRNA amplification. A -C 5 µl cDNA were electrophoresed on 1,2% agarose gels in TAE buffer at PCR cycles (cyc) given above gels. **A** The optimal number of cycles for amplification of hyphae grown in liquid culture was 16. Here, 50 µL PCR reactions were performed. **B** and **C** The optimal number of cycles for amplification in 25 µL reactions was 22 for infection cushions (B) and 24 for runner hyphae (C). All three samples (A-C) show a smear between 0,5 and 5 kb size, at the respective optimal cycle. Distinct bands are only detected in sample A and B, while a homogenous smear is visible in sample C. M: 1 kb-plus DNA size marker.

3.4.4 Illumina sequencing of infection cushions and runner hyphae

After Illumina sequencing, statistics and quality assessment of sequencing data (FastQC-format) was done by LGC Genomics using the Software CASAVA Version: 1.8.2. In table 9 the results are summed up. The total number of RAW (unprocessed) reads from cDNA libraries of runner hyphae and infection cushions shows that about 13 % more reads were obtained from the library of runner hyphae compared to infection cushions. 25 % of the raw reads from both samples were identified as linker sequences and omitted from the RAW reads of each sample. The remaining number of liker trimmed reads for runner hyphae was 84.477.235 and 69.971.732 for infection cushions. The trimmed reads represent the number of sequences to be determined. Quality scores for base calling of trimmed reads were determined by filtering reads for a minimum phred quality of 20 (see table 9 and 10). Thereby, it is shown for both tissues that the base calling of 99,7 % of the trimmed reads do not exhibit a lower accuracy than 20 (>99 % accuracy). Furthermore, the average phred quality for trimmed reads exceeded the usual value of 33 for high quality sequencing data in both samples, runner hyphae (34,9) and infection cushions (35,0) (table 9). The sequencing coverage was calculated by dividing the number of base pairs for each tissue through the total genome size of 36,1 mega bases known for *F. graminearum* Fg.PH-1-Wt. The number of sequenced bases for runner hyphae covers the genome size 120 fold, while bases of infection cushions covers the genome size 99 fold (table 9).

Table 9: Statistics and quality data of reads provided by Illumina sequencing of libraries from runner hyphae and infection cushions.

Sequencing results	Runner hyphae	Infection cushions
No. of RAW reads	105.397.626	93.327.391
No. of linker trimmed reads	84.477.235	69.971.732
No. of trimmed reads (Q20)	84.255.834	69.778.375
No. of base pairs after trimming	4.328.161.117	3.587.387.454
Sequencing coverage*	120x	99x
Average read length after trimming	51 bases	51 bases
Average Phred quality after trimming	34.9	35.0

* No. of base pairs after trimming per total genome size of 36.1 mega bases for *F. graminearum* Fg.PH-1-Wt [65].

Table 10: Phred quality scores for quality assessment of sequencing data.

Phred quality score	Probability of wrong base call	Accuracy of the base call
10	1 in 10	90%
20	1 in 100	99%
30	1 in 1,000	99.9%
40	1 in 10,000	99.99%
50	1 in 100,000	99.999%

3.4.5 Bioinformatics of sequencing data from infection cushions and runner hyphae

Mapping of sequencing reads gained from Illumina sequencing as well as differential expression analysis of infection cushions and runner hyphae was done by means bioinformatics in cooperation with Sebastian Piehler and Dr. Ulrich Güldener (Institute of Bioinformatics and Systems Biology, Munich, Germany).

3.4.5.1 Mapping of sequencing reads

The raw sequencing reads, provided in seperate FASTQ files for infection cushions and runner hyphae, were aligned to the reference genome of *F. graminearum* [89] by Sebastian Piehler and Dr. Ulrich Güldener (Institute of Bioinformatics and Systems Biology Munich, Germany) using the programm TopHat. The mapping results show that about 20% less reads of runner hyphae aligned to the reference, compared to reads of infections cushions (table 11). While 92% of the reads from infection cushions mapped to the reference genome of *F. graminearum*, only 72% of the reads from the runner hyphae mapped to the genome (table 11). In contrast to the genome alignment, mapping to the transcriptome resulted in a high amount of unmapped reads in both samples (66% for runner hyphae and 54% percent ininfection cushions (table 11). This might indicate that reads mapped to intergeneric regions. Furthermore, splicing variants of transcripts or not yet annotated genes of *F. graminearum* can be discussed to cause unmapped reads.

Table 11: **Mapping results**. Trimmed reads (Q20) of infection cushions and runner hyphae (see table 9) were aligned to the reference genome and transcriptome of *F. graminearum* strain Fg.PH-1-Wt. § Data were provided by Sebastian Piehler [101]

Alignment	Result	Runner hyphae	Infection cushions
Genome	No. mapped reads§	50.316.469	77.866.840
	No. unmapped reads§	19.461.669	6.388.768
	Mapped/total reads	72%	92%
Transcriptome	No. mapped reads§	23.606.694	38.999.231
	Unmapped reads§	46.171.471	45.256.377
	Unmapped/total reads	66%	54%
Trimmed reads (Q20)	Total no. reads	84.255.834	69.778.375

3.4.5.2 Differential expression in infection cushions and runner hyphae

Differential expression analyses of the transcriptome data of infection cushion and runner hyphae was performed by Sebastian Piehler and Dr. Ulrich Güldener (Institute of Bioinformatics and Systems Biology Munich, Germany). Four different sets of differentially expressed genes have been determined using four different approaches [101]. Only those genes were taken for further analysis, which had been assigned as differentially expressed genes by at least two of these approaches [101]. Genes were considered as differentially expressed, which showed the highest 5% of fold change in the one tissue compared to the other. The abundance estimations were made by means of Cuffdiff and resulted in 723 differentially up-regulated genes in runner hyphae compared to infection cushions and 759 up-regulated genes in infection cushions compared to runner hyphae [101]. In figure 49 a scatter plot of the expression values of runner hyphae vs. infection cushions is shown. Differentially expressed genes are represented by blue dots, while red dots are not differentially expressed genes. As marker genes for differential expression in infection cushions the *TRI*-gene-cluster is marked in the figure 49. It is demonstrated that the trichothecene biosynthesis is induced specifically in infection cushions and that the provided transcriptome data reflect tissue specific features observed by microscopy under real time conditions.

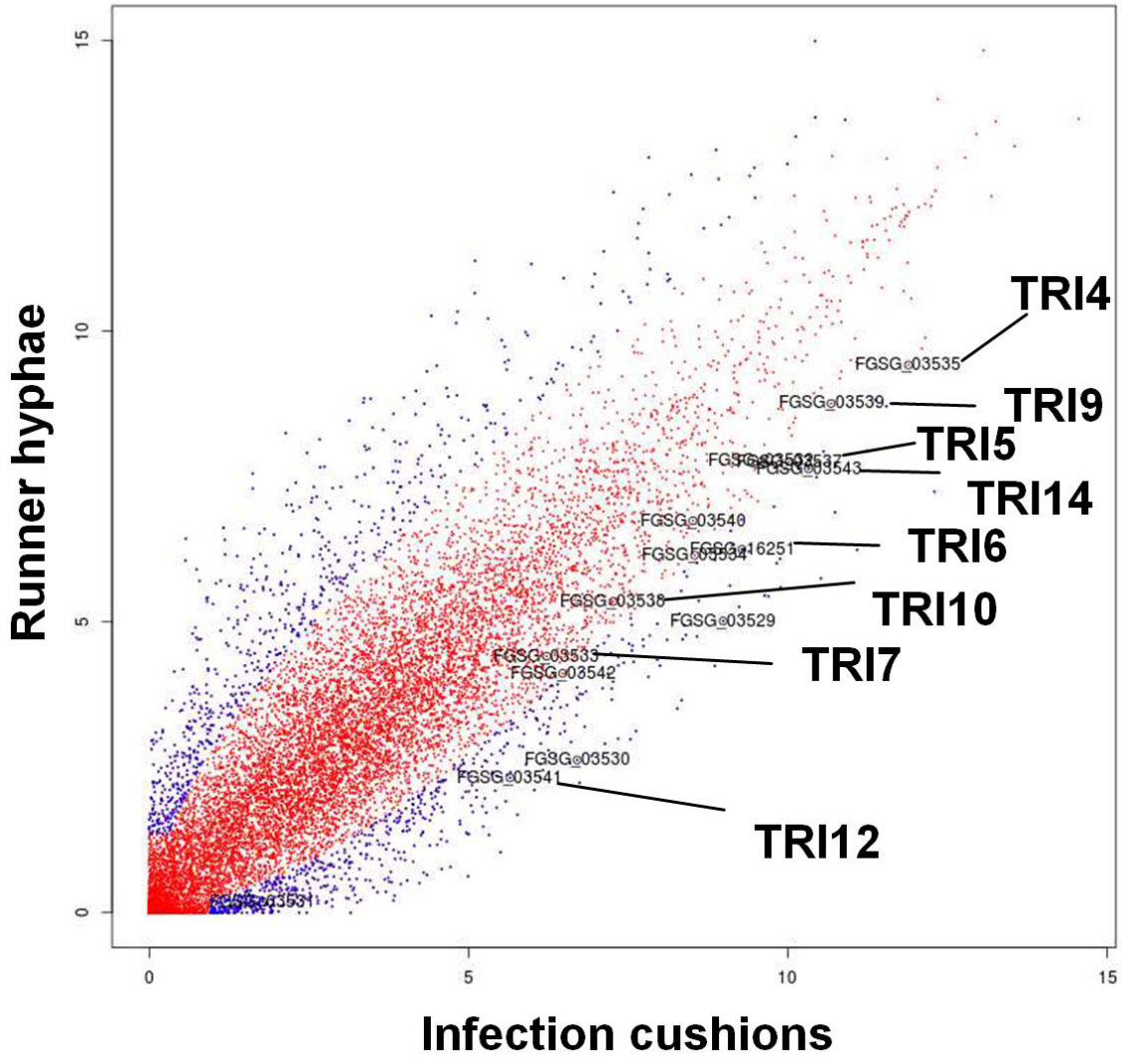

Figure 49: Scatter plot of the expression values of runner hyphae and infection cushions. Blue dots represent differentially expressed genes, while red dots are not differentially expressed genes. Genes showing the highest 5% of fold change in the respective tissue are considered as differentially expressed. The marked genes point out genes of the *TRI*-gene-cluster. The *TRI5* gene expression was observed to be highly induced in infection cushions compared to runner hyphae by fluorescence microscopy of the *TRI5prom*::*GFP* strain. Source: The figure was created and provided by Sebastian Piehler [101], however, the names of *TRI*-genes have been marked afterwards for better clarity.

4 Discussion

4.1 Infection structures of different wild type and reporter strains of *F. graminearum*

4.1.1 The *TRI5prom::GFP* reporter strain represents the wild type of *F. graminearum* during initial infection of wheat

In previous works the initial infection stages I-III on wheat floret tissues, as well as formation of compound appressoria of *F. graminearum* during infection were observed and described [104]. All observations were initially made during studies using the reporter strain *TRI5prom::GFP*. The constitutive expression of dsRed in the mycelium of the reporter strain enabled live cell microscopy of hyphae development during plant infection. The reporter strain used contains an additional genetic modification, which enabled microscopic monitoring of the trichothecene production in the mycelium in real time. Thereby, the induction of trichothecenes specifically in infection structures was observed. Despite the genetic modifications no phenotypic effect was observed for the *TRI5prom::GFP* strain under *in vitro* growth and *in vivo* during wheat spike infection compared to the wild type [22]. Nevertheless, it was important to control the wild type-like phenotype of the *TRI5prom::GFP* strain with regard to the initial infection stages observed and, in particular, the development of compound appressoria. Consequently one objective of the presented work was to perform similar infections with the wild type *F. graminearum* Fg.8/1-Wt and to investigate by means of microscopy. The studies revealed that the infection stages and infection structures are exhibited by the wild type (figure 8) as observed for the *TRI5prom::GFP* strain (Figure 5 and 14) and other fungal plant pathogens e.g. *R. solani* [105]. Due to bleaching the chlorophyllic tissue of infected glumes and paleas by ethanol, necrotic lesions of the plant co-localised to infection cushions of the Fg.8/1-Wt (figure 8, A) were visible as observed for the *TRI5prom::GFP* strain ([18], figure 22, A andC). The observation that lesions develop mainly around bigger or matured infection cushions is consistent with descriptions of lesion formation of *R. solani* [61].

4.1.1.1 The wild type strains Fg.8/1-Wt and Fg.PH-1-Wt form compound appressoria

In the following it was tested, whether the formation of compound appressoria formation was restricted on the *F. graminearum* wild type isolate 8/1. In order to answer this question the *F. graminearum* wild type isolate Fg.PH-1-Wt was investigated for the formation of compound appressoria by means of microscopy as done for Fg.8/1-Wt. However, in contrast to the Fg.8/1-Wt (figure 8), true colour images of Fg.PH-1-Wt (figure 9) are shown, because a colour camera was available for the microscope Axio Imager Z1 at the date when experiments were performed with Fg.PH-1-Wt. The formation of compound appressoria by Fg.PH-1-Wt was expected, since so-called coral-like hyphal structures with lobed, thickened, and branched hyphae were described using *F. graminearum* Fg.PH-1-Wt [16, 17]. In contrast to the latter named studies, which were not focused on exploring infection structures, Rittenour and Harris published [106] a comprehensive microscopic investigation in 2010 about initial infection and penetration of glumes of wheat. The authors clearly documented two different structures, named coral-like hyphal mats [16, 17, 106] and bulbous infection hyphae [14]. We suggest that the coral-like hyphal mats described are similar to infection cushions, whereas the bulbous infection hyphae correlate to foot structures. Lobed and thickened infection structures, which were observed by microscopy of *F. graminearum* PH-1 on wheat [16] and barley [107] are assumed to be identical to lobate appressoria shown here and named after similar structures of many other phytopathogenic fungi [44], e.g. *Rhizoctonia solani*, [52, 59], *Botrytis cinerea* [60], and *Sclerotinia sclerotiorum* [44, 54]. Apart from morphological similarities between coral-like infection structures observed by Rittenour and Harris, 2010 [106] and infection cushions shown here, the time points after inoculations at which respective structures appear differed in the two studies. Rittenour and Harris observed coral-like infection structures already at 24 hpi on glumes, while infection cushions appeared on glumes at 7 dpi in our studies. The incongruence in this concern might be explained by different conditions in infection assays performed by the respective investigators. While 100 conidia were applied per floret tissue (glume and palea) in the assays presented, the 10 fold amount of conidia was used by Rittenour and Harris for inoculation of glumes. Furthermore, in contrast to Rittenour and Harris, who used refrozen glumes for inoculation, fresh glumes were used here. It is assumed that defence reactions of

refrozen plant cells are reduced compared to fresh cells of glumes. Thus, a faster infection of refrozen glumes compared to fresh glumes might be explained. The evidence of compound appressoria formation for both wild type isolates (Fg.PH-1-Wt and Fg.8/1-Wt) indicates that the genetic basis responsible for compound appressoria formation is conserved along different isolates of *F. graminearum*.

4.1.1.2 The reporter strains Fg.8/1-Wt-GFP and Fg.PH-1-Wt-dsRed form compound appressoria

After showing that compound appressoria are formed by genetically unmodified wild type strains Fg.PH-1-Wt and Fg.8/1-Wt it was tested, whether this observation can be made for reporter strains of the respective wild type isolates. By applying fluorescence microscopy on similar infected glumes and paleas, compound appressoria were identified for both, the Fg.8/1-Wt-GFP strain (figure 10) and Fg.PH-1-Wt-dsRed strain (figure 11) without significant differences between each other and the corresponding wild types. Both wild type-like reporter strains express the respective fluorescence protein constitutively in the cytoplasm due to the control of the *gpdA* promoter from *A. nidulans*. This feature enabled z-stack imaging and the generation of maximum intensity projections (MIP) from z-stacks of different infection structures. Thereby the three dimensional structure of infection structure was assessable and more detailed structural and cellular characteristics of infection cushions, lobate appressoria, and foot structures became visible for both isolates (figures 10 and 11). The penetration of the inoculated plant epidermis by compound appressoria Fg.8/1-Wt-GFP and Fg.PH-1-Wt-dsRed was demonstrated by two approaches. Firstly, infection structures were shown to proceed into the underlying epidermal cells by different focal planes of the z-series (figure 12). Hyphae of lobate appressoria were observed, which proceed in focal planes deeper than the outer epidermal layer. Plant penetration through lobate appressoria of the Fg.8/1-Wt-GFP and Fg.PH-1-Wt-dsRed strain was therefore evidential. Secondly, studying histological cross sections of paleas infected with the Fg.8/1-Wt-GFP or the Fg.PH-1-Wt-dsRed strain several penetration pegs were identified, which emanated from infection cushions (figure 13). Further invasion of subepidermal layers of paleas was identified by intracellulary hyphae of the Fg.8/1-Wt-GFP and PH-1-Wt-dsRed

strain (figure 13). Finally, this demonstrated that the reporter strains Fg.8/1-Wt-GFP and Fg.PH-1-Wt-dsRed exhibit infection stages and infection structures (figure 10 and 11) with morphological characteristics similar to the respective *F. graminearum* wild type strains (figure 8 and 9). This proves that the reporter strains reflect the wild type during initial infection and with regard to formation of infection structures. The use of reporter strains in microscopic studies in infection structures gained several advantages with regard to microscopic studies. On the one hand, it was beneficial for the clarity of microscopic images to apply fluorescence microscopic approaches (e.g. z-stack images, MIP generation) to study infection structures. In contrast to that, images of wild type strains from bright field microscopy provide information about only one focal plane of the sample. On the other hand, it was necessary to provide adequate wild type controls to investigate initial infection and infection structures of different deletion and overexpression mutants of *F. graminearum*, which express either GFP or dsRed constitutively. Some of the mutants investigated were in the genetic background of Fg.8/1-Wt and some in the background of Fg.PH-1-Wt (details see 2.1.2). Therefore, microscopy was done with both *F. graminearum* wild type isolates.

4.2 Penetration mechanisms of *F. graminearum* on wheat husks

In order to characterise compound appressoria of *F. graminearum* structurally and biologically the *TRI5prom::GFP* strain was used. After it was shown that the infection stages and infection structures of the *TRI5prom::GFP* strain [18] (figure 14) are similar to the corresponding wild type strains (Fg.8/1-Wt (figure 8) and Fg.8/1-Wt-GFP (figure 10)), it was approved that the *TRI5prom::GFP* strain reflects the wild type infection. Then the *TRI5prom::GFP* strain was used representatively to study infection structures of *F. graminearum* on the macroscopic and microscopic level. The *TRI5prom::GFP* strain was beneficial for microscopic studies on infection structures by the following reasons: 1.) Pre-selection and preparation of inoculated plant samples with high abundance of infection structures were possible under a fluorescence stereomicroscope, due to the constitutive fluorescence of dsRed in the mycelium of the *TRI5prom::GFP*

strain. 2.) This feature also enabled to control the vitality of hyphae sampled for ultrastructural studies (e.g. LSM, TEM; and SEM). 3.) By GFP fluorescence of the *TRI5prom::GFP* strain it was possible to select samples with infection structures, which show toxin production for further microscopic studies. Thus, at the same time observations were also gained about toxin production during penetration. The role of toxins during infection is discussed separately in section 4.3.. In the following section the focus is on the general observations with regard to biological, pathological, and structural characteristics of *F. graminearum*, which were gained by combining different histological and microscopic techniques.

4.2.1 Development of compound appressoria of *F. graminearum*

During stage II of wheat infection foot structures, lobate appressoria, and infection cushions were observed, which are described as different developmental stages of infection cushion formation for other fungal pathogens e.g. *R. solani* [52, 61], *B. cinerea* [60], and *S. sclerotiorum* [44]. A scheme that illustrates the development of infection cushions by *R. solani* is provided by Armentrout and Downer [61]. Lesions appeared when infection cushions were fully developed [61] with regard to size and structural complexity [102]. This is consistent with our observations that lesions develop mainly around bigger infection cushions with dense mycelium (figure 1, A). The model of Armentrout and Downer described for *R. solani* reflects the infection stages that were identified for *F. graminearum* on wheat in previous studies [18]. The increasing size and complexity of cellular structures observed during the time of infection supports the idea of a developmental process. Five different morphological types of infection cushions with a different degree of morphological complexity are distinguished for *R. solani* [102]. A higher complexity of infection cushions correlates with increasing resistance of the host cultivar. Different morphological types of infection cushions of *F. graminearum* were not observed studying infection cushions of different wheat cultivars including Nandu and Sumai3 with low (Nandu) and high resistance (Sumai 3) towards FHB [18]. This observation is in agreement with previous publication, in which no major differences were observed between the resistant wheat

cultivar Sumai 3 and susceptible cultivar Wheaton during initial infection and invasion of glumes with *F. graminearum* [16]. It is published about *S. sclerotiorum* that the complexity of infection cushions varied dependent on the different host species [108]. Simple appressoria formed on leaves of lettuce, oilseed rape, and *Phaseolus vulgaris*, while complex appressoria were observed on leaves of *Phaseolus coccineus* and *Chrysanthemum spp.*. Interestingly, varrying degrees of appressorial complexity appeared on hypocotyl surfaces of *Phaseolus vulgaris*. Indeed, the morphology of infection cushions of *F.graminearum* is highly heterogeneous (shape, height, number of cells/complexity). Nevertheless, it was unclear how to distinguish between different developmental stages and different morphological types of infection cushions [18]. Most probably several abiotic factors that influence fungal growth and development, like humidity, temperature, and exposure of light might also influence the development of compound appressoria. Exposure with light has been shown to influence infection cushion formation of *R. solani* [61]. In contrast to infected cotton hypocotyls incubated with light, infected hypocotyls incubated in the dark exhibit no infection cushions. Interestingly, the absence of infection cushions of dark-grown plants was restored by applying sucrose [61]. The presence of exogenous nutrient sources such as plant exudates as well as sucrose generally promoted increase of branching frequency during cushion development of *R. solani* on artificial surfaces [61, 109]. In this context nutrients are discussed to be necessary for the production of mucilage of *R. solani* [61, 109]. The presence of mucilage seem to be necessary for adhesion of hyphae of *R. solani* to inoculated surfaces [61, 63] and thigmotropic growth, which results in infection cushion formation [61]. In addition, mucilage has been shown to be involved in agglomeration of hyphae that form infection cushions of *S. sclerotiorum* [54]. Thus, a combination of multiple factors including the availability of nutrients and exposure of light influence infection cushion formation of *R. solani*. As already mentioned, development of infection cushions of *R. solani* can be induced on artificial surfaces under certain conditions. Consistently, infection cushions of other pytopathogenic fungi, including *S. sclerotiorum*, *B. cinerea* [44, 61, 108], and many classical appressoria forming fungi [45] can be induced on artificial surfaces, such as glass and plastic surfaces. Usually the hardness and /or hydrophobicity are main factors for the induction of appressoria of other phytopathogenic fungi. Since we were not able to induce compound appressoria formation *in vitro* on agar plates or artificial surfaces, such as glass or different plastic surfaces (data not shown), a host factor or additional nutritions

seem to be necessary for compound appressoria formation of *F. graminearum*. Currently, they were observed only *in planta*. However, more experiments are necessary to elucidate the conditions that influence infection cushion formation of *F. graminearum in vitro* and *in vivo*. Moreover, additional hosts of *F. graminearum* e.g. barley, maize and rice should be investigated with regard to compound appressoria development, to test for a host dependence on wheat. The corresponding results will further elucidate the relevance of compound appressoria formation in other *F. graminearum*-host-interactions. In addition, different *Fusarium species* should be studied with regard to compound appressoria formation. Rodriguez-Galvez and Mendgen published 1995 [110] a study about the infection process of *F. oxysporum* on cotton root tips and indicate similarities to the observations made with *F. graminearum* [18] and other infection cushion devoloping fungi [44]. They observed that germinated conidia of *F. oxysporum* did not immediately penetrate the root, but colonised the root surface and produced a dense net-like mycelium [110]. In addition to that surface hyphae of *F. oxysporum* were described to grow irregularly and produced branches, which penetrated cotton root tip cells. In agreement to runner hyphae of *R. solani* [61, 62] superficial hyphae of *F. oxysporum* grew along the anticlinal cell walls of the host surface [110]. This growth behaviour, however, was not observed for runner hyphae of *F. graminearum* on the wheat floret tissues studied here. Nevertheless, the observations about the infection process of *F. oxysporum* on cotton root tips make this pathosystem especially interesting for studies on compound appressoria formation.

4.2.2 Epidermal penetration by compound appressoria

Although direct penetration of epidermal cells by infection hyphae, infection cushions, and lobate appressoria was evident by LSM z series from previous works [18], several details regarding the penetration process remained unknown. LSM z-scans of the plant surface (tangential/top view) showed hyphae of lobate appressoria and infection cushions proceeding into the epidermal layer of wheat floret tissues, however, penetration pegs were not clearly visible by the LSM approaches performed. Firstly, the z resolution of the series was not sufficient to identify the penetration peg without a

doubt, even not in 3D reconstructions (figure 15). To improve the z-resolution and visualise penetration pegs of infection cushions by means of live cell microscopy, longitudinal sections of infection cushions on the plant were scanned by LSM z-series (figure 17). Although penetration pegs and epidermal colonisation was strongly indicated by the LSM results (figure 15 and 17), the detection of plant cell wall by its autofluorescence was not consistent and reliable enough to study direct penetration of the plant. Therefore, a second disadvantage during fluorescence microscopy was the plant cell wall detection by a not yet characterised autofluorescence, which exhibited varying intensity along the plant sample (figure 17, B). Nevertheless, this technique enabled live cell imaging of the fungus on the plant without applying artificial dyes to the pathosystem. Also, a strong reduction of the natural autofluorescence of the plant cell wall underneath infection cushions provided hints for alterations of the plant cell wall caused by compound appressoria (figure 15). Observing 3D reconstructions it appeared, as if the plant cell wall was degraded below infection cushions. However, SEM of compound appressoria revealed that all compound appressoria were closely attached to the inoculated plant surface (figure 16). Consequently, the loss of cell wall autofluorescence does not reflect a loss of entire cell wall material, but more likely the alteration (degradation, synthesis or modification) of certain cell wall compounds. The chemical identity of these components remains unknown, although different cell wall compounds can be discussed in this regard. It was shown by immuno-gold labelling that *F. culmorum* and *F. graminearum* produced CWDE such as cellulases, xylanases, and pectinases at early stages of infection in wheat spikes [12, 20, 111]. Fungal pathogens can secrete various extracellular enzymes that may be involved in virulence. The disruption of genes encoding pectinolytic enzymes from *Aspergillus flavus*, *B. cinerea,* and *Claviceps purpurea* resulted in the reduction of virulence on respective host plants [9]. A comparative analysis of genomes of the infection cushion forming fungi, *S. sclerotiorum* and *B. cinerea* revealed pectin to be a major nutrient source [112]. Different CWDE have been detected in various *Fusarium spp*. depending on the host and plant tissue infected [9]. The importance of lipases for phytopathogenicity of *F. graminearum* has been shown previously [70, 73, 113]. Moreover, modifications of the plant cell wall can occur by fungal enzymes targeting phenolic compounds. In order to provide access of depolymerases to the backbone wall polymers, particularly from plant hosts of the Gramineae family, fungal feruloyl esterases are secreted, which hydrolyze phenolic groups and, thus, cleave cross-linkadges of arabinoxylan to other

cell wall components [9]. By hemithin LR White sections and toluidine blue staining it was observed that the host cell wall underneath infection cushions is perforated by several penetration pegs (figure 18, A and 20, B). Penetration pegs inside the epidermal cell wall were identified more definitely by toluidine blue staining LR White sections than by fluorescence microscopy, because the plant cell wall is visible more clearly by toluidine staining than by autofluorescence. Furthermore, the thinner LR White sections improve clarity of images compared to free hand cross sections used for fluorescence microscopy. Many defined penetration pores in the outer epidermal cell wall underneath infection cushions observed by SEM (figure 23) further demonstrate numerous penetration pegs that are formed by infection cushions of *F. graminearum* on wheat. This has been shown by similar experiments for *S. sclerotiorum* [54] and *R. solani* [53, 63] by ultrastructural studies. For *R. solani*, in early literature in the 70s, it was debated whether one penetration peg or several pegs are formed at the center of an infection cushion [114]. In addition to that, more than one penetration peg was observed arising from lobate appressoria (figure 19), as it is typically described for lobate appressoria [44]. Consistent with the observation that necroses are visible mainly around bigger cushions, necrotic lesions of cotton hypocotyls infected with *R. solani* are related to the developmental stage/ cellular complexity of infection cushions [61]. In summary, it is demonstrated by the presented studies that both types of compound appressoria of *F. graminearum* penetrate by penetration pegs as it is described for other fungal plant pathogens which form similar types of infection structures. Wounding of the plant due to a high amount of penetration pores might induce hypersensitive reactions that may lead to necrotic reactions surrounding infection cushions (figure 8 A; 22, A and C). Following reaction to pathogen attack, defense responses of the plant commonly involve a production of ROS, the strengthening of the cell wall by oxidative cross-linking of cell wall components, or cell wall appositions with callose or phenolic compounds [115, 116]. A rapid production of ROS has been observed after wounding and can serve as an oxidant for lignification [117, 118]. Pannecoucque and Höfte [62] reported 2009 about an increase of phenolic compound and callose as plant defenses of cauliflower infection by *R. solani*. In the case of the infection cushion producing pathogens *S. sclerotiorum* and *B. cinerea*, the redox status and apoptosis of the host following pathogen attack appear to be crucial for the disease to develop [112]. Genes of *S. sclerotiorum* responsible in lesion formation were identified in EST analysis by Sexton et al., 2006 [119]. The authors compared the transcription of infection cushions

of *S. sclerotiorum* with mycelia grown on agar and lesions formed during infection of *Brassica napus*. In the leaf lesion library the most abundant EST showed homologies (57% amino-acid identity) to a metallothionein from dermatophyte ascomycete *Microsporum canis*. It was demonstrated by Q-PCR that this gene is expressed about two fold higher during infection of leaves than in mycelia grown in axenic culture. Seven amino acids of this metallothionein are identical to those of a metallothionein essential for cuticle penetration in *M. oryzae* [119]. One EST identified in the leaf lesion library showed homology to a cellobiohydrolase I from *Thermoascus aurantiacus*.

4.2.3 Compound appressoria show subcuticular growth

Subcuticular growth of hyphae related to infection cushions and lobate appressoria was demonstrated through different microscopic techniques such as SEM, TEM, and LM (figure 24). Severe alterations of the cuticula, like irregular differences in thickness and cracks of the plant surface, were visible exclusively around compound appressoria by SEM (figure 24, A and B) and supported by LM (figure 24 C) and TEM (figure 24 D and E). Subcuticular growth by lobed hyphae and colloid infection structures, which exhibited thick and ramified hyphae were observed for *F. graminearum* during wheat and barley infection in previous studies [14, 16, 120]. Furthermore, subcuticular growth is a common mode of penetration that is described for infection cushions of *R. solani* [63, 109, 121], *S. sclerotiorum* [69], and *B. cinerea* [112, 122]. The ability of *R. solani* to form infection cushions on red kidney hypocotyls was related to the cuticle thickness of the plant tissue and cultivar resistance [109]. Thus, hints for possible ways to increase plant resistance during FHB might be provided. If an increase of cuticle thickness of wheat plants prevents infection by *F. graminearum*, this will have to be elucidated in future studies. Several other fungal pathogens also exhibit subcuticular growth, although in differing extenses dependent on the fungus, pathosystem, and conditions. Usually, subcuticular hyphae are characterized structurally by flat, branched fungal cells growing between the cuticle and the epidermal cell walls [16]. One of the best known, and predominantly, subcuticular growing fungi is *Venturia inaequalis*, the causal agent of the most important apple disease. For this pathogen cuticle degradation

appeared to be important for pathogenicity [123]. In *V. inaequalis* two genes, cin1 and cin3, are significantly up-regulated during subcuticular growth on cellophane sheets [124]. However, this does not reflect the *in planta* situation. Although, the effects of cutinase disruption were studied in various fungal pathogens, the function of cutinase for pathogenicity remained questionable [9]. Disruption of cutinase genes in *Nectria haematococca* and other fungal pathogens did not affect their ability to adhere to plant surfaces or to penetrate the host cuticle [125, 126]. Cutinase disruption mutants of fungal plant pathogens showed defects in plant infection only in minor cases [127]. It is commonly argued that isoenzymes of cutinases complement the phenotype in single deletion mutants. Despite the contradicting results, cutin monomers have been shown to induce germination and appressorium formation of several fungal pathogens [128]. Moreover, cutin can serve as a chemical signal that results in induction of fungal cutinase expression [128].

4.2.4 Husks of wheat can be invaded through silica cells

An invasion through papillae silica cells by infection cushions and lobate appressoria was remarkable, when analysing the penetration of compound appressopria by SEM, LM, TEM, and LSM (figure 25). Current studies on detached wheat glumes also suggest papillae silica cells as sites of invasion by *F. graminearum* [14]. The authors observed that subcuticular and bulbous infection structures of *F.graminearum* wild type strain Fg.PH-1-Wt were associated with papillae silica cells of wheat glumes. Congruently to our results with *F. graminearum*, hyphae ramified through the pits of the bases of the papillae silica cells and invades epidermal cells. This observation was made in bioassays with detached glumes and intact wheat plants [14]. However, penetration of unspecialised epidermal cells was observed at a similar frequency, especially by SEM (figure 23). In addition compound appressoria are also formed in the absence of papillae silica cells e.g. on inoculated caryopses of wheat [18]. Consequently, the presence of papillae silica cells is not necessary to induce compound appressoria of *F. graminearum*. This assumption is supported by the observations that hyphae often passed papilla without invading them [14]. Solid deposits of silicon

dioxide are formed by many plants at certain intracellular and extracellular locations [129, 130]. The deposits are commonly named phytoliths or plant rocks in literature. Many plants produce phytoliths. The role of silicon (Si) in plant resistance against pathogen attack has been implicated by studies on different pathogen-plant-systems, including dicots and monocots [131, 132]. Plant phytoliths differ in the location on the plant organ, in size and shape with respect to plant species. Phytoliths may exhibit characteristic morphologies used for taxonomic determination in several scientific disciplines [133]. Solid depositions of silicon in plant cells are suggested to increase the natural resistance of plants by acting as a physical barrier against abiotic and biotic stresses. The physiological and molecular mechanisms of silicon metabolism and transport are nearly unknown, at present [132, 131]. It was indicated that specific proteins are involved in the regulation of silification in plants [131]. Incorporation of silicon in plant cells seems to take place by binding to organic cell wall compounds including polysaccharides, proteins, phenolic polymers, e.g. lignin and lipids. It can be assumed that silicon dioxide is involved in cross linking of other cell wall components and probably stabilizes the plant apoplast. Increased resistance of agricultural plants against fungal pathogens by silicon fertilisation through the soil was demonstrated in green house and field experiments. Moreover, silicon fertilized rice leaves of resistant and susceptible cultivars exhibited an increased amount of silicon deposits as well as size of silica cells, especially at the side of inoculation with *M. oryzae* [134]. The results indicate an involvement of plant silification for initial establishment of *M. oryzae* on rice. This suggestion is supported by Hayasaka et al., 2008 [135] who provided evidences that silicon in the leaf epidermis of rice may prevent appressorial penetration. An active role of silicon resistance to powdery mildew (*Blumeria graminis f. sp. tritici*) infection was further indicated in wheat [136]. It was shown that disease symptoms of wheat leaves inoculated with *B. graminis f. sp. tritici* were strongly reduced when wheat plants were fertilized with silicon. Histological and ultrastructural studies revealed defense reactions, including papilla formation, production of callose, and the release of phenolics in silicon treated leaf epidermal cells [136]. An increased production of flavonoids and phytoalexins was detected in leaves of silicon treated cucumber plants following powdery mildew infection [137]. A further indication for an increased plant defense following silicon treatment was provided by the accumulation of phenolic compounds and an enhanced activity of chitinases, peroxidises, and polyphenoloxydases in cucumber plants during infection by *Pythium spp*.

4.2.5 Stomata penetration is an alternative path to enter wheat husks

Concerning the penetration strategy of *F. graminearum,* it is described that the fungus enters floret tissues of cereals by direct penetration via infection hyphae or by natural openings, such as stomata [16, 17, 120]. Due to previous observations made by microscopy, it was suggested that stomata are one primary court for *F. graminearum* to enter husk tissues. Stomatal penetration was described also for *F. culmorum* [20] and *F. nivale* [138] duringwheat infection and several other *Fusarium* spp. [64, 139]. Surprisingly, during entire fluorescence microscopy and SEM studies, entering of wheat floret tissues via stomata were observed only very rarely. Although hyphae frequently grew along or above stomata during surface colonisation in stage I, they did not enter the pore of stomata. Nevertheless, stomata penetration can occur as it was observed during stage II (figure 26). Despite the obvious possibility for the fungus to enter wheat husks by stomata, it has to be pointed out that this was a more exceptional event with regard to the entire observations of this study. Compared to stomata penetration, epidermal penetration by compound appressoria was far more abundant. With respect to this result, it must be considered that stomata are present on adaxial surfaces of glumes in discontinuous rows [16] and represent only a minor percentage of the entire surface inoculated. Thereby, it is possible that penetration through stomata can be observed more frequently when the density of stomata is higher, e.g. on wheat leaves and stems. Summarising the observations, it is concluded that the penetration of stomata is an alternative way for *F. graminearum* to invade floret tissues during FHB infection independent of infection structures. Interestingly, the same observations with regard to stomatal penetration are described for *R. solani* [52, 62], *S. sclerotiorum* [54], and *B. cinerea* [60]. In contrast to that plant penetration through stomata can be highly specific and regulated for other phytopathogenic fungi. For instance, *U. appendiculatus* differentiates appressoria in response to the contact with a ridge formed by the stomatal lips of the guard cell [45]. Thereby the surface signal is perceived by the first 10 µm of the hyphal tip of *U. appendiculatus*.

4.3 The trichothecene biosynthesis is induced in infection structures of *F. graminearum*, but dispensable for initial infection of wheat

The reporter strain enabled microscopic monitoring of the trichothecene production during infection by the expression of GFP under the control of the promoter of the *TRI5* gene, which is a key enzyme during tichothecene biosynthesis. Due to the constitutive expression of dsRed in all cells of the *TRI5prom::GFP* strain, parts of the mycelium without toxin induction were visualised in parallel. The induction of trichothecenes was visible by a strong GFP fluorescence particularly in infection structures (figure 14). As mentioned above, the formation of compound appressoria in general was observed first during studies using the reporter strain *TRI5prom::GFP* [18]. In the study presented here, additional microscopic images of *TRI5* induction in infection structures are provided (figure 14- 26). Thereby, the striking difference in *TRI5* induction between runner hyphae and infection structures was visualised in more detail. The difference in toxin induction in different hyphae might be related to different biological functions of runner hyphae and infection structures. Runner hyphae of plant symbiotic mycorrhiza fungi build an epiphytical network and have specialised functions in absorption of nutrients from the soil, while plant penetrating and colonizing hyphae provide nutrition, such as sugars from the plant [58]. An analogous biological function can be suggested for epiphytic runner hyphae and compound appressoria of *F. graminearum*, with the general difference that nutrition absorbed by runner hyphae on wheat florets can only be derived from the plant surface (e,g. cuticular waxes, cutin, pollen grains). Interestingly, a strong *TRI5* induction was observed for infection structures with a different degree of cellular complexity. Infection cushions, lobate appressoria, and foot structures showed toxin induction by GFP fluorescence (figure 14, B-D). Despite the differences in morphology, all infection structures of phytopathogenic fungi have the penetration peg in common [44-46]. Penetration pegs of infection structures are a thin hyphae specialised in the breaking plant cell walls. Consequentially, penetration pegs are most likely those hyphae that contact the cytoplasm of the host at first. The cytoplasm of the host is the location where trichothecenes act by binding to the 60S ribosomal subunits of the translation machinery of the host [28]. The induction of trichothecenes in infection structures in order to expose host cells immediately with mycotoxins via penetration pegs might be biologically reasonable. However, an effect of trichothecenes during initial infection was not supported by previous infection studies with *TRI5*

knockout mutants on wheat [30, 33, 36]. The studies revealed that the trichothecene deficient mutant is still able to infect the inoculated wheat spikelet in the absence of trichothecenes. In addition, no affect on infection stages and formed infection structures was observed for the trichothecene deficient *F. graminearum* reporter strain Δ*TRI5-GFP* by microscopy (figure 29). Cellular and structural morphology of infection structures was similar to the wild type, thus, an effect of trichothecenes in development of infection structures can be excluded. In addition, brownish lesions were also observed under trichothecene deficient conditions. Consequentially, not trichothecenes but cellular destructions are more likely to be responsible for necrotic lesions surrounding infection cushions. This is contrary to previous publication that DON causes plant necrosis at very low concentrations [29]. It can be suggested that necrosis at infection cushions reflect defense responses of the plant following pathogen attack e.g. oxidative burst [16, 118, 140, 141], apoptosis or cell wall modifications [142, 143]. The observation of a specific mycotoxin induction in fungal infection structures is completely unique description in phytopathology with one exception. The only expression data about infection cushions available at present are from the fungal pathogen *S. sclerotiorum* [119]. It was shown that several ESTs identified in the library of *in vitro* grown infection cushions displayed similarity to genes of the aflatoxin biosynthetic pathway in *Aspergillus spec*.. However, it should be mentioned that *S. sclerotiorum* is not described as an aflatoxin producing fungi. No further information about the expression profiles of compound appressoria exists in scientific literature that could support a specific mycotoxin induction in infection structures. Furthermore, mycotoxin induction in compound appressoria is a unique observation for fungal plant pathogens until now. Mutants of other mycotoxin producing phytopathogenic fungi, in which other mycotoxin pathways are tagged by reporter genes, might clarify this observation in the future. Generally, fungal secondary metabolites, including toxins are regulated by central carbon, nitrogen, and pH regulatory systems [144]. Several Nitrogen and carbon sources as well as low pH play key roles in regulation of mycotoxins such as sterigmatocystin and aflatoxin produced by *Aspergillus* species, [145, 146]. Many nitrogen containing substances like various amines were identified that significantly induce *TRI5* expression [37]. The amine putrecine induced *TRI5* expression and mycotoxin production *in vitro* to levels observed during infection [37]. In addition, it was demonstrated that low extracellular pH is required for DON production in axenic culture. A combination of low pH and amines results in

significantly enhanced expression of the *TRI5* gene and increased DON production. Consistent with previous publications, that showed that ammonium induces *TRI5* expression and DON production *in vitro* [40, 41], we observed *TRI5* induction in hyphae of the *TRI5prom::GFP* mutant on agar plates containing ammonium, but not with nitrate (figure 27, C). It was further shown that the *TRI5prom::GFP* penetrates cellophane membranes on nitrate containing medium, but not if ammonium is the available nitrogen source (figure 28). Previously López-Berges et al., 2010 published silimar results for *F. graminearum*; *F. oxysporum,* and the rice blast fungus *M. oryzae*. The authors observed that hyphae of the species named penetrated cellophane foil with nitrate in the medium of agar plates, but not with ammonium [103]. It can be discussed, whether *TRI5* induction is suppressed by nitrate or not induced under its presence. Similarly, it possible that ammonium is either an inducer of the *TRI5* expression or is not suppressed under the presence of ammonium. The function of trichothecene production of *F. graminearum* during penetration of cellophane remains unknown. However, cellophane penetration assays with a *TRI5* deletion mutant of *F. graminearum* may answer this question in future experiments. The nitrogen pathway is suggested to act as a trigger for the expression of infection-related genes in plant pathogenic fungi. Many genes induced under nitrogen starvation are also up-regulated during plant infection [147-149]. In addition, genes required for pathogenicity of *M. oryzae*, such as MPG1 encoding a hydrophobin [150] and the avirulence gene AVR9 of *Cladosporium fulvum*, were strongly up-regulated *in planta* and under nitrogen limiting conditions [151]. Therefore, nitrogen limitation has been proposed as a key signal for activating the expression of virulence genes [103, 152]. Nitrogen limited conditions are most likely to correspond with the situation during epiphytic growth of *F. graminearum* on wheat husks. Following this assumption it can be suggested that the loss of nitrogen may trigger genes important for initial penetration of the plant cell wall. Nutritions derived by the host, including nitrogen compounds, are accessible after penetration. The favoured availablability of nitrogen might reflect the situation *in vitro* assays on ammonium containing medium. Furthermore, it can be suggested that penetration-related genes are either repressed or not induced under nitrogen starvation (ammonium), while the biosynthesis of DON is induced. The induction of DON production following initial penetration might explain why infection structures and initial infection of a DON deficient *TRI5* deletion mutant was not altered (figure 29). The production of DON and its distribution inside the plant [153] could be involved in the suppression of plant

defense reactions at later stages of infection, because a *TRI5* deletion mutant is not able to pass the rachis [21, 22]. A host specific effect of trichothecenes during spike infection of wheat is indicated, because a DON deficient mutant of *F. graminearum* acts as the wild type during infection of barley [21, 33] and maize [33]. In spike infection of barley the wild type and the *TRI5* mutant both exhibited a reduced spread through the rachis, compared to wheat infections [21]. During infection of maize cobs the wild type produces high levels of DON, however, the DON deficient mutant colonises and cobs similar to wild type [33]. The question remains why DON is induced, even though it does not contribute to the virulence of the fungus on maize and barely. Other virulence factors of FHB that have been characterized to varying degrees for *F. graminearum* [9], and most probably other not yet discovered factors, might play a role regarding the initial infection, which may act independently of DON, as it is described for the virulence factor lipase 1 of *F. graminearum* [70]. The expression of pathogenesis related (PR) proteins, such as a peroxidase (PR1), a β-1,3-glucanase (PR-2), and a chitinase (PR3) was shown to be unregulated in wheat following *F. graminearum* infection [16]. It can be speculated that trichothecenes inhibit the biosynthesis of infection induced PR-proteins, which may defend the plant from fungal attack

4.4 Investigation of different mutants of *F. graminearum* for defects in penetration

Different deletion or overexpression mutants of *F. graminearum* were used for microscopic investigation of the initial infection stages and infection structures on wheat husks (paleas and glumes). The mutants selected for this purpose exhibited reduced FHB symptoms on wheat spikes in previous experiments, performed by different researchers in the group of Prof. Dr. Wilhelm Schäfer (Phytopathology and Genetics, Biocenter Klein Flottbek, University of Hamburg, Germany). One of the mutants (OE *DHS-GFP*), however, caused stronger FHB symptoms compared to the wild type. Another mutant (OE *DHS/DOHH-GFP*) showed no difference to the wild type in previous spike infection. Additional mutants investigated were chosen for microscopic studies on infection structures, because deletion mutants of the respective

homologous gene in other phytopathogenic fungi are known to be related to infection structure induction, formation or function.

4.4.1 The lipase *FGL1* of *F. graminearum* is not important for initial infection

Deletion of the lipase1 gene of *F. graminearum* (*FGL1*) has no negative influence on germination and surface colonisation, as the typical stage 1 was displayed on inoculated glumes and palea as typical for the wild type. Specialised infection structures, including foot structures, lobate appressoria and complex infection cushions (figure 30) developed without morphological and functional differences to the wild type. The secreted enzyme (*FGL1*) of *F. graminearum* is a member of a large class of triacylglycerol lipases [113]. They can catalyze the hydrolysis and the synthesis of ester bonds [70]. These lipases can cleave triacylglycerol substrates into glycerol and free fatty acids. Lipases might be responsible during pathogenesis by degrading wax, cuticle and cell wall compounds. Lipases of phytopathogenic fungi are also suggested to play a nutritional role during certain stages of infection. *FGL1* gene expression of *F. graminearum* was induced already 1 day after inoculation of wheat spikes, thus, a role of the lipase during early stages of infection was assumed [113]. Disruption of *FGL1* gene led to repression of the extracellular lipolytic activity in axenic culture and to reduced symptoms in wheat and maize infections [70]. The deletion mutant was restricted to the inoculated spikelet of wheat [70]. In other pytopathogenic fungi, first indications were provided that secreted lipases act as virulence factors in plant infection [72]. The lipase inhibitor, ebelactone B repressed the lipolytic activity of the lipase1 of *F. graminearum in vitro* and reduced disease severity *in planta* [70]. Due to the presented results, it can be concluded that the activity of *FGL1* is not important for *F. graminearum* to gain nutrition by digestion of cuticular waxes/ lipids during germination and colonisation of the wheat surface, because fungal growth during stage I was not reduced. This, however, does not exclude that other lipases of *F. graminearum* are important in this concern. Trail 2009 reported a number of 27 putative triacylglycerol lipases among 67 putative lipases in the genome of *F. graminearum* [3]. Thus, complementation of the *FGL1* deletion phenotype by

other lipases of *F. graminearum* can be assumed. Moreover, it is shown that *FGL1* is not dispensable for the formation and function of compound appressoria of *F. graminearum* on wheat.

4.4.2 The *GPMK1* MAP kinase of *F. graminearum* is important for the penetration of the plant cell wall

By different microscopic studies it is demonstrated that the *GPMK1* mutant of *F. graminearum* forms compound appressoria like the wild type (figure 31). This is different to previous descriptions from the rice blast fungus *M. oryzae*, [74], *Pyrenophora teres* [76] and many other appressoria forming fungi [154], where the homologous MAP kinase gene is involved in appressoria formation. This contradiction to other phytopathogenic fungi indicates a different regulation mechanism for compound appressoria formation of *F. graminearum* as described for other phytopathogenic fungi. The difference might be explained by the different development of compound appressoria compared to the classical appressoria, which are formed by the majority of fungi investigated in MAP kinase pathways. While compound appressoria develop after extensive epiphytic spread by hyphae, classical appressoria types, like those of *M. oryzae* and *P. teres,* are formed immediately after germination at the tip of the germ tube. It can be suggested that different regulatory pathways might be involved during germination as compared to epiphytic colonisation. It is assumed that the *GPMK1* of *F. graminearum* regulates other processes than appressoria formation. This suggestion is supported by the finding that the homologous MAP kinase Smk1 of the compound appressoria producing fungi *S. sclerotiorum* regulates sclerotia development and hyphal growth, but an involvement in plant infection is not reported [155]. Consistently, *GPMK1* deletion mutant of *F. graminearum* was unable to form perithecia, was reduced in conidiation and showed an altered growth phenotype *in vitro* [73]. Moreover, the results indicate that the Δ*GPMK1-GFP* mutant of *F. graminearum* is still able to penetrate the cuticle and to colonise wheat floret tissues by subcuticular hyphae (figure 32, B and C). Subcuticular growth was also observed during infection of glumes with Δ*GPMK1-GFP* mutant from the *F. graminearum* wild type strain Fg.PH-1-

Wt [14]. Coralloid infection structures forming subcuticular hyphae of the Δ*GPMK1-GFP* mutant were previously observed on inoculated glumes by light microscopy [14]. However, in contrast to Rittenour and Harris, 2010 [14], who did not observe bulbous infection hyphae of the Δ*GPMK1-GFP* mutant, in our studies, foot structures and lobate appressoria were formed by Δ*GPMK1-GFP* mutant similar to the wild type. Under the assumption that foot structures are early stages of infection cushion formation, it seems reasonable that both infection cushions and foot structures are observed. Detailed microscopic studies are necessary to clarify the contradiction concerning bulbous infection hyphae of Δ*GPMK1-GFP* mutants in different wild type strains of *F. graminearum* (Fg.8/1-Wt and Fg.PH-1-Wt). Despite the ability to grow subcuticular, Δ*GPMK1-GFP* mutant was unable to break the plant cell wall, although infection structures developed normally. A function of the MAP kinase for penetration is concluded by the absence of penetration pores in the plant cell wall in SEM studies, after infection cushions of the Δ*GPMK1-GFP* mutant were removed from the plant (figure 32, D). In addition to that, epidermal and subepidermal tissue colonisation underneath infection cushions was not observed, although infection cushions were fully developed with regard to cellular complexity (figure 31 and 32, A). In agreement with the conclusion that Δ*GPMK1-GFP* mutant is unable to penetrate the plant cell wall and, therefore, most likely limited in sources nutrition, stagnation of fungal development at stage II is observed. In several infections with the Δ*GPMK1-GFP* mutant, stage II lasted over 20 days without proceeding to stage III. An impairment of the Δ*GPMK1-GFP* mutant in stage III is in agreement with the *in vitro* phenotype of the mutant. The mutant exhibits a reduced formation of aerial hyphae and conidiation, both characteristics for stage III. It is further indicated that the metabolism of the *GPMK1* mutant is reduced, because the GFP fluorescence of the mycelium decreased with ongoing time of infection. This might be explained by a lower fitness of the mutant due to limited nutrition. Interestingly, in *M. oryzae* surface recognition and the initiation of appressorium formation are mediated by the cAMP signalling, while late stages of appressorium formation, penetration and hyphal growth after penetration are regulated by the *PMK1* pathway [154]. Previously it was published that Δ*GPMK1-GFP* mutant of *F. graminearum* regulates the early induction of extracellular endoglucanase, xylanolytic, and proteolytic activities as well as the overall induction of secreted lipolytic activities [73]. Together with the results presented here, it can be speculated

that secreted enzymes, induced by the MAP kinase *GPMK1,*might be important for *F. graminearum* to break through the plant cell wall of wheat husks.

4.4.3 The *PLS1* tetraspanin mutant of *F. graminearum* is delayed in epiphytic growth, but not defective in penetration

The *PLS1* (*FgPLS1*) of *Fusarium graminearum* encodes a protein, called tetraspanin, and was suggested to be involved in breaking the plant cell wall by penetration pegs of infection structures. Previous studies showed that *PLS1* deletion mutants were reduced in infection of wheat spikes compared to the wild type [78]. Thus, the deletion mutant Δ*PLS1-GFP* was investigated for a defect in penetration during infection of wheat paleas and glumes. The *MgPLS1* deletion mutants of *M. oryzae* develop melanized appressoria, but were unable to form functional penetration pegs. The homologous gene in *C. lindemuthianum* (*ClPLS1*) is additionally required for the correct positioning of the penetration peg at the base of the appressorium [82]. In contrast, *FgPLS1* deletion mutants differ dramatically from previously described *PLS1* deletion mutants of other plant pathogenic fungi. By microscopic and histological studies of the infection process it was shown that *FgPLS1* deletion mutants of *F. graminearum* are delayed in epiphytic growth (figure 33) but still able to form complex infection structures (figure 34 and 36, A nad B). Penetration of the plant by the *FgPLS1* deletion mutants takes place (figure 35, B and 36, C and C), although at a much lower rate. Therefore, *FgPLS1* is required quantitatively for the spread of the fungus on the plant surface and its penetration inside plant tissues. Finally, after a weak colonisation of the inoculated spikelet, the *FgPLS1* deletion mutant is unable to colonise the rachis of the adjacent spikelet. This observation is similar to the pathogenicity defect observed for the lipase and toxin biosynthesis deficient mutants that can not colonise rachis. These shared defects of pathogenicity mutants highlight the importance of the rachilla and rachis as an efficient barrier to the systemic spread of *F. graminearum* [21, 70]. Indeed, *MgPLS1* and *PaPLS1* encoding proteins are suspected to act with other proteins such as the NADPH oxidases encoded by *NOX2* family [156, 157] in a morphogenetic pathway, that is involved in different re-polarisation processes of fungal cells (appressorium penetration

pore, ascospore germination). However, the specific mechanism by which tetraspanin proteins are recruited for different morphogenetic processes is not known. Animal tetraspanins are involved in organizing membrane proteins microdomains, so-called lipid rafts [158, 159]. Fungal tetraspanins are involved in polarized and directed growth in filamentous fungi [81] and the yeast *Saccharomyces cerevisiae*. Future experiments on *FgPLS1* should focus on its localisation in different fungal tissues (e.g. conidia, germ tubes, runner hyphae and infection structures) as well as its cellular localisation in certain membranes (e.g. plasma membrane, tonoplast, microsomes) to rule out the function of this gene for *F. graminearum*.

4.4.4 The *FAC* adenylate cyclase of *F. graminearum* is necessary for compound appressoria formation

The results from microscopic studies performed with the AC mutant of *F. graminearum* indicate a similarity to the regulation of penetration in *M. oryzae*. As mentioned above, the surface recognition and the initiation of appressorium formation are mediated by the cAMP signaling in *M. oryzae*. Adenylate cyclase deletion mutants of *M. oryzae MAC1* were unable to form appressoria on a hydrophobic surface and are apathogenic on its host plant [86, 154]. A regulation of appressoria formation by cAMP signalling pathways was also shown for other phytopathogenic fungi, such as *Cochliobolus heterostrophus*, *Colletotrichum lagenarium*, *Colletotrichum gloeosporioides,* and *P. teres* [154]. A similar phenotype was observed with the Δ*FAC-dsRed* mutant of *F. graminearum*. The mutant did not form compound appressoria, such as lobate appressoria and infection cushions (figure 37 and 38). Although small infection structures, such as foot structures and infection hyphae, were observed by LSM and SEM studies (figure 38, A and B), plant penetration was an acceptional event on paleas (figure 38, C) and absent on glumes (figure 38, D). A defect in penetration of inoculated paleas by Δ*FAC-dsRed* mutant is also indicated by the absence of hyphae in tissue cross sections of paleas (figure 39, B). 1,16-hexadecanediol is described as a chemical signal for the activation of an adenylate cyclise that induces appressorium formation of *M. oryzae* [83]. For the rice blast fungus *M. oryzae* it is proposed that chemical and

physical (hydrophobic surface) stimuli are involved in the induction of appressorium formation. At present nothing is known about physical or chemical signals that induce compound appressoria of *F. graminearum*. It should be ruled out in experiments in the future, which factors and conditions are involved in this regard. Moreover, the cAMP/PKA pathway is involved in regulation of hyphal growth and asexual/sexual sporulation in many fungi [83, 84, 86]. Deletion mutants of the adenylate cyclase gene *MAC1* of *M. oryzae* display reduced vegetative growth as well as defects in conidiation and conidial germination [85]. A defect in conidiation is also observed for many deletion mutants of adenylate cyclases of other phytopathogenic fungi [83]. Surprisingly, we observed an enhanced sporulation of the Δ*FAC-dsRed* mutant during infection of wheat paleas and glumes (figure 37). At 4 dpi conidia were developed at runner hyphae and at conidia of the primary inoculums. This indicates that the adenylate cyclase of *F. graminearum* regulates the suppression of conidiation. Interestigly, the deletion mutant of a G-protein alpha-subunit gna-3 from the filamentous fungus *Neurospora crassa* exhibits premature and dense conidiation [160]. The gna-3 mutant produced conidia in liquid culture, under darkness, although conidiation is suppressed under the conditions in the wild type situation. Conidia of *N. crassa* develop at aerial hyphae, which are shorter at the gna-3 mutant compared to the wild type. Supplementation with exogenous cyclic AMP (cAMP) restored wild type like conidiation in the *gna-3* strains. The conidiation and aerial hypha defects of the D*gna-3* strain are similar to those of a previously characterised adenylyl cyclase mutant, *cr-1* of *N. crassa* [161]. The predicted amino acid sequence of *GNA-3* is most similar to the G-protein alpha-subunit from the saprophytic fungus *Podospora anserine*. It should be investigated in ongoing studies, whether a homologous *GNA*-3 gene exists in the genome of *F. graminearum*. In case that the deletion mutant displays a similar phenotype like the Δ*FAC-dsRed* mutant, an activation of the adenylate cyclase by the alpha-subunit can be assumed. Thereby, the *FAC* medited cAMP signal transduction pathway in *F. graminearum* would be clarified further.

4.4.5 *DHS* and *DOHH* regulate the speed of compound appressoria development and disease severity

Microscopic investigation of initial infection of paleas and glumes inoculated with overexpression mutants of the enzymes, deoxyhypusine synthase *DHS* (OE *DHS-GFP* mutant) and deoxyhypusine hydroxylase (OE *DOHH-GFP* mutant) of *F. graminearum* as well as the double mutant of both (OE *DHS/DOHH-GFP* mutant) indicate a regulatory function of these enzymes during pathogenic interaction of the fungus on wheat, as suggested previously [87]. The *DHS* and *DOHH* emcoding enzymes catalyze the activation of the eukaryotic initiation factor 5A (eIF-5A) by two enzymatic steps [94]. The activated eIF-5A transports a certain, so far unknown, subset of cellular mRNAs from the nucleus to the ribosomes and, thereby initiates their translation [162, 163]. The constitutively GFP expressing reporter mutant OE *DHS-GFP* is faster in the entire process of infection on paleas and glumes, because all typical infection stages of the wild type appear earlier compared to the wild type. Moreover, the development of infection structures seems to be enhanced, because a high density of compound appressoria (figure 40) was observed at earlier time points after inoculation as typical for the wild type. The opposite phenotype during infection was observed with the OE *DOHH-GFP* mutant (figure 41, A and B). The mutant does not form compound appressoria types on glumes and paleas of wheat and caused no necroses, although the germination and epiphytic growth was not affected (figure 41, A and B). The results lead to the conclusion that the development of compound appressoria of *F. graminearum* is regulated by the transport of mRNAs through the eIF-5A. Interestingly, the double mutant showed a similar infection behavior as the wild type in comparable studies (figure 41, C and D). Following this result, it can be assumed that the overexpression of both enzymes in the OE *DHS/DOHH-GFP* mutant causes a balanced relation between *DHS* and *DOHH* in the cell, and, thus, shows a wild-type-like phenotype. The phenotype described for the three overexpression mutants (OE *DHS-GFP*, OE *DOHH-GFP*, and OE *DHS/DOHH-GFP*) supports previous observations in spike infections of wheat with these mutants [87]. The expression of *DHS* [88] *DOHH* and eIF-5A of *F. graminearum*, during the early stages of wheat spike infection have been shown previously [70, 87]. Thereby, the function of the eIF-5A mediated mRNA transport pathway during the initial steps of plant-fungal interaction of FHB on wheat is

supported. Recent studies using the inhibitor CNI-1493 to suppress the *DHS* enzyme in *F. graminearum* showed an effect on fungal germination *in vitro* and *in planta* [88]. Functions of the *DHS* enzyme in cell viability and fungal proliferation are assumed [88] as described for *S. cerevisiae* [164]. Moreover, mammal cells treated with inhibitors of *DHS* or *DOHH* fail to proliferate [94]. Cell proliferation might also play a role during compound appressoria development of *F. graminearum,* since the multicellular nature of these structures implies enhanced fungal growth by cell divisions.

4.5 Molecular characterisation of infection structures

4.5.1 Laser microdissection of infection structures

Following the aim to provide tissue specific expression profiles of infection cushions and runner hyphae, it was necessary to collect and accumulate each tissue type separately. Therefore, laser microdissection was applied to isolate infection cushions and runner hyphae (figure 6, 46 and 47). LMD has been used successfully to study gene expression in different plant-microbe interactions [165, 166]. However, only a few studies in this regard are available where LMD was applied on fungal systems, e.g. mycorrhizal fungi [166, 167] or pathogenic fungi [168-175]. The fundamental features of the current laser microdissection techniques are visualisation of the cells by a microscope and removal of the cells or tissue of interest by a laser. Two fundamentally different LMD systems are available using either ultraviolet (UV) or infrared (IR) lasers, or a combination of both lasers [176-178]. In the presented study the UV laser dissection system called PALM MicroBeam was applied. In UV systems a narrow laser beam is used to ablate away unwanted tissue next to cells of interest, which remain intact [177, 178]. By ablating the adjacent rim of unwanted tissue, non-specific adherence of tissue to the cap is avoided [177]. The remaining cells of interest are then catapulted under pressure onto an overhanging cap. In contrast to the ablation of tissue, where the laser is continuously active and directly focused on the sample, the catapulting takes place by single laser impulses focused below the target cells. IR laser

pulse melts ethylene vinyl acetate (EVA) film inside a cap and isolates cells from object slides by heating and cooling [176, 177]. Due to use of cold laser in UV-systems, risk of damaging samples by isolation is reduced compared to heat generating IR Systems [177, 178]. Furthermore, in IR systems the direct contact of the cap to the isolated sample is more susceptible for contaminations with unwanted material, than contact free UV systems. The different technical principles of UV and IR systems, as well as general features and advantages of both systems are summarised in table 12. Different technical variants of UV- and IR systems from different companies are commercially available, however, all of them share the same basic function of laser dissection.

Table 12: Overview of the different features of ultraviolet (UV) and infrared (IR) laser microdissection systems [178]

	UV	IR
Operating wavelength	320–400 nm	812 nm
Focusing width	Shorter wavelength allows focusing of the laser light in the sub-micron range More precise cutting enables single cell and subcellular microdissection	Focusing diameter of the laser beam can be adjusted from 7.5 to 30 µm Subcellular microdissection is impossible
Sample retrieval	Photovolatilisation of cells surrounding a selected area subsequently: ejection against gravity, falling by the force of gravity or separation by electrostatic forces (depending on the system) Contact-free	Transfer of laser energy to a thermolabile polymer thus forming a polymer-cell composite Not contact-free (higher risk of contamination with non-selected material)
Impact on cellular biomolecules	High photon density (cold laser) Minimal heat generation. Absorption maxima of DNA, RNA and proteins lie outside the operating wavelength. No harm to DNA, RNA and proteins	Generated heat (90°C) may potentially be harmful, but the thermal effect is transient. Alterations in DNA, RNA and protein content are not measurable

4.5.2 RNA isolation from LMD-Samples

To isolate infection cushions (IC) and runner hyphae (RH) by laser microdissection to isolate the RNA of each tissue several requirements had to be fulfilled:

Both tissues had to be transferred on a microscope slide, while the plant must be removed. The plant was removed in order to maximise the signal-to-noise ratio for fungal gene expression analysis [169, 175]. In the presented thesis, the plant tissue was removed after a small piece of glume with ICs and RH was pressed on an adhesive glass slide. This strategy was possible only with dried plant samples, because fresh (wet) samples did not stick to the slide (data not shown). In order to provide sticky microscopy slides, glass slides were covered with Liquid Cover Glass (Zeiss). Liquid Cover Glass is usually taken to improve the image quality of samples in microdissection approaches. The polymeric resin Liquid Cover Glass is shown to have no effect on subsequent DNA and RNA analysis from microdissected samples (personal communication at Zeiss Microscopy Laboratory, Munich, Germany). Alternatively, a tape transfer system is described to transfer paraffin embedded sections of *A. thaliana* tissues on slides [179] as well as for microdissection of forensic specimens [178]. Actually, adhesive tape was used successfully to remove ICs and RH from the plant (figure 22). However, it was not possible to isolate ICs or RH from the tape by laser catapulting, due to the strong adhesion of the mycelium to the tape. Furthermore, the tape impaired the clarity of microscopy during microdissection by interferring in the optical path. The method using Liquid Cover Glass on glass slides was used, since structural maintenance of the hyphal architecture as it developed *in planta* was demonstrated (figure 46, D and E). Moreover, RNA integrity in samples had to be preserved, since low RNA integrity effects subsequent transcription analysis [180-183]. Different preparation and fixation protocols are published, which provide high integrity of RNA from microdissected plant samples [177, 184, 185] and mammals [176, 177, 186, 187]. Dehydrated samples are predominately used for microdissection approaches in order to inactivate RNases. The importance of tissue dehydration in LMD has previously been described [172, 186]. Clement-Ziza et al., 2008 [186] showed for LMD samples of neurons and glial cells that dehydration of the samples is a key factor for maintaining RNA integrity. They demonstrated that RNA integrity was increased, when cryosections of frozen cells were incubated in ethanol during slide preparation and

microdissection compared to aqueous solutions [186]. Moreover, preparing the sample with high concentrated alcoholic solutions stabilised RNA as efficiently as performing LMD under a flow of argon [186]. Organic fixatives are commonly used for LMD approaches for chemical cross-linking of biomolecules and preservation of the cellular structure [177, 185]. Cross-linking fixatives, such as formalin and aldehydes, are described to maintain good histological integrity, but reduce RNA yield significantly [169, 181, 185]. In contrast, methanol and ethanol are described to be preferred in order to achieve good yields of RNA [177, 181, 185]. For laser dissected plant cells Farmer's fixation (3:1 ethanol:acetic acid) is frequently reported to maintain good histological and RNA integrity [177, 181, 185]. Ethanol-acetic acid fixation has been successfully applied for LMD and microarray analysis of plant tissues [188, 189]. Hacquard et al., 2010 [172] used laser microdissection for expression analysis on the basidiomycete *Melampsora larici-populina* infected leaf sections. A drastic impact of water and temperature during preparation of EAA-fixed, paraffin-embedded sections on RNA integrity was demonstrated [172]. Isolation of intact RNA from laser-isolated paraffin sections was unsuccessful using the conventional method of slide mounting, where paraffin ribbons were floated onto a bead of diethylpyrocarbonate (DEPC) water and mounted onto a slide [172]. In contrast to that, a direct transfer onto microscope slides without water and dry sections led to a drastic increase of RNA integrity [172]. In addition, the use of low-melting paraffin with at 37°C significantly improved RNA integrity compared to conventional paraffin where 58°C is necessary for paraffin impregnation of samples. In this study dehydration with 99,9% ethanol cooled on ice was performed with glume tissues containing infection cushions and runner hyphae of *F. graminearum*. Thereby, RNase activities were inactivated. Fixation of fungal protoperithecia by ethanol was performed prior to laser microdissection for RNA-seq analysis very recently [174]. Moreover, lyophilization was performed to gain freeze dried and fixed samples. By using dry glume tissues containing infection cushions and runner hyphae, it was possible to transfer infection cushions and runner hyphae on sticky microscope slides without releasing RNases derived from aquos vacuoles of the plant or the fungus. In order to avoid RNase activites during rehydration of infection cushions and runner hyphae on the slide from humidity in air, dissection was performed not longer than 60 min at RT. Adhesive isolation caps with isolated tissue were immediately transferred in a freezer at -80°C and stored until RNA isolation was performed (over night). To achieve sufficient amounts of dissected infection cushions

and runner hyphae material for mRNA isolation, individual isolations (content of individual adhesive caps) were pooled. The quality of total RNA from hyphae under the preparation procedure used for LMD samples was validated by means of photometry and gel electrophoresis. Since high RNA purity determined by photometry provides information about contamination with proteins and/or aromatic substances, but not about the integrity of the RNA, gel electrophoresis of total RNA was performed (figure 42). By distinct 18S and 28S ribosomal RNA bands in samples with high and low amount of starting material (30-2,5 mg DW) it was checked that the RNA is not degraded during ethanol fixation and lyophilization (figure 42). The most precise and reliable methods to determine the integrity of total RNA down to 200 pg, are technologies applied by the Agilent 2100 Bioanalyzer (Agilent Technologies, USA) and the Experion system (Bio-Rad Laboratories, USA) [182]. In Experion systems RNA samples are electrophoretically separated on micro-fabricated chips and detected via laser induced fluorescence dyes. By a RNA ladder as a mass and size standard the RNA integrity of the sample is estimated by the 18S and 28S ribosomal RNA bands. In the literature, mRNA quality with a 28S/18S rRNA ratio >2.0 is regarded as perfect [182, 190]. Another tool for RNA quality assessment is available for the Agilent Bioanalyzer 2100 Technologies is the determination of the RNA Integrity Number (RIN) [182, 191]. Quality estimation of total RNA by RIN numbers relies on a standardised numbering system from 1 to 10, with 1 being the most degraded and 10 being the most intact RNA. RIN values are also determined by fluorescence curves and 18S and 28S peaks from capillary gel electrophoresis. Here, the software uses an algorithm for data interpretation and classification by RIN values. Considerring that total RNA contains only a small proportion of mRNA (2–4%), while the main amount of RNA is ribosomal RNA (80–90%, rRNA) and transfer RNA (5–15%, tRNA) [192], it can be questioned, whether estimations based on the non-targeted ribosomal RNA are valid to make a definite statement on the mRNA quality [182]. Lab-on-chip capillary gel electrophoresis is currently the method of choice to determine RNA integrity, however, mRNA isolation instead of total RNA isolation was performed in our studies to generate sequencing libraries. Therefore, RIN determination by 18S and 28S peaks is not possible in this application. Alternatively, amplified mRNA (cDNA) was checked for degradation by electrophoresis (figure 48). When fragmented RNA is used as template for amplification, the resulting cDNA products appear on ethidium bromide gels as a strong signal with low molecular weight (50-500 bp). Hence, respective signals were not

observed for amplified mRNA of hyphae from liquid culture (figure 48, A), infection cushions and runner hyphae (figure 48, B and C) the RNA integrity was controlled. Q-PCRs targeting 5' ends of fungal transcripts can be performed, in addition to the gene specific Q-PCRs shown in this thesis (figure 45). Furthermore, Southern-blots targeting specific transcripts of *F. graminearum* can be used to for quality assessment of cDNA libraries.

4.5.3 cDNA libraries of infection cushions and runner hyphae

Experiments for next generation sequencing or microarray analysis usually require RNA in larger quantities (1-3 µg) than are available from microscopic biological samples [192, 193] especially from biopsies, forensic or laser microdissection [185]. It can be considered that plant and animal cells typically contain 10-100 pg of total RNA per cell [184] and a only a small proportion of 2-4 % (approx. 0,2-4 pg) is mRNA[192]. Therefore, RNA amplification is necessary for single cell and LMD samples. For our approach it was necessary to achieve sufficient RNA amounts (3 µg total) from both infection cushions and runner hyphae for expression profiling by next generation sequencing. Different PCR-based amplification systems are commercially available from different companies and have been compared experimentally [193-196]. The method for cDNA library production as performed for infection cushions and runner hyphae was established according to Le et al., 2005 [197], who performed comparative expression analysis from 20 manually isolated maize egg and 25 central cells by SSH. They applied mRNA isolation and amplification by SMART-PCR prior to LD-PCR (long distance PCR) to generate 6-8 µg cDNA from each tissue [197]. The SMART (switching mechanism at the 5' end of the RNA transcript) PCR system has been developed originally in order to amplify full-length cDNAs for construction of clone libraries and microarray hybridisation [193, 198]. The first-strand synthesis by SMART-PCR is primed with certain oligo(dT) sequences and performed by the SMARTScribe reverse transcriptase. With its terminal transferase activity the enzyme adds a few additional nucleotides to the 3' end of the cDNA, when the 5' end of the mRNA template is reached. SMARTScribe RT then switches templates and continues

replicating to the end of the oligonucleotide [199]. The resulting, single-stranded (ss) cDNA and the introduced sequences at both ends of the cDNA-RNA hybrids serve as universal priming sites for end-to-end cDNA amplification using LD- PCR. Through the SMART mechanism contaminants during amplification like prematurely terminated cDNAs, genomic DNA, or other RNAs species (e.g. rRNA, tRNA, miRNA, siRNA) are avoided. The effectiveness of SMART-PCR based amplification from isolated mRNA in identifying differentially expressed and cell type-specific transcripts of relatively low abundance is demonstrated by Le et al., 2005 [197]. Validation of expression profiles derived from SSH was done by Q-PCR. Additionally, the specific localisation of transcripts was confirmed by *in situ* hybridisation [197]. The Arcturus RiboAmp and Clontech SMART-PCR are two commonly used methods for RNA amplification, which have been compared using low amounts (50 ng) of total RNA isolated from mouse livers and kidneys [193]. Differential expression profiles from microarray analysis were compared between both techniques as well as with unamplified samples. Thereby they conclude from their results that SMART is preferable compared to Arcturus RiboAmp, when low amounts of total RNA are used. For SMART-amplified samples most genes were correctly assigned as differentially expressed by microarray analysis, when compared with public expression databases on the transcript and protein levels [193]. Caretti et al., 2008 [195] performed a comparison of amplifications of a colon biopsy subjected to laser microdissection with purification of an estimated 1 nanogram of RNA per specimen; they compared the two cycles Arcturus and the one cycle Nugen amplification methods and found the Arcturus method to show the lowest variance and highest correlation. Lang et al., 2009 [196] compared three commonly applied PCR based RNA amplification techniques with sub-nanogram input concentration of total RNA (0,25 ng- 3,3 ng). Microarray data from respective amplification method were validated for 37 genes by Q-PCR [196]. It was shown that each of the three tested amplification methods provides acceptable accuracy and reliability of gene expression data from sub-nanogram input of total RNA [196]. However, in studies from Lang et al., 2009 [196] SMART-PCR amplification as applied in our studies was not investigated. However, Subkhankulova and Livesey 2006 [194] compared T7-based linear amplification, SMART-PCR amplification and global PCR amplification for expression profiling by microarray analysis on the single cell level using mouse fibroblast or ovarian tissue. It was estimated by the authors that a single eukaryotic animal cell contains approximately 0.1 pg of mRNA or 10 pg of total RNA. In this

study 10 ng total RNA was used in all PCRs, to avoid a random representation of different species of mRNA in each aliquot of templates. Comparing microarray results from different PCR amplification methods with those from unamplified RNA, it was shown that results from PCR amplification are more reliable than linear amplification for detecting true expression differences between samples. SMART amplification had a higher true-positive rate than global amplification, but at the expense of a considerably lower absolute discovery rate and a systematic compression of observed expression ratios. The smallest total number of differentially expressed genes was identified using SMART amplification. However, the percentage of true positive differentially expressed genes was much higher for SMART amplified samples (80%) as compared to global amplification (53% true positives), and linear amplification (34-40%), when compared to expression data from unamplified RNA. RNA After validation of amplified and unamplified samples by Q-PCR, amplified samples showed a high validity for microarray analysis using sub-nanogram quantities of total RNA, [194, 196]. PCR-based amplification methods have a number of potential advantages over linear isothermal amplification: it is faster, more cost effective, with an almost unlimited degree of amplification [194, 200, 201]. The disadvantage of PCR-based exponential amplification, such as SMART, is the possible introduction of systemic biases in differential expression data [194], especially in the case of increased cycle numbers [201]. The decision, which amplification method to use for expression profiling of limiting biological samples depends on several factors, such as the quality and quantity of RNA, laboratory facilities, and the experimental goal.

4.5.4 RNA sequencing of infection cushions and runner hyphae libraries provides depth sequencing data with a high accuracy

In order to follow the main aim of this thesis to identify fungal genes specifically activated in infection cushions and runner hyphae, two major challenges had to be overcome. First, a low amount of mRNA from laser microdissected samples requires a high sensitivity for transcript detection. Second, no expression data about infection cushions and runner hyphae *in planta* are published for any other fungi. Thus, candidate

genes for targeted Q-PCR analysis or hybridisation based approaches were unknown. Unlike hybridisation-based technologies, next generation sequencing (NGS) methods are not limited to known transcripts. From the cDNA libraries of runner hyphae and infection cushions 3 µg were used for Illumina sequencing at LGC Genomics (Berlin, Germany). All NGS sequencing technologies e.g. Roche-454 and SOLiD Illumina enable the so-called 'massively parallel' sequencing that differs significantly from conventional Sanger capillary sequencing [192, 202]. Although NGS technologies show specific differences, all of them share certain attributes [192]. First, the preparation steps are fewer and faster than for Sanger sequencing. For instance, a bacterial cloning step to produce sequencing libraries is not necessary. Instead production of a library for NGS starts by ligating synthetic DNAs (adapters) onto each fragment of the library to be sequenced. Second, all platforms require the library fragments to be amplified on a solid surface (glass slides or microbeads). The amplification step is needed to gain sufficient signal for optical detection systems. Third, these instruments perform polymerase based sequencing reactions in a series of repeating steps that are detected automatically by fluorescence dyes. Solid-phase amplification in Illumina technologies is used to produce randomly distributed, clonally amplified clusters per fragment of the library. This procedure can produce up to 200 million spatially separated template clusters, providing ends for primer hybridisation, needed to initiate the NGS reaction [192]. As summed up in table 9 an enormous number of reads (50 pb each) were achieved for both, runner hyphae (>105 million reads) and infection cushions (>93 million reads). After the linker sequences were omitted from the RAW reads, about 75% of raw reads remained for both samples (84.477.235 reads of RH and 69.971.732 reads of IC). The linker trimmed reads represent the number of sequences derived from the respective biological sample. The mean accuracy for base calling (Phred quality [203-205]) of these reads was shown to be excellent (between 99.9% and 99.99%) for both runner hyphae and infection cushions (table 9 and 10). Moreover, 99,7 % of the linker trimmed reads (sequences to be determined) have been shown to exhibit an Phred quality of >99 %. Therefore, the overall accuracy of sequence determination for both samples is demonstrated. The resulting total number of bases determined from linker trimmed reads of runner hyphae library was approx. 4,3 giga bases and 3,6 giga bases for the infection cushion library. This shows that the total number of bases in the genome of *F. graminearum* (36,1 mega bases [65]) is covered 120 fold by the bases determined in runner hyphae, but 99 fold by those of infection cushions. Although approximately 13 % more RAW reads were

obtained from the library of runner hyphae compared to infection cushions, this effect might be neglected considering the high degree of sequencing coverage for both samples. Thus, it is demonstrated that high quality NGS data were gained for both samples of runner hyphae and infection cushions. The sequencing depths that can be achieved using NGS techniques, such as Illumina sequencing, are known to allow much higher sensitivity compared to hybridisation based microarrays approaches [192]. Microarrays allow only relative abundance measurements of RNA transcripts and suffer from high background and cross-hybridisations [192]. Less abundant genes give low signal-to-noise ratios in the array hybridisations. Consequently, minor changes in gene expression levels from different biological samples are not detected by microarray approaches [192]. Due to the low signal-to-noise ratios and high levels of reproducibility for both technical and biological replicates [192], RNA-Seq is the method of choice for highly sensitive expression profiling. Another advantage of RNA-Seq data is the ability to detect intron-exon-boundaries of genes and, thus, to identify splice variants. RNA-Seq data can are also used for de novo annotation purposes [174, 192, 206], including single nucleotide polymorphisms (SNPs). NGS has been used in combination with laser microdisection to study gene expression in plants [207, 208], mammals [187, 209], and in fungi [174, 210].

4.5.5 Transcriptome profiles from infection cushions and runner hyphae mirror microscopic observations

The Illumina sequencing data form infection cushions and runner hyphae were mapped to the reference genome of *F. graminearum* [89] by using the programm TopHat [99]. Genome mapping, differential expression analysis and statistics were done by Sebastian Piehler and Dr. Ulrich Güldener (Institute of Bioinformatics and Systems Biology, Munich, Germany). The mapping results showed 20% less reads of runner hyphae aligned to the reference genome, compared to reads of infections cushions. While 92% of the reads from infection cushions mapped to the reference genome of *F. graminearum*, only 72% of the reads from the runner hyphae were aligned, respectively (table 11). In contrast to the genome alignment, mapping to the

transcriptome resulted in a high amount of unmapped reads (54% percent ininfection cushions and 66% for runner hyphae) in both samples. The unmapped reads indicate intergeneric regions, splicing variants of transcripts or not yet annotated genes of *F. graminearum*. Other reasons for unmapped reads can be complex exon-exon junctions, miRNA, and small ncRNA. Such situations could potentially be identified by more sophisticated or combined alignment strategies [192]. After mapping, differentially expressed genes in runner hyphae and infection cushions were identified by combining four different data sets. Comparable strategies have been applied previously in similar analytical purposes [211, 212]. Finally, genes were considered as differentially expressed, which showed the highest 5% of fold change in the one tissue compared to the other. The abundance estimations were made by means of the Cuffdiff tool in the Cufflinks software [99, 100] and resulted in 723 differentially up-regulated genes in runner hyphae compared to infection cushions and 759 up-regulated genes in infection cushions compared to runner hyphae. A scatter plot of the expression values of runner hyphae vs. infection cushions demonstrates that genes of the trichothecene (TRI)-cluster are differentially expressed in infection cushions but not in runner hyphae(figure 49). This is consistent with microscopic results of the *TRI5prom::GFP* reporter strain, because the *TRI5* gene was shown to be specifically induced in infection structures (figure 14). This leads to the conclusion that the expression profiles provided for runner hyphae and infection cushions mirror the living situation of the fungus *in planta*.

4.5.6 Laser microdissection combined with RNA-Seq are powerful tools to explore plant-pathogen interactions

The second data set about organ specific transcriptom of fungi from combined laser microdissection and RNA-sequencing (RNA-seq) is provided here. Teichert et al., 2012 [174] used laser microdissection and RNA-seq to determine gene expression patterns in young fruiting bodies and non-reproductive mycelia of the ascomycete *Sordaria macrospora*. In the last named study nearly equal approaches were used, including cDNA library production by SMART-PCR amplification, Illumina HiSeq 2000, genome

mapping by TopHat. Moreover, the expression of a strongly up-regulated pheromone precursor in protoperithecia was confirmed by fluorescence microscopy of GFP expression under the control of the promoter of the pheromone precursor sequences. Several *in planta* profiling studies using bulk infected tissues have led to the identification of many genes expressed during infection [213-215]. However, changes in *in planta* fungal gene expression could not be monitored [169, 175]. Using an Affymetrix chip more than 7.000 of *F. graminearum* transcripts (50% of all genes) can be detected in whole tissue of infected barley [213]. At very early stages (e.g. 2 dpi), only 900 fungal genes (7% of all genes) could be detected, most likely as a result of less fungal biomass. hybridisation has been shown to improve signal-to-noise by gene sets enriched in pathogen-derived cDNAs [216], but gives only rough quantitative information and is not sufficient to generate a global, staged transcription pattern [169]. In general, expression profiling approaches of pathogens *in planta* results in high background noise, hence it is difficult to physically separate fungal hyphae from of host tissue [169, 175]. Laser microdissection has been applied to *in planta* expression profiling with microarray techniques of the maize (Zea mays) anthracnose stalk rot fungus *Colletotrichum graminicola*, and, thus, identified 437 fungal genes that are upregulated *in planta* [169]. The methods used by Tang et al., 2006 [169] were successfully applied to analyse gene expression profiles of *F. graminearum* hyphae during infection of wheat coleoptiles at different stages of infection [175]. Stage-specific gene expression patterns were distinguished that were related to distinct metabolic strategies [175]. By the recent publications using laser microdissection for large scale expression profiling in plant pathogen interactions [169, 174, 175], the power of combined microscopic and molecular approaches is demonstrated. One major methodical achievement in this thesis is the use of fungal tissues grown on wheat glumes for laser microdissection, but without isolating the plant. Thereby, the background noise, caused by the plant, was minimized in subsequent expression analysis. At the end, the first transcriptome data of runner hyphae and infection cushions from a fungal plant pathogen under *in planta* conditions are provided here. Nevertheless, the bioinformatic analyses are still in an ongoing process. Functional classification results, as well as pathway mapping of highly expressed genes in runner hyphae and infection cushions will probably elucidate the molecular differences between both tissues in the near future.

5 Summary

It was discovered very recently that *Fusarium. graminearum* forms specialised infection structures, so-called compound appressoria during infection of floret tissues of wheat [18]. Furthermore, a specific mycotoxin induction in infection structures was initially observed [18]. Therefore, one aim of the presented study was to clarify the penetration mechanism of compound appressoria formed by *Fusarium graminearum* on wheat husks. By applying various microscopical techniques, including LM (light microscopy), LSM (laser scanning microscopy), SEM (scanning electron microscopy), and TEM (transmission electron microscopy) developmental, structural, and functional characteristics of compound appressoria were revealed. The combination of 3D imaging by LSM with electron microscopy provided a detailed insight in the cellular complexity and the penetration mechanism of lobate appressoria and infection cushions of *F. graminearum* on wheat husks (paleas and glumes). Multiple penetration pegs at infection cushions, subcuticular colonisation, and a dense colonisation of the plant tissue below infection cushions indicate a high impact of these infection structures for disease severity. Several possibilities for *F. graminearum* to enter wheat husks were identified. In summary, an unknown complexity of the penetration strategy of *F. graminearum* during FHB on wheat was discovered. Concerning this, striking similarities to other fungi, including *R. solani* and *S. sclerotiorum* are noted.

Microscopic observations of several mutants of *F. graminearum* provide indications that the compound appressoria formation is induced in a cAMP dependent pathway, which is mediated by an endogenous adenylate cyclase. In contrast to that, the *GPMK1* MAP kinase pathway in *F. graminearum* is dispensable for induction and development of infection structures, but essential for penetration of the plant cell wall of wheat. Surprisingly, the deletion mutant of the tetraspanin encoding gene *PLS1* of *F. graminearum* was not defective in plant penetration, as it is described for several other phytopathogenic fungi. The speed of fungal development during initial infection in general and with regard to infection structures seems to be regulated by a hyposine dependent pathway with a possible function in specific mRNA transport. The deletion mutant of the lipase1, a known virulence factors for systemic FHB infection by *F. graminearum*, showed no defect during initial infection stages and infection structures. This supports former suggestions that lipase1 is important at the rachis of wheat spikes, where the mutant gets stuck. In contrast, trichothecene production in

infection structures of *F. graminearum* is not a requisite for initial infection stages. Development of infection structures and disease symptoms are formed by the *TRI5* deletion mutant on wheat husks similar to the wild type.

In order to understand the molecular basis of infection cushions, a laser microdissection (LMD) approach was established. Thereby, several hundred runner hyphae and infection cushions were collected, mRNAs from both tissues isolated, and amplified by SMART-PCR to provide tissue specific cDNA libraries. Next generation sequencing of the resulting libraries by Illumina HiSeq 2000 determined the sequences with a high accuracy. Over 13.800 genes of *F. graminearum* were identified in runner hyphae and infection cushions by mapping to the reference genome. The transcriptome profiles of runner hyphae and infection cushions revealed more than 700 hundred differentially expressed genes in both tissues. Microscopic observations from a *TRI5prom::GFP* reporter strain *in planta* and differential expression results are congruent. Thereby, an authentic representation of the respective living situation by the corresponding expression data set is implied. The first transcriptome data of runner hyphae and infection cushions from a fungal plant pathogen under *in planta* conditions are provided here. In summary, the power of combined microscopic and molecular approaches to analyse cell type-specific gene expression during fungal-plant-interactions is demonstrated in this thesis.

6 Zusammenfassung

Es ist erst seit sehr kurzer Zeit bekannt, dass *Fusarium graminearum* während der Infektion von Weizenblüten multizelluläre Appressorien bildet [18]. Darüber hinaus wurde erstmalig eine spezifische Induktion von Mykotoxinen in Infektionsstrukturen beobachtet [18]. Daher war es ein Ziel der hier präsentierten Arbeit, den Penetrationsmechanismus multizellulärer Appressorien von *F. graminearum* auf Weizenspelzen aufzuklären. Durch die Anwendung verschiedener mikroskopischer Techniken, wie Lichtmikroskopie, LSM (laser scanning microscopy), REM (Rasterelektronenmikroskopie), TEM (Transmissionselektronenmikroskopie) konnten neue Erkenntnisse über die Struktur, Entwicklung und Funktion multizellulärer Appressorien von *F. graminearum* erlangt werden. Die Kombination aus 3D-Aufnahmen und Elektronenmikroskopie lieferte neue, detaillierte Einblick in die zelluläre Komplexität sowie den Penetrationsmechanismus von gelappten Appressorien und Infektionskissen des Pilzes auf Spelzen von Weizen. Im Rahmen der Studie wurde gezeigt, dass gelappten Appressorien und Infektionskissen Weizenspelzen mit mehreren Penetrationsstiften durchbohren können und die Pflanze zusätzlich durch subkutikuläres Wachstum schädigen. Eine dichte Kolonisierung des pflanzlichen Gewebes durch Infektionskissen sowie Nekrosen die durch Infektionskissen entstehen lassen darüber hinaus den Schluss zu, dass Infektionskissen eine entscheidende Rolle bei der Pathogenese spielen. Alternative Wege um in das Innere von Weizenspelzen zu gelangen, wie z.B. über Stomata oder Silikatzellen, wurden ebenfalls beobachtet. Es wird eine bisher unbekannte Komplexität bezüglich der Penetrationsmechanismen von *F. graminearum* auf Weizen deutlich.

Mikroskopische Untersuchungen von Mutanten von *F. graminearum* deuten darauf hin, dass die Bildung multizellulärer Appressorien durch eine endogene Adenylat-Zyklase in einen cAMP vermittelten Signaltransduktionsweg induziert wird. Hingegen scheint die MAP kinase *GPMK1* des Pilzes für die Penetration der pflanzlichen Zellwand verantwortlich zu sein. Entgegen der Ergebnisse, die von anderen phytopathogenen Pilzen bekannt sind, ist das *PLS1* Gen von *F. graminearum* nicht notwendig für die erfolgreiche Penetration der Pflanze. Es konnten jedoch Hinweise dafür geliefert werden, dass die Entwicklung des Pilzes und der Infektionsstrukturen auf Weizenspelzen durch den Transport spezieller mRNAs reguliert wird.

Deletionsmutanten der bekannten Virulenzfaktoren des FHB an Weizen, *FGL1* und *TRI5*, zeigten hingegen keine Beeinträchtigung bezüglich der Infektion von Weizenspelzen gegenüber dem Wildtyp. Da beide Mutanten nicht in der Lage sind Weizenähren über den Rachisknoten der Ähre hinaus systemisch zu kolonisieren, kann von einer Funktion der Virulenzfaktoren zu einem späteren Zeitpunkt der Weizeninfektion ausgegangen werden.

Mit dem Ziel Erkenntnisse über die molekularen Grundlagen und Regulationsmechanismen von Infektionskissen zu erhalten wurde Laser-Mikrodissektion angewendet. Dadurch wurden hunderte Laufhyphen und Infektionskissen von *F. graminearum* separat gesammelt und deren mRNA isoliert. Durch SMART-PCR konnten cDNA Bibliotheken von Laufhyphen und Infektionskissen hergestellt werden. Die Nukleotidsequenzen der amplifizierten Transkripte wurden mittels Illumina HiSeq 2000 Sequenzierung mit hoher Genauigkeit bestimmt. Durch den Vergleich der ermittelten Sequenzen mit dem Referenzgenom von *F. graminearum* wurden mehr als 13.800 Gene des Pilzes in Laufhyphen und Infektionskissen identifiziert. Unterschiede in der Expression von Laufhyphen und Infektionskissen konnten durch differenzielle Expressionsanalysen nachgewiesen werden. Anhand der Transkriptionsanalysen wurden in Laufhyphen und Infektionskissen über 700 differentiell regulierte Gene ermittelt. Desweiteren bestätigen die Expressionsprofile von Laufhyphen und Infektionskissen Ergebnisse mikroskopischer Untersuchungen mit dem *TRI5prom::GFP* Reporterstamm während der Infektion von Weizenspelzen. Dadurch wurde überprüft, dass die Expressionsprofile der Situation im lebendenden System entsprechen. Letztlich wurden im Rahmen dieser Arbeit erstmalig Transkriptomdaten von Infektionskissen und Laufhyphen eines phytopathogenen Pilzes auf seiner Wirtspflanze geliefert. Insgesamt wird durch diese Arbeit das Potential kombinierter mikroskopischer und molekularer Methoden für zellspezifische Expressionsstudien in Pathogen-Pflanze-System demonstriert.

7 Future perspectives

The expression data of runner hyphae and infection cushions has to be validated by Q- PCR for several genes of *F. graminearum* to approve the reproducibility and reliability of the data. Following validation of highly differentially regulated genes in infection cushions, deletion fungal mutants of the respective gene can be created by plasmid mediated homologous recombination. The resulting mutants can be studied microscopically for the ability to form infection structures. The results might give a rise for genetic targets to suppress infection cushion formation of the fungus by specific inhibitors. Suppression of infection structure development might be relevant in FHB infection in wheat fields, because infection structure of the fungus produce trichothecenes such as DON at the initial stages of infection and enables the penetration of wheat tissues. The ongoing bioinformatic analyses of the transcriptome data including functional classification of differentially expressed genes and identification of different metabolic and signaling pathways in runner hyphae and infection cushions will provide new insights into the biological and molecular characteristics of runner hyphae and infection cushions. One the one hand, unique data about compound appressoria of fungal plant pathogens will be provided. On the other hand, comparison of the provided expression data from infection cushions with similar data from infections structures of other phytopathogenic fungi, such as *S. sclerotiorum*, *R. solani* and *M. oryzae*, may reveal the global transcriptional pattern of the penetration process in fungal plant pathogens. In order to identify the transcriptional pattern underlying penetration of wheat florets by penetration pegs of *F. graminearum*, comparative analyses with transcription data from infection cushions of the *GPMK1* deletion mutant can be performed. The genes which show strong differences in gene expression in the non penetrating infection cushions of the *GPMK1* are most likely those genes that are involved in breaking the plant cell wall by penetration pegs. For this purpose laser dissection combined with subsequent RNA sequencing approaches will be the method of choice. Another valuable achievement for the future will be the establishment of other “omic” analysis, such as proteomics and metabolomics, in laser miocrodissection approaches to elucidate the biological, molecular and chemical processes in plant-pathogen interactions in a comprehensive manner.

8 References

1. Bai S, Shaner G: **Scab of wheat: prospects for control**. *Plant Disease* 1994, **78**(8):760-766.
2. McMullen M, Jones R, Gallenberg D: **Scab of wheat and barley: a re-emerging disease of devastating impact**. *Plant Disease* 1997, **81**(12):1340-1348.
3. Trail F: **For blighted waves of grain: *Fusarium graminearum* in the postgenomics era**. *Plant Physiology* 2009, **149**(1):103-110.
4. O'Donnell K, Kistler HC, Tacke BK, Casper HH: **Gene genealogies reveal global phylogeographic structure and reproductive isolation among lineages of *Fusarium graminearum*, the fungus causing wheat scab**. *Proceedings of the National Academy of Sciences* 2000, **97**(14):7905-7910.
5. Goswami RS, Kistler HC: **Heading for disaster: *Fusarium graminearum* on cereal crops**. *Mol Plant Path* 2004, **5**(6):515-525.
6. Tóth B, Mesterházy Á, Horváth Z, Bartók T, Varga M, Varga J: **Genetic variability of central European isolates of the *Fusarium graminearum* species complex**. *European Journal of Plant Pathology* 2005, **113**(1):35-45.
7. Karugia G, Suga H, Gale L, Nakajima T, Tomimura K, Hyakumachi M: **Population structure of the *Fusarium graminearum species* complex from a single Japanese wheat field sampled in two consecutive years**. *Plant Disease* 2009, **93**(2):170-174.
8. Wang C, Zhang S, Hou R, Zhao Z, Zheng Q, Xu Q, Zheng D, Wang G, Liu H, Gao X: **Functional analysis of the kinome of the wheat scab fungus *Fusarium graminearum***. *PLoS Pathogens* 2011, **7**(12):e1002460.
9. Kikot GE, Hours RA, Alconada TM: **Contribution of cell wall degrading enzymes to pathogenesis of *Fusarium graminearum*: a review**. *Journal of Basic Microbiology* 2009, **49**(3):231-241.
10. O'Donnell K, Ward TJ, Geiser DM, Kistler HC, Aoki T: **Genealogical concordance between the mating type locus and seven other nuclear genes supports formal recognition of nine phylogenetically distinct species within the *Fusarium graminearum* clade**. *Fungal Genetics and Biology* 2004, **41**(6):600-623.
11. Kang ZS, Buchenauer H: **Cytology and ultrastructure of the infection of wheat spikes by *Fusarium culmorum***. *Mycological Research* 2000, **104**:1083-1093.
12. Wanjiru WM, Kang ZS, Buchenauer H: **Importance of cell wall degrading enzymes produced by *Fusarium graminearum* during infection of wheat heads**. *European Journal of Plant Pathology* 2002, **108**(8):803-810.
13. Pearce RB, Strange RN, Smith H: **Glycinebetaine and choline in wheat: Distribution and relation to infection by *Fusarium graminearum***. *Phytochemistry* 1976, **15**(6):953-954.
14. Rittenour W, Harris S: **An *in vitro* method for the analysis of infection-related morphogenesis in *Fusarium graminearum***. *Molecular Plant Pathology* 2010, **11**(3):361.
15. Strange RN, Smith H: **Fungal growth stimulant in anthers which predisposes wheat to attack by *Fusarium graminearum*.** *Physiological and Molecular Plant Pathology* 1971, **1**(2):141-144, IN145, 145-150.
16. Pritsch C, Muehlbauer GJ, Bushnell WR, Somers DA, Vance CP: **Fungal development and induction of defense response genes during early infection of wheat spikes by *Fusarium graminearum***. *Molecular Plant-Microbe Interactions* 2000, **13**(2):159-169.
17. Boddu J, Cho S, Kruger WM, Muehlbauer GJ: **Transcriptome analysis of the barley-*Fusarium graminearum* interaction**. *Molecular Plant-Microbe Interactions* 2006, **19**(4):407-417.
18. Boenisch M, Schäfer W: ***Fusarium graminearum* forms mycotoxin producing infection structures on wheat**. *BMC Plant Biology* 2011, **11**(1):110.

19. Ribichich KF, Lopez SE, Vegetti AC: **Histopathological spikelet changes produced by *Fusarium graminearum* in susceptible and resistant wheat cultivars**. *Plant Disease* 2000, **84**(7):794-802.
20. Kang Z, Buchenauer H: **Ultrastructural and immunocytochemical investigation of pathogen development and host responses in resistant and susceptible wheat spikes infected by *Fusarium culmorum***. *Physiological and Molecular Plant Pathology* 2000, **57**(6):255-268.
21. Jansen C, von Wettstein D, Schäfer W, Kogel KH, Felk A, Maier FJ: **Infection patterns in barley and wheat spikes inoculated with wild-type and trichodiene synthase gene disrupted *Fusarium graminearum***. *Proceedings of the National Academy of Sciences* 2005, **102**(46):16892-16897.
22. Ilgen P, Hadeler B, Maier FJ, Schäfer W: **Developing kernel and rachis node induce the trichothecene pathway of *Fusarium graminearum* during wheat head infection**. *Molecular Plant-Microbe Interactions* 2009, **22**(8):899-908.
23. Brown NA, Urban M, Van de Meene AML, Hammond-Kosack KE: **The infection biology of *Fusarium graminearum*: Defining the pathways of spikelet to spikelet colonisation in wheat ears**. *Fungal Biology* 2010, **114**(7):555-571.
24. Desjardins AE, Hohn TM: **Mycotoxins in plant pathogenesis**. *Molecular Plant-Microbe Interactions* 1997, **10**(2):147-152.
25. Marasas WFO, Nelson PE, Toussoun TA: **Toxigenic *Fusarium species*. Identity and mycotoxicology**: Pennsylvania State University; 1984.
26. Snijders C: **Fusarium head blight and mycotoxin contamination of wheat, a review**. *European Journal of Plant Pathology* 1990, **96**(4):187-198.
27. Guenther JC, Trail F: **The development and differentiation of *Gibberella zeae* (anamorph: *Fusarium graminearum*) during colonization of wheat**. *Mycologia* 2005, **97**(1):229-237.
28. Rocha O, Ansari K, Doohan FM: **Effects of trichothecene mycotoxins on eukaryotic cells: A review**. *Food Additives and Contaminants* 2005, **22**(4):369-378.
29. Cutler HG: **Trichothecenes and their role in the expression of plant disease**. In: *Biotechnology for crop protection* Edited by Hedin PA, Menn JJ, Hollingworth RM, vol. 379. Washington DC: The American Chemical Society Symp. Ser.; 1988: 50-72.
30. Proctor RH, Hohn TM, McCormick SP: **Reduced virulence of *Gibberella zeae* caused by disruption of a trichothecene toxin biosynthetic gene**. *Molecular Plant-Microbe Interactions* 1995, **8**(4):593-601.
31. Desjardins AE, Proctor RH, Bai GH, McCormick SP, Shaner G, Buechley G, Hohn TM: **Reduced virulence of trichothecene-nonproducing mutants of *Gibberella zeae* in wheat field tests**. *Molecular Plant-Microbe Interactions* 1996, **9**(9):775-781.
32. Bai GH, Desjardins AE, Plattner RD: **Deoxynivalenol-nonproducing *Fusarium graminearum* causes initial infection, but does not cause disease spread in wheat spikes**. *Mycopathologia* 2002, **153**(2):91-98.
33. Maier FJ, Miedaner T, Hadeler B, Felk A, Salomon S, Lemmens M, Kassner H, Schäfer W: **Involvement of trichothecenes in fusarioses of wheat, barley and maize evaluated by gene disruption of the trichodiene synthase (Tri5) gene in three field isolates of different chemotype and virulence**. *Mol Plant Path* 2006, **7**(6):449-461.
34. Kimura M, Tokai T, Takahashi-Ando N, Ohsato S, Fujimura M: **Molecular and genetic studies of *Fusarium* trichothecene biosynthesis: Pathways, genes, and evolution**. *Bioscience, Biotechnology, and Biochemistry* 2007, **71**(9):2105-2123.
35. Desjardins AE, Hohn TM, McCormick SP: **Trichothecene biosynthesis in *Fusarium species*: chemistry, genetics, and significance**. *Microbiology and Molecular Biology Reviews* 1993, **57**(3):595-604.
36. Hohn TM, Desjardins AE: **Isolation and gene disruption of the Tox5 gene encoding trichodiene synthase in *Gibberella pulicaris***. *Molecular Plant-Microbe Interactions* 1992, **5**(3):249-256.
37. Gardiner DM, Kazan K, Manners JM: **Nutrient profiling reveals potent inducers of trichothecene biosynthesis in *Fusarium graminearum***. *Fungal Genetics and Biology* 2009, **46**(8):604-613.

38. Gardiner DM, Osborne S, Kazan K, Manners JM: **Low pH regulates the production of deoxynivalenol by *Fusarium graminearum***. *Microbiology- Society for General Microbiology* 2009, **155**:3149-3156.
39. Doohan FM, Weston G, Rezanoor HN, Parry DW, Nicholson P: **Development and use of a reverse transcription-PCR assay to study expression of Tri5 by *Fusarium species in vitro* and *in planta***. *Applied and Environmental Microbiology* 1999, **65**(9):3850-3854.
40. Covarelli L, Turner AS, Nicholson P: **Repression of deoxynivalenol accumulation and expression of Tri genes in *Fusarium culmorum* by fungicides *in vitro***. *Plant Pathology* 2004, **53**(1):22-28.
41. Lemmens M, Haim K, Lew H, Ruckenbauer P: **The effect of nitrogen fertilization on Fusarium head blight development and deoxynivalenol contamination in wheat**. *Plant Pathology* 2004, **152**(1):1-8.
42. Evans CK, Xie W, Dill-Macky R, Mirocha CJ: **Biosynthesis of deoxynivalenol in spikelets of barley inoculated with macroconidia of *Fusarium graminearum***. *Plant Disease* 2000, **84**(6):654-660.
43. Frank AB: **Über einige neue und weniger bekannte Pflanzenkrankheiten**, vol. 1: Berichte der Deutschen Botanischen Gesellschaft; 1883.
44. Emmett R, Parbery D: **Appressoria**. *Annual Review of Phytopathology* 1975, **13**(1):147-165.
45. Mendgen K, Hahn M, Deising H: **Morphogenesis and mechanisms of penetration by plant pathogenic fungi**. *Annual Review of Phytopathology* 1996, **34**(1):367-386.
46. Howard RJ, Valent B: **Breaking and entering: host penetration by the fungal rice blast pathogen *Magnaporthe grisea***. *Annual Reviews in Microbiology* 1996, **50**(1):491-512.
47. Deising HB, Werner S, Wernitz M: **The role of fungal appressoriain plant infection**. *Microbes and Infection* 2000, **2**(13):1631-1641.
48. de Jong JC, McCormack BJ, Smirnoff N, Talbot NJ: **Glycerol generates turgor in rice blast**. *Nature* 1997, **389**(6648):244-244.
49. Howard RJ, Ferrari MA, Roach DH, Money NP: **Penetration of hard substrates by a fungus employing enormous turgor pressures**. *Proceedings of the National Academy of Sciences* 1991, **88**(24):11281-11284.
50. Horwitz B, Sharon A, Lu S, Ritter V, Sandrock T, Yoder O, Turgeon B: **AG protein alpha subunit from *Cochliobolus heterostrophus* involved in mating and appressorium formation**. *Fungal Genetics and Biology* 1999, **26**(1):19.
51. Braun E, Howard R: **Adhesion of *Cochliobolus heterostrophus* conidia and germlings to leaves and artificial surfaces**. *Fungal Genetics and Biology* 1994, **18**(3):211-220.
52. Weihold A, Sinclair J: **Penetration, colonization and host response**. In: *Rhizoctonia species: Taxonomy, molecular biology, ecology, pathology and disease control.* Edited by Sneh B, Jabaji-Hare S, Neate S, Dijst G. Dordrecht, The Netherlands: Kluwer Academic Publishers; 1996: 163-175.
53. Hofman TW, Jongebloed PHJ: **Infection process of *Rhizoctonia solani* on *Solanum tuberosum* and effects of granular nematicides**. *European Journal of Plant Pathology* 1988, **94**(5):243-252.
54. Huang L, Buchenauer H, Han Q, Zhang X, Kang Z: **Ultrastructural and cytochemical studies on the infection process of *Sclerotinia sclerotiorum* in oilseed rape**. *Journal of Plant Diseases and Protection* 2008, **115**(1):9-16.
55. Jamaux I, Gelie B, Lamarque C: **Early stages of infection of rapeseed petals and leaves by *Sclerotinia sclerotiorum* revealed by scanning electron microscopy**. *Plant Pathology* 1995, **44**(1):22-30.
56. Boyle C: **Studies in the physiology of parasitism VI. infection by *Sclerotinia Libertiana***. *Ann Bot-London* 1921(3):337.
57. Friese CF, Allen MF: **The spread of VA mycorrhizal fungal hyphae in the soil: inoculum types and external hyphal architecture**. *Mycologia* 1991, **83**(4):409-418.
58. Varma A, Hock B: **Mycorrhiza: Structure, function, molecular biology, and biotechnology** 2edn. Heidelberg, Germany: Springer Publishing; 1999.

59. Keijer J, Sinclair JB: **Plant-pathogen interactions of *Rhizoctonia spp.*** In: *Rhizoctonia species: taxonomy, molecular biology, ecology, pathology and disease control.* Edited by Sneh B, Jabaji-Hare S, Neate S, Dijst G. Dordrecht, The Netherlands: Kluwer Academic Publishers; 1996: 147-174.
60. Tenberge K: **Infection sites and infection structures**. In: *Botrytis: biology, pathology and control.* Edited by Elad Y, Williamson B, Tudzynski P, Delen N. Dordrecht, The Netherlands: Kluwer Academic Publishers; 2004: 74-84.
61. Armentrout VN, Downer AJ: **Infection cushion development by *Rhizoctonia solani* on cotton**. *Phytopathology* 1987, **77**(4):619-623.
62. Pannecoucque J, Höfte M: **Interactions between cauliflower and *Rhizoctonia* anastomosis groups with different levels of aggressiveness**. *BMC Plant Biology* 2009, **9**:95.
63. Matsuura K: **Scanning electron microscopy of the infection process of *Rhizoctonia solani* in leaf sheaths of rice plants**. *Phytopathology* 1986, **76**(8):811-814.
64. Kang ZS, Zingen-Sell I, Buchenauer H: **Infection of wheat spikes by *Fusarium avenaceum* and alterations of cell wall components in the infected tissue**. *European Journal of Plant Pathology* 2005, **111**(1):19-28.
65. Cuomo CA, Gueldener U, Xu JR, Trail F, Turgeon BG, Di Pietro A, Walton JD, Ma LJ, Baker SE, Rep M *et al*: **The *Fusarium graminearum* genome reveals a link between localized polymorphism and pathogen specialization**. *Science* 2007, **317**(5843):1400-1402.
66. Bluhm BH, Zhao X, Flaherty JE, Xu JR, Dunkle LD: **RAS2 regulates growth and pathogenesis in *Fusarium graminearum***. *Molecular Plant-Microbe Interactions* 2007, **20**(6):627-636.
67. Marshall DS, Rush MC: **Infection cushion formation on rice sheaths by *Rhizoctonia solani***. *Phytopathology* 1980, **70**(10):947-950.
68. Demirci E, Döken MT: **Host penetration and infection by the anastomosis groups of *Rhizoctonia solani* Kühn isolated from potatoes**. *Turkish Journal of Agriculture and Forestry* 1998, **22**:609-613.
69. Huang HC, Kokko EG, Erickson RS: **Infection of alfalfa pollen by *Botrytis cinerea***. *Botanical Bulletin of Academia Sinica* 1999, **40**:101-106.
70. Voigt C, Schäfer W, Salomon S: **A secreted lipase of *Fusarium graminearum* is a virulence factor required for infection of cereals**. *The Plant Journal* 2005, **42**(3):364-375.
71. Berto P, Comménil P, Belingheri L, Dehorter B: **Occurrence of a lipase in spores of *Alternaria brassicicola* with a crucial role in the infection of cauliflower leaves**. *Federation of European Microbiological Societies Microbiology Letters* 2006, **180**(2):183-189.
72. Comménil P, Belingheri L, Dehorter B: **Antilipase antibodies prevent infection of tomato leaves by *Botrytis cinerea***. *Physiological and Molecular Plant Pathology* 1998, **52**(1):1-14.
73. Jenczmionka NJ, Maier FJ, Lösch AP, Schäfer W: **Mating, conidiation and pathogenicity of *Fusarium graminearum*, the main causal agent of the head-blight disease of wheat, are regulated by the MAP kinase gpmk1**. *Current Genetics* 2003, **43**(2):87-95.
74. Xu JR, Hamer JE: **MAP kinase and cAMP signaling regulate infection structure formation and pathogenic growth in the rice blast fungus *Magnaporthe grisea***. *Genes and development* 1996, **10**(21):2696-2706.
75. Lev S, Sharon A, Hadar R, Ma H, Horwitz BA: **A mitogen-activated protein kinase of the corn leaf pathogen *Cochliobolus heterostrophus* is involved in conidiation, appressorium formation, and pathogenicity: diverse roles for mitogen-activated protein kinase homologs in foliar pathogens**. *Proceedings of the National Academy of Sciences* 1999, **96**(23):13542-13547.
76. Ruiz-Roldán MC, Maier FJ, Schäfer W: **PTK1, a mitogen-activated-protein kinase gene, is required for conidiation, appressorium formation, and pathogenicity of**

***Pyrenophora teres* on barley**. *Molecular Plant-Microbe Interactions* 2001, **14**(2):116-125.

77. Di Pietro A, García-Maceira FI, Meglecz E, Roncero MIG: **A MAP kinase of the vascular wilt fungus *Fusarium oxysporum* is essential for root penetration and pathogenesis**. *Molecular Microbiology* 2004, **39**(5):1140-1152.
78. Nguyen, L. N: **Importance of secreted lipases for virulence of the phytopathogenic fungus *Fusarium graminearum***. *Dissertation* Hamburg, Germany: University of Hamburg; 2008.
79. Clergeot PH, Gourgues M, Cots J, Laurans F, Latorse MP, Pépin R, Tharreau D, Notteghem JL, Lebrun MH: **PLS1, a gene encoding a tetraspanin-like protein, is required for penetration of rice leaf by the fungal pathogen *Magnaporthe grisea***. *Proceedings of the National Academy of Sciences* 2001, **98**(12):6963-6968.
80. Gourgues M, Brunet-Simon A, Lebrun MH, Levis C: **The tetraspanin BcPls1 is required for appressorium-mediated penetration of *Botrytis cinerea* into host plant leaves**. *Molecular Microbiology* 2004, **51**(3):619-629.
81. Veneault-Fourrey C, Parisot D, Gourgues M, Laugé R, Lebrun M, Langin T: **The tetraspanin gene ClPLS1 is essential for appressorium-mediated penetration of the fungal pathogen *Colletotrichum lindemuthianum***. *Fungal Genetics and Biology* 2005, **42**(4):306-318.
82. Veneault-Fourrey C, Barooah M, Egan M, Wakley G, Talbot N: **Autophagic fungal cell death is necessary for infection by the rice blast fungus**. *Science's STKE* 2006, **312**(5773):580.
83. Lee N, D'Souza CA, Kronstad JW: **Of smuts, blasts, mildews, and blights: cAMP signaling in phytopathogenic fungi**. *Annual Review of Phytopathology* 2003, **41**(1):399-427.
84. D'Souza CA, Heitman J: **Conserved cAMP signaling cascades regulate fungal development and virulence**. *Federation of European Microbiological Societies Microbiology Reviews* 2006, **25**(3):349-364.
85. Choi W, Dean RA: **The adenylate cyclase gene MAC1 of *Magnaporthe grisea* controls appressorium formation and other aspects of growth and development**. *The Plant Cell Online* 1997, **9**(11):1973-1983.
86. Yan X, Li Y, Yue X, Wang C, Que Y, Kong D, Ma Z, Talbot NJ, Wang Z: **Two novel transcriptional regulators are essential for infection-related morphogenesis and pathogenicity of the rice blast fungus *Magnaporthe oryzae***. *PLoS Pathogens* 2011, **7**(12):e1002385.
87. Woriedh, M.: **Cloning, expression and functional characterization of deoxyhypusine synthase from the pathogenic fungus *Fusarium graminearum* Schwabe (teleomorph *Gibberella zeae*), wheat (*Triticum aestivum* L.) and maize (*Zea mays* L.)**. *Dissertation.* Hamburg,Germany: University of Hamburg 2011.
88. Woriedh M, Hauber I, Martinez-Rocha AL, Voigt C, Maier FJ, Schröder M, Meier C, Hauber J, Schäfer W: **Preventing Fusarium head blight of wheat and cob rot of maize by inhibition of fungal deoxyhypusine synthase**. *Molecular Plant-Microbe Interactions* 2011, **24**(5):619-627.
89. Güldener U, Mannhaupt G, Münsterkötter M, Haase D, Oesterheld M, Stümpflen V, Mewes HW, Adam G: **FGDB: a comprehensive fungal genome resource on the plant pathogen *Fusarium graminearum***. *Nucleic Acids Research* 2006, **34**(suppl 1):D456-D458.
90. Shirane N, Masuko M, Hayashi Y: **Light microscopic observation of nuclei and mitotic chromosomes of *Botrytis species***. *Phytopathology* 1989, **79**(7):728.
91. Zadoks JC, Chang TT, Konzak CF: **A decimal code for the growth stages of cereals**. *Weed Research* 1974, **14**(6):415-421.
92. Miedaner T, Reinbrecht C, Schilling AG: **Association among aggressiveness, fungal colonization, and mycotoxin production of 26 isolates of *Fusarium graminearum* in winter rye head blight**. *Journal of Plant Diseases and Protection* 2000, **107**(2):124-134.

93. Maier FJ, Maiz S, Losch AP, Lacour T, Schäfer W: **Development of a highly efficient gene targeting system for *Fusarium graminearum* using the disruption of a polyketide synthase gene as a visible marker**. *Federation of European Microbiological Societies Yeast Research* 2005, **5**(6-7):653-662.
94. Park M, Nishimura K, Zanelli C, Valentini S: **Functional significance of eIF5A and its hypusine modification in eukaryotes**. *Amino Acids* 2010, **38**(2):491-500.
95. Leach J, Lang B, Yoder O: **Methods for selection of mutants and *in vitro* culture of *Cochliobolus heterostrophus***. *Journal of General Microbiology* 1982, **128**(8):1719-1729.
96. Nirenberg H: **A simplified method for identifying *Fusarium spp.* occurring on wheat**. *Canadian Journal of Botany* 1981, **59**:1599-1609.
97. Reynolds ES: **The use of lead citrate at high pH as an electron-opaque stain in electron microscopy**. *The Journal of cell biology* 1963, **17**(1):208-212.
98. Kircher M: **Understanding and improving high-throughput sequencing data production and analysis**. *Dissertation.* Leipzig, Germany: University of Leipzig, Germany; 2011.
99. Trapnell C, Pachter L, Salzberg SL: **TopHat: discovering splice junctions with RNA-Seq**. *Bioinformatics* 2009, **25**(9):1105-1111.
100. Trapnell C, Williams BA, Pertea G, Mortazavi A, Kwan G, Van Baren MJ, Salzberg SL, Wold BJ, Pachter L: **Transcript assembly and quantification by RNA-Seq reveals unannotated transcripts and isoform switching during cell differentiation**. *Nature biotechnology* 2010, **28**(5):511-515.
101. Piehler S: **Differential gene expression analysis of the infection process of *Fusarium graminearum* using RNA-seq**. *Diploma.* Munich, Germany: Ludwig Maximilian University Munich, Technische Universität München; 2012.
102. EI-Samra IA, El-Faham YM, Kamara AM: **Selective induction of infection cushions by *Rhizoctonia solani* in relation to host responses**. *Phytopathologische Zeitschrift* 1981, **102**:122-126.
103. López-Berges MS, Rispail N, Prados-Rosales RC, Di Pietro A: **A nitrogen response pathway regulates virulence functions in *Fusarium oxysporum* via the protein kinase TOR and the bZIP protein MeaB**. *The Plant Cell Online* 2010, **22**(7):2459-2475.
104. Boenisch MJ, Schäfer W: ***Fusarium graminearum* forms mycotoxin producing infection structures on wheat**. *BMC Plant Biology* 2011, **11**(1):110.
105. Pannecoucque J, Höfte M: **Interactions between cauliflower and Rhizoctonia anastomosis groups with different levels of aggressiveness**. *BMC Plant Biology* 2009, **9**(1):95.
106. Rittenour WR, Harris SD: **An *in vitro* method for the analysis of infection-related morphogenesis in *Fusarium graminearum***. *Molecular Plant Pathology* 2010, **11**(3):361-369.
107. Boddu J, Cho S, Kruger WM, Muehlbauer GJ: **Transcriptome analysis of the barley-*Fusarium graminearum* interaction**. *Molecular Plant-Microbe Interactions* 2006, **19**(4):407-417.
108. Tariq VN, Gutteridge C, Jeffries P: **Comparative studies of cultural and biochemical characteristics used for distinguishing species within *Sclerotinia***. *Transactions of the British Mycological Society* 1985, **84**(3):381-397.
109. Stockwell V, Hanchey P: **The role of the cuticle in resistance of beans to *Rhizoctonia solani***. *Phytopathology* 1983, **73**(12):1640-1642.
110. Rodriguez-Galvez E, Mendgen K: **The infection process of *Fusarium oxysporum* in cotton root tips**. *Protoplasma* 1995, **189**(1):61-72.
111. Kang Z, Buchenauer H: **Ultrastructural and cytochemical studies on cellulose, xylan and pectin degradation in wheat spikes infected by *Fusarium culmorum***. *Journal of Phytopathology* 2001, **148**(5):263-275.
112. Amselem J, Cuomo CA, van Kan JAL, Viaud M, Benito EP, Couloux A, Coutinho PM, de Vries RP, Dyer PS, Fillinger S: **Genomic analysis of the necrotrophic fungal**

pathogens *Sclerotinia sclerotiorum* and *Botrytis cinerea*. *PLoS Genetics* 2011, **7**(8):e1002230.

113. Feng J, Liu G, Selvaraj G, Hughes GR, Wei Y: **A secreted lipase encoded by LIP1 is necessary for efficient use of saturated triglyceride lipids in *Fusarium graminearum***. *Microbiology* 2005, **151**(12):3911-3921.
114. Fukutomi M, Takada H: **Ultrastructure of infection process of *Rhizoctonia solani* Kuhn in cucumber hypocotyls**. *Annals of the Phytopathological Society of Japan* 1979, **45**(4):453.
115. Hückelhoven R: **Cell wall-associated mechanisms of disease resistance and susceptibility**. *Annu Rev Phytopathol* 2007, **45**:101-127.
116. Shetty NP, Jørgensen HJL, Jensen JD, Collinge DB, Shetty HS: **Roles of reactive oxygen species in interactions between plants and pathogens**. *European Journal of Plant Pathology* 2008, **121**(3):267-280.
117. Collmer A, Keen NT: **The role of pectic enzymes in plant pathogenesis**. *Annual Review of Phytopathology* 1986, **24**(1):383-409.
118. Mika A, Boenisch MJ, Hopff D, Lüthje S: **Membrane-bound guaiacol peroxidases from maize (Zea mays L.) roots are regulated by methyl jasmonate, salicylic acid, and pathogen elicitors**. *Journal of Experimental Botany* 2010, **61**(3):831-841.
119. Sexton AC, Cozijnsen AJ, Keniry A, Jewell E, Love CG, Batley J, Edwards D, Howlett BJ: **Comparison of transcription of multiple genes at three developmental stages of the plant pathogen *Sclerotinia sclerotiorum***. *Federation of European Microbiological Societies Microbiology Letters* 2006, **258**(1):150-160.
120. Bushnell WR, Hazen BE, Pritsch C: **Histology and physiology of Fusarium head blight**. In: *Fusarium Head Blight of Wheat and Barley.* Edited by Leonard KJ, Bushnell WR. St. Paul: APS Press; 2003: 44-83.
121. Flentje NT: **Studies on *Pellicularia filamentosa* (Pat.) Rogers. III Host penetration, and resistance, and strain spezialisation** *Transactions of the British Mycological Society* 1957, **40**:322-326.
122. L'Haridon F, Besson-Bard A, Binda M, Serrano M, Abou-Mansour E, Balet F, Schoonbeek HJ, Hess S, Mir R, Léon J: **A permeable cuticle is associated with the release of reactive oxygen species and induction of innate immunity**. *PLoS Pathogens* 2011, **7**(7):e1002148.
123. Koller W, Parker D, Becker C: **Role of cutinase in the penetration of apple leaves by *Venturia inaequalis***. *Phytopathology* 1991, **81**(11):1375.
124. Kucheryava N, Bowen J, Sutherland P, Conolly J, Mesarich C, Rikkerink E, Kemen E, Plummer K, Hahn M, Templeton M: **Two novel *Venturia inaequalis* genes induced upon morphogenetic differentiation during infection and *in vitro* growth on cellophane**. *Fungal Genetics and Biology* 2008, **45**(10):1329.
125. Stahl DJ, Schäfer W: **Cutinase is not required for fungal pathogenicity on pea**. *The Plant Cell Online* 1992, **4**(6):621-629.
126. Stahl DJ, Theuerkauf A, Heitefuss R, Schäfer W: **Cutinase of *Nectria haematococca* (*Fusarium solani f. sp. pisi)* is not required for fungal virulence or organ specificity on pea**. *Molecular Plant-Microbe Interactions* 1994, **7**(6):713-725.
127. Li D, Ashby AM, Johnstone K: **Molecular evidence that the extracellular cutinase Pbc1 is required for pathogenicity of *Pyrenopeziza brassicae* on oilseed rape**. *Molecular Plant-Microbe Interactions* 2003, **16**(6):545-552.
128. Woloshuk CP, Kolattukudy P: **Mechanism by which contact with plant cuticle triggers cutinase gene expression in the spores of *Fusarium solani f. sp. pisi***. *Proceedings of the National Academy of Sciences* 1986, **83**(6):1704-1708.
129. Jones L, Handreck K: **Silica in soils, plants and animals**. *Advances in Agronomy* 1967, **19**(1):107-149.
130. Sangster A: **Intracellular silica deposition in immature leaves in three species of the Gramineae**. *Annals of Botany* 1970, **34**(1):245-257.

131. Fauteux F, Rémus-Borel W, Menzies JG, Bélanger RR: **Silicon and plant disease resistance against pathogenic fungi**. *Federation of European Microbiological Societies Microbiology Letters* 2005, **249**(1):1-6.
132. Cai K, Gao D, Chen J, Luo S: **Probing the mechanisms of silicon-mediated pathogen resistance**. *Plant Signaling and Behavior* 2009, **4**(1):1-3.
133. Ball TB, Gardner JS, Anderson N: **Identifying inflorescence phytoliths from selected species of wheat (*Triticum monococcum, T. dicoccon, T. dicoccoides, and T. aestivum*) and barley (*Hordeum vulgare* and *H. spontaneum*)(Gramineae)**. *American Journal of Botany* 1999, **86**(11):1615-1623.
134. Cai K, Gao D, Luo S, Zeng R, Yang J, Zhu X: **Physiological and cytological mechanisms of silicon-induced resistance in rice against blast disease**. *Physiologia Plantarum* 2008, **134**(2):324-333.
135. Hayasaka T, Fujii H, Ishiguro K: **The role of silicon in preventing appressorial penetration by the rice blast fungus**. *Phytopathology* 2008, **98**(9):1038-1044.
136. Bélanger R, Benhamou N, Menzies J: **Cytological evidence of an active role of silicon in wheat resistance to powdery mildew (*Blumeria graminis f. sp. tritici*)**. *Phytopathology* 2003, **93**(4):402-412.
137. Fawe A, Abou-Zaid M, Menzies J, Bélanger R: **Silicon-mediated accumulation of flavonoid phytoalexins in cucumber**. *Phytopathology* 1998, **88**(5):396-401.
138. Malalasekera RAP, Sanderson FR, Colhoun J: ***Fusarium* diseases of cereals: IX. Penetration and invasion of wheat seedlings by *Fusarium culmorum* and *F. nivale***. *Transactions of the British Mycological Society* 1973, **60**(3):453-IN457.
139. Kang Z, Huang L, Buchenauer H: **Ultrastructural and cytochemical studies on infection of wheat spikes by *Microdochium nivale***. *Journal of Plant Diseases and Protection* 2008 **111**(4):351-361.
140. Keller T, Damude HG, Werner D, Doerner P, Dixon RA, Lamb C: **A plant homolog of the neutrophil NADPH oxidase gp91phox subunit gene encodes a plasma membrane protein with Ca2+ binding motifs**. *The Plant Cell Online* 1998, **10**(2):255-266.
141. Yoda H, Hiroi Y, Sano H: **Polyamine oxidase is one of the key elements for oxidative burst to induce programmed cell death in tobacco cultured cells**. *Plant Physiology* 2006, **142**(1):193-206.
142. Olson P, Varner J: **Hydrogen peroxide and lignification**. *The Plant Journal* 2002, **4**(5):887-892.
143. Bhuiyan NH, Selvaraj G, Wei Y, King J: **Role of lignification in plant defense**. *Plant Signaling and Behavior* 2009, **4**(2):158-159.
144. Yu JH, Keller N: **Regulation of secondary metabolism in filamentous fungi**. *Annual Review of Phytopathology* 2005, **43**:437-458.
145. Kachholz T, Demain AL: **Nitrate repression of averufin and aflatoxin biosynthesis**. *Journal of Natural Products* 1983, **46**(4):499-506.
146. Keller NP, Nesbitt C, Sarr B, Phillips TD, Burow GB: **pH regulation of sterigmatocystin and aflatoxin biosynthesis in *Aspergillus spp***. *Phytopathology* 1997, **87**(6):643-648.
147. Coleman M, Henricot B, Arnau J, Oliver RP: **Starvation-induced genes of the tomato pathogen *Cladosporium fulvum* are also induced during growth *in planta***. *Molecular Plant-Microbe Interactions* 1997, **10**(9):1106-1109.
148. Donofrio N, Oh Y, Lundy R, Pan H, Brown D, Jeong J, Coughlan S, Mitchell T, Dean R: **Global gene expression during nitrogen starvation in the rice blast fungus, *Magnaporthe grisea***. *Fungal Genetics and Biology* 2006, **43**(9):605.
149. Divon H, Ziv C, Davydov O, Yarden O, Fluhr R: **The global nitrogen regulator, FNR1, regulates fungal nutrition-genes and fitness during *Fusarium oxysporum* pathogenesis**. *Molecular Plant Pathology* 2006, **7**(6):485.
150. Talbot NJ: **On the trail of a cereal killer: Exploring the biology of *Magnaporthe grisea***. *Annual Reviews in Microbiology* 2003, **57**(1):177-202.

151. Ackerveken G, Dunn R, Cozijnsen A, Vossen J, Broek H, Wit P: **Nitrogen limitation induces expression of the avirulence gene avr9 in the tomato pathogen *Cladosporium fulvum***. *Molecular and General Genetics MGG* 1994, **243**(3):277-285.
152. Snoeijers SS, Pérez-García A, Joosten MHAJ, De Wit PJGM: **The effect of nitrogen on disease development and gene expression in bacterial and fungal plant pathogens**. *European Journal of Plant Pathology* 2000, **106**(6):493-506.
153. Kang Z, Buchenauer H: **Studies on the infection process of *Fusarium culmorum* in wheat spikes: Degradation of host cell wall components and localization of trichothecene toxins in infected tissue**. *European Journal of Plant Pathology* 2002, **108**(7):653-660.
154. Zhao X, Mehrabi R, Xu JR: **Mitogen-activated protein kinase pathways and fungal pathogenesis**. *Eukaryotic Cell* 2007, **6**(10):1701-1714.
155. Chen C, Harel A, Gorovoits R, Yarden O, Dickman MB: **MAPK regulation of sclerotial development in *Sclerotinia sclerotiorum* is linked with pH and cAMP sensing**. *Molecular Plant-Microbe Interactions* 2004, **17**(4):404-413.
156. Malagnac F, Bidard F, Lalucque H, Brun S, Lambou K, Lebrun MH, Silar P: **Convergent evolution of morphogenetic processes in fungi: Role of tetraspanins and NADPH oxidases 2 in plant pathogens and saprobes**. *Communicative and Integrative Biology* 2008, **1**(2):180-181.
157. Brun S, Malagnac F, Bidard F, Lalucque H, Silar P: **Functions and regulation of the Nox family in the filamentous fungus *Podospora anserina*: a new role in cellulose degradation**. *Molecular Microbiology* 2009, **74**(2):480-496.
158. Hemler ME: **Targeting of tetraspanin proteins-potential benefits and strategies**. *Nature Reviews Drug Discovery* 2008, **7**(9):747-758.
159. Charrin S, le Naour F, Silvie O, Milhiet P, Boucheix C, Rubinstein E: **Lateral organization of membrane proteins: tetraspanins spin their web**. *Biochemical Journal* 2009, **420**:133-154.
160. Kays AM, Borkovich KA: **Severe impairment of growth and differentiation in a *Neurospora crassa* mutant lacking all heterotrimeric Gα proteins**. *Genetics* 2004, **166**(3):1229-1240.
161. Terenzi HF, Flawiá MM, Torres HN: **A *Neurospora crassa* morphological mutant showing reduced adenylate cyclase activity**. *Biochemical and Biophysical Research Communications* 1974, **58**(4):990-996.
162. Zanelli CF, Valentini SR: **Is there a role for eIF5A in translation?** *Amino Acids* 2007, **33**(2):351-358.
163. Lee SB, Park JH, Kaevel J, Sramkova M, Weigert R, Park MH: **The effect of hypusine modification on the intracellular localization of eIF5A**. *Biochemical and Biophysical Research Communications* 2009, **383**(4):497-502.
164. Dias CAO, Cano VSP, Rangel SM, Apponi LH, Frigieri MC, Muniz JRC, Garcia W, Park MH, Garratt RC, Zanelli CF: **Structural modeling and mutational analysis of yeast eukaryotic translation initiation factor 5A reveal new critical residues and reinforce its involvement in protein synthesis**. *Federation of European Biochemical Societies Journal* 2008, **275**(8):1874-1888.
165. Ramsay K, Jones MGK, Wang Z: **Laser capture microdissection: a novel approach to microanalysis of plant-microbe interactions**. *Molecular Plant Pathology* 2006, **7**(5):429-435.
166. Balestrini R, Gomez-Ariza J, Klink VP, Bonfante P: **Application of laser microdissection to plant pathogenic and symbiotic interactions**. *Journal of Plant Interactions* 2009, **4**(2):81-92.
167. Gomez SK, Harrison MJ: **Laser microdissection and its application to analyze gene expression in arbuscular mycorrhizal symbiosis**. *Pest Management Science* 2009, **65**(5):504-511.
168. Howard RJ, Bourett TM, Czymmek KJ: **Essential Microscopy-based Technology for Studies of Fungal Pathogen-Plant Host Interactions**. *Microscopy and Microanalysis* 2004, **10**(S02):218-219.

169. Tang W, Coughlan S, Crane E, Beatty M, Duvick J: **The application of laser microdissection to in planta gene expression profiling of the maize anthracnose stalk rot fungus *Colletotrichum graminicola***. *Molecular Plant-Microbe Interactions* 2006, **19**(11):1240-1250.
170. Tremblay A, Shuxian LI, Scheffler BE, Matthews BF: **Laser capture microdissection and expressed sequence tag analysis of uredinia formed by *Phakopsora pachyrhizi*, the causal agent of Asian soybean rust**. *Physiological and Molecular Plant Pathology* 2008, **73**(6):163-174.
171. Tremblay A, Li S, Scheffler B, Matthews B: **Laser capture microdissection and expressed sequence tag analysis of uredinia formed by *Phakopsora pachyrhizi*, the causal agent of Asian soybean rust**. *Physiological and Molecular Plant Pathology* 2009, **73**(6):163-174.
172. Hacquard S, Delaruelle C, Legue V, Tisserant E, Kohler A, Frey P, Martin F, Duplessis S: **Laser capture microdissection of uredinia formed by *Melampsora lahci-populina* revealed a transcriptional switch between biotrophy and sporulation**. *Molecular Plant-Microbe Interactions* 2010, **23**(10):1275-1286.
173. Chandran D, Inada N, Hather G, Kleindt CK, Wildermuth MC: **Laser microdissection of *Arabidopsis* cells at the powdery mildew infection site reveals site-specific processes and regulators**. *Proceedings of the National Academy of Sciences* 2010, **107**(1):460-465.
174. Teichert I, Wolff G, Kück U, Nowrousian M: **Combining laser microdissection and RNA-seq to chart the transcriptional landscape of fungal development**. *BMC Genomics* 2012, **13**(1):511.
175. Zhang XW, Jia LJ, Zhang Y, Jiang G, Li X, Zhang D, Tang WH: **In Planta Stage-Specific Fungal Gene Profiling Elucidates the Molecular Strategies of *Fusarium graminearum* Growing inside Wheat Coleoptiles**. *The Plant Cell Online* 2012, **24**(12):5159-5176.
176. Espina V, Wulfkuhle JD, Calvert VS, VanMeter A, Zhou W, Coukos G, Geho DH, Petricoin EF, Liotta LA: **Laser-capture microdissection**. *Nature Protocols* 2006, **1**(2):586-603.
177. Domazet B, MacLennan GT, Lopez-Beltran A, Montironi R, Cheng L: **Laser capture microdissection in the genomic and proteomic era: targeting the genetic basis of cancer**. *International Journal of Clinical and Experimental Pathology* 2008, **1**(6):475.
178. Vandewoestyne M, Deforce D: **Laser capture microdissection in forensic research: a review**. *International Journal of Legal Medicine* 2010, **124**(6):513-521.
179. Cai S, Lashbrook CC: **Laser capture microdissection of plant cells from tape-transferred paraffin sections promotes recovery of structurally intact RNA for global gene profiling**. *The Plant Journal* 2006, **48**(4):628-637.
180. Goldsworthy SM, Stockton PS, Trempus CS, Foley JF, Maronpot RR: **Effects of fixation on RNA extraction and amplification from laser capture microdissected tissue**. *Molecular Carcinogenesis* 1999, **25**(2):86-91.
181. Kerk NM, Ceserani T, Tausta SL, Sussex IM, Nelson TM: **Laser capture microdissection of cells from plant tissues**. *Plant Physiology* 2003, **132**(1):27-35.
182. Fleige S, Pfaffl MW: **RNA integrity and the effect on the real-time qRT-PCR performance**. *Molecular Aspects of Medicine* 2006, **27**(2):126-139.
183. Copois V, Bibeau F, Bascoul-Mollevi C, Salvetat N, Chalbos P, Bareil C, Candeil L, Fraslon C, Conseiller E, Granci V: **Impact of RNA degradation on gene expression profiles: assessment of different methods to reliably determine RNA quality**. *Journal of Biotechnology* 2007, **127**(4):549-559.
184. Nelson T, Tausta SL, Gandotra N, Liu T: **Laser microdissection of plant tissue: what you see is what you get**. *Annual Review of Plant Biology* 2006, **57**:181-201.
185. Day RC, McNoe LA, Macknight RC: **Transcript analysis of laser microdissected plant cells**. *Physiologia Plantarum* 2006, **129**(2):267-282.
186. Clement-Ziza M, Munnich A, Lyonnet S, Jaubert F, Besmond C: **Stabilization of RNA during laser capture microdissection by performing experiments under argon**

atmosphere or using ethanol as a solvent in staining solutions. *RNA* 2008, **14**(12):2698-2704.

187. Wang WZ, Oeschger FM, Lee S, Molnár Z: **High quality RNA from multiple brain regions simultaneously acquired by laser capture microdissection**. *BMC Molecular Biology* 2009, **10**(1):69.
188. Nakazono M, Qiu F, Borsuk LA, Schnable PS: **Laser-capture microdissection, a tool for the global analysis of gene expression in specific plant cell types: identification of genes expressed differentially in epidermal cells or vascular tissues of maize**. *The Plant Cell Online* 2003, **15**(3):583-596.
189. Casson SA, Spencer MWB, Lindsey K: **Laser-capture microdissection to study global transcriptional changes during plant embryogenesis**. *Methods in Molecular Biology* 2008, **427**:111.
190. Sambrook J, Russell DW: **Molecular Cloning: A Laboratory Manual.** New York, USA: Cold Spring Harbor CSH Laboratory Press; 2001.
191. Mueller O, Lightfoot S, Schroeder A: **RNA integrity number (RIN)-standardization of RNA quality control**. *Agilent Application Note, Publication* 2004:1-8.
192. Costa V, Angelini C, De Feis I, Ciccodicola A: **Uncovering the complexity of transcriptomes with RNA-Seq**. *Journal of Biomedicine and Biotechnology* 2010, **2010**.
193. Wilhelm J, Muyal JP, Best J, Kwapiszewska G, Stein MM, Seeger W, Bohle RM, Fink L: **Systematic comparison of the T7-IVT and SMART-based RNA preamplification techniques for DNA microarray experiments**. *Clinical Chemistry* 2006, **52**(6):1161-1167.
194. Subkhankulova T, Livesey FJ: **Comparative evaluation of linear and exponential amplification techniques for expression profiling at the single-cell level**. *Genome Biology* 2006, **7**(3):R18.
195. Caretti E, Devarajan K, Coudry R, Ross E, Clapper ML, Cooper HS, Bellacosa A: **Comparison of RNA amplification methods and chip platforms for microarray analysis of samples processed by laser capture microdissection**. *Journal of Cellular Biochemistry* 2008, **103**(2):556-563.
196. Lang JE, Magbanua MJM, Scott JH, Makrigiorgos GM, Wang G, Federman S, Esserman LJ, Park JW, Haqq CM: **A comparison of RNA amplification techniques at sub-nanogram input concentration**. *BMC Genomics* 2009, **10**(1):326.
197. Le Q, Gutierez-Marcos JF, Costa LM, Meyer S, Dickinson HG, Lörz H, Kranz E, Scholten S: **Construction and screening of subtracted cDNA libraries from limited populations of plant cells: a comparative analysis of gene expression between maize egg cells and central cells**. *The Plant Journal* 2005, **44**(1):167-178.
198. Zhu YY, Machleder EM, Chenchik A, Li R, Siebert PD: **Reverse transcriptase template switching: A SMART™ approach for full-length cDNA library construction**. *Biotechniques* 2001, **30**(4):892-897.
199. Chenchik A, Zhu YY, Diatchenko L, Li R, Hill J, Siebert PD: **Generation and use of high-quality cDNA from small amounts of total RNA by SMART PCR**. In: *Gene cloning and analysis by RT-PCR*. Edited by Larrick. PDSaJW. Madison, USA: BioTechniques Books; 1998: 305-319.
200. Vernon SD, Unger ER, Rajeevan M, Dimulescu IM, Nisenbaum R, Campbell CE: **Reproducibility of alternative probe synthesis approaches for gene expression profiling with arrays**. *The Journal of molecular diagnostics: JMD* 2000, **2**(3):124.
201. Petalidis L, Bhattacharyya S, Morris GA, Collins VP, Freeman TC, Lyons PA: **Global amplification of mRNA by template switching PCR: linearity and application to microarray analysis**. *Nucleic acids research* 2003, **31**(22):e142-e142.
202. Mardis ER: **A decade's perspective on DNA sequencing technology**. *Nature* 2011, **470**(7333):198-203.
203. Ewing B, Hillier LD, Wendl MC, Green P: **Base-calling of automated sequencer traces usingPhred. I. Accuracy assessment**. *Genome Research* 1998a, **8**(3):175-185.
204. Ewing B, Green P: **Base-calling of automated sequencer traces usingPhred. II. error probabilities**. *Genome Research* 1998b, **8**(3):186-194.

205. Cock PJA, Fields CJ, Goto N, Heuer ML, Rice PM: **The Sanger FASTQ file format for sequences with quality scores, and the Solexa/Illumina FASTQ variants**. *Nucleic Acids Research* 2010, **38**(6):1767-1771.
206. Nagalakshmi U, Wang Z, Waern K, Shou C, Raha D, Gerstein M, Snyder M: **The transcriptional landscape of the yeast genome defined by RNA sequencing**. *Science* 2008, **320**(5881):1344-1349.
207. Torti S, Fornara F, Vincent C, Andres F, Nordström K, Göbel U, Knoll D, Schoof H, Coupland G: **Analysis of the Arabidopsis shoot meristem transcriptome during floral transition identifies distinct regulatory patterns and a leucine-rich repeat protein that promotes flowering**. *The Plant Cell Online* 2012, **24**(2):444-462.
208. Matas AJ, Yeats TH, Buda GJ, Zheng Y, Chatterjee S, Tohge T, Ponnala L, Adato A, Aharoni A, Stark R: **Tissue-and cell-type specific transcriptome profiling of expanding tomato fruit provides insights into metabolic and regulatory specialization and cuticle formation**. *The Plant Cell Online* 2012, **23**(11):3893-3910.
209. Chen H, Liu Z, Gong S, Wu X, Taylor WL, Williams RW, Matta SG, Sharp BM: **Genome-wide gene expression profiling of nucleus accumbens neurons projecting to ventral pallidum using both microarray and transcriptome sequencing**. *Frontiers in Neuroscience* 2011, **5**.
210. Cox MP, Eaton CJ, Scott DB: **Exploring molecular signaling in plant-fungal symbioses using high throughput RNA sequencing**. *Plant Signaling and Behavior* 2010, **5**(11):1353-1358.
211. Dietterich TG: **Ensemble methods in machine learning**. In: *Multiple classifier systems*. Corvallis, USA Springer Berlin Heidelberg; 2000: 1-15.
212. Aßfalg J, Gong J, Kriegel HP, Pryakhin A, Wei T, Zimek A: **Supervised ensembles of prediction methods for subcellular localization**. *Journal of Bioinformatics and Computational Biology* 2009, **7**(02):269-285.
213. Güldener U, Seong KY, Boddu J, Cho S, Trail F, Xu JR, Adam G, Mewes HW, Muehlbauer GJ, Kistler HC: **Development of a *Fusarium graminearum* Affymetrix GeneChip for profiling fungal gene expression *in vitro* and *in planta***. *Fungal Genetics and Biology* 2006, **43**:316-325.
214. Stephens AE, Gardiner DM, White RG, Munn AL, Manners JM: **Phases of infection and gene expression of *Fusarium graminearum* during crown rot disease of wheat**. *Molecular Plant-Microbe Interactions* 2008, **21**(12):1571-1581.
215. LyØse E, Seong KY, Kistler HC: **The transcriptome of *Fusarium graminearum* during the infection of wheat**. *Molecular Plant-Microbe Interactions* 2011, **24**(9):995-1000.
216. Sugui JA, Deising HB: **Isolation of infection-specific sequence tags expressed during early stages of maize anthracnose disease development**. *Molecular Plant Pathology* 2002, **3**(4):197-203.

9 Eidesstattliche Versicherung

Name: Boenisch

Vornamen: Marike Johanne

Hiermit erkläre ich an Eides statt, dass ich die vorliegende Dissertation selbstständig verfasst und keine anderen als die angegebenen Quellen und Hilfsmittel benutzt habe.

Marike Johanne Boenisch

Hamburg, den 04. Februar 2013

10 List of publications

Accepted publications

Bormann J., Ilgen P., Boenisch M. J. and W. Schäfer. „**Mykotoxinbildung durch *Fusarium graminearum* in der Weizenähre**“. BIOspektrum. 19(6): 612-615. (2013)

Staerkel C., Boenisch M. J., Kröger C., Bormann J., Stahl D. and W. Schäfer. “**CbCTB2, an O-methyltransferase is essential for biosynthesis of the mycotoxin cercosporin and infection of sugar beet by *Cercospora beticola***” BMC Plant Biology 13(1):1-11. (2013)

Boenisch M. J. and W. Schäfer. "***Fusarium graminearum* forms mycotoxin producing infection structures on wheat**" BMC Plant Biology 11(1): 110. (2011)

Publications in progress

Boenisch M. J., Scholten S., Piehler S.,Münsterkötter M., Güldener U. Bormann J. and W. Schäfer. **“Laser microdissection and transcriptomics of infection cushions formed by *Fusarium graminearum*”** (Research article)

Bormann J., Boenisch M. J., Brückner E., Firat D. and W. Schäfer. ”**The adenylyl cyclase controls the switch from vegetative to pathogenic lifestyle of *Fusarium graminearum* on wheat”** (Research article)

Nguyen L. N., Boenisch M. J., Le G. T. T., Lambou K., Barbisan C., Staerkel C., Lebrun M. H. and W. Schäfer. “**The tetraspanin FgPls1 is involved in novel developmental and pathogenicity functions of the wheat scab fungus *Fusarium graminearum***” (Research article)

Talks and poster presentations on scientific conferences

„XI International Fungal Biology Conference"
Karlsruhe, Germany, 29.09 - 03.10. 2013 (Talk)

"27th Fungal Genetics Conference"
Asilomar, USA. 12.-17. 03. 2012 (Poster)

„Jahrestagung der Vereinigung für Allgemeine und Angewandte Mikrobiologie"
Karlsruhe, Germany, 03.-06. 04. 2011 (Talk)

"10th VAAM Symposium of Molecular Biology of Fungi"
Marburg, Germany, 11.-14. 04. 2011 (Talk)

"National Fusarium Head Blight Forum 2010" of the United States Wheat and Barley Scab Initiative (USWBSI), Milwaukee, USA, 07.-09. 12. 2010 (Invited talk)

"Fusarium Satellite Meeting" of the "10th European Conference on Fungal Genetics"
Amsterdam, The Netherlands, 28.-29. 03. 2010 (Talk)

11 Acknowledgments

Zunächst möchte ich mich herzlich bei Herrn Prof. Dr. Wilhelm Schäfer bedanken. Er hat mir im Rahmen meiner Promotion ermöglicht sowohl molekularbiologische, als auch diverse Imaging-Verfahren anzuwenden und miteinander zu kombinieren. Ich danke ihm für seine Begeisterung dafür Unsichtbares sichtbar zu machen und scheinbar Unmögliches möglich zu machen. Desweiteren möchte ich mich bei Prof. Dr. Christian Voigt bedanken, der mir im Rahmen meiner Doktorarbeit die Verwendung der Mikroskope LSM 780 und PALM Microbeam gestattet hat. Dr. Stefan Scholten möchte ich einen außerordentlichen Dank aussprechen. Neben der Erfahrung, der Zeit und der materiellen Unterstützung, war Stefans Begeisterung und Ehrgeiz während unserer Zusammenarbeit eine großartige Hilfe und Motivation. Bei Sebastian Piehler und Dr. Ulrich Güldener möchte ich mich für die sehr aufwendige und ambitionierte Arbeit bezüglich der bioinformatischen und statistische Auswertung der Sequenzdatensätze von Laufhyphen und Infektionskissen bedanken. Einen ganz besonderen Dank möchte ich zudem an Elke Woelken, Renate Walter, Karen Dehn und Dr. Frank Friedrich richten. Durch die fantastische Zusammenarbeit und Unterstützung wurden viele histologische und elektronenmikroskopische Untersuchungen in dem zeitlichen Rahmen der Arbeit erst möglich. Für die freundliche Hilfsbereitschaft und die gute Teamarbeit in allen Bereichen des Laboralltags sowie der Hochschullehre möchte ich mich bei meinen Arbeitskollegen Birgit Hadeler, Cathrin Kröger, Christiane Berkenharn, Jakob Bönninghausen, Thuat van Nguyen, Antje Blümke , Marcel Naumann, Dr. Jörg Bormann und Dr. Ana Lilia Martínez-Rocha herzlich bedanken. Meinen Projektstudenten Jakob Weber, Birgit Schiller, Elena Brückner und Lisa Charadi möchte ich für das Interesse an meinem Forschugsprojekt, die ehrgeizige Mitarbeit und eine schöne Zeit danken. Brigitte Doormann möchte ich ganz besonders für ihr offenes Ohr, die wertvolle mentale Unterstützung und die Korrekturlesungen diverser Manuskripte danken. Bei Dr. Hartwig Lüthen und Dr. Sabine Lüthje möchte ich mich ganz besonders dafür bedanken, dass sie sich die Zeit genommen haben, mich in allen Belangen des täglichen „Uni-Wahnsinns“ bestmöglich zu beraten und zu unterstützen.

Bei einigen sehr wertvollen Menschen möchte ich mich hier bedanken, die einen großen Anteil an dieser Arbeit haben, da sie in den letzten Jahren meine Wegbegleiter und private Stütze waren. Dabei möchte ich Mathias Bading, Jasmin Rother und Jan Waage nennen, auf die ich stets zählen konnte. Daniel TJ Takoeta möchte ich herzlich für das Korrekturlesen meiner Arbeit danken. Desweiteren danke ich Retriever-Dame Dagmar und dem treuen Benchmob für den Ausgleich.

Von ganzem Herzen möchte ich meinen Eltern und meinem Bruder danken, die mich in jeder Lebenslage unterstützt und aufgebaut haben. Ich bin unglaublich dankbar, dass es euch gibt, denn ohne Euch hätte ich das nicht geschafft. Das hier ist für uns vier.

gez. Marike Johanne Boenisch